Advanced Composites and Hybrid Materials (2024) 7:130
https://doi.org/10.1007/s42114-024-00913-7

REVIEW

Research progress in the development of transition metal chalcogenides and their composite-based electrode materials for supercapacitors

E. S. Sowbakkiyavathi[1,2] · S. P. Arunachala Kumar[1] · Dheeraj K. Maurya[1] · B. Balakrishnan[1] · John Zhanhu Guo[3] · A. Subramania[1]

Received: 4 August 2023 / Revised: 3 October 2023 / Accepted: 28 May 2024 / Published online: 1 August 2024

Abstract

Supercapacitors revealing excellent power density have arisen as the most promising candidates for supporting the major developments in energy storage devices. Supercapacitor attracts many emerging mobile devices for addressing energy storage and harvesting issues. The supercapacitor is similar to a conventional capacitor. Moreover, many researchers studied the improvement of energy and power density so that they can be applied extensively. The electrochemical performance of supercapacitor depends on various factors like electrode materials, electrolyte, and the range of voltage used. Most researchers mainly focused on the development of new electrode materials which yield better performance for the application of supercapacitors. This review work summarizes the introduction of supercapacitors and the recent advanced development of a variety of electrode materials in supercapacitors and production methods. In particular, transition metal chalcogenide–based electrode materials are focused here. Also, this review précises the improvement of the electrochemical performance of supercapacitor by incorporating or doping highly active materials like MWCNT, graphene, CNT, reduced graphene oxide, metal-based compounds, and polymers. The enhancement of specific capacity by altering the morphology and developing electrode with new morphological structures is deeply discussed in this review. Recently, trimetallic chalcogenides and its composites are emerged as new promising electrode materials which deliver large specific capacitance with excellent cycling stability and rate performance have also been reported here.

Keywords Supercapacitor · Metal chalcogenide · Transition metal chalcogenide · Electrode material

1 Introduction

The increase in population and economic growth across the world leads to increase in the usage of fossil fuels for various purposes. This leads to two main environmental issues: exhaustion of existing fossil fuels and environmental pollution, i.e., global warming due to the emission of greenhouse gas. These issues compel us to create and market environmentally responsible, economically viable, and sustainable energy sources [1]. Sustainable renewable energy from nature can be utilized as the energy source using various technologies from the sun, wind, ocean, hydropower, etc. [2]. Energy storage systems play the prominent role in intermittent nature of the renewable energy sources and increase the power transmission into the grid [3, 4]. Batteries, supercapacitors, and fuel cells are the major energy storage systems that store and deliver the energy at the time of requirement by the principle of electrochemical energy

E. S. Sowbakkiyavathi and Arunachala Kumar S. P. contributed equally to this work.

✉ John Zhanhu Guo
zguo10@utk.edu; a.subramania@gmail.com

✉ A. Subramania
a.subramania@gmail.com; zguo10@utk.edu

[1] Electro-Materials Research Laboratory, Centre for Nanoscience and Technology, Pondicherry University, Puducherry 605 014, India

[2] Department of Physics, Sathyabama Institute of Science and Technology, Chennai 600 119, India

[3] Mechanical and Construction Engineering, Faculty of Engineering and Environment, Northumbria University, Newcastle Upon Tyne NE1 8ST, UK

conversion. Batteries are well established and have wide range of application from simple electronic equipment such as clock and toys to automobile vehicle such as EMV. But there are some drawbacks in battery technologies such as less power densities, low cycle life, higher recharging time period, and rise in temperature during operation and hazardous to the environment [5]. These downside impulses to develop new alternative and efficient energy storage systems lead to the supercapacitors. Supercapacitors (SCs) or ultracapacitor is an electrochemical device with high power density than batteries and larger capacitance than the conventional capacitors. SCs have greater advantages such as higher power densities, high efficiency, high specific capacitance, and wide operating temperature. Moreover, they are environmental friendliness and charge quickly and deliver high power at a short period and build a gap between batteries and conventional capacitors. Due to these advantages, they are used for specific applications that require quick charge discharge and long life cycle than the long period of energy storage.

Supercapacitors can be classified as either electrochemical double-layer capacitor (EDLC) or pseudocapacitors based on their energy storage potential. While considering the charge storage mechanism, there are two main charge storage principles in capacitors: double-layer capacitance, electrostatic storage of energy by separation of charge in a Helmholtz double layer, and pseudocapacitance, electrochemical storage of energy by faradic redox reaction. Variation in mechanism and choice of electrodes lead to three different classifications: electric double-layer capacitors (EDLCs), pseudocapacitors (PCs), and hybrid capacitors (HCs).

EDLCs store charges electrostatically in the formed double layer at the interface of two electrodes. It uses carbon-based materials such as activated carbon (AC), carbon nanosheets, single-walled and multi-walled carbon nanotubes (CNT), carbon aerogel, graphene, graphene oxides, and mesoporous carbon to store energy [5]. PCs are a type of supercapacitors that store charges by a Faradaic mechanism based on fast and highly reversible surface or near-surface redox reactions. When a potential is applied, fast and reversible Faradaic reactions (redox reactions) take place on the electrode material similar to batteries results in Faradic current. PCs uses metal oxides (RuO_2, MnO_2, NiO, MoO_2, V_2O_5, etc.), metal chalcogenides (MnSe, CoSe, MoS, etc.), metal nitrides (VN, TiN, RuN, etc.), and conducting polymers (polypyrrole, polyaniline, polythiophene, etc.) as electrode materials for SCs. In EDLCs, non-Faradic reaction takes places where the electrode material is undisturbed leads to long life cycle of the SCs but outcomes with low energy density. On the other hand, pseudocapacitors undergo Faradic mechanism for the charging and discharging process on the surface of electrodes offer high energy density than the EDLC at the price of low cycle life and rate capability. Since both types have different disadvantages, the combination of both types can improve the efficiency of the supercapacitors. Hybrid supercapacitors are another type with a combination of both electric double capacitors and pseudocapacitors working principle for the charging and discharging process in supercapacitors. The different parameters of EDLCs, PCs, and HSCs are given in Table 1. The carbon-based electrode's non-Faradaic charge-discharge reaction and the other electrodes surface confined Faradaic reaction combine to provide large energy densities and good cyclic stability. In both mechanisms, large surface area, appropriate pore-size distribution, and high conductivity are essential properties of the electrode materials to attain large capacitance [6].

Supercapacitors are devices that are accomplished for managing and providing high power densities than the batteries at the time of requirement. It also has high cycle life (greater than 100 times) than the conventional batteries [8, 9]. Even though it delivers hundred to thousand times higher power at the same volume, its energy density is much lower (5–50 times) than the batteries. This limits the application of SCs to the necessity of high power bursts and is

Table 1 Parameter comparisons of electric double-layer capacitors, pseudocapacitors, and hybrid supercapacitors

Parameters	EDLC	PC	HSC
Charge storage	Electrostatically, i.e., by the formation of a double layer (non-Faradic process)	Electrochemically, i.e., Faradic process (redox reaction)	Both electrostatically and electrochemically, i.e., by non-Faradic process on a carbon electrode and by Faradic process on another electrode
Electrodes	Carbon-based electrode	Metal oxides (MOs), nitrides (MNs), chalcogenides (MXs), and conducting polymers (CP)	Both carbon-based electrodes and MOs, MNs, MXs, CP
Energy density	Low	High	High
Power density	High	Low	High
Cycle life	High	Low	Moderate

Information is gathered from the research article by Pandolfo et al. [7]

not essential for high energy storage capacity (high energy density). The application of SCs in the industrial field is mostly for military purposes, and in automotive industries, they are used in electric vehicles coupled with batteries for maximum efficiency [10]. SCs serve as a bridge between traditional capacitors and batteries since the batteries have higher energy density but lower power density and cycle lives when compared to traditional capacitors. The characteristics of the capacitors, supercapacitors, and batteries are given in Table 2. This energy and power densities characteristic between energy storage devices were clearly explained using Ragone plot that plots the value of specific energy (Wh kg^{-1}) versus specific power (W kg^{-1}). This plot can only relate the energy and power densities of the energy storage system and does not deal with other parameters such as eco-friendliness, cost, safety, and life cycle [6]. These need to be analyzed separately for the complete understanding of the energy storage device limitation and its advantages.

Supercapacitors consists of two electrode separated by ion permeable membrane called separator, to avoid conduct between two electrodes that leads to short circuit. Separator is soaked in electrolyte and provides the ionic charge transfer between the two electrodes. The separator membranes should also have high electrical resistance, high ionic conductivity, and low thickness for the better performance. The major issues in supercapacitor are the energy density which is much lower than the batteries. In order to provide for the better application, the energy density needs to be increased by various measures. The energy and power densities of the SCs are calculated by [11]

$$E = \frac{1}{2}CV^2 \ (Wh\ kg^{-1})$$

$$P = \frac{V^2}{4R} \ (Wkg^{-1})$$

where V is the cell voltage (V), C is the specific capacitance (F g^{-1}), and R is the internal resistance of the supercapacitor.

To increase the power densities of SCs, the internal resistance of the cell which is the sum of electrode resistance and electrolyte resistance has to be reduced, although the internal resistance of the SCs is much lower than batteries due to the fast and rapid recombination of positive and negative charges even in Faradic process. To increase the energy density of the SCs, both specific capacitance and cell voltage have to be increased since they are linearly proportional. Cell voltage of the SCs depends on the electrode material and electrolyte. But the operating voltage of the SCs is determined by electrolyte stability window. For aqueous electrolyte, the operating voltage will be around 1.2 V since water molecules decompose into oxygen and hydrogen at voltage above 1.23 V. But organic electrolyte has the operating voltage around 3.5 V, and ionic electrolyte has the wide stability window ranging from 3 to 6 V. Hence, choosing suitable electrolyte for the SCs can improve its operating potential window and thus increases the energy density of the device. Then, energy density is also directly proportional to its capacitance, so increasing the capacitance increases the energy density. In order to increase the overall cell capacitance, specific capacitance of the individual electrode has to be improved. Thus, the development of electrode materials for the SCs becomes the hot area of research work in energy storage system. The specific capacitance of the material C_s is [11]

$$C_s = \varepsilon\frac{A}{d} \ (Fg^{-1})$$

where ε is the permittivity of the free space and A and d are the surface area of the electrode and distance between two electrodes. Specific capacitance is directly proportional to the surface area of the electrode to hold the charge physically by electric double layer; thus, the nanomaterials which have increased surface area to volume ratio can be used as electrode materials for SCs. Furthermore, PCs also require high active sites for Faradic reaction (redox reaction) on the electrode surface, and thus, nanomaterials increase high

Table 2 Shortened characteristics of capacitors, supercapacitors, and batteries

Characteristics	Capacitor	Supercapacitor	Battery
Charge storage	Electrostatically (non-Faradic)	Electrostatically or electrochemically (Faradic) or both	Chemical reaction
Specific energy (Wh kg^{-1})	< 0.1	1–10	10–100
Specific power (W kg^{-1})	> > 10,000	500–1000	< 1000
Discharging time	10^{-6} to 10^{-3}	Sec to min	Min to hrs
Charging time	10^{-6} to 10^{-3}	Sec to min	1–5 h
Efficiency (%)	Almost 100	85–95	70–85
Cycle life	Infinite	> 500,000	Up to 1000
Cell voltage	6–800 V	2.3–2.7 V/Cell	1.2–12 V/Cell
Operating temperature	− 20 to 100 °C	− 60 to + 100 °C	− 20 to 65 °C

Comparison between batteries and supercapacitors [1]

active sites in the surface of the electrode. The supercapacitors are made of different nanomaterials as the electrodes such as carbon-based materials (activated carbon, carbon nanotubes, graphene, mesoporous carbon, etc.), metal oxides (ruthenium oxide, manganese oxide, nickel oxide, etc.), conducting polymers (polyaniline, polypyrrole, etc.), and their composite materials.

2 Electrode materials

The capacitance of the SCs depends on the specific surface area of the material, but they are not fully accessible when it comes in contact with the electrolyte used and the capacitance of the electrode materials also not linearly increased with increases in specific surface area. Along with surface area, pore size and pore-size distribution also play a prominent role in the capacitance of the SCs electrode. Largeot et al., in their experiments, show that when pore size of the electrode material is almost close to the size of the ions in the electrolyte yields the maximum double-layer capacitance [12]. Higher or smaller pore size decreases the capacitance of the materials. Thus, the capacitance is strongly depending on the electrochemically accessible surface area of the electrode.

2.1 Carbon materials

The carbon-based materials are mainly known for their specific surface area. Different carbon materials are used as electrodes for SCs. From the research work suggested by Conway et al., the carbon-based materials are used for the double-layer-type capacitor with three main unique properties such as (1) high specific surface area, (2) good inter- and intraparticle conductivity in pore matrices, and (3) good accessibility by electrolyte in the pores of the carbon materials [13]. These carbon materials mainly include activated carbons, carbon aerogels, carbon nanotubes, mesoporous carbon, and graphene.

Activated carbons are the first choice of the electrode materials for the EDLC-type capacitor. These are porous carbon materials with porous structure consists of micropores (less than 2 nm), mesopores (2–50 nm), and macropores (greater than 50 nm) to attain high specific surface area but has low electrical conductivity (1200–2500 S m^{-1}) [14]. An activated carbon electrode having a specific surface area of approximately 1000 m^2 g^{-1} has the capacitance of 100 F g^{-1} (100 μF cm^{-2}) [15]. Carbon aerogels are known to be one of the world's lightest material with high specific surface area (SSA) and density. It has low internal resistance, thus provides high power density [16]. Chien et al. developed carbon aerogels with a capacitance of 104 F cm^{-3} that yields an energy density of 90 Wh kg^{-1} and a power density of 20 Wh kg^{-1} [17]. Carbon nanotubes (CNTs) are produced by the physical process of decomposition of hydrocarbons that forms two types of CNTs based on precursors single-walled CNT and multi-walled CNTs. The SWCNTs have the high theoretical specific surface area (1315 m^2 g^{-1}), but MWCNTs have lower SSA [18]. Chen et al. developed 50-nm diameter SWCNT on graphitic foil, with good electrochemical stability and yields specific capacitance of 115.7 F g^{-1}. Emmenegger et al. produced well-aligned MWCNTs that grow on aluminum films with diameters ranging from 5 to 100 nm, producing a high volumetric capacitance of 120 F cm^{-3} [19]. Graphene is the one carbon atom thick sheet made up of sp^2 lattice in polyaromatic honeycomb crystal lattice. They are suitable for good performance energy storage devices due to their excellent physicochemical properties. The highlighted properties are large surface area, good chemical and thermal stability, wide potential window, and abundant surface functional group [20]. Stoller et al. reported that specific capacitance of the prepared graphene is 205 F g^{-1}, and its energy density is 28.5 Wh kg^{-1} [21]. The carbon-based material has many advantages such as high surface area, good chemical, and thermal stability, but the major limitation is electrochemically accessible surface area by the electrolyte in the electrode and low energy density due to the formation of electric double layer.

2.2 Metal oxides

The metal oxide–based electrode materials provide higher energy density than the carbon-based materials due to its charge storage mechanism. These materials store charge by electrochemical Faradic reaction between the electrode and electrolyte in the appropriate potential windows. Some unique properties are required for the metal oxides to be used as the electrode materials for the supercapacitors are as follows: (1) the metal can exist in two or more oxidation states, (2) the oxides should be electronically conductive, and (3) free movement of proton intercalation between oxide lattices [13]. Transition metal oxides are explored widely due to its high conductivity, chemical stability, and variable valence.

Apart from the various transition metal oxides, ruthenium oxide (RuO_2) is one of the most explored TMOs due to its high reversible faradic reaction (redox reaction), three distinct oxidation states by Ru, wide potential window (1.2 V), high specific capacitance, superior proton conductivity, better thermal stability, and long cycle life [22]. In acidic medium, fast reversible electron transfer and electron adsorption take place resulting in high specific capacitance. Zheng et al. reported that the amorphous RuO_2 in the sulfuric acid electrolyte (acidic medium) exhibits a maximum capacitance of 720 F g^{-1} [23]. The internal resistance of the RuO_2 is much lower than the other electrodes that yield

high power and energy densities, but the availability of the materials is fewer which causes higher cost and shows poor performance in higher current densities. Long et al. reported the hydrous ruthenium oxide (RuO_2 0.5 H_2O) that has a specific capacitance of approximately 900 F g^{-1} and high electrical conductivity [24]. Due to the environmental hazards and high cost of RuO_2 leads to the better replacement by manganese oxide (MnO_2). In comparison with RuO_2, MnO_2 shows relatively low cost, low toxicity, environment safety, and high theoretical capacitance almost equal to 1300 F g^{-1} (for RuO_2, 1358 F g^{-1}) [25]. Hu et al. reported several MnO_2 thin film–based systems that reach the specific capacitances of about 600 F g^{-1} in some aqueous electrolytes such as KCl, KOH, K_2SO_4, and Na_2SO_4 at the operating potential window of between 0.9 and 1.2 V [26]. Cobalt oxide (Co_3O_4) is another transition metal oxide and is also investigated due to its high theoretical capacitance of about 3560 F g^{-1}, better reversibility, and better electrochemical performance. Wang et al. investigated the 3D hollow cobalt oxide which yields the capacitance of around 820 F g^{-1} at 5 mV s^{-1}, and nanoporous Co_3O_4 prepared by solvothermal method yields an energy density of about 42.3 Wh kg^{-1} [27, 28]. Nickel oxide is also considered one of the prominent electrodes for the supercapacitors mainly for the alkaline electrolyte due to its high theoretical capacitance, low cost, and environmental friendliness. Yang et al. synthesized NiOO in cubic structure with various calcination temperatures; the maximum capacitance of the material yields around 700 F g^{-1} at 250 °C [29]. Vanadium oxide (V_2O_5) has also been investigated due to its wide potential window and its variation in oxidation state that yields fast redox reaction in bulk and surface of the vanadium material. Lee and Goodenough prepared the amorphous V_2O_5 by quenching the bulk vanadium pentoxide powders at 950 °C, yielding the maximum capacitance of 350 F g^{-1} in aqueous KCl electrolyte [30].

2.3 Conducting polymers

Conducting polymer–based electrodes are used for the supercapacitors due to its various properties such as low cost, flexibility, and low internal resistance and also have high potential densities, high porosity, and adjustable redox activity by the surface modification through various chemical processes. In conducting polymers, the charge storage takes place by faradic redox process, i.e., during the charging and discharging process, the movement of the ions occurs in the backbone of the polymer chain without any structural alternations. The conducting polymer SCs are classified into three types based on the p-doped polymer and n-doped polymer such as (1) type I (symmetric) p-p doped same polymer, (2) type II (asymmetric) p-p′ doped different polymer (e.g., polypyrrole/polythiophene), and (3) type III (symmetric) n-p doped polymers. Among these types, type III is considered the advanced conducting polymer supercapacitors based on their design and their energy storage mechanism [31, 32]. The conducting polymers in supercapacitors are polyaniline, polypyrrole, polythiophene, and PEDOT. Polyaniline (PANI) is the lightweight polymer and has high conductivity, low cost, and mechanical stability and possess high theoretical capacitance used as the electrode materials for the SCs. Lie et al. investigated PANI in pure form as the electrode materials and yields a capacitance of 815 F g^{-1} [33]. Polypyrrole (PPY) is also a conducting polymer mainly known for its simple preparation method, p-doped valence, high conductivity, and stability. It also has greater density and higher flexibility than the other conducting polymer electrodes. Kim et al. studied the polymer-based electrodes with carbon materials by developing polypyrrole with carbon fiber yields the specific capacitance of about 600 F g^{-1} at the scan rates of 30 mV s^{-1} [34]. Polythiophene and its derivatives are both p- and n-doped polymers that can be prepared by chemical oxidative polymerization. Zhou et al. reported that the polythiophene prepared from Triton X-100 shows a maximum capacitance of 117 F g^{-1} [35]. The main limitation of using polymers based supercapacitors as the electrode is the swelling and shrinkage of the polymer electrode while continuing for long life cycle.

2.4 Transition metal chalcogenides

The main criteria for the electrode material selections are multiple oxidation states, superior conductivity, and electrochemically active. Even though conducting polymers, metal oxides, and carbon-based materials exhibit these key characteristics, their applications are limited. For example, conducting polymers are inexpensive and environmentally friendly but have limited operation across the potential window, and swelling and shrinkage of the electrode leads to the need for alternative measures in supercapacitor. Metal oxides have a high energy density, but electrochemical instability and surface deformation lead to further applications [10]. Transition metals have various advantages such as multiple oxidation state and good pseudocapacitive behavior, and they received great attention due to their anisotropic properties. These transition metals with chalcogenides (S, Se, Te) have gained attention in past decades due to their high specific power, stability, and life cycle and offer better tolerance in environmental safety measures than the other energy storage devices in electronic devices and in EMV [36]. TMCs have application of the various fields such as in energy harvesting (solar cells, fuel cells), energy storages (batteries, supercapacitors), electronics (LED, sensors), and memory-based devices due to their excellent properties such as flexibility, additional reactive sites for catalysis and redox reaction, improved conductivity by reduction

of internal resistance, low mean path, and quantum effect [37, 38]. Generally, Chalcogenide-based materials have improved electrochemical performance with high electrical conductivity and stability; selenide-based materials are a new class of electrode material with rich redox chemistry, superior electrical conductivity and stability. Chalcogenide-based research is highly concentrated in SC-based devices because of these improved applications. Compared with sulfide and selenides, telluride with transition metals are rarely reported, since in periodic table, telluride is placed in the same group of chalcogenides between metal and non-metals, then it possess some unique properties such as good conductivity and better stability like the other chalcogenides that are reported [39].

Transition metal chalcogenides are appealing for a variety of applications, including energy conversion and storage, due to their changing band gaps, distinctive stoichiometry, tunable structure, and materials. Due to their benefits of high theoretical capacitance, transition metal chalcogenides are anticipated to meet the high energy storage requirements of supercapacitors. The most remarkable feature of metal chalcogenides is their changeable active sites, which are made possible by their rich component and electronic structure and make them suitable materials for the creation of extremely effective electrodes for supercapacitors. The low symmetry anisotropic (1D and 2D) transition metal chalcogenides (TMCs) have attracted a lot of attention due to their novel electrical and catalytic properties, which have applications in electrochemical energy storage, chemical sensing, and next-generation optoelectronics. Metal tellurides, metal selenides, and metal sulfides have demonstrated exceptional cycle stability and high power density and have been used in supercapacitor applications. In an electrochemical energy storage system, the electrochemical performance of electrodes is influenced by their morphology, chemical content, synthesis method, and crystalline structure. The most often reported crystal structures in electrochemical energy storage applications are layer and spinel structures. At the same time, the disadvantage of TMCs as supercapacitors regarding low energy density has been identified as a significant challenge in the furtherance of supercapacitor technologies. It also has limited synthesis strategies and low stability, which lowers the performance of supercapacitors. The development of high-performance electrode materials is one of the most involved strategies for overcoming the problem of low energy density. Based on the researchers report on the transition metal chalcogenides, herein, we have detailed the use of transition metal chalcogenides as the electrode material for the supercapacitors.

3 Synthesis methods

3.1 Co-precipitation method

Co-precipitation is a technique for making multi-component oxides by precipitating intermediate chemicals like oxalates or hydroxides. If the reaction is well controlled, dopants can also be added to the mixed oxides. This technology has been shown to be useful for the synthesis of advanced energy materials such as cathodes in rechargeable M-ion batteries and solid fossil fuels. The washing and drying of the hydroxide or oxalate intermediate chemical cause little difficulty in generating nanoparticles by co-precipitation. It is possible to create high-quality nanomaterials via co-precipitation techniques.

3.2 Sol–gel method

The wet chemical approach of sol–gel synthesis of metal oxides is widely utilized to make materials for coatings, optical, energy, catalysis, separation (chromatography), electronics, and sensors. A typical sol–gel approach starts with the addition of a metal salt or metal alkoxide to water (elevated temperature or catalyst may also be used), which then undergoes a hydrolyzed reaction to produce a metal hydroxide colloid or nanoparticles. After the precursor has been hydrolyzed to the required quantity, a suspension is created by adding a stabilizing agent, such as nitric acid. A sol or stable suspension of hydroxide nanoparticles is obtained at this moment. One of the most significant advantages of sol–gel procedure is that the sol can be employed in a variety of processes to create a film of material, including dip coating, spin coating, drop position, aerosol processing, coating, and many more. After the solution has been deposited and the water has been removed during drying, a stiff gel will form. The pace of gelation determines the particle size and porosity of the finished material; therefore, it is a crucial processing step. The gel is an amorphous substance that can be burned to convert it into the final oxide layer once it has dried (Fig. 1). Sol–gel process can be used to make a wide range of oxide nanoparticles, including Al_2O_3, Fe_2O_3, NiO, SnO_2, TiO_2, WO_3, ZnO, ZrO_2, and $BaTiO_3$. Many of these pure oxides can be employed as the active element in gas sensors, and various investigations have been conducted in this sector using the sol–gel process. Sol–gel processes can be used to introduce dopants to materials with fine stoichiometry control. Sol–gel produced antimony-doped SnO_2 and niobium-doped TiO_2 which are two specific instances in gas sensing research. These are only a few examples of the current interest in sol–gel method as a means of

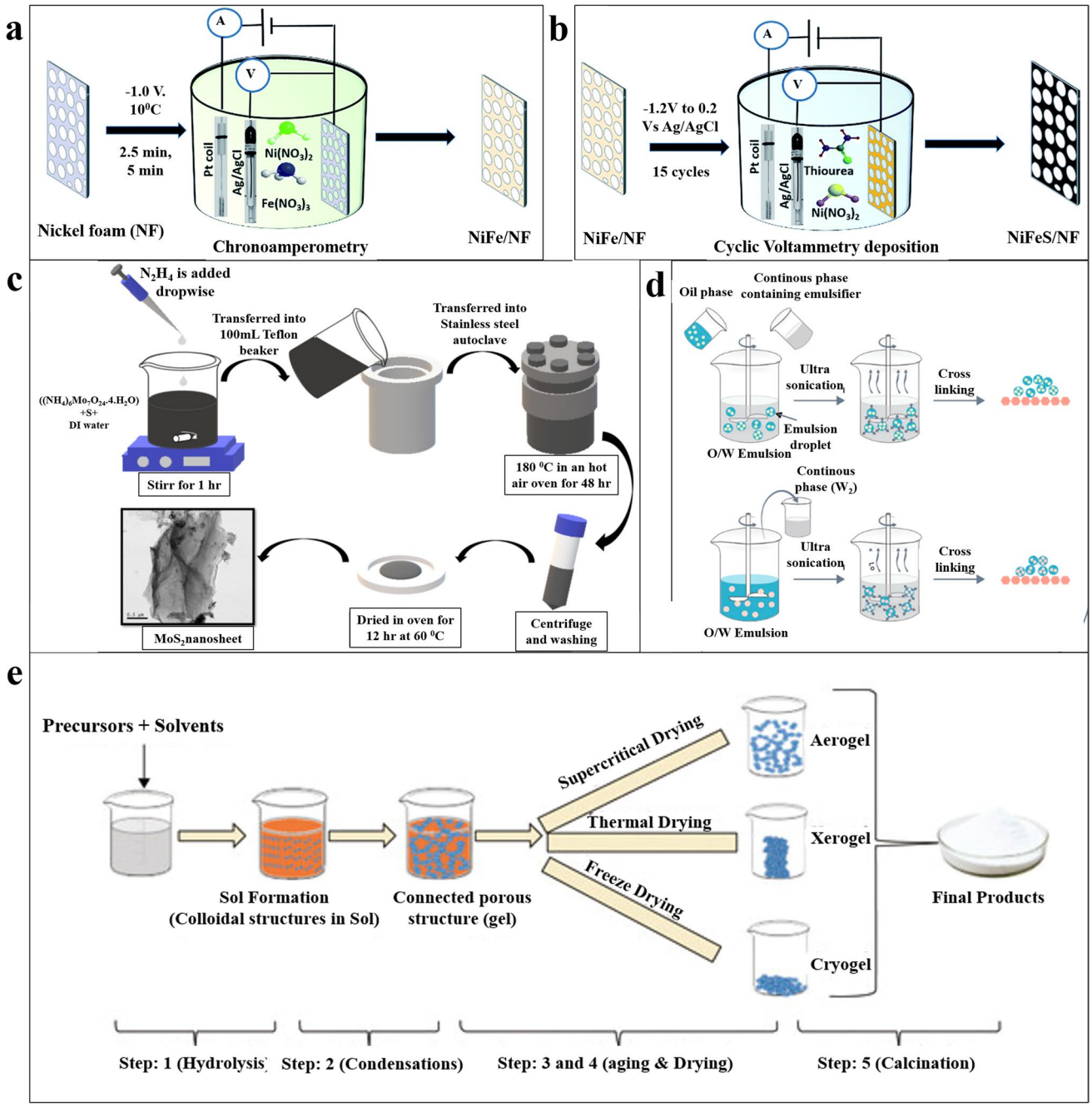

Fig. 1 Schematic representation of synthesis of nanoparticles. a, b Electrodeposition method image is reproduced with permission from ref. [40] under Creative Commons Attribution-Non Commercial 3.0 Unported License by Royal Society of Chemistry. c Hydrothermal method image is reproduced with permission from ref. [41] under Copyright © 2020 Elsevier B.V. d Emulsion method image is reproduced with permission from ref. [42] under Creative Commons Attribution License CC BY, Copyright © 2020 by MDPI. e Sol–gel method image is reproduced with permission from ref. [43] under Creative Commons Attribution License CC BY, Copyright © 2021 Bokov et al.

producing high-performance oxide nanoparticles. Sol–gel technique for producing oxide nanoparticles has various advantages, including a vast number of precursors accessible, which allows reactions to be customized to create an almost infinite variety of specially doped materials to meet the specific application. Particle size control is achieved by carefully controlling the reaction condition. The initial step in the sol–gel method is to establish a stable suspension, which offers a lot of benefits for depositing materials on microsensors.

3.3 Hydrothermal synthesis

Many of the mechanisms were first clarified for mineral systems by Morey, who coined the term hydrothermal. When it comes to ceramic nanomaterial processing, hydrothermal synthesis is described as an aqueous chemical reaction in a sealed container at a temperature that generates an elevated pressure on its own. The synthesis of completely crystalline nanoparticles can be achieved at low temperatures, between 100 and 374 °C, which are the boiling and critical points for water, respectively. Hydrothermal processing has several advantages, including high purity (> 99.5%) and chemical homogeneity, small particle size (up to 5 nm), narrow particle size distribution, single-step processing, low energy consumption, quick reaction time, low-cost equipment, and the ability to generate metastable compounds, and, most importantly, no calcination is required for many materials because they are fully crystallized by the reaction. One of the reasons oxide nanostructures created using hydrothermal synthesis has increased in popularity over the last decade is the fact that nanomaterials including one-, two-, and three-dimensional structures can be synthesized to a fully crystalline state (Fig. 1).

3.4 Solvothermal method

Solvothermal synthesis is analogue to hydrothermal synthesis, but instead of water, it uses organic solvents. It provides various advantages over other approaches. First, solvothermal conditions allow for fast solution convection. The mild environment allows for the careful control of nanoparticle size, shape distribution, and crystallinity, as well as the formation of crystals with few lattice defects. Second, the low boiling point of the organic solvent involved can result in a larger reaction pressure when carried out at high temperatures, which aids in the crystallization process. Third, the mild temperature allows specific structural properties of precursors to be transmitted into products, allowing for product morphology control. Solvents can also give functional groups, which can be used to synthesis new materials by reacting with the precursors or products. Finally, solvothermal synthesis can limit the release of hazardous vapor during some reaction systems, such as those involving toxic starting ingredients. The sealed system not only helps with "green chemistry," but it also effectively lowers the risk of oxidation and contamination from the atmosphere or oxygen, which is critical for high-purity products. As a result, the solvothermal approach was investigated as a convenient route for synthesizing $CulnS_2$, $AglnS_2$, and CulnSe2 nanoparticles from single-source precursors in order to control the size and shape of nanoparticles. One-step solvothermal synthesis can be used to generate nanoparticles directly through singe molecules of relative precursors acting as building blocks.

3.5 Emulsion synthesis

Microemulsion processing is a crucial synthetic technology because it may produce oxide nanoparticles, whereas large-scale emulsion processing produces particles in the order of micrometers. Microemulsions are optically transparent dispersions of two immiscible liquids, such as water and oil, that are thermodynamically stable. Surfactant mixtures are used to lower the interfacial tension to near zero (less than 0.001 mN m^{-1} in some situations), allowing the two phases to disperse spontaneously by thermal motion. Domain sizes in equilibrium water (assuming a water-in-oil microemulsion) range from 10 to 100 nm, depending on the surfactant type and concentration. The nucleation, nanoparticle formation, intermediate growth (for colloids), and eventual coagulation and flocculation of colloidal and nanoparticles are a complicated process that includes relationships between nucleation, nanoparticle formation, intermediate growth (for colloids), and eventual coagulation and flocculation. All these variables are influenced by the interactions of molecular species in the microemulsion. The presence of surfactant film acting as stabilizer for the oxide particles allows for successful microemulsion synthesis of oxide materials because particle nucleation occurs simultaneously in a large number of micelles (spherical water droplets stabilized by surfactants in the oil medium) with well-isolated nucleation sites. The sizes of the colloids or nanoparticles generated are directly determined by the sizes of these emulsified droplets. Surfactant-stabilized water micelles act as nano-sized reactors for executing synthetic processes. Only when the nucleation and growth stages are tightly segregated do monodispersed particles emerge (one of the advantages of microemulsion synthesis). Controlling the molar ratio of water to surfactant allows the size of emulsified water droplets to be adjusted, making it possible to regulate the size of oxide nanoparticles generated using this process. The microemulsion synthesis process provides excellent dispersion, small particle size distribution, and shape control, making it a very appealing method for oxide nanoparticle creation (Fig. 1). According to Shi and Verweij, one component of microemulsion preparation that must be considered is particle purification following synthesis. Their findings revealed that non-agglomerated nanoparticles with diameters smaller than 5 nm could be created and that homogenous coatings could be made after thorough cleaning method. Microemulsion processing has been used to make SnO_2 nanoparticles in the size range of 3–5 nm, but no sensing data with materials made this way is available.

3.6 Electrodeposition method

Electrodeposition is a process of transfer of electrons to the ions in a solution; a thin layer of one metal is deposited

on top of a thin layer of another metal to adjust its surface properties. This bottom-up fabrication method is adaptable and can be used for a broad range of applications. Due to its capacity to fabricate one-dimensional nanostructures such as nanoribbons, nanorods, nanowires, and nanotubes, electrodeposition has gained prominence in recent years.

4 Single metal chalcogenides and its composites

4.1 Cadmium chalcogenides

Cadmium sulfide (CdS) is broadly studied ultracapacitive TMSs because it possesses variable sulfide states which help fast and successive redox reactions. It is an n-type semiconductor with a narrow band gap of approximately 2.4 eV. It has advantages like high discharge rates, excellent morphology with high surface area, high energy density, and virtuous environmental stability with long cycle life. Also, cadmium has a very little toxicity in nature. Various groups reported the use of CdS as electrodes in the application of energy storage devices. For the first time, Xu and his co-workers reported CdS on nickel foam as electrodes with a gravimetric capacitance of 909 F g^{-1}. Oloore et al. developed CdS QDs and organohalide perovskite-based bilayer electrodes through facile and inexpensive solution process coating for the use of symmetric electrochemical capacitors [44]. Finally, he showed that the supercapacitors developed with cadmium sulfide with methyl ammonium bismuth iodide (MAPI3) electrodes displayed the highest areal capacitance of 141 μF cm^{-2} and power density of 12.7 mW cm^{-2} and energy density of 23.8 mWh cm^{-2} with stability retention of 87% after 4000 cycles.

Chen et al. prepared CdS NPs anchored 3D graphite cage for supercapacitor study [45]. As a result, the 3D CdS/graphite cage displayed a better specific capacitance of 511 F g^{-1} at 5 A g^{-1}. Also, he prepared a 3D CdS/graphite/rGO asymmetric supercapacitor with an energy density of 30.4 Wh kg^{-1} at a power density of 800 W kg^{-1} with cycling stability of 90.1% after 5000 cycles at 10 A g^{-1}. Patil et al. synthesized Ag NWs@CdS core–shell nanostructured electrodes and showed the areal capacitance of ~ 2662 mF. cm^{-2} at 10 mV s^{-1} and 810 mF. cm^{-2} at 45 mA [46]. Later, Patil et al. synthesized core–shell nanostructures of Co_3O_4@CdS on a nickel foam using a one-pot hydrothermal method and SILAR method [47]. The core–shell Co_3O_4@CdS electrode-based symmetric supercapacitor showed a better specific capacitance of 360 F g^{-1} and 99 F g^{-1} at 10 mV s^{-1} with stability retention of 92% after 2000 cycles. He et al. suggested that G-CdS nanocomposite through a one-pot solvothermal process and displayed high electrochemical behavior with excellent stability [48]. Wang et al. synthesized hierarchical Ni_3S_2@CdS core–shell nanostructures on nickel foam using the hydrothermal method for the first time [49]. Ni_3S_2@CdS core–shell nanostructure electrode-based asymmetric supercapacitors exhibit an excellent energy density of 127.5 Wh kg^{-1} at 2 mA. cm^{-2} with cycling stability of 130% after 4000 charge–discharge cycles at 6 mA. cm^{-2}. Based on this, Safdar et al. enhanced the capacitive performance of electrochemical capacitors by developing Ni_3S_2/CdS through hydrothermal method followed by successive ionic layer adsorption and reaction deposition (SILAR) techniques [50]. They showed a specific capacity of 545.6 C g^{-1} at 1 A g^{-1} with excellent stability of 103% after 5000 charge–discharge cycles at 5 A g^{-1}. Also, recently, mixed metal oxide–based materials like Mn/Fr oxides, Ni/Mn oxides, and Mn/Ni/Co oxide have explored high enhancement in the performance of electrochemical devices. Based on this concern, De Adhikari et al. synthesized a mixed system of CdS-$CoFe_2O_4$@rGO nanohybrid through a simple hydrothermal method for high-performance supercapacitors, which exhibits a high specific capacitance of 1487 F g^{-1} at 5 A g^{-1} current density with good capacitance retention of 78% even after 5000 cycles.

Related to sulfides, selenides could be potentially better candidates, as selenium displays more metallicity with higher electronic conductivity (1×10^{-3} S m^{-1}). During the pseudocapacitive reaction, selenides retain better cycling stability without the formation of polyselenide intermediates. Though selenides have good electrochemical properties, preparing selenides with better rate performance and higher specific capacity is still a challenge. To overcome these obstacles, Zhai et al. proposed a system of mixed metal selenide (Co_9Se_8/CdSe) on nickel foam via selenization method and developed a cell (Fig. 2). He stated that the developed cell shows excellent power density and energy (57.6 Wh kg^{-1} at 10.9 kW kg^{-1} or 68.0 Wh kg^{-1} at 1.20 kW kg^{-1}) with better cycling stability of 80.9% after 1000 cycles at 2 A g^{-1}.

Cadmium selenide belongs to the II–VI group compound semiconductor, and it is extensively used in the application of optoelectronics, solar cells, light-emitting diodes, laser diodes, etc. For the first time, Bae et al. reported on semiconducting CdSe QDs as electrodes on electrochemical capacitors. In this study, they used a complex hot injection method to prepare CdSe QDs [52]. Following this, Pawar et al. prepared CdSe electrodes through the chemical bath deposition method with various reaction times for the application of electrochemical supercapacitors [53]. He reported that CdSe deposited at a reaction time of 8 h exhibited superior supercapacitive performance with an excellent areal capacitance and energy density of 1.285 mF. cm^{-2} and 4.015 Wh kg^{-1}.

Cadmium telluride (CdTe) belongs to the II–VI semiconducting periodic table with a direct band gap of 1.47 eV under room temperature. It is an appropriate material for the application of photovoltaics because of its high absorption coefficient property. However, it is a single crystal with a

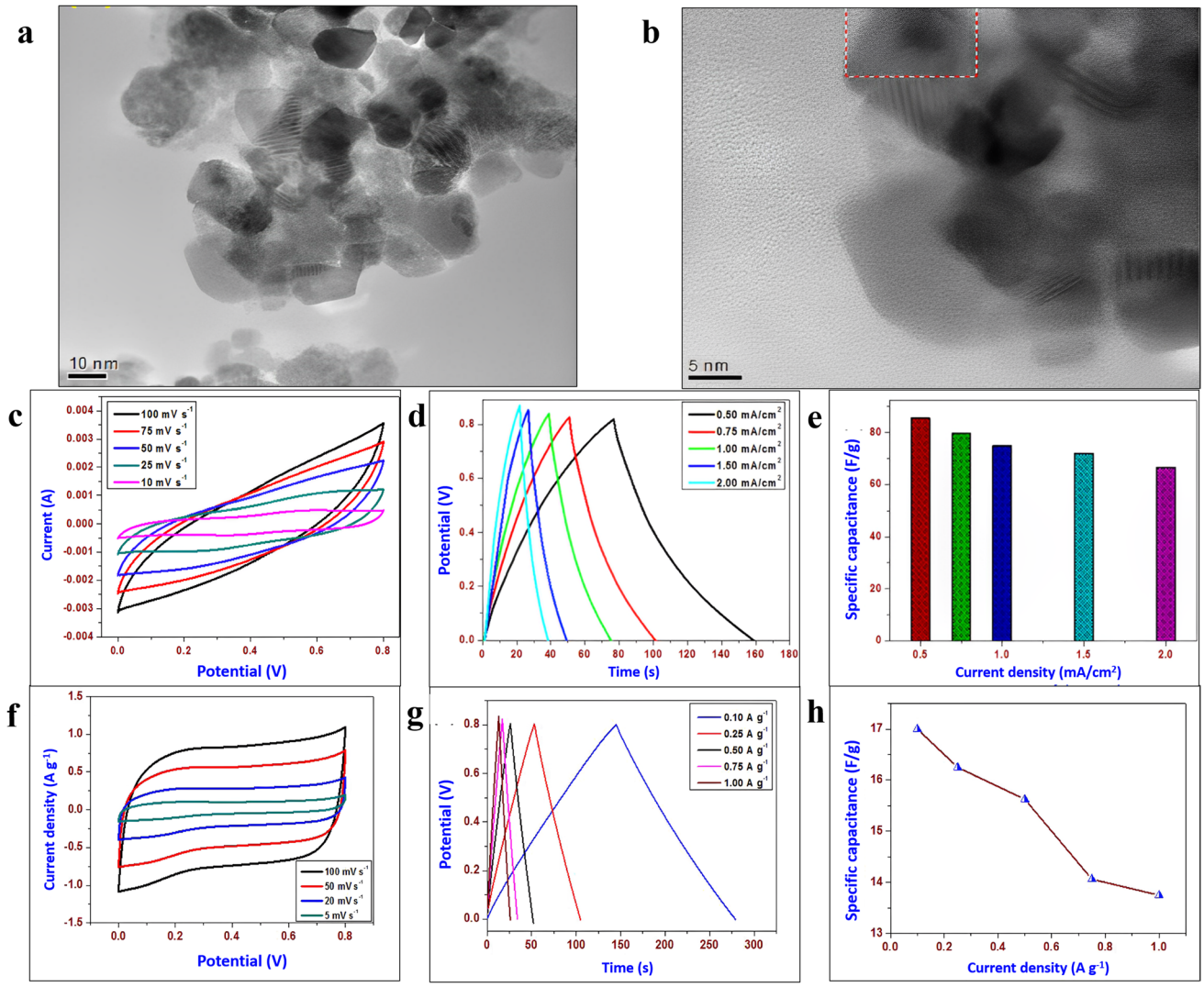

Fig. 2 **a**, **b** High resolution transmission electron micrographs of RuS_2 nanoparticles **c–e** 3-cell electrochemical performance of RuS_2 in 0.5 M H_2SO_4 electrolyte. **f–h** Electrochemical performance of RuS_2 symmetric cell supercapacitors, image is reproduced with permission from ref [51] under Copyright © 2016 Elsevier Ltd

zinc blende structure, but it also exists in the wurtzite and hexagonal structure. Even though the preparations of CdTe are well studied, most of the study compacts with the optical and structural characterization. Concerned by the excellent potential and properties of CdTe NRs, Manikandan et al. made an effort to know its electrochemical behavior and its role in energy storage devices. In this study, he proposed that the prepared CdTe NRs offers an outstanding specific capacitance performance of 438 F g^{-1} at 2 mA. cm^{-2} over the other CdTe-based supercapacitors [54].

4.2 Mercury chalcogenides

Mercury sulfide (HgS) is a binary compound belonging to II and VI group elements with an optical band gap between 1.9 and 2.6 eV. Due to its band gap property, mercury sulfides show its auspicious applications in catalysts, IR detectors, photoconductors, photo-electrochemical cells, solid-state solar cells, etc. Various methods such as hydrothermal microwave-assisted and wet chemical route are used to synthesis HgS nanostructures with various structural morphologies like nanoparticles, dendrite-form, star-shape, rod-like structures. HgS has explored several applications like electrostatic imaging, ultrasonic transducing, image sensors, and photoelectric conversion devices. Though HgS has excellent characteristics, more consideration has not been paid yet towards energy storage uses. For the first time, Pande et al. synthesized HgS with cauliflower-like surface architecture by using the SILAR method under room temperature for the application of supercapacitors [55]. HgS electrode-based

capacitor exhibits a maximum specific capacitance and energy density of 446 F g^{-1} at 2 mV s^{-1} and 15.45 Wh kg^{-1}. Also, Pande et al. synthesized mercury sulfide/MWCNT nanocomposite through a "dip and dry" process followed by successive ionic layer adsorption and reaction method [56]. This nanocomposite exhibits a higher specific capacitance of 946.43 F g^{-1} at the scan rate of 2 mV s^{-1} with excellent cycling stability of 93% even after 4000 charge–discharge cycles. Also, HgS/MWCNT nanocomposite-based electrodes possess high specific energy and power densities of 42.97 Wh kg^{-1} and 1.60 kW kg^{-1}. This shows that HgS-based materials have a decent application in the domain of energy storage devices for the future scope.

4.3 Ruthenium chalcogenides

A ruthenium semiconducting compound is one of the most promising TMCs with excellent technological uses such as fuel cells and water splitting. It has a narrow band gap of 1.85 eV with superior stability towards photoelectrolysis of water under visible light. Because of its multiple valence states and rich redox chemistry, ruthenium-based material is recognized as the remarkable electrochemical properties. Ruthenium-based materials like metallic ruthenium, Ru complexes, amorphous and crystalline RuO_2, and hydrous RuO_2 are investigated for several electrochemical applications such as electrocatalysis, sensors, batteries, and supercapacitors. Although studies on energy storage of TMCs are rapidly increasing and ongoing, the effectiveness of RuS_2 as an electrode for energy storage devices is not examined yet. On the other hand, ruthenium disulfide (RuS_2) is proven to be an excellent catalyst material compared to MoS_2. Thus, for the first time, Krishnamoorthy et al. demonstrated the preparation of cubic RuS_2 NPs through the sonochemical method and used as an electrode for the application of electrochemical supercapacitors [51]. The prepared cubic RuS_2 NP-based electrode delivered an excellent specific capacitance of 85 F g^{-1} at 0.5 mA. cm^{-12} with retention stability of 96.15% capacitance over 5000 cycles (Fig. 2).

Bolagam et al. synthesized RuS_2/TRGO composite through the hydrothermal method which delivers a specific capacitance of 193 F g^{-1} at 5 mV s^{-1} with excellent cyclic stability and rate performance. But so far, there is still no report on the use of ruthenium disulfide ($RuSe_2$) as the electrode material for the use of supercapacitors. Thus, Yun et al. prepared crystalline $RuSe_2$ nanoparticles through the hydrothermal method followed by thermal treatment at 650 °C under an argon atmosphere (shown in Fig. 2) [57]. For the first time, the prepared crystalline $RuSe_2$ NPs were utilized as a pseudocapacitive supercapacitor electrode for which it showed a specific capacitance of 100.8 F g^{-1} at 0.2 A g^{-1} with superior cycle stability and excellent rate performance.

4.4 Silver chalcogenides

Mo et al. synthesized graphene sheets/Ag_2S composite through a facile solvothermal method [58]. The electrochemical performance of graphene sheets/Ag_2S was carried out on a modified glassy carbon electrode in a three-electrode cell. Gs-Ag_2S showed an enhanced specific capacitance of 1063 F g^{-1} and could be employed as better supercapacitor materials for future electronic devices. Carbon allotropes such as activated carbons, single- and multi-walled carbon nanotubes, graphene, and fullerenes have been investigated thoroughly due to their moderate specific capacitance and long cycle stability. Hybrid materials showed enhanced physical and chemical properties with excellent mechanical flexibility and conductivity. But they have some limitations such as expensive and time-consuming synthesis process, high contact resistance at the interface of electrode/current collector, and low power density. Therefore, an effort has been developed in adding new materials which can be carbon-free and synthesized easily. Based on this, Nair et al. synthesized Cds/Ag_2S through the cation exchange process for the application of supercapacitors [59]. They used toxic cadmium ions in the initial synthesis but obtained Ag_2S nanowires and showed the highest specific capacitance of 268.4 F g^{-1} at 1.5 mA. cm^{-2} in a 1.5 M NaOH electrolyte. Pawar et al. used a facile, low-cost, successive ionic layer adsorption and reaction (SILAR) method for the preparation of Cu_2S-Ag_2S composite electrode on nickel foam [60]. The prepared electrodes showed a high specific capacity of 772 C/g at a scan rate of 10 mV s^{-1} than the individual electrodes with a capacity retention of 89% after 2000 cycles (Fig. 3).

4.5 Tantalum chalcogenides

Till now, various TMDs have been studied extensively. Especially, tantalum diselenide ($TaSe_2$), as a metallic nature with a layered low dimension electric conductor, has been studied for its charge density wave property, field emission, phonon, thermal property, and superconductivity. Depending on the coordination of tantalum atoms, there are various polymorphic forms for tantalum diselenide crystal. They are 1 T (T, trigonal), 2H (H, hexagonal), and 3R (R, rhombohedral) polytypes. In the past few decades, polymorphism in tantalum diselenide leads to various physical properties like the metallic property of 2H and semiconducting behavior for 1 T and 3R polytypes. Up to date, there were no reports about the direct preparation of $TaSe_2$ nanobelts. For the first time, Wang et al. synthesized a 3D conductive quasi-array based on 2H-$TaSe_2$ nanobelts directly on a tantalum foil through one-step surface-assisted chemical vapor transport technique [61]. Also, they used conductive quasi-array-based 2H-$TaSe_2$ as a substrate for the in situ electrodeposition of polypyrrole to form cylinder-like composite nanostructures

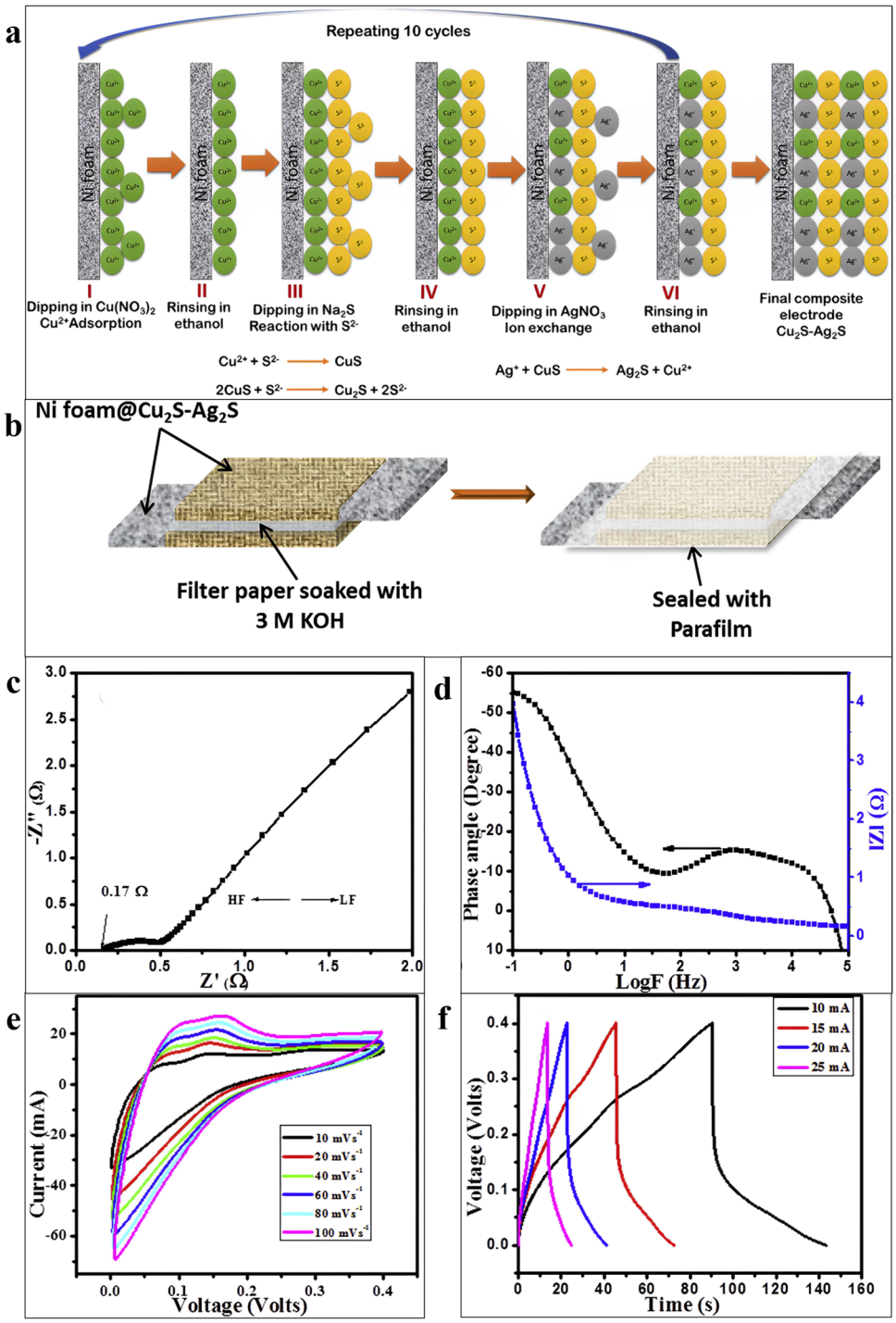

Fig. 3 **a** Schematic diagram of the different stages in the SILAR process for Cu_2S-AgS composite electrode. **b** Schematic illustration of the fabrication of symmetric supercapacitor device. **c–f** Electrochemical studies of symmetric Cu_2S-Ag_2S supercapacitor electrode, image is reproduced with permission from ref [60] under Copyright © 2017 Elsevier Ltd

and developed a symmetric supercapacitor from the composite. It showed a high areal capacitance of 835 mF.cm^{-2} at 2 mV s^{-1} with excellent initial capacitance maintained at 98.7% even after 10,000 cycles.

Other than sulfides and selenides, telluride-based materials have not prepared widely due to its deficiency of phase diagrams and high melting points. This type of crystals exists due to the interaction of ionic, metallic, and covalent bonds. Especially, quite low electronegative nature of tellurium in transition metal tellurides commonly leads to complex opposition between metals and non-metals for the electrons and, as significant, to valence electron localization. It is quite interesting to note that tantalum telluride ($TaTe_2$) has been studied to have a distorted 1 T structural property with a space group of C2/m. Generally, Te-based materials have remained unexplored practically. But in the

past decades, the thermoelectric and electronic properties of this $TaTe_2$ were studied. For the first time, Chakravarty et al. make an effort to prepare $TaTe_2$ nanosheets through a simple microwave-assisted method and employed for the use of supercapacitors [62]. They stated that the supercapacitor developed with $TaTe_2$ nanosheets as anode and platinum as cathode exhibits a coulombic efficiency of 95%, while the cycle-to-cycle decrease in capacity was less than 5% and also, the maximum discharging or charging capacity was less than 2.4 mV s^{-1} which is desirable for the characteristic behavior of supercapacitor.

4.6 Titanium chalcogenides

Titanium chalcogenides are one of the most important TMDCs, which have sizable band gaps, so these materials are used for the application of electronic and optoelectronic components. Titanium-based chalcogenides belong to IV or V group elements of the periodic table with a narrow band gap. Especially, titanium disulfide (TiS_2) is the layered structures like molybdenum and tungsten with the form of S-Ti-S unit structure, whereas the sulfur atoms in two hexagonal planes are separated by a plane of Ti atoms. The bond between Ti and S is the covalent bond of interactions, whereas the adjacent S-Ti-S layers are bonded through weak Van der Waals force of interactions. Various methods such as hydrothermal method, chemical vapor deposition (CVD) technique, solid assisted reaction, and physical ablation were employed for the preparation of TiS_2. But the electrochemical performance of TiS_2 was not reported widely. Parvaz et al. prepared TiS_2 nanodiscs through solid-state reaction (SSR) method and studied their electrochemical behavior for supercapacitor applications [63]. The observed results indicate the possibility of TiS_2 as a better electrode material for the application of supercapacitor.

4.7 Zinc chalcogenides

Like other metal oxides, nanostructured metal sulfides have received more attention towards researchers and exposed approachable pseudocapacitive performance. The two or more valence states present in the sulfide and better theoretical capacity of sulfur deliver good characteristic behavior of the capacitor. Among various metal sulfides, zinc sulfide (ZnS) is a significant II–VI semiconductor material with a wide band gap of 3.5–3.8 eV and two possible crystal structures, namely, sphalerite and wurtzite. Much application has been proposed with ZnS nanomaterials like electronics, optoelectronics, photovoltaics, and energy storage devices. Jayalakshmi et al. studied the performance of the capacitor of ZnS nanoparticles in various electrolytes. Recent studies demonstrated that the usage of carbon-based materials like CNTs and graphene into ZnS NP has decreased the band gap and could be applied for several applications including energy storage devices. Based on this, Ramachandran et al. prepared ZnS-decorated graphene nanocomposites through the facile solvothermal method and used as an electrode to examine their electrochemical behavior in 6 M KOH electrolyte towards supercapacitor applications [64]. This nanocomposite electrode achieved a specific capacitance of 197.1 F g^{-1} at 5 mV s^{-1} with initial capacitance maintained at 94.1% after 1000 cycles. Similarly, Hou et al. prepared CNT-decorated hierarchical ultrathin ZnS nanosheets through the facile method as an electrode for supercapacitor applications [65]. The results revealed that the ZnS@CNT electrode-based flexible all-solid-state supercapacitor obtained the specific capacitance of 159.6 F g^{-1} with long cycling stability. Iqbal et al. deposited ZnS nanoweb onto the Ni foam having predeposited graphene oxide thin layer through the hydrothermal method [66]. This electrode holds an excellent specific capacitance of 3052 F g^{-1} at a scan rate of 2 mV s^{-1}. According to the galvanostatic charge–discharge profile, the specific capacitance is calculated to be 2400.3 F g^{-1} at 3 mA. cm^{-2}. The power and energy densities obtained for GO-supported ZnS nanoweb is 4407.73 W kg^{-1} and 120 Wh kg^{-1}, respectively. Javed et al. grow ZnS nanospheres on a flexible carbon textile (CT) using the hydrothermal method [67]. The ZnS-CT-based electrode possesses a specific capacitance of 747 F g^{-1} at 5 mV s^{-1} and directly applied as a binder-free electrode for the fabrication of symmetric flexible full solid-state supercapacitor. The ZnS-CT-based supercapacitor delivers a better capacitive behavior with a maximum areal capacitance of 56.25 F cm^{-2}, C_{sp} of 540 F g^{-1} at 5 mV s^{-1} with initial capacitance maintained at 94.6% even after 5000 cycles.

However, ZnS-based electrode material still experiences a low operating voltage, energy density, and specific capacitance for practical commercial uses. To rectify these drawbacks, an effective methodology is to fabricate composites of zinc sulfides with an excellent metal-based pseudocapacitive material. Based on this concern, Sabari Arul et al. have attempted to fabricate ZnS/MnS nanocomposite-based symmetric supercapacitor device with high specific energy and power densities and long cycle stability [68]. The results revealed that ZnS/MnS nanocomposite-based electrode achieved a specific capacitance of 884 F g^{-1} at 2 mV s^{-1} (Fig. 4). Finally, the utmost energy and power densities of ZnS/MnS NC-based symmetric supercapacitor are 91 Wh kg^{-1} and 7.78 kW kg^{-1} with long cycling stability after 5000 cycles. Li et al. synthesized a novel cactus-like ZnS/Ni_3S_2 nanohybrid for the first time through a facile two-step hydrothermal method as an electrode material for high-performance asymmetric supercapacitor [69]. It delivered a high specific capacitance of 2093 F g^{-1} at 1 A g^{-1} with excellent initial capacitance maintained even at higher current density (72% at 10 A g^{-1}). The asymmetric supercapacitor assembled with ZnS/Ni_3S_2 electrode exhibits high

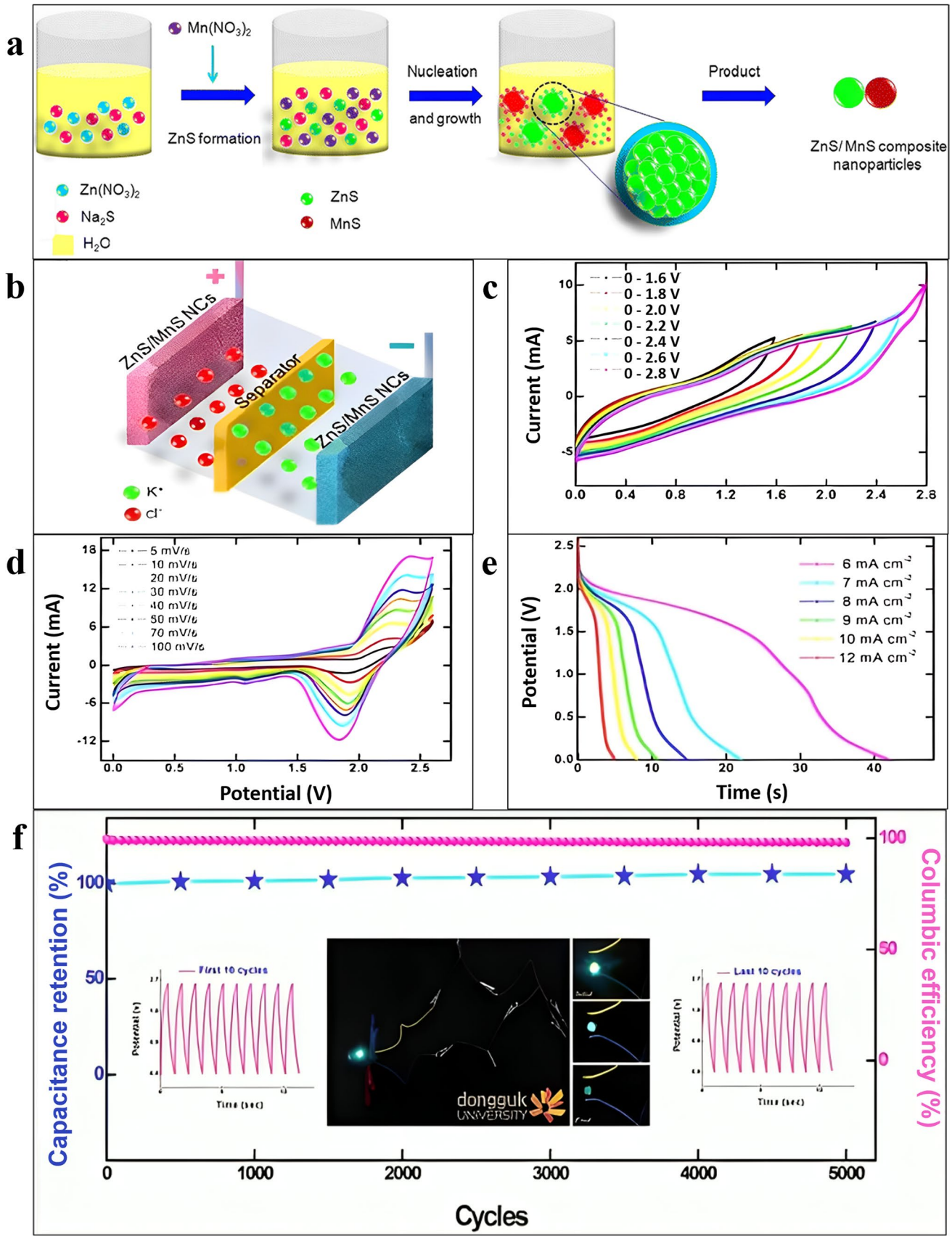
a
Mn(NO3)2
ZnS formation
Nucleation
and growth
Product
ZnS/ MnS composite
nanoparticles
Zn(NO3)2
Na2S
H2O
ZnS
MnS
b
ZnS/MnS NCs
Separator
ZnS/MnS NCs
K+
Cl-
c
0 - 1.6 V
0 - 1.8 V
0 - 2.0 V
0 - 2.2 V
0 - 2.4 V
0 - 2.6 V
0 - 2.8 V
Current (mA)
d
5 mV/s
10 mV/s
20 mV/s
30 mV/s
40 mV/s
50 mV/s
70 mV/s
100 mV/s
Current (mA)
Potential (V)
e
6 mA cm-2
7 mA cm-2
8 mA cm-2
9 mA cm-2
10 mA cm-2
12 mA cm-2
Potential (V)
Time (s)
f
Capacitance retention (%)
Columbic efficiency (%)
Cycles
First 10 cycles
Last 10 cycles
dongguk
UNIVERSITY

◂**Fig. 4** **a** Schematic illustration of the growth mechanism of ZnS/MnS NCs. **b** Assembled ZnS/MnS NCs//ZnS/MnS NC SSC device. **c**–**f** Electrochemical performance of SSC device (**c**) at different operating voltages, **d** CV curves at diverse scan rates, **e** GCD curves at various current densities, **f** cycling stability for 5000 cycles. Inset shows the GCD curves at initial/final cycles, and symmetric devices lit a green LED image are reproduced with permission from ref. [68] under Copyright © 2017, Springer-Verlag GmbH, Germany

energy and power density of 51.2 Wh kg^{-1} and 849.4 W kg^{-1}, respectively.

Recent reports demonstrate that the composite of two kinds of transition metal sulfides with carbon-based materials has enhanced the electrochemical properties with excellent photocatalytic efficiency and a wider range of solar energy absorption than the single component sulfide. On this concern, for the first time, Li et al. prepared ZnS NWs/Cu_7S_4 NPs/rGO nanocomposite through a one-pot hydrothermal method and utilized as an electrode material for supercapacitor [70]. The ZnS/Cu_7S_4/rGO nanocomposite-based electrode achieved an ultimate specific capacitance of 1114 F g^{-1} at 1 A g^{-1} with initial capacitance holding at 88% after 5000 cycles. The ZnS/Cu_7S_4/rGO NC-based asymmetric supercapacitor was fabricated, which achieved the energy and power densities of 22 Wh kg^{-1} and 595 W kg^{-1} with 77% of initial capacitance sustained after 5000 cycles.

Wei et al. synthesized graphitic C_3N_4/ZnS-based electrode using a one-step calcination process with various mass ratios under the N_2 atmosphere [71]. The specific capacitance of g-C_3N_4/ZnS exhibits a maximum specific capacitance of 497.7 F g^{-1} at 1 A g^{-1} with capacitance retaining at 80.4% at 5 A g^{-1} after 1000 cycles. The symmetric supercapacitor developed with a g-C_3N_4/ZnS-based electrode achieved an energy and power density of 10.4 Wh kg^{-1} and 187.3 W kg^{-1} with long cycling stability. Cao et al. prepared a double-layer hollow structure of Cu_7S_4/NiS through a self-generated sacrificial template method and used as an electrode material for high-performance supercapacitor [72]. The Cu_7S_4/NiS composites with three different particle sizes are prepared, and they exhibit a high specific capacitance of 1204 F g^{-1}, 1028 F g^{-1}, and 857 F g^{-1} at a current density of 1 A g^{-1}, and 85.8%, 84.32%, and 80.13% of its initial capacitance were sustained after 1000 cycles. Binder-free cupric ion-containing zinc sulfide nanoplate-like structures were developed by Hussain et al. utilizing a practical solvothermal method. The developed electrode material displays exceptional coulombic efficiency (99%) and a specific capacitance of 545 F g^{-1} at a current density of 1 A g^{-1} after 5000 cycles [73].

4.8 Vanadium chalcogenides

Vanadium disulfide (VS_2) is a family of transition metal sulfides, comprised of two-dimensional layered structures with the vanadium metal sandwiched by two sulfur atoms. This slack structure is bonded by weak Van der Waals force of interactions, forming an interlayer spacing of 5.76 Å, which enables the electrons and ions to transport from one valence shell to another. At the same time, because of its low cost and wide range of sources, vanadium disulfide is studied extensively towards energy storage devices. To date, very few reports have emerged regarding the preparation of vanadium disulfide through the chemical route for the application of supercapacitors. Feng et al. used VS_2 ultrathin nanosheets as an electrode material for supercapacitors and obtained a maximum specific capacitance of 4760 μF.cm^{-2}. According to literature, for the first time, Pandit et al. developed nanostructured VS_2 through the SILAR method and functioned as an electrode material for a flexible symmetric all-solid-state supercapacitor [74]. It yields a specific power of 1.5 kW kg^{-1} (specific capacitance of 25.9 Wh kg^{-1}) at a voltage window of 1.6 V. Guo et al. reported the synthesis of ultrathin VS_2 TMD nanoplates with in-plane and out-of-plane defects through simple colloidal chemical method [75]. These rich-defect nanoplates are used as anode material for supercapacitor application, which provides an ultrahigh specific capacitance of 2200 F g^{-1} at 1 A g^{-1}. The fabricated asymmetric supercapacitor obtained a better energy density of 66.54 Wh kg^{-1} at a power density of 0.75 kW kg^{-1} with long cycling constancy over 5000 cycles.

The addition of carbonaceous materials to vanadium disulfide helps to enhance its energy storage properties. In TMD/carbonaceous composites, carbonaceous-based materials are known to be a conductive channel that enhances the contact between the electrolyte and electrode interface. Masikhwa et al. developed an asymmetric supercapacitor with VS_2 nanosheets and activated carbon and achieved a maximum specific capacitance of 155 F g^{-1} at 1 A g^{-1} current density as an asymmetric supercapacitor and exhibits 42 Wh kg^{-1} of energy density, 700 W kg^{-1} of power density with ~ 99% of initial capacitance maintained over 5000 cycles at 2 A g^{-1} [76]. Later, Pandit et al. prepared hexagonal structured VS_2 NPs onto the MWCNTs matrix through a facile chemical route [77]. It exhibits a maximum capacitance of 830 F g^{-1} with long cycle steadiness at 95.9% over 10,000 cycles. Fabricated VS_2/MWCNT-based flexible solid-state symmetric supercapacitor obtained a high specific capacitance of 182 F g^{-1} at 2 mV s^{-1} with 42 Wh kg^{-1} of specific energy and 93.2% of long cycling stability over 5000 cycles. Meyer et al. successfully synthesized carbon-supported vanadium disulfide nanocomposites through hydrothermal synthesis which exhibits specific capacitance of 33 F g^{-1} at 1 mA. cm^{-2} [78]. Also, Fang et al. reported the preparation of cauliflower-like nanocomposite made up of ultrathin VS_2 nanosheets and ZnO nanospheres through in situ growth of ZnO nanospheres on the ultrathin VS_2 nanosheets by simple solution method and examined as electrode materials for

supercapacitors [79]. The cauliflower-like nanocomposite exhibits a high specific capacitance of 2695.7 F g^{-1} at 1 A g^{-1} with initial capacitance holding at 92.7% over 5000 cycles.

As another form of vanadium sulfide, vanadium tetrasulfide (VS_4) stands out in TMSmaterials. It exhibits a 1D chain structure with an interchain distance of 5.83 Å. The sulfur atom present in vanadium tetrasulfide is in the form of S_2^{2-} and bonded to the adjacent V atoms. This sparse chain structure offers enough space for the insertion and extraction of electrolyte ions and accelerates the progress of the reaction. The capacity of VS_4 is higher than that of VS_2 since the sulfur content in VS_4 is high and it plays a very predominant role as an active reactant in the electrochemical reaction. The use of graphene or other carbon-based material with vanadium will surely improve both the specific capacitance and cycle performance compared to the pure form. Ou et al. synthesized V_5S_8/graphite nanosheets which exhibits a specific capacitance of 1112 mA h/g at 0.1 A g^{-1} in Li battery and remains 846 mAh g^{-1} after 700 cycles. Kalam et al. prepared hierarchal porous vanadium sulfide/rGO (V_3S_4/rGO) composite using the hydrothermal method and used as electrode material for supercapacitor [80]. The V_3S_4/rGO composite electrode offers a maximum specific capacitance of 520 F g^{-1} at 1 A g^{-1} current density with excellent cyclic stability of 99.6% over 2000 cycles (Fig. 5). Zhang et al. synthesized flower-like VS_4/rGO composite and used in aluminum-ion batteries which provides a promising capacity and coulombic efficiency of 90% after 1000 cycles. Sun et al. developed a promising anode with vanadium sulfide on reduced graphene oxide (VS_4/rGO) for sodium-ion battery and exhibits a capacity of 362 mAh/g [81]. Wang et al. successfully prepared patronite VS_4 anchored on carbon nanocubes with a petal-shaped structure consisting of nanolayers using a one-step hydrothermal method [82]. The VS_4/CNT composite-based electrode offers a specific capacitance of 330 F g^{-1} at 1 A g^{-1} which is exceeding that of pure VS_2. The VS_4/CNT electrode-based symmetric supercapacitor (SSC) exhibits a spectacular areal capacitance of 676 mF. cm^{-2} with an energy and power density of 51.2 Wh kg^{-1} and 30.95 W kg^{-1} at 2.2 V. Ratha et al. prepared both VS_4/rGO- and VS_4/CNT-based electrodes and examined their electrochemical behavior in 0.5 M of K_2SO_4 solution. The VS_4/CNT nanosheets exhibit a capacitance of 231 F g^{-1}, while VS_4/rGO brought a specific capacitance of 492 F g^{-1} at 1 mV s^{-1} under the two-electrode system. Based on this concern, Wang et al. planned to combine CNTs and rGO with VS_4, which show better electrochemical performance than the pure phase [83]. They prepared 3D VS_4/CNTs/rGO through the hydrothermal method and used as an electrode material for the application of supercapacitors. It explored a remarkable capacitance of 497 F g^{-1} (Fig. 5). The symmetric supercapacitor developed with VS_4/CNTs/rGO electrode exhibits an areal capacitance of 1003.5 mF. cm^{-2} with energy and power density of 72.07 Wh kg^{-1} and 14.69 W kg^{-1} at 0.5 mA. cm^{-2}.

Vanadium diselenide (VSe_2) is consists of two Se atoms sandwiching with one V atom in between them forming layered structures stacked through weak Van der Waals force of interaction. VSe_2 has hexagonal crystal structures and exists in both 2H and 1 T phase with metallic nature. Due to the strong electron correlation between the adjacent V atoms and high charge density wave induced structural instability, VSe_2 obtains an excellent potential to be exploited in the application of energy storage and conversion devices. According to the report, to date, both VS_2 and VSe_2 are shown metallic nature, while other TMCs are insulators or semiconductors with few of them possess superconducting behavior as well. Recently, it has been observed that in contrast to TMCs with semiconducting nature, those having metallic nature show ultrahigh conductivity and used as an appropriate material for supercapacitor applications. Also, vanadium diselenide (VSe_2) has been reported to have versatile electronics behavior which is beneficial for the realization of futuristic nano-devices. Additionally, its unique activities towards intercalation reactions, VSe_2, have been stated to display promising energy storage properties as active components in the cathode material of Li-ion batteries. Hybridization of these highly conductive TMCs with carbon-based material would surely enhance their overall supercapacitor performances. Since the graphene hybrid of VS_2 is proved to be a better alternative for energy storage devices, enhanced performance is expected from VSe_2/rGO hybrid. On this concern, Marri et al. reported the preparation of VSe_2/rGO with various concentrations of GO through a one-step hydrothermal method for the first time [85]. The supercapacitor performance of VSe_2/$rGO_{0.3}$ showed a high specific capacitance of ~ 680 F g^{-1} at a current density of 1 A g^{-1}. Moreover, it acquires a high energy and power density of ~ 212 Wh kg^{-1} and ~ 3.3 kW kg^{-1} with capacitance retention of ~ 81% over 10,000 charge–discharge cycles. Chemical synthesis was employed by Xu et al. in 2021 to create VSe_2 nanoparticles anchored on an N-doped hollow carbon sphere. An improved specific capacitance of 1030 F g^{-1} at 1 A g^{-1} is observed in the produced electrode material. With a power density of 701.91 W kg^{-1}, the asymmetric supercapacitor made with an activated carbon anode and VSe2@NC cathode has a high energy density of 85.41 Wh kg^{-1}. It also has a high-stable cycling performance with 90% retention after 2000 cycles [86]. Additionally, Ramu et al. created binder-free patronite (VS4) flower-like nanostructures that are facilely fabricated on carbon cloth (CC) using a simple hydrothermal process [87]. With exceptional energy and power densities of 74.4 Wh cm^{-2} (28.6 Wh kg^{-1}) and 10,154 W cm^{-2} (9340 W kg^{-1}), respectively, the IL-based symmetric supercapacitor

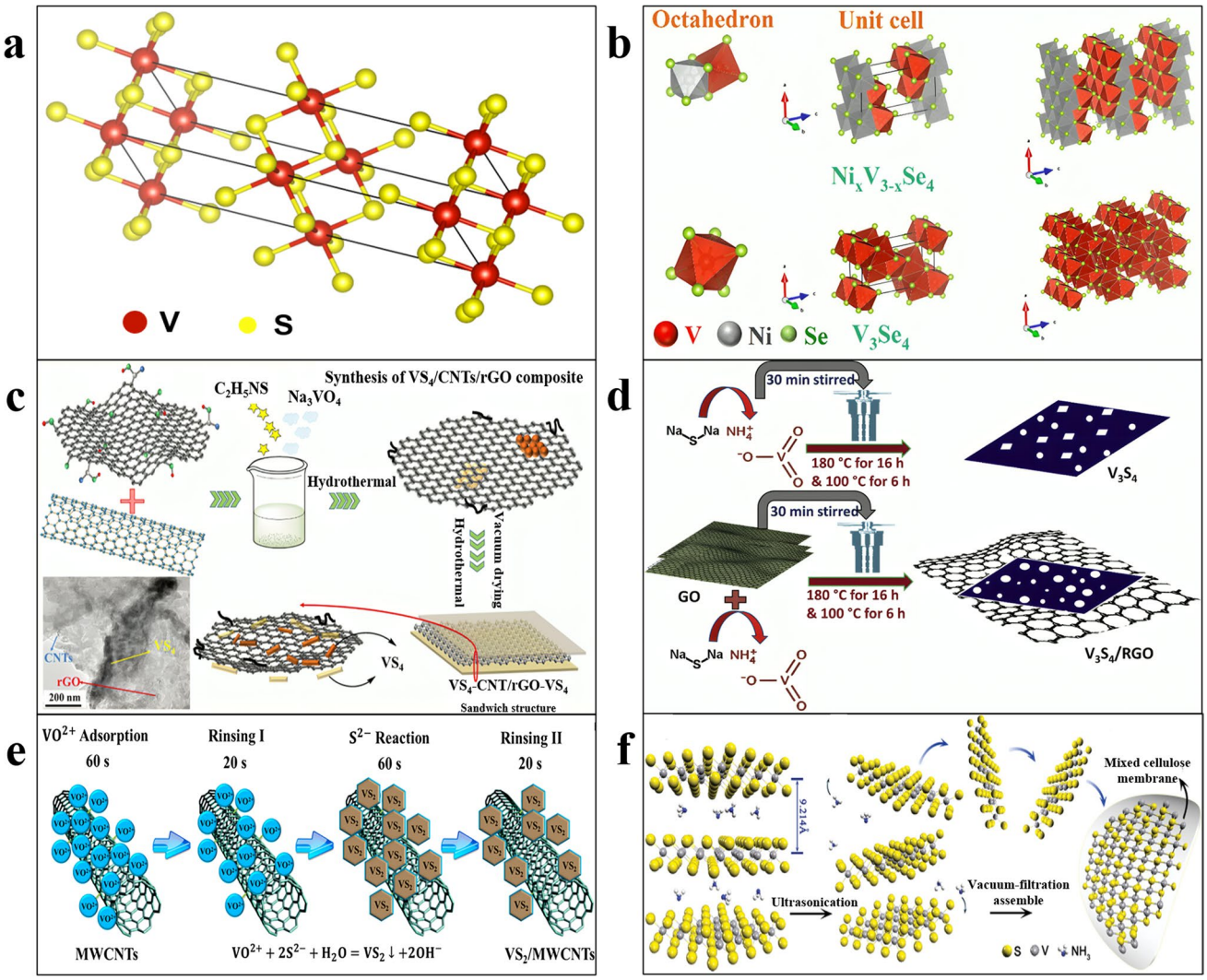

Fig. 5 Structural formation of **a** VS_2 and **b** $Ni_xV_{3-x}Se_4$ and V_3Se_4, images are reproduced with permission from ref. [84] under Copyright © 2019, American Chemical Society. **c–f** Different schematics for the synthesis of various vanadium chalcogenides: **c** synthesis of VS_4/CNTs/rGO composites by simple one-step hydrothermal method, images are reproduced with permission from ref. [83] under Copyright © 2020 Elsevier Inc.; **d** synthesis of V_3S_4/rGO composites by hydrothermal method, images are reproduced with permission from ref. [80] under Copyright © 2018 Taiwan Institute of Chemical Engineers, published by Elsevier B.V.; **e** synthesis of VS_2 hexagons on MWCNTs by using simple and cost-effective successive ionic layer adsorption and reaction (SILAR) method, images are reproduced with permission from ref. [77] under Copyright © 2017 American Chemical Society; **f** synthesis of all-in-solution VS_2 ultrathin nanosheets, images are reproduced with permission form ref. under Copyright © 2011 American Chemical Society

is built and exhibits a high areal capacitance of 536 mF. cm^{-2} (206 F g^{-1}) and remarkable cycling endurance (93%) as well. Molybdenum sulfide (MoS_2) @ vanadium sulfide (VS_2) and tungsten sulfide (WS_2) @ VS_2 hybrid nanoarchitectures were created by Hussain et al. using a simple one-step hydrothermal process. The electrodes produced have high specific capacitances of 513 and 615 F g^{-1}, respectively, at 2.5 A g^{-1}. The asymmetric device, which was created using WS_2@VS_2 electrodes, has a high specific capacitance of 222 F g^{-1} at an applied current of 2.5 A g^{-1} and a specific energy of 52 Wh kg^{-1} at power density of 1 kW kg^{-1} [88].

4.9 Tungsten chalcogenides

Many researchers have stated that among various transition metal dichalcogenides (TMDCs), tungsten disulfide (WS_2) is a low-cost, graphene-like alternative material that offers many applications in the field of energy-related devices such as solar cells, photocatalysts, supercapacitors, and Li-ion batteries. Tungsten disulfide (WS_2) has a hexagonal crystal structure (space group of P63/mnc) made up of three stacked atomic layers (S-W-S) bonded together by weak Van der Waals force. The interlayer spacing of the adjacent atoms is ~ 0.61 nm, which is higher than that of graphite (0.33 nm).

These stacked layers will provide space for the insertion and extraction of Li^+ ions. Although WS_2 is a potentially promising material for energy storage devices, its poor electronic conductivity, the catalytic property of the bulk form, low specific capacitance, poor volume expansion, and agglomeration properties have restricted its practical applications. To overcome these demerits, several approaches have been explored. Use of carbon-based materials, conducting polymers, metal oxides could suppress the abovesaid defects. Chen et al. reported a novel 3D WS_2 nanotubes/graphene hybrid with unique sandwich-type geometry through one-pot hydrothermal for Li-ion batteries. Ratha et al. synthesized WS_2 nanosheet with reduced graphene oxide through the hydrothermal method [89]. The WS_2/rGO hybrids exhibit a specific capacitance of 350 F g^{-1} at 2 mV s^{-1}, which is about 5 times higher than the pure WS_2 and and 2.5 times higher than the pure rGO nanosheets. Tu et al. synthesized well-constructed WS_2/rGO nanosheets by a simple molten salt process as the electrode material for SCs [90]. It yields a massive specific capacitance of 2508.07 F g^{-1} at a scan rate of 1 mV s^{-1} with capacitance retention of 98.6% over 5000 cycles. Similarly, several methods have been taken to address the limitations of WS_2 and to improve its electrical contact between the catalyst. Generally, 2D mesoporous nanosheets have received much attention because of their superior properties compared to their conventional bulk materials. Shang et al. prepared interwoven WS_2 nanoplates supported on carbon fiber cloth (WS_2/CFC) through a facile solvothermal method [91]. The electrochemical behavior of WS_2/CFC delivers a specific capacitance of 399 F g^{-1} at 1 A g^{-1}. Moreover, WS_2/CFC exhibits long cycling stability 99% of initial capacitance retaining for over 500 cycles. Similarly, Qiu et al. reported the preparation of tungsten disulfide/active carbon fiber nanocomposite through electrospinning, one-pot carbonization, and activation, and followed by a hydrothermal process [92]. The nanocomposite displays a high specific capacitance of 600 F g^{-1} at 1 A g^{-1}. The fabricated quasi-solid-state asymmetric supercapacitor obtains an approachable specific capacitance of 237.7 F g^{-1} at 1 A g^{-1}.

The performance of the nanostructured electrode is deeply dependent upon the surface area, electric and ionic conductivity, compact dimensions, reactivity, etc. Normally, mesoporous structured based materials offer a high specific surface area for easy ionic transportation. In the previous report, mesoporous structure materials display several attractive features and have recognized to be potentially favorable anode materials for Li-ion batteries. Based on this literature report, herein, Ansari et al. have prepared porous WS_2 consists of few-layered nanosheets through the hydrothermal method and used as electrode material for supercapacitor [93]. It displays a specific capacitance of 241.5 F g^{-1} at 0.75 A g^{-1} with long cycling stability over 2000 cycles.

Like sulfide, tungsten selenide (WSe_2) is also considered a promising electrode material for the use of energy storage devices due to its wide and direct band gap. But, due to its low electronic conductivity and easy aggregation because of a high specific area, it limits its future application. To solve these hindrances, a profitable way is to associate metal selenide with nanostructured carbon-based materials like mesoporous carbon, CNT, graphene, and rGO. Inspired by previous reports, for the first time, Gopi et al. successfully prepared nanosheet-like tungsten diselenide with rGO hybrid through facile one-step hydrothermal route for the application of supercapacitor [94]. The WSe_2/rGO nanocomposite electrode-based supercapacitor displays a high specific capacitance of 389 F g^{-1} at a current density of 1 A g^{-1} with long capacitance retention of 98.7% over 3000 cycles, and it also delivered an energy and power density of 34.5 Wh kg^{-1} and 400 W kg^{-1}, respectively.

Compared to two-dimensional metal sulfides and selenides, telluride (Te)-based TMDs are metallic, which results in a fast transport rate of ions at the electrodes/electrolyte interface to raise the specific capacitance. Thus, the electrochemical studies of 2D Te-based TMDs are vital. Recent reports have stated that 1Td WTe_2 is a type-II Weyl semimetal, making it show abnormal physical performance like a positive quantum spin hall gap for monolayers and extreme magnetoresistance. Also, the transport rate properties of atomically thick 1Td WTe_2 exposed a superconducting nature below 2.5 K. The outstanding physical characteristics of 1Td WTe_2, especially high electrical conductivity, encourage us that atomically thick 1 Td WTe_2 deserves specific consideration as an auspicious electrode material for energy storage devices, particularly, supercapacitors. However, to date, the reports on the application of Te-based TMDs in supercapacitors are quite infrequent. Here, for the first time, Yu et al. reported the single-crystal 1Td WTe_2 exfoliated nanosheets by liquid phase exfoliation method, which are assembled into air-stable films and further all-solid-state flexible supercapacitors [95]. The 1Td WTe_2 nanosheet-based supercapacitor delivers a mass capacitance of 221 F g^{-1} and stack capacitance of 74 F. cm^{-3}. Moreover, they also display excellent volumetric energy and power density of 0.01 Wh cm^{-3} and 83.6 W cm^{-3} with capacitance retention of ~ 91% over 5500 cycles.

4.9.1 Iron chalcogenides

Iron sulfides (commonly known as fool's gold) are one of the most promising candidates for energy storage devices due to their cost-effectiveness, environmental benignity, and low abundance nature. The solubility of sulfur in iron results in a multitude of stoichiometry, which leads to the formation of iron sulfides in multi-valent states like troilite (FeS), pyrite (FeS_2), and greigite (Fe_3S_4). Furthermore,

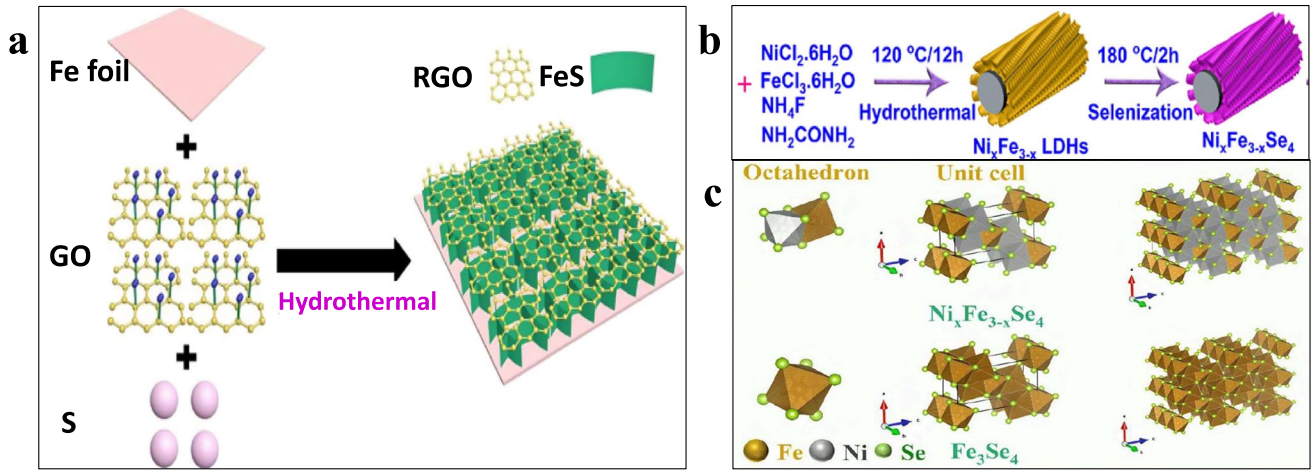

Fig. 6 Schematic representation of the formation of iron chalcogenides. **a** FeS/RGO nanocomposite by in situ growth method, image is reproduced with permission from ref. [97] under Copyright © 2017 Elsevier Ltd. **b** $Ni_XFe_{3-X}Se_4$ and **c** structural configuration of $Ni_XFe_{3-X}Se_4$ nanoarray, images are reproduced with permission from ref. [84] under Copyright © 2019, American Chemical Society

for the past decades, many researchers have attempted to prepare FeS thin film using various synthesis approaches. Karade et al. first reported the preparation of FeS thin-film electrodes was investigated by the SILAR method at room temperature. They also reported the use of FeS thin films as efficient electrodes in liquid configuration and developed the symmetric flexible solid-state supercapacitor device using PVA-$LiClO_4$ as a gel electrolyte at a potential window of 2 V [96]. The fabricated supercapacitor gained a specific capacitance of 4.62 F g^{-1} at 0.75 mA with an energy density of 2.56 Wh kg^{-1}. It yields capacitance retention of 91% over 1000 cycles along with bending of device up to 175°. Moreover, few uses of FeS in supercapacitors may attribute to the large change in volume during the charging and discharging process. The expansions of volume can extent up to 200% to cause the pulverization of FeS which results in poor cycle stability. To solve this, an effective technique is coating a carbon layer on the FeS surface or reducing the size of FeS. Also, combining with active materials may alleviate the volume change, thereby increasing the cyclability, which enhances their conductivity. Based on the concern, Zhao et al., a porous FeS/rGO composite was prepared by in situ grown on Fe foil surface and directly used as an electrode material for supercapacitor [97]. It displays an excellent specific capacitance of 300 F g^{-1} (900 mF. cm^{-2}) with 97.5% of capacitance retention over 2000 cycles.

As one kind of iron sulfide, FeS_2 has been investigated as an electrode material for supercapacitors. Chen et al. prepared pyrite (FeS_2) nanobelts through the facile hydrothermal method for enhancing the performance of aqueous pseudocapacitor. But the practical application of iron-based electrodes was hindered by some problems like large volumetric expansion, low rate capability, low capacity retention, and poor inherent conductivity. To rectify these defects, composite of iron sulfides with carbon-based materials, conducting polymers or metal oxides, is approachable. Thus, Sridhar et al. reported the one-pot two-step method for the preparation of carbon nanofiber (CNF) cross-linked FeS_2 networks through the microwave method [98]. The prepared 3D mesoporous FeS_2/CNF electrodes yield a maximum capacitance of 612 and 342 F g^{-1} at 5 and 100 mV s^{-1} with initial capacitance retained at 97% even after 2000 cycles (Fig. 6). Javed et al. synthesized FeS_2 nanospheres supported on carbon paper which exhibits a better electrochemical performance towards energy storage device and yields a high energy and power density of 44 Wh kg^{-1} and 175 W kg^{-1}, respectively. Zhong et al. developed a supercapacitor with a hierarchical $FeS_2@Fe_2O_3$ heterostructure which displays an excellent capacitance performance to the bare Fe_2O_3 [99]. Pei et al. developed the FeS_2/GNS electrode for supercapacitor which yields a theoretical capacitance of 313.6 F g^{-1}. Sun et al. synthesized FeS_2 nanoellipsoids through a rapid microwave-assisted method to use as an anode material for supercapacitor [100]. It displays a specific capacitance of 515 C/g at 1 A g^{-1} with energy and power density of 64 Wh kg^{-1} and 271.2 W kg^{-1} with initial capacitance maintained at 91% of initial capacitance after 5000 cycles. Zhang et al. prepared a novel $Fe_7S_8@Fe_5Ni_4S_8$ flower center/petal hierarchical nanostructure via a one-step solvothermal method, which achieved a specific capacitance of 670.4 C/g at 1 A g^{-1}. The constructed supercapacitor based on $Fe_7S_8@FeNi_4S_8$ composite electrode exhibits high energy and power density of 49.9 Wh kg^{-1} and 770.0 W kg^{-1} with 88.9% of capacitance retention after 10,000 cycles. Selenium-enriched hybrid $NiSe_2@Fe_3Se_4$ (NFS) nanocomposites were prepared by Manikandan et al. and which are easily

deposited on Ni-foam utilizing the chemical bath deposition (CBD) method. The maximal areal capacity of the deposited $NiSe_2$@Fe_3Se_4 for 36 h (NFS@36 h) is 6.05 C/cm^2 at 6 mA. cm^{-2}. The NFS@36 is used as the positive electrode in a hybrid supercapacitor (HSC), and biomass-derived O, N enriched activated carbon is used as the negative electrode and exhibits superior specific energy of 52 Wh kg^{-1} at 398 W kg^{-1} specific power. Additionally, after 10,000 charge/discharge cycles at 5 A g^{-1}, the device shows a remarkable cycling endurance, with a specific capacitance retention rate of 92% [101].

4.9.2 Manganese chalcogenides

Manganese sulfide (MnS) is typically a p-type semiconductor with a wide band gap of 3.1 eV, since Mn has multiple oxidation states, due to outstanding properties such as economical and eco-friendly nature, and high electronic conductivity of ~ 3.2×10^3 S cm^{-1} than their corresponding hydroxides or oxides [102]. It exists in three different phases, namely, rock-salt structure with α-phase, zinc blende structure with β-phase, and wurtzite structure with γ-phase, respectively (Fig. 7). MnS could be used for charge storage purposes through redox reactions along with non-Faradaic processes. Furthermore, the layered crystal structure of MnS could facilitate the easy intercalation and de-intercalation of electrolyte ions thereby boosting the electrochemical stability of a supercapacitor. Although among various polymorphs of MnS, alpha-phase of MnS is the most stable one, and few reports are available for the use of electrode material in energy storage devices. Tang et al. prepared MnS nanocrystals of hollow spindle-like nanospheres and tetrapod nanorods via the hydrothermal method and yields a specific capacitance of 704 F g^{-1} and 400.6 F g^{-1}, respectively [103]. Li et al. synthesized 2D MnS nanosheets through the hydrothermal method and investigated their electrochemical performance for supercapacitors [104]. The alpha-MnS nanosheet electrode demonstrated a high specific capacitance of 667.40 F g^{-1} at 1 mV s^{-1} and 344.51 F g^{-1} at 0.5 A g^{-1} with initial capacitance retained at 93% over 5000 cycles. Pujari et al. prepared cubic microfibers MnS thin films through the chemical bath deposition (CBD) method which revealed a high specific capacitance of 747 F g^{-1} at 1 mA. cm^{-2} with initial capacitance sustained at 85% over 2000 cycles (Fig. 7) [105]. Quan et al. reported the preparation of α-MnS NPs with nitrogen-doped rGO through a simple one-step solvothermal method and fabricated MnS/N-rGO//N-rGO electrode-based asymmetric supercapacitor with a specific capacitance of 77.9 F g^{-1}. Mohamed et al. prepared α-MnS nanoflakes/rGO nanosheets through the facile one-step hydrothermal method and used for the application of supercapacitors [106]. The hybrid supercapacitor device was fabricated using α-MnS/rGO and activated carbon as a positive and negative electrode. It exhibits a high energy and power density of 38.13 Wh kg^{-1} and 850 W kg^{-1}, respectively. Tang et al. used the hydrothermal approach to create porous manganese sulfide (MnS/GO-NH3) nanocrystals based on the Kirkendall effect [107]. It exhibited a high specific capacitance of 390.8 F g^{-1}, and the developed MnS/GO-NH_3 electrode-based ASC devices demonstrate specific capacitance of 73.63 F g^{-1} with energy and power density of 14.9 Wh kg^{-1} and 4.6 kW kg^{-1}, respectively. Naveenkumar et al. successfully electrodeposited MnS on graphene-wrapped Ni foam substrate as an electrode for supercapacitor application [108]. It delivered a specific capacitance of 2220 F g^{-1} at 0.5 A g^{-1} with initial capacitance retained at 94.6% over 1000 cycles. Ragupathi et al. employed sol–gel method to prepare graphitic carbon nitride–doped MnS nanocomposites for supercapacitor application. It yields a maximum specific capacitance of 463.32 F g^{-1} at 10 mV s^{-1} with initial capacitance maintained at 98.6% over 2000 cycles [109].

Chen et al. synthesized MnS nanocrystals through the hydrothermal method and developed MnS/activated carbon electrode-based asymmetric supercapacitor which displayed a maximum specific capacitance of 73.63 F g^{-1} at 1 mV s^{-1}. Javed et al. prepared MnS nanoparticles onto the carbon textile through the hydrothermal method and developed a solid-state symmetric supercapacitor with high energy and power density of 52.03 Wh kg^{-1} and 1.2 kW kg^{-1}, respectively. Kumbhar et al. successfully prepared novel MnS nanoclusters on nickel foam by the SILAR method and used them as an electrode to examine their capacitance performance [113]. It presents a high specific capacitance of 828 F g^{-1} at 5 mV s^{-1} with capacitance retention of 85.2% over 5000 cycles. Also, the ASC was fabricated using MnS@NF and reduced graphene oxide as a positive and negative electrode, which displays high energy and power density of 34.1 Wh kg^{-1} and 12.8 kW kg^{-1} with initial capacitance holding at 86.5% after 2000 cycles.

Additionally, the laminar nanostructure of manganese sulfide (wurtzite structure) accelerates the penetration of electrolyte and the easy ionic intercalation, which promotes its intrinsic electrochemical reactivity for the capacitive property. Chen et al. fabricated asymmetric supercapacitor using rod-like γ-MnS nanocrystal and porous eggplant derives activated carbon as a positive and negative electrode. They showed a specific capacitance of 110.4 F g^{-1} at 0.5 A g^{-1} and possess an energy and power density of 37.6 Wh kg^{-1} and 181.2 W kg^{-1} with the initial capacitance were upholding at 89.87% over 5000 cycles. But, due to poor cycle life and low electrical conductivity, only a little attention has been paid for γ-MnS to use as an electrode material for supercapacitor. As an electrode material, the coating of graphene is one of the efficient ways to raise conductivity. If nanostructured graphene is used as the matrix material

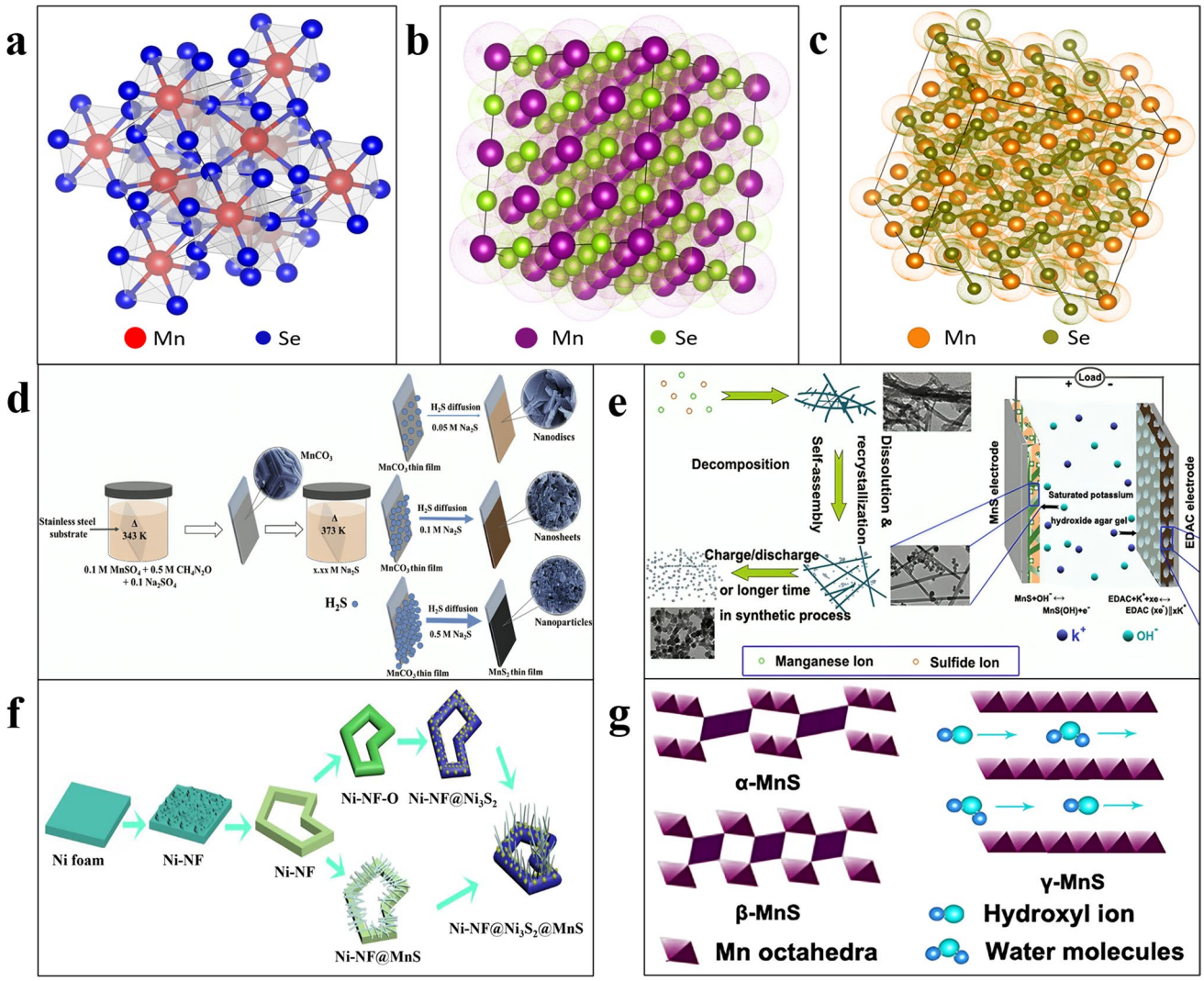

Fig. 7 Structural formation of different manganese chalcogenides: **a** MnS_2, **b** MnSe, **c** $MnSe_2$. **d–f** Schematic representation of various synthesis processes of manganese sulfides. **d** Controlled sulfurization of $MnCO_3$ thin film into different morphological MnS_2, image is reproduced with permission from ref. [110] under Copyright © 2019 Elsevier Ltd. **e** Hydrothermal synthesis of γ-MnS2 with ASCs device, image is reproduced with permission from ref. [111] under Copyright © 2016 Springer Nature. **f** Facial in situ hydrothermal approach combined with etching and pre-oxidization process for the synthesis of Ni_3S_2@MnS composite, image is reproduced with permission from ref [112]. under Copyright © 2017 Elsevier Ltd. **g** Structures of manganese sulfide: α-MnS (rock salt type), β-MnS (zinc blende type), and γ-MnS (wurtzite type), image is reproduced with permission from ref. [111] under Copyright © 2016 Springer Nature

for MnS-based composite, it not only well accommodates the MnS particles, but additionally offers a significant electrode and electrolyte contact for the charge transfer process. Based on the abovesaid considerations, Li et al. synthesized gamma-phase manganese sulfide (γ-MnS)/rGO composite through a one-pot solvothermal method. The electrochemical performance of fabricated γ-MnS/rGO electrode-based supercapacitor possesses an enhanced specific capacitance of 802.5 F g^{-1} at 5 A g^{-1}, and there is no decrease of its initial capacitance values even after 2000 cycles. Arul et al. prepared γ-MnS NPs through a simple chemical process [114]. For the first time, they attempted to deposit the synthesized MnS NPS on homemade graphite/scotch tape, as a binder-free flexible conducting electrode with a maximum specific capacitance of 112 F g^{-1} at 5 mV s^{-1} and cycling permanency of 93% of its initial capacitance even after 2000 cycles. Zhang et al. successfully prepared γ-MnS/rGO composite through a facile one-pot hydrothermal method and used as electrode materials for ASC [115]. It exhibits a specific capacitance of 547.6 F g^{-1} at 1 A g^{-1} with initial capacitance sustaining at 65% over 5000 cycles (Fig. 8).

As comparable to manganese sulfide (MnS), manganese selenide (MnSe) is a typical p-type semiconductor with a

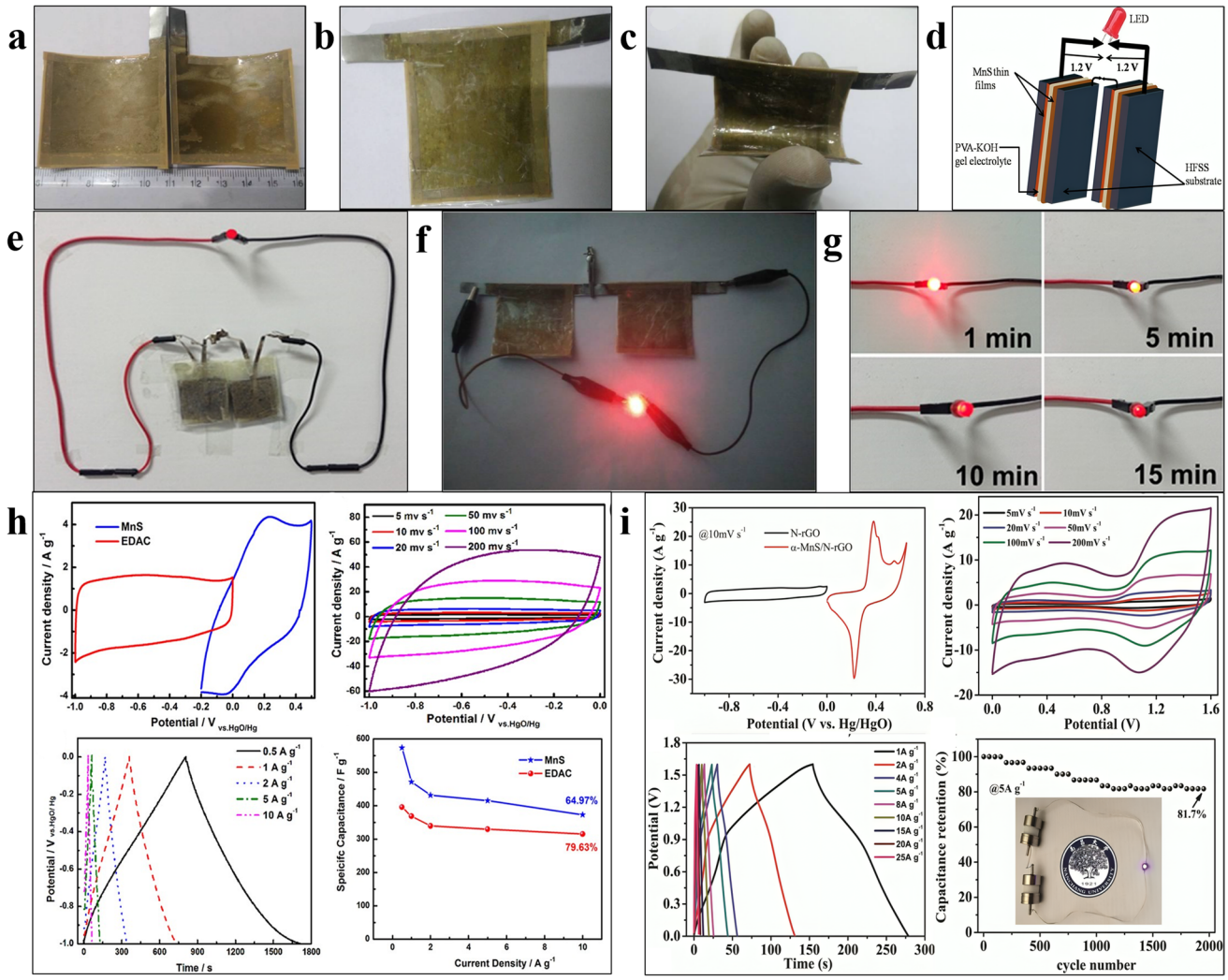

Fig. 8 **a**–**c** Digital snapshots of prepared two MnS thin films with PVA-KOH gel electrolyte as a device. **d** Schematic of MnS thin-film symmetric supercapacitor. **f** A photograph presenting red LED illumination by connecting two symmetric devices in series, image is reproduced with permission from ref [105] under Copyright © 2016 Elsevier Ltd. **e**, **g** A red LED powered by two assembled MnS//EDAC ASC devices in series. **h** Electrochemical studies of MnS and EDAC electrodes, image is reproduced with permission from ref. [111] under Copyright © 2016 Springer Nature. **i** Electrochemical performance of α-MnS/N-rGO hybrid//N-rGO asymmetric devices, image is reproduced with permission from ref. [116] under Copyright © 2016 Elsevier Ltd

band gap of 2.0 eV. It possesses a low electron resistance with high ionic conductivity. MnSe has high electrical conductivity than MnO (~4.2 eV) and MnS (~3.2 eV). There are three different phases of MnSe, namely, the cubic NaCl phase or rock-salt phase (α-MnSe), the cubic zinc blende phase (β-phase), and hexagonal wurtzite phase (γ-phase) (Fig. 7). Among other phases, the rock-salt phase is thermodynamically stable, whereas the zinc blende phase is highly stable and observed as a minor impurity phase and the wurtzite phase is said to be metastable. Due to harsh growth form particularly in liquid, it is very difficult to synthesis MnSe nanostructures. Very few reports are available so far for the synthesis of MnSe nanostructures including α-MnSe nanoparticles and nanocubes, β-MnSe nanowires, and γ-MnSe nanorods. Kim et al. synthesized α-phase MnSe nanoparticles with a maximum specific capacitance of 96.76 F g^{-1} at 0.1 mA. cm^{-2}, although preparation of thermodynamically stable rock-salt (α-phase) phase MnSe nanostructures is still a challenge. For the first time, Javed et al. successfully synthesized single-phase hierarchical MnSe microflowers assembled by nanosheets via a facile-solvothermal method used as efficient electrode material for symmetric supercapacitor [117]. Remarkably, it showed outstanding electrochemical specific capacitance of 200 F g^{-1} at 1 A g^{-1} with an energy density of 55.42 Wh kg^{-1} and 97.15% of initial capacitance maintained over 5000 cycles.

Tang et al. reported a simple one-step solvothermal method to synthesis the nanocellular rock-salt phase of

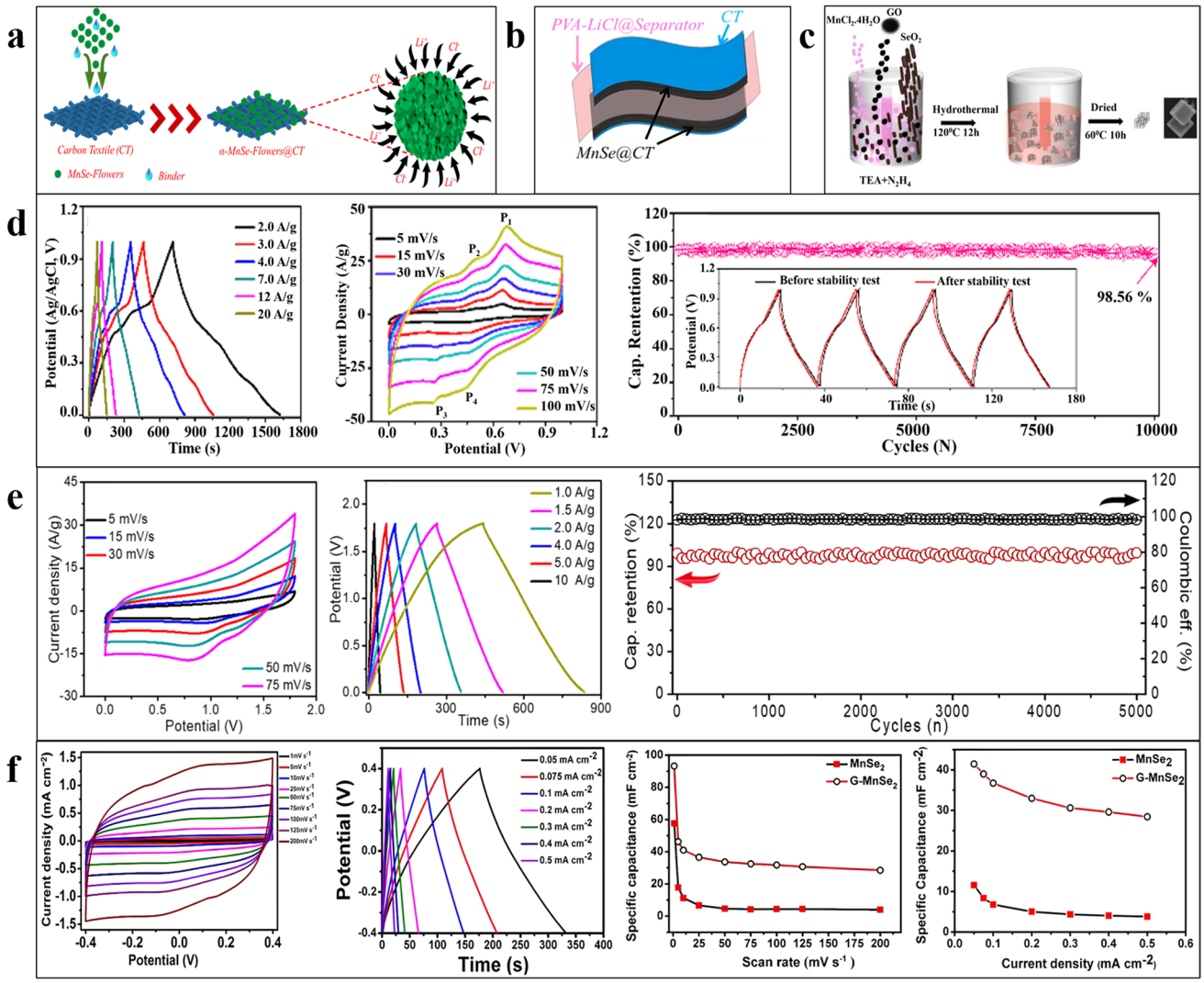

Fig. 9 **a** Fabrication of electrode on flexible carbon textile using α-MnSe nanospheres by one-step solvothermal method. **b** Schematically representation of flexible MnSe@CT symmetric SC. **b** Schematically representation of flexible MnSe@CT symmetric SC **e** Electrochemical measurements of MnSe@CT electrode in aqueous electrolyte. **f** Electrochemical performance of symmetrical MnSe@CT based symmetrical SC in LiCl hydrogel electrolyte, image is reproduced with permission from ref [117] under Copyright © 2019 Elsevier B.V. **c** The schematic representation of the synthesis of the cubic G-$MnSe_2$ hybrid material. **f** Electrochemical performance of cubic $MnSe_2$ and G-$MnSe_2$ symmetric cells, image is reproduced with permission from ref [121]. under Copyright © 2017 Wiley-VCH Verlag GmbH & Co

MnSe and investigated its electrochemical behavior towards energy storage devices [118]. The MnSe faradic electrode displays a high capacity of 84.7 mAh/g at 10 mV s^{-1} with long cycling stability and good rate capability. The MnSe electrode-based supercapacitor was developed which exhibits its large energy and power density of 39.6 μWh cm^{-2} and 0.96 mW cm^{-2}, respectively. Sahoo et al. used hydrothermally prepared α-MnSe as an electrode material for symmetric supercapacitor [119]. It delivered a maximum specific capacitance of 96.76 F g^{-1} at 0.1 mA. cm^{-2} with a corresponding energy density of 8.60 Wh kg^{-1} over 2000 cycles. The developed α-MnSe electrode-based symmetric supercapacitor exhibits a specific capacitance of 23.44 F g^{-1} at 0.1 mA. cm^{-2} with a potential window of 0.8 V. Ranganatha et al. prepared γ-MnS/rGO composite through a one-pot solvothermal method and studied their electrochemical performance as supercapacitor electrode materials (Fig. 9) [120]. The maximum specific capacitance of γ-MnS/rGO is 1009 C/g at 1 A g^{-1} with an initial capacitance retained at 82% after 2000 cycles, whereas pristine γ-MnS offers only 480 C/g of specific capacitance 1 A g^{-1} with a capacity maintained at 64%.

On the other hand, $MnSe_2$ also possess a similar crystal structure and other intrinsic physical and chemical properties

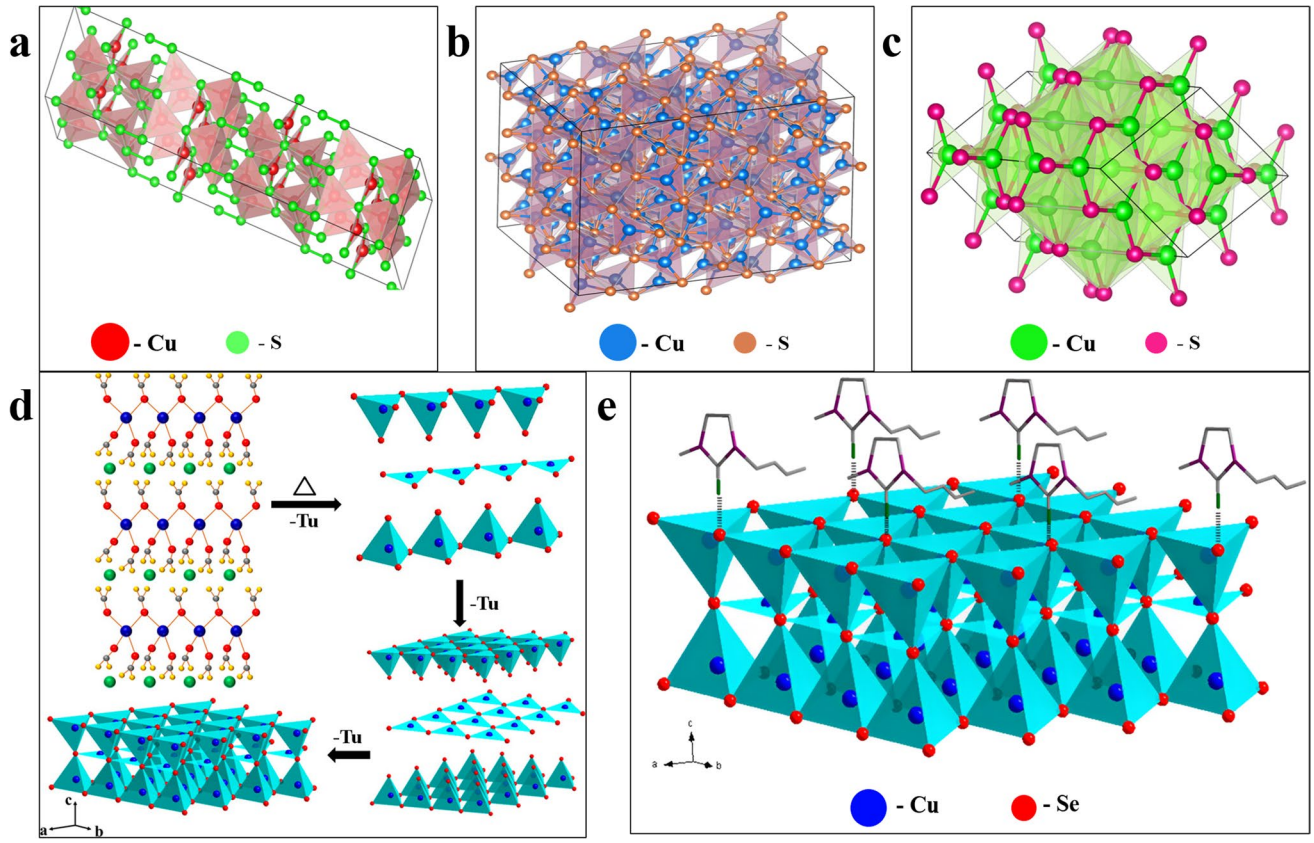

Fig. 10 **a**–**c** Schematic illustration of the different CuS: **a** CuS, **b** Cu_2S, **c** Cu_7S_4. **d**, **e** Phase transformation: **d** $Cu(Tu)_3Cl$ into CuS, **e** $[Bmim]^+$ ions on the surface of the CuS layer, images are reproduced with permission from ref [126] under Copyright © 2015 American Chemical Society

as like other metal TMDs. $MnSe_2$ has many advantages including low toxicity, low cost, and earth-abundant material; basically, pristine metal dichalcogenides have some intrinsic disadvantages like low chemical stability, low specific capacitance, rate capability, and poor cycle life which hinders their electrochemical energy storage performance on a device scale. The abovementioned drawbacks are overcome by combining them with high-conductive materials like carbon and graphene to form a hybrid structure. On this concept, Balamuralitharan et al. synthesized 2D cubic $MnSe_2$ and reduced graphene oxide–decorated $MnSe_2$ ($MnSe_2$/rGO) through a facile hydrothermal method [121]. The electrochemical energy storage performance of $MnSe_2$ and $MnSe_2$/rGO hybrid-based electrodes was examined and used for supercapacitor application for the first time. The specific capacitance of $MnSe_2$ electrode is ~ 57.8 mF. cm^{-2}, whereas $MnSe_2$/rGO hybrid electrode has a high specific capacitance of 93.3 mF. cm^{-2}. The fabricated $MnSe_2$ symmetric supercapacitor exhibits excellent capacitance retention of 80% over 4500 cycles, whereas $MnSe_2$/rGO-based SC displays 106% of its initial capacitance sustained over 4500 cycles under similar conditions (Fig. 9). Wet chemical synthesis of manganese sulfoselenide nanoparticles anchored graphene oxide nanocomposite was carried out by Yasoda et al. As a supercapacitor electrode, GO-MnSSe produced a specific capacitance of 603 F g^{-1} at 0.1 A g^{-1} in 1 M KCl. The constructed two-electrode device displayed a decent retention of 67% after 9000 cycles, with a specific capacitance of 98.5 mF. cm^{-2} at 80 µA cm^{-2} [122].

4.9.3 Copper chalcogenides

Copper sulfide (CuS) is typically a p-type semiconductor with a band gap of 1.2^{-2} eV and becomes a potentially promising candidate for SCs owing to low cost, abundant availability, large theoretical capacity, and environmental benignity. It has diverse stoichiometric forms based on their crystal structure extending from orthogonal to hexagonal, which includes covellite (CuS), spionkopite ($Cu_{1.39}S$), geerite ($Cu_{1.6}S$), anilite ($Cu_{1.75}$), digenite ($Cu_{1.8}S$), djurleite ($Cu_{1.95}S$), chalcocite (Cu_2S), and villamaninite (CuS_2) (Fig. 10). Till now, there are only a few reports on CuS on supercapacitor applications. Huang et al. reported CuS nanosheets using a solvothermal method and used them as electrode for supercapacitor. It exhibits an outstanding electrochemical capacitance of

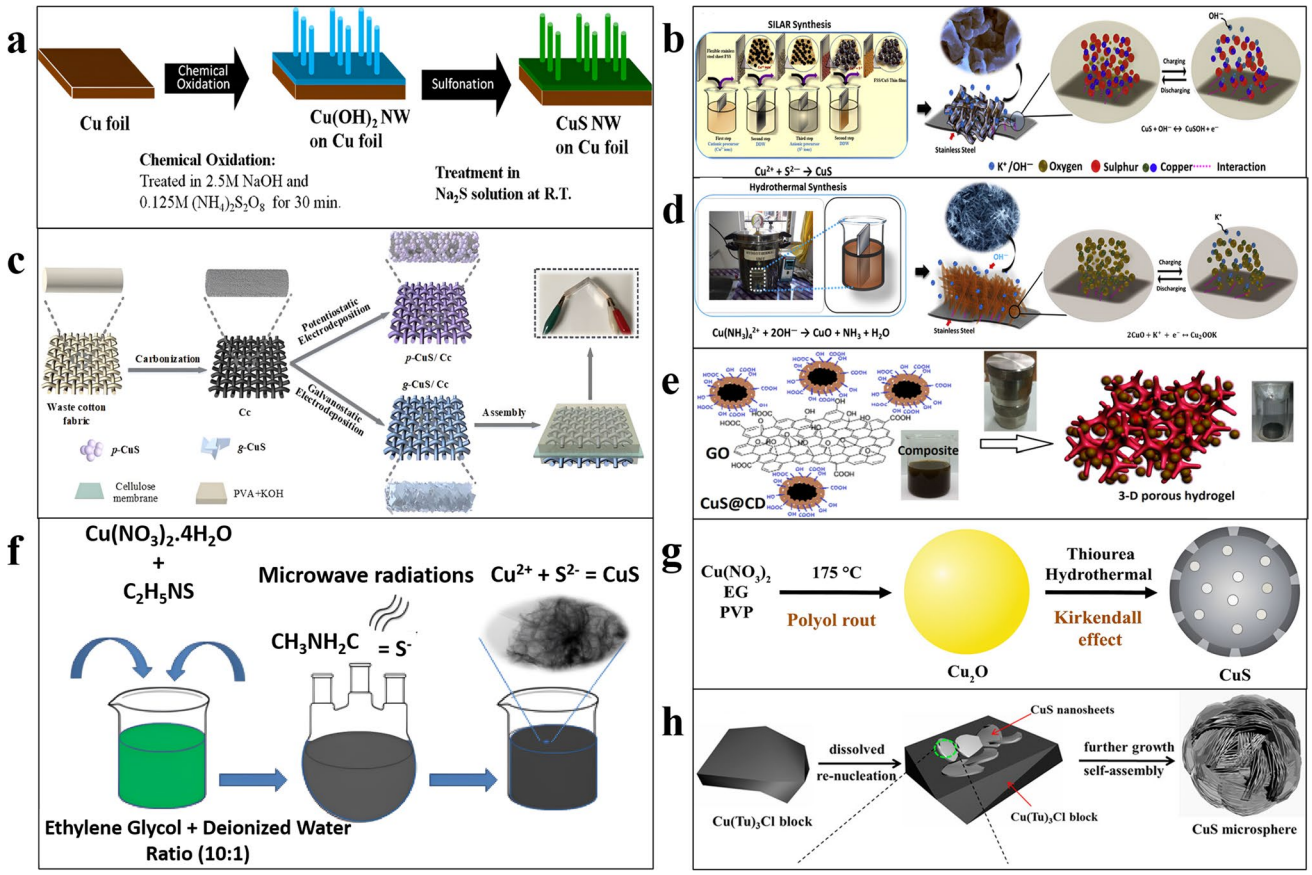

Fig. 11 **a**–**h** Different synthesis methods for the preparation of copper sulfides: **a** CuS nanowire array on Cu foil by simple wet chemical process, image is reproduced with permission from ref [125]. under Copyright © 2014 Elsevier Ltd. **c** Preparation of CuS at carbon cloth by electrodeposition technique, image is reproduced with permission from ref [127]. under Copyright © 2018 Elsevier Ltd. **b**, **d** Preparation of CuS thin films on flexible stainless steel by SILAR and hydrothermal method, image is reproduced with permission from ref. [128] under Copyright © 2019 Elsevier Ltd. **e** CuS@CD–GO 3D porous hydrogels prepared using one-pot hydrothermal method, image is reproduced with permission from ref [129]. under Copyright © 2017 Elsevier Ltd. **f** Preparation of CuS nanosheets using microwave irradiation method, image is reproduced with permission from ref. [130] under Copyright © 2019 Elsevier Ltd. **g** CuS nano-hollow sphere prepared by hydrothermal method using PVP, image is reproduced with permission from ref [124]. under Copyright © 2016 Elsevier B.V. **h** Solvothermal method for 3D CuS structure using ionic liquid precursors, images are reproduced with permission from ref [126] under Copyright © 2015 American Chemical Society

833.3 F g^{-1}. Excellent electrochemical behavior with a better specific capacitance of 101.34 F g^{-1} was reported by Krishnamoorthy et al. by developing SC based on CuS nanoparticles by the hydrothermal method. Huang et al. reported a one-step solvothermal method with different morphologies of CuS nanosheets and used it as a supercapacitor electrode material [123]. The prepared CuS nanosheets displayed a specific capacitance of 833.3 F g^{-1} at 1 A g^{-1} as compared to CuS-CTAB (378.9 F g^{-1}) and CuS-SDBS (232.4 F g^{-1}). Heydari et al. synthesized CuS nano-hollow spheres with nanoporous structure through a facile method (Fig. 11) [124]. It displayed a marvelous specific capacitance of 948 F g^{-1} at 1 A g^{-1} with a rate capability of 46% of the initial capacitance retention at 50 A g^{-1}. Yu-Kuei et al. reported CuS nanowire preparation through liquid–solid reaction, which exhibits a specific capacitance of 305 F g^{-1} and 87% of original capacitance obtained over 5000 cycles (Figs. 11 and 12) [125].

To date, many CuS architectures have been developed for SCs like microspheres, nanowires, nanoflowers, nanosheets, nanotubes, and nanoplatelets. Unfortunately, their energy density, rate performance, and cycle stability are less well than expected. So, to overwhelm these issues, structural and compositional engineering may pay an effective way to improve the electrochemical performance of CuS. Durga et al. studied coriander leaf-like CuS nanostructures on nickel foam for SC applications [132]. It showed a high specific capacitance of 5029.28 F g^{-1} at 4 A g^{-1} with an energy density of 169.73 Wh kg^{-1} and 107% of capacitance retention over 2000 cycles. Bulakhe et al. synthesized three-dimensional copper sulfide with various morphologies through the SILAR method and used as an electrode

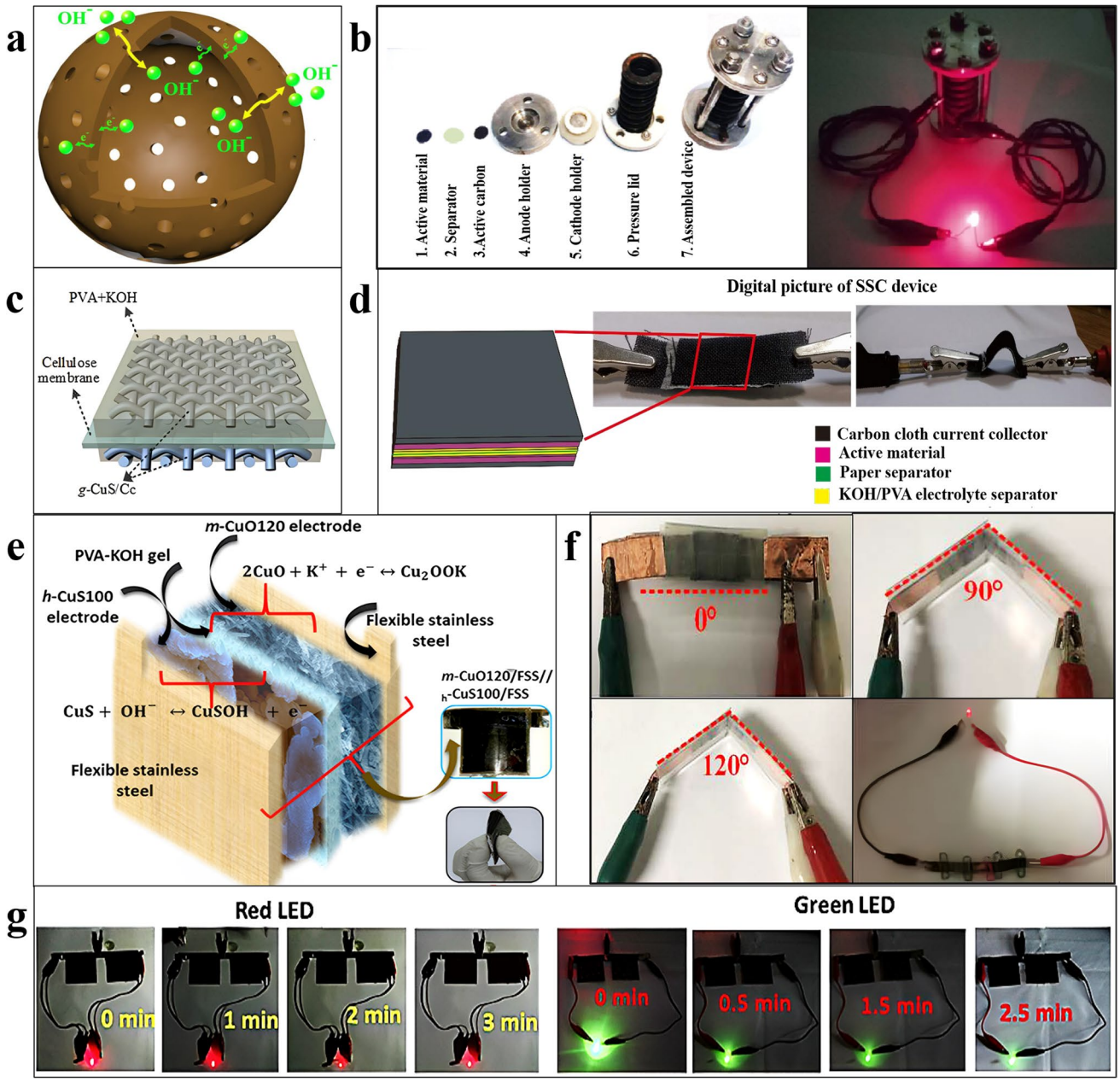

Fig. 12 **a** Schematic illustration of CuS nano-hollow spheres, image is reproduced with permission from ref [124]. under Copyright © 2016 Elsevier B.V. **b** Two-electrode device components and photograph of CuS//AC device lit red LED, image is reproduced with permission from ref. [130] under Copyright © 2019 Elsevier Ltd. **c**, **f** Schematic illustration of g-CuS/CC symmetric devices and its bending photograph, image is reproduced with permission from ref [127]. under Copyright © 2018 Elsevier Ltd. d Schematic illustration of the EDTA-$Cu_{1.8}S$ composite flexible SSC device (optical photographs of the SSC device under normal and bent), image is reproduced with permission from ref [131] under Copyright © 2018 Elsevier Ltd. **e**, **g** Schematic illustrations of CuS asymmetric flexible solid-state supercapacitor devices on flexible stainless steel. **g** AFSSCs devices lit red and green LED method, image is reproduced with permission from ref. [128] under Copyright © 2019 Elsevier Ltd

material for high-performance SCs [133]. The maximum specific capacitance of flowers like and integrated nanotubes were observed to be 761 and 470 F g^{-1} at 5 mV s^{-1}.

Various nanostructure CuS-based electrode materials were investigated and fabrication for the application of supercapacitor. Still, owing to the lack of rate capability and the dead surface of CuS, it is far beyond the commercial application. Recently, a hybrid supercapacitor has received much greater attention towards energy storage devices. The combination of several materials with CuS would improve their capacitor efficiency. Based on this concern, Zeraati et al. prepared CuS nanowires through a chemical route on

Cu substrates, and their electrochemical performance was compared with the case that these nanowires are coated with SiC (Fig. 11) [134]. The SiC-coated CuS exhibits a specific capacitance of 3370 F g^{-1} with 98.4% capacity sustained over 1000 cycles. Cui et al. reported rGO-wrapped 3D CuS nano-erythrocytes through the solvothermal method, which exhibits an energy and power density of 16.7 Wh kg^{-1} and 681 W kg^{-1} and 90.8% of the initial capacitance maintained over 10,000 cycles at 2 A g^{-1} [135]. The fiber-shaped SC based on PANI/CuS/PET was developed by Ba et al. and reported a specific capacitance of 29 mF. cm^{-2} with 93.1% of capacitance retention over 1000 cycles [136]. Hou et al. prepared hierarchical structured CuS grown on MWCNT with a specific capacitance of 566.4 F g^{-1} and retention of 94.5% of its initial capacitance after 5000 cycles [137].

Copper sulfide (Cu_2S or chalcocite)–based supercapacitor displayed less specific capacitance owing to its inadequate charge transfer barriers at the electrode and electrolyte interface and low specific capacitance. Hence, researchers exploited the composites of Cu_2S electrodes for the study of the supercapacitor. Alshammari et al. reported the preparation of a new hybrid core silver nanowires (Ag NWs) with shell copper sulfide (Cu_2S) nanostructure by the SILAR method, which unveils a specific capacitance of 603 F g^{-1} (stainless steel substrate) and 707 F g^{-1} (Ni foam substrate) with an energy and power density of 10.01 Wh kg^{-1} and 25.33 Wh kg^{-1} at 0.2 mA (Fig. 11) [138]. Hong et al. prepared 1D single-crystalline Cu_2S nanostructures by solution-based direct synthesis process and used as electrode materials for SC [139]. It displayed a specific capacitance of 750 mF. cm^{-2} at 2 mA. cm^{-2} with 90.5% of the initial capacitance sustained over 20,000 cycles. Liu et al. prepared hierarchical Cu_2S nanorods with various crystal phases by a simple hydrothermal method, which exhibits a specific capacitance of 346 mF. cm^{-2} (hexagonal phase) at 5 mA. cm^{-2} with 90% of original capacitance retention over 2000 cycles [140]. Zhao et al. prepared the Cu_2S microsphere by reducing copper sulfate with ascorbic acid in sodium thiosulfate solution and used as electrode materials for SC [141]. It showed a specific capacitance of 444.2 F g^{-1} at 1 A g^{-1} with 87% of initial primary capacitance retained over 6000 cycles.

As one of the non-stoichiometric CuS, copper sulfide with Cu:S ratio of 1.75 is usually known as anilite ($Cu_{1.75}S$ or Cu_7S_4). It is the most stable Cu-rich crystal structure in the system of Cu_xS, where the S atoms in Cu_7S_4 form a rigid cubic lattice, thereby offers a crystalline pathway for the embedding of electrolyte ions (Fig. 10). While the Cu ions around the S sublattice are superionic with "liquid-like mobility," such definite transportation of the ionic behavior of Cu is vital to enhance the pseudocapacitive performance. For the first time, Javed et al. fabricated a flexible solid-state supercapacitor based on faradic redox active material of Cu_7Se_4 nanowires through a modified hydroxide-mediated approach [142]. It showed a high specific capacitance of 400 F g^{-1} at 10 mV s^{-1} and energy and power density of 35 Wh kg^{-1} and 200 W kg^{-1} with 95% capacitance retention over 5000 cycles. Also, Liu et al. adopted the calcination-vulcanization method to prepare Cu_9S_8@C for the first time [143]. Then, they deposited it onto a carbon fiber cloth. Furthermore, they prepared polypyrrole/Cu_9S_8@C-CC nanocomposite-based electrodes through the electrochemical deposition method and used for SC application. The specific capacitance of PPy/Cu_9S_8@C-CC electrodes was found to be 270.72 F g^{-1} at 10 mV s^{-1} with 80.36% of capacitance retention after 3000 cycles. Zhou et al. synthesized porous $Cu_{7.2}S_4$ sub-microspheres through ion-exchange reaction, which displayed a specific capacitance of 491.5 F g^{-1} at 1 A g^{-1} and 82% of capacitance retention even after 1000 cycles [144]. Xu et al. prepared $Cu_{1.92}S$ nanorod accompanying CuS nanoribbons grown on copper foam and as electrode materials for asymmetric supercapacitor application [145]. It showed a high energy and power density of 35 Wh kg^{-1} and 266 W kg^{-1} with 88% of capacitance retention after 5000 charge–discharge cycles. Wang et al. prepared several kinds of copper sulfides, namely CuS, Cu_7S_4, and Cu_9S_5, through the liquid phase synthesis process [146]. They reported that the snowflake-like morphology of Cu_7S_4 offers a special path for the diffusion of ions. It exhibits a high specific capacitance of 1303.01 F g^{-1} at 5 A g^{-1} with 98.84% of capacitance retention after 1000 cycles.

Copper selenides (Cu_2Se) is a p-type semiconducting material. Copper selenides are binary composites and can be produced in many stoichiometric arrangements as reported in various forms like CuSe, $CuSe_2$, Cu_2Se, Cu_3Se_2, Cu_5Se_4, and Cu_7Se_4 as well as non-stoichiometric compositions like $Cu_{2-x}Se$. For $Cu_{2-x}Se$, Se atoms are placed in face-centered cubic positions, while Cu ions are placed in superionic states. Copper selenide is prepared in several phases such as monoclinic, cubic, tetragonal, and hexagonal. Several researchers have reported the various syntheses of zero-dimensional, one-dimensional, and two-dimensional Cu_2Se nanomaterials through several methods such as hydrothermal, solvothermal, hot injection technique, liquid phase deposition, and sonochemical method. It has advantages including multiple oxidation states and high electrical conductivity than metal oxides, which could offer better electrochemical properties. Thus, copper selenide is widely used in the application of gas sensors, catalysts, thermoelectric devices, rechargeable lithium, and sodium batteries, but only a few reports are available for copper selenides towards energy storage applications. Pazhamalai et al., using a straightforward hydrothermal technique, created hierarchical $CuSe_2$ nanoneedles synthesized on Cu foil and tested their electrochemical properties to serve as a binder-free electrode for supercapacitor applications [147]. The galvanostatic

charge–discharge technique displayed that $CuSe_2$ nanoneedles/Cu electrode displayed a high specific capacitance of 1037.5 F g^{-1} at 0.25 mA. cm^{-2}. Also, since morphology is a key factor in designing nanomaterials with controlled functional properties, Shinde et al. demonstrated the supercapacitor application of Cu_2Se electrodes with various morphologies through electrodeposition method [148]. The well-designed morphologies of Cu_2Se nanostructures have been used for fabricating supercapacitor devices. Among various morphologies, the nanodendrite-like morphology of Cu_2Se exhibits a maximum specific capacitance of 688 F g^{-1} at 5 mV s^{-1}. To enhance the intrinsic conductivity of metal chalcogenides and to reduce the dissolution of selenide species during cycling, the only suitable approach is to prepare nanometer-sized materials with conductive additives. On this concern, Jin et al. prepared 1D CNTs@C with $Cu_{2-x}Se$ nanospheres through a facile solvothermal method and investigated as an electrode material for supercapacitor (Fig. 13) [149]. It exhibits better specific capacitance of 302.7 F g^{-1} at a constant current density of 1 A g^{-1} with opening capacitance retained at 86.9% over 2000 cycles. The summary on copper chalcogenide–based electrode materials with various synthesis methods and their supercapacitor performances are given in Table 3.

4.9.4 Cobalt chalcogenides

Cobalt sulfide is one of the semiconducting TMCs with multiple oxidation states for high electronic conduction and easy charge transfer. It acts as an excellent electrode material for energy storage devices owing to inexpensive, good electrochemical performance, and environmentally friendly nature. It exists in various phases like CoS, CoS_2, Co_3S_4, Co_9S_8, and $CoS_{1.097}$, respectively. Each phase of cobalt sulfide has its own merits. Various studies on CoS_2 denote that CoS_2 micro/nanostructures with several structural morphologies like octahedrons, hollow sphere, hierarchical mesoporous microsphere, ellipsoids, worm-like, nanocomposites, and nanocubes, which improve the electrochemical behavior of CoS_2 for energy storage devices. Many synthesis methods like hydrothermal, microwave assisted, solid-phase reaction, solvothermal, and ion-exchange reaction were studied so far. Kumar et al. prepared CoS electrodes through a facile chemical bath deposition method with various solvent on nickel foam [167]. When utilized as electrode material for high-performance supercapacitor, CoS prepared with ethanol solvent exhibits a high specific capacitance of 41.36 F g^{-1} at 1.5 A g^{-1} with excellent cycling permanency and rate performance. Zhang et al. synthesized cobalt disulfide (CoS_2) nanodendrites through a one-step solvothermal method, which delivered a maximum specific capacitance of 311.06 F g^{-1} at 1 A g^{-1} with 80.22% of initial capacitance preservation after 3000 charge–discharge cycles [168]. Amaresh and co-workers fabricated cubic CoS_2 nanoparticles based supercapacitor through single-step microwave-mediated method [169]. The specific capacitance of phase pure cubic CoS_2 nanoparticles was found to be 52 F g^{-1} at 0.7 A g^{-1} with 80% initial capacitance retaining even after 10,000 cycles. Liu et al. successfully prepared hierarchical cobalt sulfide/cobalt basic salt nanocomposite using a vapor-phase hydrothermal method for the application of supercapacitor [170]. It yields a high specific capacitance of 1984 F g^{-1} at 1 A g^{-1}, excellent rate capability of 78.6% capacitance retention, and cycle stability of 90.2% of its initial capacitance maintained even after 5000 cycles.

Chen et al. prepared Co_3S_4 nanosheet arrays through in situ shape and phase transformation synthesis and used as efficient electrode material for high-performance supercapacitors [171]. It showed a specific capacitance of 1081 F g^{-1} at 1.61 A g^{-1}, areal capacitance of 2.69 F. cm^{-2} and 2.37 F. cm^{-2} at 4.12 mA. cm^{-2} with the primary capacitance holding at 96.2% after 3000 cycles. Aloqayli et al. prepared cobalt sulfide (Co_9S_8) for flexible, durable, and high-performance supercapacitors via a facile technique [172]. It showed a high specific capacitance of 7358 mF. cm^{-2} with excellent cycle stability after 5000 cycles. Ghosh et al. prepared hierarchical Co_3S_4 on reduced graphene oxide hydrogel@Ni foam through the hydrothermal method and utilized it as electrode material for the fabrication of the supercapacitor. The aqueous asymmetric supercapacitor fabricated with the Ni@rGO-Co_3S_4 electrode displayed a specific capacitance of 1369 F g^{-1} at 1.5 A g^{-1} and holds 96.6% of the initial capacitance after 3000 cycles at even higher current density of 12 A g^{-1} [173].

Liu and co-workers for the first time used a one-step solvothermal process to create new networked ultralong $CoS_{1.097}$ nanotubes, which they used as an active material for supercapacitor applications [174]. It showed a maximum specific capacitance of 764 F g^{-1} at 2 A g^{-1} and 85% of original capacitance retaining after 500 cycles. Cao et al. synthesized 2D $CoS_{1.097}$/N-doped carbon nanocomposite through a facile method for the first time [175]. The supercapacitor developed with $CoS_{1.097}$/N-doped carbon yields a high specific capacitance of 360.1 F g^{-1} at 1.5 A g^{-1} with high-rate capability and recollects 56.8% of its initial capacitance at a current density of 1.5 A g^{-1}. Chang et al. utilized a facile synthesis for the preparation of Co_9S_8/Ni_3S_2 double-size nanoparticles decorated on rGO [176]. The supercapacitor was assembled with Co_9S_8/Ni_3S_2/rGO-based electrode material, which exhibits a maximum specific capacitance of 1929.1 F g^{-1} at 1 A g^{-1} with 92.8% of retained capacitance after 1000 cycles at a higher current density of 10 A g^{-1}. Zhu et al. prepared hexagonal prism-like hierarchical Co_9S_8@$Ni(OH)_2$ core–shell nanotubes on carbon fibers through electrodeposition process [177]. The high-performance supercapacitor fabricated with Co_9S_8@$Ni(OH)_2$ electrode possesses

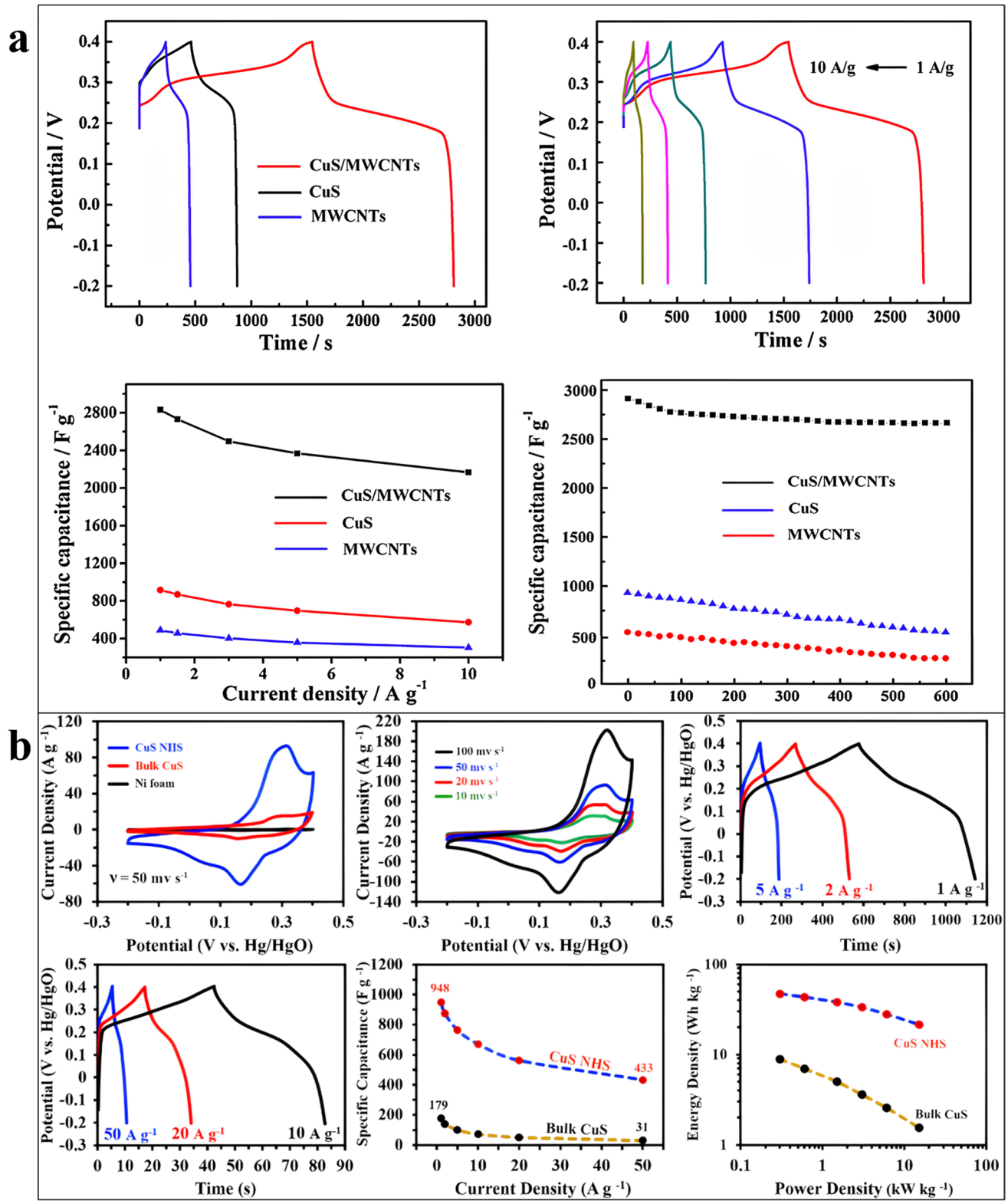

Fig. 13 Electrochemical performance of various copper chalcogenides and its composites, images are reproduced with permission from ref. [124] and [150] under Copyright © 2016 Elsevier B.V

Table 3 Summary of copper chalcogenide–based electrode materials with various synthesis methods and their supercapacitor performances

Electrode material	Method of synthesis	Specific capacitance	Capacitance retention	Ref
3D carbon dot supported on CuS/GO	Hydrothermal method	920 F g^{-1} @ 1 A g^{-1}	90% over 5000 cycles	[129]
CuS/nitrogen-doped GN	One-step hydrothermal method	379 F g^{-1} @ 1 A g^{-1}	72.46% over 500 cycles	[151]
Fe-doped CuS	Hydrothermal method	516.39 F g^{-1} @ 5 mV s^{-1}	-	[152]
CuS/MWCNT	Hydrothermal method	2831 F g^{-1} @ 1 A g^{-1}	90% over 600 cycles	[150]
CuS/acetylene black	Solvothermal method	2981 F g^{-1} @ 1 A g^{-1}	92% over 600 cycles	[153]
$CuS^{-1}40$	One-step hydrothermal method	1000.2 F g^{-1} @ 1 A g^{-1}	94.7% over 1000 cycles	[154]
CuS/rGO	Solvothermal route	2317.8 F g^{-1} @ 1 A g^{-1}	96.2% over 1200 cycles	[155]
CuS nanoparticle	Sonochemical method	62.77 F g^{-1} @ 5 mV s^{-1}	-	[156]
CuS hollow microflowers		536.7 F g^{-1} @ 8 A g^{-1}	83.6% over 20,000 cycles	[157]
CuS nanosheets	Microwave-assisted method	2535 F g^{-1} @ 1 A g^{-1}	88% over 10,000 cycles	[130]
CuS@PbS	Chemical bath deposition	1004.42 F g^{-1} @ 2.85 A g^{-1}	97.1% after 3000 cycles	[158]
g-CuS/Cc	Electrodeposition method	4676 mF. cm^{-2} @ 2 mA. cm^{-2}	89.8% after 10,000 cycles	[127]
CuS/rGO	Solvothermal method	946 F g^{-1} @ 10 mV s^{-1}	89% over 5000 cycles	[141]
CuS microspheres	Ionic liquid precursor method	237 F g^{-1} @ 0.5A g^{-1}	74% after 3000 cycles	[126]
CuS/rGO	Solvothermal method	368.3 F g^{-1} @ 1 A g^{-1}	88.4% after 1000 cycles	[159]
3D CuS on the active carbon layer	Solvothermal method	247 F g^{-1} @ 0.5 A g^{-1}	92% after 5000 cycles	[160]
CuS spherical cluster	Melt spinning method	713 F g^{-1} @ 1 A g^{-1}	61% after 2000 cycles	[161]
EDTA-$Cu_{1.8}S$	Solvothermal method	1050.0 F g^{-1} @ 1 A g^{-1}	81.5% after 2000 cycles	[131]
Ni-doped CuS	Hydrothermal method	400 F g^{-1} @ 5 mV s^{-1}	-	[162]
PPy/CuS/BC	In situ synthesis	580 F g^{-1} @ 0.8 mA. cm^{-2}	73% after 300 cycles	[163]
CuS@PPy	Solvothermal method	427 F g^{-1} @ 1 A g^{-1}	88% after 1000 cycles	[164]
Flower-like CuS	Solvothermal method	597 F g^{-1} @ 1 A g^{-1}	80% after 1000 cycles	[165]
CuS/$Cu(OH)_2$	Solvothermal method	845.5 F g^{-1} @ 1 mA. cm^{-2}	78.6% after 1000 cycles	[166]

a high specific capacitance of 149.44 mAh/g at 1 A g^{-1} with initial capacitance engaged at 97.3% after 5000 cycles. Han et al. designed a supercapacitor based on a porous Co_9S_8 nanosheet array on nickel foam through a facile synthesis [178]. It exhibits a good electrochemical performance with a specific capacitance of 1098.8 F g^{-1} at 0.5 A g^{-1} and holds 87.4% of its initial capacitance of the first cycle even after 1000 cycles and has a good rate performance of 54.6% at 10 A g^{-1}.

Cobalt selenide (CoSe) has semiconducting nature with a lower optical band gap. Among Co-based compounds, CoSe has potentially outstanding electrical conductivity owing to its metallic property of Se. Also, compared with the sulfide and oxides, selenium possesses lower electronegativity with a larger ionic radius. The electron in the outermost orbital of cobalt has a weak attraction with Se; hence, the weakly bound electrons offer electroactive reaction sites for redox reaction and thereby enhance the overall kinetics of the electrochemical reaction. Additionally, $CoSe_2$ has been proved to possess excellent electrochemical activity and studied to be a negative electrode for supercapacitor. Consequently, it is expected that $CoSe_2$ could be used as positive material for supercapacitor application. However, the study on $CoSe_2$ for SC positive electrode is worth exploring and rarely reported. Chen et al. synthesized bifunctional bamboo-like $CoSe_2$ arrays through thermal annealing technique for high-performance supercapacitor [179]. It obtained a specific capacitance of 544.6 F g^{-1} at 1 mA. cm^{-2}. The fabricated ACS based on the $CoSe_2$ electrode possesses an energy and power density of 20.2 Wh kg^{-1} and 144.1 W kg^{-1} at 10 mA. cm^{-2}. Bose et al. prepared Co_3Se_4 nanosheets embedded on N-CNT as an electrode active material for supercapacitor through pyrolysis and solvothermal method, which exhibits a specific capacitance of 114 F g^{-1} at 2 mV s^{-1} with 96% of its initial capacitance obtained even after 5000 cycles [180]. Peng and co-workers, using a straightforward low-temperature solvothermal technique, created an asymmetric supercapacitor constructed on nanosheets of cobalt selenide that resemble petal-like morphology [181]. It yields an energy and power density of 21.1 Wh kg^{-1} and 400 W kg^{-1}, and after 5000 cycles, the initial capacitance retained at 93.8%.

Kirubasankar et al. hydrothermally prepared in situ grown CoSe onto graphene nanosheets as electrode material for ASC [182]. The CoSe-G nanohybrid electrode presented a high specific capacitance of 1037 F g^{-1} at 5 mV s^{-1}. The asymmetric supercapacitor fabricated with the CoSe-G electrode possesses an energy and power density of 45.5 Wh kg^{-1} and 1.1 kW kg^{-1} and recollects 81% of its initial capacitance after 5000 cycles. Zhang et al. successfully prepared ASC based on porous cobalt selenide thin films

(CoSe) through electrodeposition method, which yields a specific capacitance of 510 F g^{-1} at 1 A g^{-1} and retains 91% of its original capacitance over 5000 cycles [183]. Zhao et al. synthesized tremelliform $Co_{0.85}Se$ nanosheets through a simple solvothermal technique and utilized them as an electrode active material for supercapacitor [184]. It yields an energy and power density of 17.8 Wh kg^{-1} and 3.57 kW kg^{-1}, and after 2000 charge–discharge cycles, the primary capacitance of the material remains 93%. Zhang et al. employed self-templated technique to fabricate a high-performance supercapacitor based on N-doped $CoSe_2$/C double-shelled dodecahedral [185]. It exhibits a specific capacitance of 658 F g^{-1} at 2 A g^{-1} and retains 62.6% of its initial capacitance after 2000 charge–discharge cycles.

Due to good thermal, electrical, and magnetic properties, cobalt telluride (CoTe) has received much attention in the field of electrocatalysis, solar cells, photocatalysis, batteries, biosensors, and water splitting. The nanostructures CoTe have revealed several applications, especially in energy generation and storage. For the preparation of two-dimensional CoTe-based material, high temperature and reducing atmosphere are required, which makes it difficult and expensive for the large-scale production and fabrication of supercapacitors. Hence, for the first time, Manikandan et al. synthesized cobalt telluride through a hydrothermal route and used it as electrode material for the fabrication of SC [186]. It showed a high specific capacitance of 170 C/g at 0.5 A g^{-1}. The fabricated CoTe-based supercapacitor displayed an energy and power density of 40.7 Wh kg^{-1} and 800 W kg^{-1} at 1 A g^{-1} with capacitance holding at 85% over 10,000 cycles. Xiao et al. successfully synthesized highly dispersed CoTe electro through a one-step solvothermal route [187]. The synthesized regular CoTe nanowire electrode material exhibits a specific capacitance of 643.6 F g^{-1} at 1 A g^{-1} with 76.9% retention of its initial capacitance after 5000 cycles. The asymmetric supercapacitor-based CoTe nanowire displayed an energy and power density of 32.9 Wh kg^{-1} and 800.27 W kg^{-1} at 1 A g^{-1}, and after 5000 charge–discharge, it exhibits 90.5% of capacitance retention, showing good cycle performance. Mao et al. prepared $CoTe_2$ nanoflowers through a facile solvothermal method for supercapacitor applications [188]. The electrochemical performance of $CoTe_2$-based supercapacitor exhibits a high specific capacitance of 460 F g^{-1} at 1.5 A g^{-1} with 91% of its initial capacitance holding over 5000 cycles. Bhat and co-workers prepared $CoTe_2$ nanomaterial via the anion-exchange reaction method and utilized as electrode material for the application of supercapacitor, stating an electrochemical capacitance of 360 F g^{-1}. Ye et al. improved the supercapacitor performance with CoTe//AC electrode material through a facile hydrothermal route [189]. It displayed a maximum specific capacitance of 622.8 F g^{-1} at 1 A g^{-1}. The summary of various methods for the synthesis of cobalt chalcogenides based electrodes and their supercapacitor performances are given in Table 4.

4.9.5 Nickel chalcogenides

Among the family of transition metal sulfides, NiS-based material earned much attention owing to its low cost, simple fabrication, high electrical conductivity, and low toxicity nature. It exists in various stoichiometric forms and thermodynamically stable crystal structures like NiS, NiS_2, Ni_3S_2, Ni_3S_4, Ni_6S_5, Ni_7S_6, and Ni_9Se_8. Till now, many studies reported the use of nickel sulfide–based supercapacitor. But, the practical applications of nickel sulfides are hesitated because of their poor cycling stability and rate performance. To enhance the performance, designing, fabricating hierarchical nanostructures, compositing pseudocapacitive materials, and preparing materials directly on the current collectors are the main strategies. Du et al. prepared nanosheet-assembled hollow micro- and nanostructure NiS with different shapes like ellipsoid shaped, cube shaped, and capsule shaped through various morphological α-Fe_2O_3 templates [235]. Among these, the capsule-shaped NiS-based electrode yields a maximum specific capacitance of 1159 F g^{-1} at 2 A g^{-1} current density. The assembled ASC device with capsule-shaped NiS//rGO@Fe_3O_4 exhibits high energy and power density of 43.7 Wh kg^{-1} and 664 W kg^{-1} with 83.3% of initial capacitance retention even after 5000 charge–discharge cycles. Gaikar et al. worked on the growth of interconnected nanorods and nanoplates of NiS on the Ti substrate via a simple chemical bath deposition method and used it as electrode material for SCs [236]. It yields a high specific capacitance of 788 F g^{-1} at 1 mA. cm^{-2} current density with a better rate capability of 640 F g^{-1} at 50 mA. cm^{-2}, and 98% of the initial capacitance was retained after 1000 cycles. The assembled NiS electrode-based supercapacitor exhibits an energy and power density of 27.4 Wh kg^{-1} and 3.05 kW kg^{-1}, respectively. Fu et al. synthesized a novel honeycomb-like Ni_3S_2 nanosheet array electrode through a facile synthesis for supercapacitor applications [237]. It displayed a high specific capacity of 151.2 mAh/g at 3 A g^{-1} with excellent cycling stability and rate performance. Akbarzadeh et al. reported the electrochemical performance of NiS_2 nanocubes prepared by using a facile solvothermal method for high-performance supercapacitor [238]. It yields a high specific capacitance of 2077 F g^{-1} at a current density of 0.65 A g^{-1} with excellent cycling stability and rate performance. Gou et al. synthesized a hollow sphere of NiS_2 by employing a two-step hydrothermal method and castoff as electrode material for the supercapacitor [239]. It achieves a high specific capacitance of 1382.0 F g^{-1} at 1 A g^{-1} and 506.1 F g^{-1} at 20 A g^{-1} of current density. It retained the specific capacitance of 451.1 F g^{-1} after 5000 charge–discharge cycles at 10 A g^{-1}. For the first

Table 4 Summary of cobalt chalcogenide–based electrode materials with various synthesis methods and their supercapacitor performances

Electrode material for supercapacitor	Method of synthesis	Specific capacitance	Capacitance retention	Reference
Mesoporous $Co_{0.85}Se$ nanosheets on Ni foam	One-step hydrothermal method	1378 F g^{-1} @ 1 A g^{-1}	95.5% after 1000 cycles	[190]
$Co_{0.85}Se$ nanosheet	Microwave-assisted method	1580 F g^{-1} @ 1 A g^{-1}	87% after 10,000 cycles	[191]
$CoSe_2$ nanoarray	Selenization reaction	759.5 F g^{-1} @ 1 mA. cm^{-2}	94.5% after 5000 cycles	[192]
Bundle-like $Co_{0.85}Se$ nanotube on Ni foam	Ion-exchange reaction	1394 F g^{-1} @ 4 A g^{-1}	84.2% after 2000 cycles	[193]
$Co_{0.85}Se$ nanosheets on Ni foam	One-step hydrothermal method	1528 F g^{-1} @ 1 A g^{-1}	92% after 5000 cycles	[194]
Ultrathin CoSe nanosheet	Hydrothermal synthesis	70.6 mAh/g @ 1 A g^{-1}	95.4% after 20,000 cycles	[195]
CoS nanowires	Hydrothermal method	508 F g^{-1} @ 2 mA. cm^{-2}	81.2% after 500 cycles	[196]
CoS/CNT composite	Annealing method	2140 F g^{-1} @ 10 mV s^{-1}	91% after 1500 cycles	[197]
2D CoS_x	Sulfidation process	863 F g^{-1} @ 1 A g^{-1}	64.7% after 10,000 cycles	[198]
Cobalt sulfide *Hydrangea macrophylla* nanostructure on Ni foam	One-pot method	324.17 F g^{-1} @ 10 mV s^{-1}	-	[199]
CoS/CNT	Hydrothermal process	804 F g^{-1} @ 0.5 A g^{-1}	93.4% after 1000 cycles	[200]
CoS_x-NSA on Ni foam	Chemical bath deposition	47 F g^{-1} @ 10 mV s^{-1}	84% after 3000 cycles	[201]
FG-CoS nanocomposite	Simple approach	1072 F g^{-1} @ 1 mV s^{-1}	117% after 1000 cycles	[202]
Co_3S_4-NG nanocomposite	Chemical route	2427 F g^{-1} @ 2 mV s^{-1}	98.7% after 800 cycles	[203]
CoS-NP/CoS-NS DSNB	Annealing method	980 F g^{-1} @ 1 A g^{-1}	88% after 10,000 cycles	[204]
2D CoS nanosheet	Hydrothermal method	1314 F g^{-1} @ 3 A g^{-1}	91.7% after 500 cycles	[205]
CoS_2 nanocrystals	Modified molten salt synthesis	654 F g^{-1} @ 0.5 A g^{-1}	72% after 600 cycles	[206]
CoS nanocage	Facile route	1475 F g @ 1 A g^{-1}	88.2% after 1000 cycles	[207]
CoS/g-C_3N_4	Solvothermal method	668 F g^{-1} @ 2 A g^{-1}	100% after 5000 cycles	[208]
Nanocrystalline cobalt sulfide	Chemical bath deposition	252.39 F g^{-1} @ 5 mV s^{-1}	98.9% after 1000 cycles	[209]
Cubic Co_3S_4	Hydrothermal method	505.88 F g^{-1} @ 2 mV s^{-1}	74% after 1000 cycles	[210]
Co_9S_8/NF	Atomic layer deposition	1645 F g^{-1} @ 3 A g^{-1}	80% after 1500 cycles	[211]
Co_9S_8 particles	Mechanical alloying method	55 F g^{-1} @ 0.5 A g^{-1}	100% after 1500 cycles	[212]
Flower-like $Co_{1-x}S$	Solution-based route	674 F g^{-1} @ 3 A g^{-1}	72% after 1000 cycles	[213]
Co_9S_8@C	Chemical route	99.8 F g^{-1} @ 1 A g^{-1}	86% after 10,000 cycles	[214]
CoS-0.4/MMO/rGO/NF	Electrodeposition method	3074.5 F g^{-1} @ 1 A g^{-1}	87% after 5000 cycles	[215]
CoS nanosheet	Electrochemical route	1471 F g^{-1} @ 4 A g^{-1}	100% after 1000 cycles	[216]
Co_9S_8/3D-G	Glucose-assisted hydrothermal method	1721 F g^{-1} @ 16 A g^{-1}	86% after 1000 cycles	[217]
CoS/rGO	One-step approach	550 F g^{-1} @ 1 A g^{-1}	95% after 5000 cycles	[218]
Flower-like CoS	Microwave-assisted method	586 F g^{-1} @ 1 A g^{-1}	91% after 1000 cycles	[219]
CoS_x/MWCNT	Hydrothermal method	1324 F g^{-1} @ 10 A g^{-1}	87% after 2000 cycles	[220]
3D CoS/graphene hydrogel	One-step hydrothermal route	435.7 F g^{-1} @ 0.5 A g^{-1}	82.3% after 3000 cycles	[221]
rGO/CNT/Co_3S_4	One-step hydrothermal method	977 F g^{-1} @ 1 A g^{-1}	63% after 3000 cycles	[222]
Co_3S_4/rGO hybrid	Two-step hydrothermal method	2314 F g^{-1} @ 2 mV s^{-1}	92.6% after 1000 cycles	[223]
PPy/CoS/BC	In situ method	614 F g^{-1} @ 0.8 mA. cm^{-2}	62.4% after 300 cycles	[163]
Co_9S_8 nanotube/Ni foam	Two-step hydrothermal method	1775 F g^{-1} @ 4 A g^{-1}	91.4% after 2000 cycles	[224]
Porous Co_9S_8	Two-step hydrothermal method	1056 F g^{-1} @ 5 mV s^{-1}	90% after 5000 cycles	[225]
T-NT/CoS	Electrochemical route	400 F g^{-1} @ 5 mA. cm^{-2}	80% after 1000 cycles	[226]
CoS_2 nanowire	Direct method	828.2 F g^{-1} @ 10 mV s^{-1}	97.5% after 4250 cycles	[227]
3D CoS/graphene	Two-step electrodeposited method	3785 F g^{-1} @ 1 A g^{-1}	70% after 10,000 cycles	[228]
CoS/MoS_2/CC	Microwave-assisted method	406 F g^{-1} @ 10 mA. cm^{-2}	95.27% after 10,000 cycles	[229]
Dumbbell-shaped CoS	Solvothermal method	310 F g^{-1} @ 5 A g^{-1}	95% after 5000 cycles	[230]
Mo-doped CoS HNC	Dissolution-regrowth process	781.0 F g^{-1} @ 0.5 A g^{-1}	88.0% after 10,000 cycles	[231]
3D flower-like Co_9S_8	Microwave synthesis	522 F g^{-1} @ 0.5 A g^{-1}	97.7% after 1000 cycles	[232]

Table 4 (continued)

Electrode material for supercapacitor	Method of synthesis	Specific capacitance	Capacitance retention	Reference
Co_9S_8/rGO/Ni_3S_2	Hydrothermal method	2611.9 F g^{-1} @ 3.9 A g^{-1}	91.7% after 1000 cycles	[233]
PB/PBA-derived $Co_{0.85}Se$ nanoframeworks	Precipitation method	40.8 mAh/g @ 1 A g^{-1}	89% after 3000 cycles	[234]

time, Li et al. successfully prepared Ni_7S_6 hollow spheres with mesoporous shells by a facile hydrothermal method and employed as an electrode material for supercapacitor [240]. It exhibits a high specific capacitance of 2283.2 F g^{-1} at a current density of 1 A g^{-1} with 97% of capacitance retention after 1000 cycles.

Recently, a combination of various synthesis methods appears to be a significant methodology to prepare nanophase materials with different shapes, sizes, etc. Using this perception, Nandhini et al. used the combination of microwave and hydrothermal methods for the preparation of NiS nanostructures and investigated their electrochemical performance for the fabrication of supercapacitors [241]. The result displayed that the NiS-based electrode exhibits a specific capacitance of 964 F g^{-1} at 1 A g^{-1} current density with undiminished capacitance retention after 2000 cycles. Cheng et al. studied a facile electrode fabricated using ion implantation and hydrothermal sulfurization method for the synthesis of spicules-like Ni_3S_2 shell grown on Mo nanoparticle-doped Ni foam, which displayed a special hierarchical structure [242]. It employed as electrode material for the application of supercapacitor showing a specific capacitance of 361 C/g at 1 mA. cm^{-2}, and 168% of original capacitance was obtained after 2000 cycles at a current density of 20 mA. cm^{-2}.

Compared with a single component, sulfide, the composite of binary metal sulfides, can provide rich active sites for the redox reaction and thereby increase the performance of the electrochemical reaction. Chang et al. prepared the composite of Ni_3S_2 and Co_9S_8 NPs decorated on rGO through a facile synthesis and utilized as electrode material for a high-performance supercapacitor. It showed a high specific capacitance of 1929 F g^{-1} at 1 A g^{-1} of current density which is much higher than that of Co-Ni_3Se_2 (1075.5 F g^{-1})-based electrode. It exhibits a high-rate performance of 1669.2 F g^{-1} at 20 A g^{-1} with initial capacitance retention of 92.8% after 1000 cycles. Also, Gao et al. prepared novel amorphous Ni_xS_y@CoS double-shelled polyhedral nanocages through a simple facile process for the application of supercapacitor [243]. At a current density of 2 A g^{-1}, it exhibits a remarkably high specific capacitance of 2091 F g^{-1} with long-term cycle stability and excellent rate performance. Ghosh et al. prepared hierarchical Ni_3S_4 on reduced graphene oxide hydrogel@Ni foam through the hydrothermal method and utilized as electrode material for the fabrication of supercapacitor [173]. The aqueous asymmetric supercapacitor fabricated with the Ni@rGO-Ni_3S_4 electrode displayed a specific capacitance of 987.9 F g^{-1} at 1.5 A g^{-1} and retains 97.9% of primary capacitance after 3000 cycles at a current density of 12 A g^{-1}. Chen et al. fabricated a high-performance supercapacitor with interconnected 2D/3D NiS/Ni_3S_4 composite using a one-pot hydrothermal method [244]. The 2D/3D/NiS/Ni_3S_4 composite at a current density of 1 A g^{-1} exhibits a maximum specific capacitance 1796 F g^{-1} with an original capacitance holding at 80.5% after 1000 charge–discharge cycles. Li et al. prepared 3D Ni_9S_8 nanorods embedded in oxygen incorporated MoS_2 nanosheets on carbon cloth as an efficient electrode material for supercapacitor [245]. It exhibits a high specific capacitance of 907 F g^{-1} at 2 A g^{-1} with excellent cycling stability after 1200 cycles owing to its unique mutual embedding 3D nanostructure [245].

As we know, nickel and selenium have the same electronic configuration and nearby electronegative value (Ni = 1.9, Se = 2.4). Nickel selenide can occur in various compositions like NiSe, $Ni_{0.85}Se$, $NiSe_2$, and Ni_3Se_2 at room temperature. The intrinsic metallization of nickel selenide provides high electrical conductivity, and hence, it acts as an ideal electrode material. Gu et al. prepared a novel $NiSe_2$ nanoarray supported on nickel foam by using in situ hydrothermal methods and used as an efficient electrode material for flexible hybrid supercapacitor [246]. The electrochemical behavior of $NiSe_2$ nanoarray-based electrode exhibits a high specific capacitance (262 mAh/g) with an energy density of 33 Wh kg^{-1} and cycle retention of 90.3% of its initial capacitance over 5000 charge–discharge cycles. Li et al. synthesized nickel selenide thin films with different phases through a facile electrodeposition technique and utilized as electrode material for the fabrication of asymmetric supercapacitor [247]. The result obtained shows that the specific capacitance of Ni_3Se_2 and NiSe was found to be 581.1 F g^{-1} at 1 A g^{-1} and 1644.7 F g^{-1} at 2 A g^{-1} current density, respectively. These values are much comparable to those of transition metal oxides and higher than the carbonaceous materials. The cycle stability performance of Ni_3Se_2 and NiSe thin films is 90.1% and 75.0% of initial capacitance have been achieved even after 10,000 cycles. The ASC device based on the NiSe//AC device attained an energy and power density of 0.36 mWh cm^{-3} and 33.35 mW cm^{-3}, respectively. Yu et al. prepared a network of porous ultrathin NiSe nanosheets

supported on Ni foam for the fabrication of a high-performance hybrid supercapacitor [248]. The inherent nature of NiSe attained the highest specific capacity of 443 mAh/g at a current density 3 A g^{-1}. The fabricated NiSe nanosheet network/porous carbon-based hybrid supercapacitor achieved a high energy and power density of 66.6 Wh kg^{-1} and 425 W kg^{-1} with good rate performance and cycling stability. Du et al. prepared honeycomb-like metallic $Ni_{0.85}Se$ nanosheet through a one-step hydrothermal approach [249]. The specific capacitance of $Ni_{0.85}Se$ was found to be 3105 F g^{-1} at 1 A g^{-1} with capacitance retention of 90.1% after 5000 cycles.

Very recently, Eu et al. studied the electrochemical performance of Ni_3Se_2 grown on Ni foam through a simple one-step hydrothermal method with different morphologies like irregular film, nanowire array, and microspheres [250]. The result displayed that the electrode of Ni_3Se_2@Ni with irregular film, nanowire array, and microsphere exhibits high specific capacitance of 504 F g^{-1}, 592 F g^{-1}, and 816 F g^{-1} at a current density of 10 mA. cm^{-2}. Among different morphologies, the Ni_3Se_2@Ni electrode with microsphere morphology exhibits excellent electrochemical performance for the supercapacitor application and retains 85.5% of its initial capacitance after 1000 cycles.

To further enhance the electrochemical performance of a selenide-based electrode material, only vital strategy is to dope using pseudocapacitive metal ion, which may lead to a greater abundance in the redox reaction and thereby raise the specific capacitance and improve the electrochemical performances owing to the advantage of doped metal ions and the synergistic effect of host ion and the doped metal ions. Also, it provides a free diffusion path for the fast transportation of ions and facile ion accessibility to storage sites. Gu et al. hydrothermally prepared Co-doped $NiSe_2$ nanowire for the fabrication of high performance of asymmetric supercapacitor [251]. The Co@$NiSe_2$-based electrode material delivers a high specific capacitance of 3167.6 F g^{-1} at 1 A g^{-1} current density. The asymmetric supercapacitor based on the Co@$NiSe_2$ electrode attained an energy and power density of 50.0 Wh kg^{-1} and 779.0 W kg^{-1} with excellent rate performance and cycle stability. Arul et al. fabricated supercapacitor device based on $NiSe_2$/$Ni(OH)_2$ nanocomposite electrode through a facile hydrothermal method followed by ultrasonication process [252]. It attained a high specific capacitance of 2212 F g^{-1} at 2 mA. cm^{-2}, which is higher than the pure $NiSe_2$ (326 F g^{-1}) at the same current density with a capacitance retention of 95% over 5000 cycles. Gu et al. successfully prepared nitrogen-doped rGO with $NiSe_2$ nanoparticles for a high-performance supercapacitor via a two-step process with a combination of the hydrothermal and solvothermal methods [253]. At a current density of 1 A g^{-1}, the as-prepared N-rGO/$NiSe_2$ electrode displayed a high specific capacitance of 2451.4 F g^{-1}. The assembled N-rGO/$NiSe_2$ electrode-based ASC device exhibits an energy density of 40.5 Wh kg^{-1} at a power density of 841.5 W kg^{-1} with good cycling stability and rate performance. Jiang et al. used hydrothermally synthesized Ni_3Se_2 nanosheets grown on Ni foam as electrode material for supercapacitor [254]. The as-prepared Ni_3Se_2/Ni electrode delivered a high specific capacitance of 854 F g^{-1} at a current density of 1 A g^{-1}. The device based on Ni_3Se_2/Ni//AC ASC exhibits an energy density of 23.3 Wh kg^{-1} at a power density of 398.1 W kg^{-1} with initial capacitance sustained by 91.11% after 5000 cycles. Subramania et al. prepared in situ grown NiSe-G nanohybrid through a hydrothermal process and utilized as an electrode material for the application of asymmetric supercapacitor [255]. The result has shown that the NiSe-G nanohybrid electrode possesses a high specific capacitance of 1280 F g^{-1} at 1 A g^{-1} with 98% capacitance retention after 2500 cycles. The fabricated NiSe-G electrode-based ASC delivers an energy and power density of 50.1 Wh kg^{-1} and 816 W kg^{-1}, respectively. Peng et al. prepared NiSe@$MoSe_2$ nanosheet array through a facile one-step hydrothermal method and used as electrode material for ASC [256]. The prepared NiSe@MoSe2-based electrode delivered a specific capacitance of 223 F g^{-1} at 1 A g^{-1}. The fabricated asymmetric supercapacitor maintained the initial capacitance by 91.4% even after 5000 cycles and also yields an energy and power density of 32.6 Wh kg^{-1} and 415 W kg^{-1}.

Owing to the high surface area, smaller ionization energy, high mechanical stability, increasing redox-active structures, and high electrical conductivity (Te, 2×10^2 S/m), nickel telluride (NiTe) has influenced the applications of energy storage devices. Manikandan et al. have successfully prepared NiTe nanorods through the hydrothermal method by using CTAB as a surfactant and ascorbic acid as a reducing agent [257]. NiTe-based electrode material exhibits a specific capacitance of 618 F g^{-1} at 1 A g^{-1} of current density and retains 75% of its initial capacitance after 5000 charge–discharge cycles. During this process, it exhibits a coulombic efficiency of 99% which indicates that NiTe-based electrode material has good reversibility for the supercapacitor applications. Pei Zhou et al. used a facile hydrothermal method for the preparation of NiTe rods grown on Ni foam and used as positive electrode material for the fabrication of asymmetric supercapacitors [258]. It delivered a high specific capacitance of 804 F g^{-1} at 1 A g^{-1} with remarkable cycling stability 81% of capacitance retention after 3000 cycles.

Additionally, doping is the vital approach to enhance the electrochemical performance of materials, since the crystal structure, electrical behavior, and conductivity of the materials could be altered after doping of different metal and non-metal ions. Based on this concern, Ye et al. synthesized Co ion-doped NiTe supported on Ni foam through a one-step hydrothermal method and utilized as electrode material for supercapacitor. The result reveals that the

specific capacitance of the NiTe:Co electrode is significantly improved, and the highest specific capacitance is 1645.6 F g^{-1} at 1 A g^{-1} which is higher than the pristine NiTe-based electrode (872.7 F g^{-1}). Furthermore, the supercapacitor was fabricated with NiTe:Co//AC, which delivers an energy density of 36.8 Wh kg^{-1} than NiTe//AC-based supercapacitor (24.4 Wh kg^{-1}) at same power density. Deshagani et al. changed the crystal structure of NiTe by doping selenide by using a facile hydrothermal method [259]. The prepared material exhibits a specific capacitance of 943 F g^{-1} and compared with the NiTe-based electrode shows 1.5 times. Ye et al. used a one-step hydrothermal method for the preparation of Se-doped NiTe electrode materials for SC [260]. The result shows that the Se-doped NiTe electrode exhibits a high specific capacitance of 998.2 F g^{-1} at 1 A g^{-1} which is much better than the specific capacitance of NiTe electrode (603.6 F g^{-1}). Furthermore, the ASC based on Se-doped NiTe electrode delivered a superior energy and power density of 42.7 Wh kg^{-1} and 800.6 W kg^{-1} at 1 A g^{-1} with remarkable cycling stability of 76.4% retention after 10,000 cycles.

Also, Ye et al. fabricated a high-performance asymmetric supercapacitor based on NiTe/NiSe composites in situ grown on Ni foam [261]. The NiTe/NiSe-based electrode delivered a high specific capacitance of 1868 F g^{-1} at 1 A g^{-1}. The fabricated ASC based on NiTe/NiSe//AC device showed a high energy and power density of 33.7 Wh kg^{-1} and 800 W kg^{-1} with good cycling stability of 86.2% of its initial capacitance after 5000 cycles at 2 A g^{-1}. The summary of various synthesis approaches of nickel chalcogenide–based electrode materials and their supercapacitor performances are shown in Table 5.

4.9.6 Molybdenum chalcogenides

Among several pseudocapacitive dichalcogenide materials, nanostructured MoS_2 could be employed as the most auspicious two-dimensional material for the application of supercapacitors. Molybdenum disulfide (MoS_2) is the first TMDCs used as electrode material in lithium-ion batteries since it has high energy and current density, and also, it possesses high intrinsic ionic conductivity and high redox properties. MoS_2 has a two-dimensional layered structure like graphene which offers an extended surface area for the storage of charges and possesses high theoretical capacity than the graphite material. The charge storage in nanostructured MoS_2 happens through the diffusion of electrolyte ions into the inter-layer or double-layer charging on the external surface. Manuraj et al. fabricated high-performance supercapacitors with MoS_2 nanostructures grown Ni foam substrates through a simple hydrothermal process at various times. The nanostructured MoS_2 electrode exhibits a specific capacitance of 244 F g^{-1} at 1 mV. s^{-1} with corresponding capacitance retention of 92% after 9000 charge–discharge cycles. Choudhary et al. used a direct magnetron sputtering method to develop MoS_2 thin-film supercapacitor electrodes. The 3D MoS_2 film delivered a specific capacitance of ~ 330 F. cm^{-3} with a retention of 97% of its primary capacitance after 5000 cycles [334]. Huang et al. worked on the hydrothermal synthesis of MoS_2 nanosheets as an electrode for a supercapacitor, which displayed a specific capacitance of 129.2 F g^{-1} at 1 A g^{-1} withholding 85.1% of its initial capacitance after 500 cycles [335]. Karade et al. prepared ultrathin MoS_2 nanoflake electrodes through a chemical bath deposition method for the fabrication of high-performance supercapacitors [336]. At 5 mV. s^{-1}, the homogeneous ultrathin MoS_2 nanoflake electrodes achieved a specific capacitance of 576 F g^{-1} at a current density, and after 3000 cycles, it sustained with the initial capacitance by 82%. Li et al. reported the electrochemical performance of transparent 1 T-MoS_2 nanofilm through layer-by-layer self-assembly technique for high-performance supercapacitors. It exhibits a volumetric capacitance of 220 F cm^{-3} at 0.04 mA. cm^{-2} and obtained 130.6% of the original capacitance after 5000 cycles [337].

Although MoS_2 has many merits, its lower capacitance and low cycle life result in lower electrical conductivity. To overcome these demerits, doping of TMDCS with carbonaceous or any other pseudo-active materials is the only known strategy. Gupta et al. prepared two-dimensional MoS_2 and activated functionalized CNT hybrid through a one-step hydrothermal method and employed as electrode material for supercapacitor [338]. At a current density of 0.5 A g^{-1}, it exhibits a high specific capacitance of 516 F g^{-1} with a respective energy density of 71.76 Wh kg^{-1}. Li et al. synthesized vertical MoS_2 on rGO nanosheets through the hydrothermal method, which delivered a specific capacitance of 331 F g^{-1} at 0.75 A g^{-1} with good cycling retention of 110.7% of its initial capacitance even after 15,000 cycles [339]. The assembled ASC with the MoS_2/rGO electrode achieved an energy density of 29.2 Wh kg^{-1} and a power density of 4517.7 W kg^{-1}. Ali et al. worked on a mechanically exfoliated MoS_2 sheet coupled with conductive PANI as an electrode material for the supercapacitor which exhibits a specific capacitance of 510.12 F g^{-1} at a current density of 1 A g^{-1} with corresponding capacitance retention of ~ 80% after 2500 cycles [340]. Bai et al. synthesized MoS_2/rGO/PANI through a facile two-step approach involving hydrothermal and in situ polymerization method [341]. The MoS_2/rGO/PANI composites achieved a high specific capacitance of 570 F g at a current density of 1 A g^{-1} with corresponding capacitance retention of 78.6% after 500 cycles. Chanda et al. prepared hierarchical heterostructure of MoS_2 flake anchored on the TiO_2 sphere as an electrode for SCs, which achieved a specific capacitance of 152.22 F g^{-1} at 0.1 A g^{-1} current density [342].

Table 5 Summary of nickel chalcogenide–based electrode materials with various synthesis methods and their supercapacitor performances

Electrode material for supercapacitor	Method of synthesis	Specific capacitance	Capacitance retention	Ref
NiSe microspheres	Facile one-step method	492 F g^{-1} @ 0.5 A g^{-1}	~99% after 2000 cycles	[262]
Ni_3S_2/MnS composite	Hydrothermal method	6.70 mAh/cm^2 @ 2 mA. cm^{-2}	96.5% after 1000 cycles	[112]
Flower-like $Ni_{0.85}Se$	Two-step hydrothermal method	3.35 F cm^{-2} @ 4 mA. cm^{-2}	75% after 6500 cycles	[263]
$Ni_{0.85}Se$	Hydrothermal method	103.4 F g^{-1} @ 1 A g^{-1}	90.6% after 10,000 cycles	[264]
3D-Ni_3Se_2@$Ni(OH)_2$ hybrid	In situ method	281.5 mAh/g @ 3 mA. cm^{-2}	83.6% after 10,000 cycles	[265]
NiSe on Ni foam	One-step hydrothermal method	1790 F g^{-1} @ 5 A g^{-1}	70% after 1000 cycles	[266]
Cube-like$NiSe_2$	Hydrothermal method	1044 F g^{-1} @ 3 A g^{-1}	87.4% after 20,000 cycles	[267]
$Ni_{0.85}Se$	One-step alkali salt method	1354 F g^{-1} @ 1 A g^{-1}	92.4% after 20,000 cycles	[268]
$Ni_{0.85}Se$	One-step solvothermal method	114.6 mAh/g @ 1 A g^{-1}	76% after 5000 cycles	[269]
Nanoflower sphere-like $Ni_{0.85}Se$	One-pot mixing solvothermal method	1010 F g^{-1} @ 1 A g^{-1}	82.22% after 3000 cycles	[270]
NiSe@$Co_2(CO_3)(OH)_2$	Two-step soft chemistry approach	9.56 F cm^{-2} @ 4 mA. cm^{-2}	68.1% after 3000 cycles	[271]
$Ni_{0.85}Se$/P	Selenization method	506 C/g @ 1 A g^{-1}	73% after 5000 cycles	[272]
NiS/GNS/CNT	Hydrothermal method	2377 F g^{-1} @ 2 mV s^{-1}	68% after 1000 cycles	[273]
Nanoporous net-like Ni_3S_2 thin films	One-step pulse-reversal electrodeposition method	600 F g^{-1} @ 1 A g^{-1}	84.6% after 2000 cycles	[274]
TP-Ni_xS_y/rGO composite	Hydrothermal process	807 C/g @ 1 A g^{-1}	~72% after 5000 cycles	[275]
Uniform NiS_2 hollow nanoprisms	Facial sacrificial template method	1725 F g @ 5 A g^{-1}	122.9% after 10,000 cycles	[276]
Ni_3S_2/MWCNT composite	Glucose-assisted hydrothermal method	800 F g^{-1} @ 3.2 A g^{-1}	90% after 5000 cycles	[277]
Ni_3S_2/NiS@Ni_3S_4 hybrid	One-step hydrothermal method	1031 C/g @ 2 A g^{-1}	90.3% after 3000 cycles	[278]
NiS/Ni_3S_2 hybrid nanosheets	One-step solvothermal method	315 μAh. cm^{-2} @ 1 mA. cm^{-2}	86.7% after 8000 cycles	[279]
Ni_3S_2@NF	One-step hydrothermal method	736.64 F g^{-1} @ 0.8 A g^{-1}	82% after 1000 cycles	[280]
Ni_3S_2@Ni	One-step solvothermal method	945.71 F g^{-1} @ 17.15 A g^{-1}	100% after 2000 cycles	[281]
Ni_3S_2@$Co(OH)_2$ nanowires grown on Ni foam	Facile two-step process	2139 F g^{-1} @ 2 mA. cm^{-2}	93.7% after 3000 cycles	[282]
NiS/PEDOT:PSS composite	Facile synthesis	750.64 F g^{-1} @ 1.11 A g^{-1}	91.2% after 3000 cycles	[283]
NiS/d-Ti_3C_2 nanohybrid	Solvothermal method	840.4 C/g @ 1 A g^{-1}	64.3% after 10,000 cycles	[284]
Hierarchical NiS microspheres	Trimethylamine-assisted hydrothermal method	606 C/g @ 0.5 A g^{-1}	93% after 2000 cycles	[285]
Ni_3S_2@C/rGO		1023.44 F g^{-1} @ 5 A g^{-1}	70.1% after 5000 cycles	[286]
Ni_3S_2@rGO@NiAl-LDHs composite	Hydrothermal method	2026 F g^{-1} @ 1 A g^{-1}	87.7% after 10,000 cycles	[287]
Ni_3S_2@PEDOT	Electrodeposition method	1589.3 F g^{-1} @ 2 A g^{-1}	75.5% after 2000 cycles	[288]
Ni_3S_2-Co_9S_8/NF	One-pot solvothermal method	5.37 F. cm^2 at 5 mA. cm^{-2}	80% after 1000 cycles	[289]
Ni@rGO-Ni_3S_2 composite	Two-step hydrothermal method	987.8 F g^{-1} @ 1.5 A g^{-1}	97.9% after 3000 cycles	[173]
NiS/Ni_3S_4 composite	Hydrothermal method	194.4 mAh/g @ 2 A g^{-1}	65.8% after 6500 cycles	[290]
NiS_2/ZnS composite	MOF-derived self-sacrificing route	1198 F g^{-1} @ 1 A g^{-1}	87% after 1000 cycles	[291]
Ni_3S_2 nanorod/nanowire array on Ni foam	Post hydrothermal method	4.52 F. cm^{-2} @ 1.25 mA. cm^{-2}	108.3% after 2000 cycles	[292]
Ni_3S_2@β-NiS	One-step solvothermal method	1158 F g^{-1} @ 2 A g^{-1}	97.4% after 2000 cycles	[293]
Nanostructured NiS	Alternate dip coating method	1044 F g^{-1} @ 1 mA. cm^{-2}	53.1% after 1000 cycles	[294]
Nanoporous nickel sulfide/rGO	Hydrothermal method	1312 F g^{-1} @ 5 mV. s^{-1}	86% after 500 cycles	[295]
Ni_3S_2/Ni	One-pot hydrothermal method	1293 F g^{-1} @ 5 mA. cm^{-2}	69% after 1000 cycles	[296]
Ni_3S_2 film on Ni foam	One-step hydrothermal method	2230 F g^{-1} @ 5 mA. cm^{-2}	91% after 3000 cycles	[297]
NiS_{x-n}//CC	One-step hydrothermal method	1340 F g^{-1} @ 1 A g^{-1}	94.5% after 5000 cycles	[298]
α-NiS	Phase controlled solvothermal method	800 F g^{-1} @ 0.5 A g^{-1}	81.2% after 2000 cycles	[299]
Ni_3S_4@rGO composite	In situ hydrothermal method	1830 F g^{-1} @ 2 A g^{-1}	91.4% after 10,000 cycles	[300]
Ni_3S_4@MoS_2 nanosheets/CFP	One-step hydrothermal method	1296 F g^{-1} @ 1 A g^{-1}	96.2% after 5000 cycles	[301]

Table 5 (continued)

Electrode material for supercapacitor	Method of synthesis	Specific capacitance	Capacitance retention	Ref
3D Ni_3S_2 on Ni foam	One-step hydrothermal method	1370.4 F g^{-1} @ 2 A g^{-1}	91.4% after 1000 cycles	[302]
Ni_3S_2-$Cu_{1.8}S$ nanosheet	In suit ion-exchange method and one-pot hydrothermal method	1686 F g^{-1} @ 1 A g^{-1}	95.39% after 10,000 cycles	[303]
NiS/NHCS composite	Multistep transformation approach	1150 F g^{-1} @ 1 A g^{-1}	76% after 4000 cycles	[304]
Ni_3S_2/rGO composite	Hydrothermal and pyrolysis method	1315 F g^{-1} @ 1 A g^{-1}	85.6% after 5000 cycles	[305]
3D GNs/Ni_3S_2 composite	Q-CVD technique	652.5 F g^{-1} @ 1 A g^{-1}	93% after 2000 cycles	[306]
Ni_3S_2 film	Solvothermal-assisted sulfuration method	3.42 F cm^{-2} @ 1 mA. cm^{-2}	102% after 4250 cycles	[307]
C@Ni_3S_2@MoS_2 nanorods	Hydrothermal method	1544 F g^{-1} @ 2 A g^{-1}	92.8% after 2000 cycles	[308]
NiS hollow microsphere with mesoporous shell	Hydrothermal method	1848.0 F g^{-1} @ 1 A g^{-1}	74.3% after 1000 cycles	[309]
NiS hexagonal nanoplates	Anion-exchange method	1897 F g^{-1} @ 1 A g^{-1}	100% after 4000 cycles	[310]
NiS NPs	Microwave-assisted method	845 F g^{-1} @ 1 A g^{-1}	81.6% after 1000 cycles	[311]
Mesoporous NiS hierarchical structure	Solvothermal method	11.15 F g @ 0.16 A g^{-1}	~88.57% after 5000 cycles	[312]
NiS thin film	Chemical bath deposition method	750.6 F g^{-1} @ 5 mV. s^{-1}	85.3% after 3000 cycles	[313]
NiS nanostructure	Hydrothermal method	1073.8 F g^{-1} @ 1.2 A g^{-1}	89% after 1000 cycles	[314]
NiS_2 nanocubes	Microwave-assisted method	695 F g^{-1} @ 1.25 A g^{-1}	93.4% after 3000 cycles	[315]
Graphene-wrapped Ni_3S_2 nanocubes	One-step hydrothermal method	616 C/g @ 1 A g^{-1}	92.7% after 5000 cycles	[316]
Ni_3S_2@polypyrrole/Ni foam	Hydrothermal electrodeposition method	1.13 F. cm^{-2} @ 30 mA. cm^{-2}	100.10% after 3000 cycles	[317]
NiS hierarchical hollow cubes	Anion-exchange reaction	874.5 F g^{-1} @ 1 A g^{-1}	90.2% after 3000 cycles	[318]
Ni_3S_2/CNT composite	Electrodeposition and ion-exchange method	1643 F g^{-1} @ 1 A g^{-1}	91.5% after 2000 cycles	[319]
NiS-PbS composite	Chemical bath deposition method	125.89 mAh/g @ 2 A g^{-1}	88.97% after 3000 cycles	[320]
R-NiS/rGO composite	In situ sulfuration transformation method	744 C/g @ 1 A g^{-1}	89% after 20,000 cycles	[321]
NiS NTs/Ni foam	Wet chemistry approach	752.71 μAh. cm^{-2} @ 4 mA. cm^{-2}	89.4% after 3000 cycles	[322]
N-doped GN/nickel sulfide composite	Hydrothermal method	1120 F g^{-1} @ 1 A g^{-1}	82% after 3000 cycles	[323]
Square rod-like NiS_2	General solution method followed by post-annealing technique	1020.2 F g^{-1} @ 1 A g^{-1}	93.4% after 1000 cycles	[324]
NiS/C-dot composite	Hydrothermal method	880 F g^{-1} @ 2 A g^{-1}	~99% after 2000 cycles	[325]
3D hemp-activated carbon/Ni_3S_2 composite	Electrodeposition method	2797.43 F g^{-1} @ 1 A g^{-1}	83.4% after 10,000 cycles	[326]
Carbon sphere@nickel sulfide	Low-temperature water bath method	1022 F g^{-1} @ 1 A g^{-1}	~83% after 4000 cycles	[327]
α-NiS NPs embedded carbon NRs	Phase-controlled and in situ sulfuration method	1092 F g^{-1} @ 10 A g^{-1}	100% after 2000 cycles	[328]
Cabbage-like α-NiS	Solvothermal followed by annealing method	235.88 mAh/g @ 1 A g^{-1}	87.1% after 2000 cycles	[329]
NiS/GO nanocomposite	Hydrothermal method	800 F g^{-1} @ 1 A g^{-1}	-	[330]
Ni_3S_2@CdS core–shell structure	Hydrothermal method	2100 F g^{-1} @ 2 mA. cm^{-2}	86.7% after 4000 cycles	[49]
Ni_3S_4microflower	Hydrothermal method	1797.5 F g^{-1} @ 0.5 A g^{-1}	93% after 5000 cycles	[331]
Co-Ni_3S_2@CNT/GNF	Hydrothermal method	4.1 F. cm^{-2} @ 1 mA.cm^{-2}	89.8% after 1000 cycles	[332]
CuSe-decorated $NiSe_2$ nanocubes	Hydrothermal method	376 C/g @ 1 A g^{-1}	91.7% after 10,000 cycles	[333]

Chang et al. synthesized MoS_2/PPy nanocomposite via hydrothermal approach and employed as an electrode material for the application of supercapacitor [343]. The MoS_2/PPy electrode material delivered a specific capacitance of 307.5 F g^{-1} which is much higher than the pristine MoS_2 (138.5 F g^{-1}) and polypyrrole (106.3 F g^{-1}) at a current density of 1 A g^{-1} with excellent cycling stability of 96.47% after 1000 charge–discharge cycles. For the first time, Chao et al. synthesized oxygen-incorporated MoS_2/PANI/rGO hierarchical nanosheet composite through oxygen incorporation and polyaniline intercalation method and used it as an efficient electrode material for the fabrication of SCs [344]. At a current density of 1 A g^{-1}, MoS_2/PANI/rGO hierarchical nanosheet composite exhibits a specific capacitance of 752.0 F g^{-1} using a three-electrode system. Fan et al. reported the electrochemical performance of mesoporous MoS_2/C composite through a facile hydrothermal method and employed it as an electrode for SC. The specific capacitance of MoS_2/C composite was found to be 201.4 F g^{-1} at 0.2 A g^{-1} with excellent cycling stability and rate performance, which is much higher than that of pristine MoS_2 and carbon [345]. For the first time, Niu et al. synthesized Mo_2S_3@Ni_3S_2 nanowires on a nickel foam through a simple CTAB-assisted hydrothermal method [346]. The Mo_2S_3@Ni_3S_2 nanowire electrode unveils a high specific capacitance of 998.9 F g^{-1} at 1 A g^{-1} with outstanding retention of 90.55% of its initial capacitance after 650 cycles.

The monolayer MoS_2 is known to have two phases, namely the trigonal prismatic phase and the octahedral phase. The trigonal prismatic phase is labeled as 2H with a space group of D_{3h}, while the octahedral phase is labeled as 1 T with a space group of O_h. The 2H phase is relatively stable but semiconducting and of poor conductivity, while the 1 T phase is metastable under room temperature but metallic and of better conductivity. Recently, the metallic 1 T phase was reported to be of great advantage for MoS_2 NS-based supercapacitors. But if the higher conductivity of 1 T phase and the higher stability nature of the 2H phase can be hybridized in monolayer MoS_2, both high charge transportation and large specific surface area will be gained which are the most beneficial factors for supercapacitors. Based on this perspective, Jiang et al. synthesized 1 T-2H phase hybridization of monolayer MoS_2 through a chemical exfoliated method. The electrochemical performance of 1 T-2H monolayer MoS_2 was observed to be 366.9 F g^{-1} at 0.5 A g^{-1} withholding the stability at 92.2% of its initial capacitance after 1000 cycles [347].

As like graphene, molybdenum chalcogenides, MX (where M = Mo, and X = S, Se, and Te), has a layered structure which arose as one of the most promising candidates for the sensor, phototransistors, catalysis, and energy storage devices owing to their distinctive crystal structures and diverse material properties. These types of chalcogenide materials interact through strong chemical bonds in the molecular layers, while the individual layers interact via weak Van der Waals force of attraction, materializing a graphene-like layered structure. This layered structure is favorable for the insertion and extraction of a variety of ions in the electrolyte. Among various Mo-based chalcogenides, $MoSe_2$ has received much attention in the field of energy storage devices. $MoSe_2$ has a layered structure of Se-Mo-Se, with a narrow band gap and interlayer spacing of 0.646 nm. The interlayer spacing of $MoSe_2$ is much higher than that of MoS_2 (0.615 nm) and graphite (0.335 nm). Gao et al. prepared a sphere-feature $MoSe_2$ with excellent electrochemical activity through a facile hydrothermal method [348]. The electrochemical performance of $MoSe_2$ spheres yields a high specific capacitance of 243 F g^{-1} at 0.5 A g^{-1} and recollects 90.3% of its initial capacitance over 1000 cycles at a current density of 1 A g^{-1}. For the first time, Aziz and co-workers synthesized a hierarchical nanostructure of orthorhombic Mo_9Se_{11} through colloidal processing and utilized as an electrode for the application of asymmetric supercapacitor [349]. At a current density of 5 mV. s^{-1}, it yields a specific capacitance of ~ 510 F g^{-1}. The cycle life of the Mo_9Se_{11} electrode retains about 60% of its initial capacitance after 4000 cycles. Jia et al. used a simple and facile solvothermal method for the preparation of a $MoSe_2$ microsphere composed of 2D nanosheets, and at a current density of 1 A g^{-1}, it exhibits a specific capacitance of 272 F g^{-1} [350].

Although $MoSe_2$ has several advantages, the poor electrical conductivity of $MoSe_2$ obstructs its electrochemical performance and practical application. Hence, a frequently employed strategy to further raise the electrochemical performance of $MoSe_2$ includes a novel design of hybrid nanostructures with carbon-based or any other electrically active materials. Balasingam et al. developed a new $MoSe_2$/rGO composite nanosheet using a simple and straightforward hydrothermal process and used as an electrode material for supercapacitor applications [351]. The $MoSe_2$/rGO-based electrode delivered a high specific capacitance of 211 F g^{-1} at a scan rate of 5 mV. s^{-1} and gained 180% of its primary capacitance over 10,000 cycles. Lately, isoelectronic doping in Mo-based chalcogenides has received considerable attention attributing to the impeding generation of defects and dislocations and ease of alloy formation. In this perspective, Bhat et al. worked on the preparation of tungsten-doped $MoSe_2$/graphene through a facile hydrothermal method for the supercapacitor. The W-$MoSe_2$/G electrode possesses a specific capacitance of 248 F g^{-1} with capacitance retention of 102% after 20,000 cycles. Karade et al. prepared a 2D cryptomelane-like $MoSe_2$ on MWCNT hybrid film through a "dip and dry" method followed by the CVD technique. The $MoSe_2$/MWCNT hybrid electrode exhibits a specific capacitance of 232 F g^{-1} at a current density of

1.4 A g^{-1} with an outstanding cyclic stability of 93% after 1000 cycles [352]. Huang et al. prepared a porous layered $MoSe_2$-graphene composite on nickel foam for the application of the high performance of supercapacitor [353]. It showed a high specific capacitance of 1422 F g^{-1} at 1 A g^{-1} with retention of 100.7% even after 1500 cycles.

Li et al. synthesized the 3D $MoSe_2$-acetylene black electrode through a facile hydrothermal method [354]. At a current density of 1 A g^{-1}, the 3D $MoSe_2$/AB composite shows a high specific capacitance of 2020 F g^{-1} with good cycling stability of 107.5% after 1500 cycles. He et al. synthesized $MoSe_2$ nanosheets wrapped on carbon aerogel nanospheres as an efficient electrode material for supercapacitor which showed a specific capacitance of 775.3 C/g with capacitance retention of 98% after 1500 cycles at a current density of 1 A g^{-1} [355]. Kirubasankar et al. synthesized a 2D-2D $MoSe_2$/graphene nanohybrid through a sonochemical method and employed as an electrode for supercapacitor [356]. The $MoSe_2$/graphene nanohybrid shows a maximum specific capacitance of 945 F g^{-1} at a current density of 1 A g^{-1}. The fabricated asymmetric supercapacitor with $MoSe_2$/graphene hybrid electrode yields an energy and power density of 26.6 Wh kg^{-1} and 0.8 kW kg^{-1} with better cycling stability of 88% of its initial capacitance even after 3000 cycles. Also, Kirubasankar et al. prepared 2D $MoSe_2$/$Ni(OH)_2$ nanohybrid through a one-step hydrothermal method [357]. The 2D $MoSe_2$/$Ni(OH)_2$ electrode delivered a high specific capacitance of 1175 F g^{-1} at 1 A g^{-1} which is much higher than the $Ni(OH)_2$ nanosheets (933 F g^{-1}) under same current density. The fabricated asymmetric supercapacitor based on 2D $MoSe_2$/$Ni(OH)_2$ nanohybrid achieved an energy and power density of 43 Wh kg^{-1} and 8181 W kg^{-1} with a retention of 91.6% of its initial capacitance after 5000 charge–discharge cycles. The summary on various synthesis methods of molybdenum-based electrode materials and their supercapacitor performances are shown in Table 6.

5 Bimetal chalcogenides and its composites

The combination of two different metals will improve the redox chemistry of the electroactive materials and their performance when compared to single-metal sulfides. Binary metal chalcogenides and their composites have been studied vastly owing to their extensive properties like good electrical conductivity, high catalytic activity, and redox potential and low electronegativity. But very recently, bimetal chalcogenides and its composites showed superior electrochemical performance compared to their corresponding counterparts, owing to their multiple oxidation states and high redox properties. Cai et al. developed a composite of honeycomb-like nickel manganese sulfide nanosheet on carbon cloth via a facile two-step approach, which delivers a specific capacitance of 205 mAh/g at 2 mA. cm^{-2} [397]. The fabricated supercapacitor exhibits an energy and power density of 27.3 Wh kg^{-1} and 505.2 W kg^{-1} with retaining at 75.3% of its initial capacitance after 6000 cycles. Cao et al. used a one-pot approach for the preparation of porous nickel-manganese sulfides with tunable compositions [398]. The optimized nickel-manganese sulfides employed as an electrode exhibits a specific capacitance of 1068 F g^{-1} at 1 A g^{-1} current density. Chen et al. studied the electrochemical performance of Co_xMn_{3-x} sulfides by changing Co/Mn ratios through solvothermal techniques [399]. Among various compositions, $Co_{2.5}Mn_{0.5}$ sulfide showed a high specific capacitance of 289 C/g at 1 A g^{-1} with outstanding cycling stability of 95.1% after 2000 cycles. Peng et al. reported the electrochemical performance of supercapacitor fabricated with heterostructure cobalt manganese sulfide (CMS) nanoneedle arrays by a low-temperature hydrothermal method [400]. The as-obtained CMS nanoneedles exhibit a specific capacity of 0.53 mAh. cm^{-2} at 2 mA. cm^{-2} with a cycle life of 93.7% of capacitance retaining after 1500 cycles. Bolagam et al. successfully fabricated the pseudocapacitor based on cobalt ruthenium sulfides through a simple hydrothermal method, which exhibits a specific capacitance of 75 F g^{-1} at 1 A g^{-1} with retention of 81% of its initial capacitance after 1000 cycles [401]. Pazhamalai et al. developed an ASC based on copper tungsten sulfide grown on Ni foam binder-free electrodes, which showed an outstanding specific capacitance of 2666.6 F g^{-1} at a current density of 10 mA. cm^{-2} [402]. The electrochemical behavior of copper tungsten sulfides/Ni/graphene possesses a high energy and power density of 48.57 Wh kg^{-1} and 102 μWh cm^{-2} with better cycle life over 10,000 cycles. Du et al. prepared a high-performance hybrid supercapacitor based on nanoporous nickel-copper sulfide/carbon cloth through an anion-exchange reaction, which delivers a high specific capacitance of 936 F g^{-1} at 1 A g^{-1} with better rate performance of 76% [403].

Nguyen et al. demonstrated the synthesized procedure of the bimetal selenide system of nickel-vanadium selenide ($Ni_xV_{3-x}Se_4$) and nickel–iron selenide ($Ni_xFe_{3-x}Se_4$) through a facile and simple hydrothermal method followed by selenization for flexible asymmetric supercapacitors (Fig. 14) [84]. The prepared NiV_2Se_4 and $NiFe_2Se_4$ electrodes showed a specific capacitance of ~ 329 and 261 mAh/g at a current density of 1 mA. cm^{-2} with rate performance of 79.33% and 77.78% and excellent cycling stability of 98.6% and 97.9% after 10,000 cycles, respectively. The fabricated flexible ASC based on NiV_2Se_4//$NiFe_2Se_4$ electrodes exhibits a high energy and power density of 73.5 Wh kg^{-1} and 0.733 kW kg^{-1} with capacitance retention of 96.6% after 10,000 cycles (Fig. 15). Deka et al. fabricated a supercapacitor based on copper-cobalt selenide nanowire-anchored woven carbon fiber, which showed an energy density of

Table 6 Summary of molybdenum chalcogenide–based electrode materials with various synthesis methods and their supercapacitor performances

Electrode material for supercapacitor	Method of synthesis	Specific capacitance	Capacitance retention	Ref
$MoSe_2$/Ni	Electrochemical deposition method	548 mAh/kg @ 5 mV s^{-1}	80% after 1000 cycles	[358]
$MoSe_2$@CN	Hydrothermal method	101.3 mF.cm^{-2} @ 5 mV. cm^{-2}	80% after 10,000 cycles	[359]
$MoSe_2$ NFs//$MoSe_2$NRs	Hydrothermal method	133 F g^{-1} @ 2 A g^{-1}	92% after 2000 cycles	[360]
2H-$MoSe_2$ nanosheets	Hydrothermal method	25.31 F g^{-1} @ 5 mV s^{-1}	87% after 10,000 cycles	[361]
$MoSe_2$/rGO	One-pot hydrothermal method	814.4 F g^{-1} @ 1 A g^{-1}	81.7% after 5000 cycles	[362]
MoS_2/NPG composite	One-pot hydrothermal method	588 F g^{-1} @ 1 A g^{-1}	91.67% after 5000 cycles	[363]
Mn incorporated MoS_2 nanoflowers	One-step hydrothermal method	430 F g^{-1} @ 10 A g^{-1}	77% after 5000 cycles	[364]
MoS_2/graphene	Electrospinning process	334 F g^{-1} @ 0.5 A g^{-1}	83.8% after 5000 cycles	[365]
Few-layered MoS_2	Solvothermal method	330.8 F g^{-1} @ 2 A g^{-1}	88.8% after 5000 cycles	[366]
HGRs/MoS_2/MnO_2 composite	CVD and hydrothermal method	608 F g^{-1} @ 1 A g^{-1}	89.3% after 2500 cycles	[367]
MoS_2/PANI/rGO HNSs	Hydrothermal method	330.7 F g^{-1} @ 10 A g^{-1}	81.9% after 40,000 cycles	[368]
$MoSe_2$/CNT nanocomposite	One-step hydrothermal method	74.05 F g^{-1} @ 2 A g^{-1}	80.8% after 1000 cycles	[369]
MoS_2/MWCNT	Hydrothermal and in-situ polymerization method	255.8 F g^{-1} @ 1 A g^{-1}	91.6% after 1000 cycles	[370]
MoS_2/N-doped carbon shell	Self-polymerization technique	276 F g^{-1} @ 1 A g^{-1}	90.59% after 6000 cycles	[371]
MCMoS_2/rGO	Microwave heating	265 F g^{-1} @ 10 mV s^{-1}	92% after 1000 cycles	[372]
ACFTs/MoS_2	Hydrothermal method	308.5 F g^{-1} @ 5 mV s^{-1}	97.38% after 6000 cycles	[373]
MoS_2 nanoflakes	Freeze-drying method	0.11 F g^{-1} @ 500 mV s^{-1}	~40% after 500 cycles	[374]
MoS_2/3D graphene	Hydrothermal method	2182.33 mF.cm^{-2} @ 1 mA.cm^{-2}	116.83% after 5000 cycles	[375]
MoS_2/MWCNT	Two-step hydrothermal method	452.7 F g^{-1} @ 1 A g^{-1}	95.8% after 1000 cycles	[376]
MoS_2/carbon matrix	Microwave hydrothermal method	589 F g^{-1} @ 0.5 A g^{-1}	104% after 2000 cycles	[377]
MoS_2/Mo	Hydrothermal method	192.7 F g^{-1} @ 1 mA.cm^{-2}	98% after 1000 cycles	[378]
MoS_2-Co_3S_4	Solvothermal method	1369 F g^{-1} @ 1 A g^{-1}	83% after 10,000 cycles	[379]
MoS_2/rGO@PANI	Hydrothermal-polymerized method	1224 F g^{-1} @ 1 A g^{-1}	82.5% after 3000 cycles	[380]
MoS_2/CoS_2 composite	One-step hydrothermal method	490 F g^{-1} @ 2 mV s^{-1}	93.1% after 1000 cycles	[381]
MoS_2/$NiCo_2S_4$@C HMSs	Self-template method	250 mAh/g @ 2 A g^{-1}	90.1% after 10,000 cycles	[382]
MoS_2@HCS	Glucose-assisted one-pot synthesis	458 F g^{-1} @ 1 A g^{-1}	86% after 1000 cycles	[383]
MoS_2-rGO-WS_2 composite	Simple chemical method	365 F g^{-1} @ 1 A g^{-1}	70% after 3000 cycles	[384]
MoS_2/Ni_3S_2 composite	One-pot hydrothermal method	~1.033 C/cm^2 @ 1 mA. cm^{-2}	62.5% after 10,000 cycles	[385]
Carbon-MoS_2 composite	Co-growth mechanism	1000 F g^{-1} @ 1 A g^{-1}	93% after 20,000 cycles	[386]
MoS_2/MoO_x	Microwave- assisted hydrothermal	230 F g^{-1} @ 5 mV s^{-1}	128% after 1500 cycles	[387]
O-MoS_2 microsphere	Hydrothermal method	744.2 F g^{-1} @ 1 A g^{-1}	77.8% after 10,000 cycles	[388]
carbon@MoS_2/MoO_2nanosphere	Facile method	569 F g^{-1} @ 1 A g^{-1}	81% after 5000 cycles	[389]
MoS_2/Mn_3O_4 nanostructure	Hydrothermal-chemical precipitation method	119.3 F g^{-1} @ 1 A g^{-1}	69.3% after 2000 cycles	[390]
Rambutan-like MoS_2/Carbon sphere	Two-step hydrothermal method	411 F g^{-1} @ 1 A g^{-1}	93.2% after 1000 cycles	[391]
Flower-like MnP-MoS_2	Hydrothermal method	432.3 F g^{-1} @ 1 A g^{-1}	84.4% after 2000 cycles	[392]
Flower-like MoS_2/rGO	Hydrothermal method	352 F g^{-1} @ 0.2 A g^{-1}	-	[393]
SeMoTe	Wet chemical method	1057 F g^{-1} @ 1 A g^{-1}	97% after 5000 cycles	[394]
MoS_{3-x}@3DnCF	Hydrothermal method	97.5 mF. cm^{-2} @ 0.5 mA. cm^{-2}	-	[395]
Mn-incoporated MoS_2 nanoflowers	Hydrothermal method	430 F g^{-1} @ 1 A g^{-1}	77% after 5000 cycles	[396]

191.64 mWh kg^{-1} and power density of 36.65 W kg^{-1} with retention of 77.3% of its initial capacitance [404]. Du et al. used a two-step method involving hydrothermal and cation-exchange process for the preparation of $(Ni_{0.5}Co_{0.5})_{0.85}Se$ nanosheet arrays which possesses high electrochemical properties. The supercapacitors fabricated with $(Ni_{0.5}Co_{0.5})_{0.85}Se$ possesses an energy and power density of 70.58 Wh kg^{-1} and 320.02 W kg^{-1} with 91.88% capacitance retention after 8000 charge–discharge cycles.

Guo et al. used different ratios of Ni and Co for preparing a series of ternary materials through the co-exchange method and fabricated a supercapacitor based on $Ni@Ni_{0.8}Co_{0.2}Se$

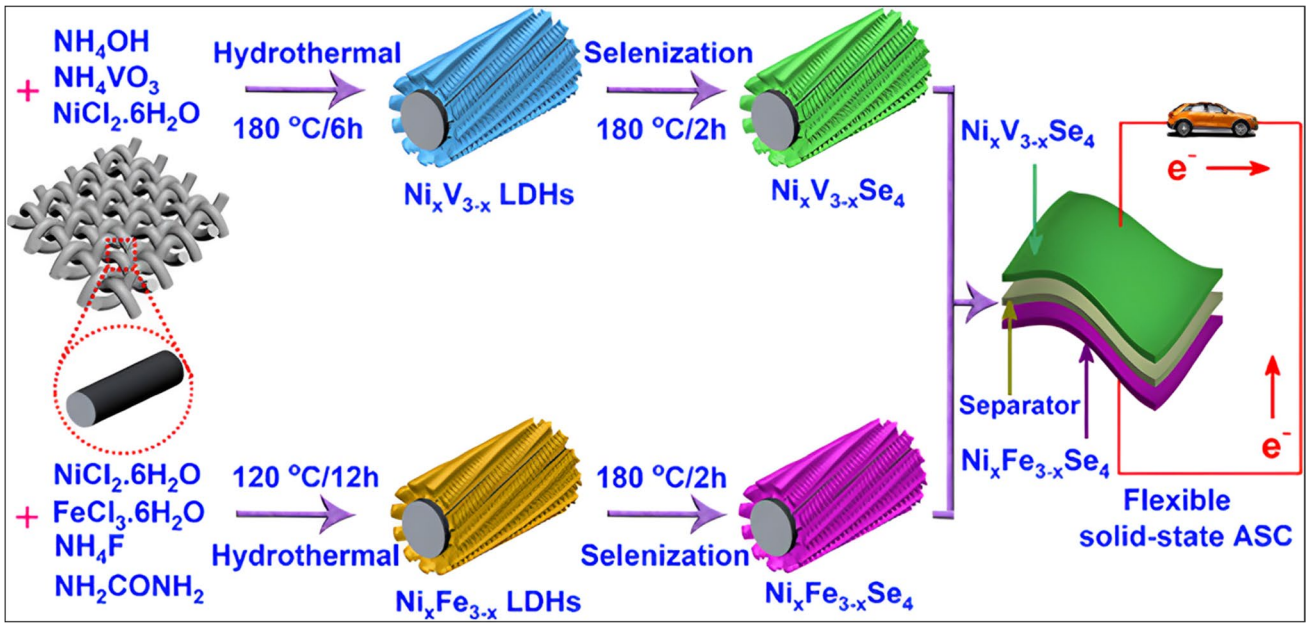

Fig. 14 Schematic representation for the design and fabrication of hierarchical $Ni_xV_{3-x}Se_4$ and $Ni_xFe_{3-x}Se_4$ nanostructures for solid-state ASCs, images are reproduced with permission from ref. [84] under Copyright © 2019, American Chemical Society

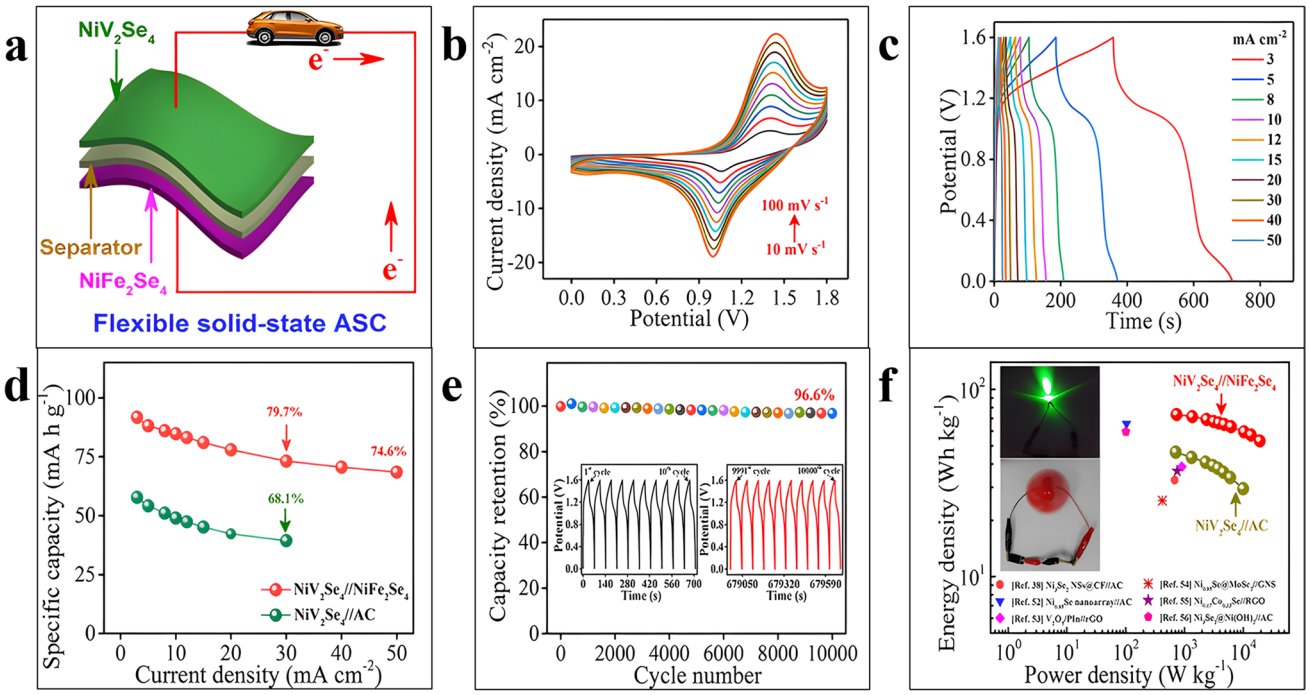

Fig. 15 Electrochemical performance of the NiV_2Se_4//$NiFe_2Se_4$ ASC device, **a** schematic illustration of the assembled ASC with NiV_2Se_4 and $NiFe_2Se_4$ electrodes, **b** CV curves of the flexible ASC at scan rates from 10 to 100 mV s^{-1}, **c** GCD curves of the flexible ASC at current densities from 1 to 50 A g^{-1}, **d** specific capacity values as a function of applied current densities for the flexible ASC, **e** cycling performance of the flexible ASC exemplified at 20 mA. cm^{-2} with 10,000 charge–discharge cycles (the inset shows the first and last ten GCD cycles), and **f** Ragone plot of the flexible ASC as compared with the reported literature, images are reproduced with permission from ref. [84] under Copyright © 2019, American Chemical Society

electrode which exhibits high energy and power density of 17 Wh kg^{-1} and 1526.8 W kg^{-1}, respectively [405]. Hu et al. designed a series of hierarchical nickel cobalt selenide NPs/NSs through a low-temperature selenization method for fabricating a high-performance supercapacitor [406]. The electrochemical performance of $Ni_{0.67}Co_{0.33}Se$ NPs/NSs at a current density of 1 A g^{-1} exhibited a large specific capacitance of 447 C/g and retains 97% of initial capacitance after 2000 cycles. Quan et al. designed a hierarchical nanostructure of nickel cobalt selenide $(Ni_{0.33}Co_{0.67})Se_2$ complex with improved electrochemical performance via a facile ion-exchange reaction [407]. The specific capacitance of the optimized complex is observed to be 827.9 F g^{-1} at a current density of 1 A g^{-1}. Wang et al. explored the improvement of the electrochemical performance of supercapacitors by preparing $Ni_{0.6}Co_{0.4}Se_2$ electrode through a hydrothermal method [408]. At 1 A g^{-1}, it exhibits a superior specific capacitance of 606.6 C/g retaining 91.0% of initial capacitance after 5000 cycles. Xie et al. investigated the electrochemical performance of the $Ni_xCo_{1-x}Se_2$ series by fabricating a high-performance asymmetric supercapacitor [409]. At 1 A g^{-1} current density, it exhibits a high specific capacitance of 1580 F g. The assembled ASC with $Ni_{0.6}Co_{0.4}Se_2$-based electrode exhibits high energy and power density of 44.1 Wh kg^{-1} and 691.3 W kg^{-1} with long cycling stability. Cheng et al. designed a novel core–shell structure $ZnCo_2S_4$ electrode through a solvothermal method, which delivered a specific capacitance of 1045.3 F g^{-1} at 2 A g^{-1} and retains 95.5% of its initial capacitance after 5000 charge–discharge cycles [410]. Elshahawy et al. prepared sulphospinel $MnCo_2S_4$ material through a controlled sulfurization method, which offers an excellent specific capacitance of 938 F g^{-1} at 20 A g^{-1} and retains about 95% of its capacitance after 5000 cycles [411]. The assembled hybrid supercapacitor delivered an energy and power densities of 43 Wh kg^{-1} at 0.801 kW kg^{-1}, respectively. Guo et al. used a straightforward hydrothermal process to create crystalline and amorphous copper-cobalt sulfide, which is then examined as an electrode material for supercapacitor applications [412]. Among various samples, the sample $CuCo_2S_4$ prepared at 150 °C attained a highest specific capacitance of 515 F g^{-1} at 1 A g^{-1} with ~ 93.3% of capacitance retention over 10,000 cycles. Huang et al. works on tip-welded ferric-cobalt sulfide hollow nanoneedles on conductive carbon fibers through a two-step sulfidation technique and researched as electrode material for supercapacitor [413]. It showed a high specific capacitance of 2282 F g^{-1} at 1 A g^{-1} with 82.3% of capacitance retention after 5000 cycles. Ai et al. worked on nanostructured $CoNi_2S_4$ with various morphologies grown on carbon cloth through a facile precursor transformation method by adjusting the anions in nickel and cobalt salts [414]. The as-prepared $CoNi_2S_4$ electrodes attained a specific capacitance of 2714 F g^{-1} at a current density of 1 A g^{-1} and retain long-term cycling stability and excellent rate capability. Beka et al. used a simple two-step hydrothermal method for the preparation of coral-like $CoNi_2S_2$ grown on NF and researched as supercapacitor electrode material [415]. The as-obtained sample exhibits a high specific capacitance of 2864 F g^{-1} at 1 A g^{-1} with extraordinary cycling life of ~ 117% over 10,000 continuous cycles. Liang et al. designed a novel hierarchical core–shell and hollow structure of $CoNi_2S_4$ using TEOA-assisted hydrothermal method and investigated their electrochemical performance for supercapacitor application [416]. The prepared $CoNi_2S_4$ nanospheres achieved an ultrahigh specific capacitance of 2035 F g^{-1} at 1 A g^{-1} with superior cycling stability of about 91.3% after 3000 cycles. Anthuvan et al. synthesized a rambutan-like cobalt–nickel sulfide ($CoNiS_4$) through a one-step hydrothermal method for improving the electrochemical performance of supercapacitor [417]. The as-synthesized $CoNi_2S_4$ sample at 1 A g^{-1} achieved a specific capacitance of 1102.22 F g^{-1} with 75% capacitance retention over 3000 cycles.

For the first time, Zhang et al. improved the electrochemical performance of supercapacitors by synthesizing nickel cobalt telluride grown on Ni foam through a simple solvothermal method followed by an ion-exchange reaction [418]. The constructed $Ni_{0.33}Co_{0.67}Te$ electrode supercapacitor possesses a specific capacity of 131.2 mAh/g at 1 A g^{-1} current density with high energy and power density of 54.0 Wh kg^{-1} and 918 W kg^{-1} and retains about 90% of initial capacitance over 5000 cycles. Chandrasekaran et al. employed a microwave-assisted approach to synthesize nanostructured tin nickel sulfide ($SnNi_2S_4$) composite and utilized it as an active material for supercapacitors [419]. The as-synthesized $SnNi_2S_4$ sample reached a high specific capacitance of 1483.42 F g^{-1} at 2 A g^{-1} with excellent retention of 97.34% of initial capacitance after 5000 charge–discharge cycles. Balamurugan et al. prepared a hierarchical copper-nickel sulfide ($Cu_{1-x}Ni_xS$) nanosheets for improving the performance of asymmetric solid-state supercapacitors using an anion-exchange method, which exhibits a high specific capacitance of 2672 F g^{-1} at 2 mA. cm^{-2} current density [420]. The constructed ASC based on $Cu_{1-x}Ni_xS$ showed high energy of ~ 94.05 Wh kg^{-1} at a power density of 1.09 kW kg^{-1} with outstanding cycling stability of 95.86% after 10,000 charge–discharge cycles. Ke et al. designed a high-performance supercapacitor based on a porous, hierarchical structured ammonium nickel molybdate/nickel sulfide/rGO composite electrode prepared by a two-step hydrothermal method [421]. At 1 A g^{-1}, the active material achieved a high specific capacitance of 150 mAh/g with better rate performance and cycling stability. Elkholy et al. reported the electrochemical activity of the $ZnMoS_4$ electrode-based supercapacitor prepared by a simple solvothermal method [422]. It exhibits a specific capacitance of

280 F g^{-1} at 0.7 A g^{-1} with 86.79% of capacitance retention after 1000 cycles. Sahoo et al. first prepared a binder-free electrode material based on copper-molybdenum sulfide on Ni foam, which delivered a specific capacitance of 663 mAh/g with a superior energy density of 23.61 Wh kg^{-1} and long-term cycling stability. Zhang et al. synthesized a novel potassium copper selenide nanowire (KCu4Se8) through a modified composite-hydroxide mediated (M-CHM) method. The synthesized KCu_4Se_8 NWs with 30 µm of length is studied for the application of solid-state supercapacitor, and their electrochemical performance was tested. It showed a specific capacitance of 25.3 F g^{-1} at 5 mV s^{-1} with excellent long-term cycling stability over 5000 cycles [423].

Even though the abovesaid binary TMCs have lots of advantages, meager cycling stability, low specific capacitance, low rate capability, etc. have hindered its practical applications. Generally, composite materials help to raise the performance of electroactive materials. Al Haj et al. synthesized N-doped graphene-encapsulated cobalt iron sulfide indicated as Co_8FeS_8@NG through the in situ hydrothermal method and utilized as an efficient electrode material for SCs [424]. It exhibits a specific capacitance of ~ 1374 F g^{-1} at 2 A g^{-1} with ~ 96.1% of capacitance retention after 10,000 cycles. The fabricated Co_8FeS_8@NG//FeS@NG ASC showed an outstanding energy and power densities of ~ 70.4 Wh kg^{-1} and 0.598 kW kg^{-1}, respectively. Xu et al. demonstrated a facile solid-state synthesis of ultrathin $Mo_{0.91}W_{0.09}S_2$ nanosheets/amorphous carbon composites for supercapacitor applications [425]. The optimized $Mo_{0.91}W_{0.09}S_2$/amorphous carbon nanosheets possess a high specific capacitance of 432.7 F g^{-1} at 1 A g^{-1} with retention of 93.8% of its initial capacitance after 500 cycles.

Diggikar et al. studied the performance of silver vanadium sulfide/PANI composite prepared by the in situ polymerization method for supercapacitor applications [426]. It revealed a high specific capacitance of 440 F g^{-1} which is exceeding the pristine PANI (128 F g^{-1}) under the same current density. Guo et al. employed a novel strategy for preparing a high-quality cobalt copper sulfide NPs anchored on N-graphene NSs (Co_2CuS_4/NG) through a simple solvothermal method [427]. This composite at a current density of 1 A g^{-1} displayed a high specific capacitance of ~ 1005 F g^{-1} with 96.3% of capacitance after 5000 cycles. Annamalai et al. synthesized a highly exposed $NiCo_2S_4$-rGO nanoporous through a simple facile technique [428]. The prepared $NiCo_2S_4$-rGO nanoporous electrode offered a specific capacitance of 1527 F g at a scan rate of 10 mV s^{-1}. The fabricated supercapacitor shows a high energy density of 60.9 Wh kg^{-1} at a power density of 1.4 kW kg^{-1} with excellent cycling stability and rate performance. Bahaa et al. proposed to design and prepare a hierarchal copper-cobalt sulfide ($CuCo_2S_4$) nanosheet arrays from a metal–organic framework, which offers an improved electroactive site for the diffusion of electrolyte ions [429]. The as-prepared $CuCo_2S_4$ exhibits a high specific capacity of ~ 409.2 mAh/g at 3 mA. cm^{-2} with ~ 94.2% of cycling stability after 10,000 cycles. The assembled supercapacitor with $CuCo_2S_4$ NS//Fe_2O_3/NG electrode exhibits an energy and power densities of ~ 89.6 Wh kg^{-1} and ~ 663 W kg^{-1}, respectively. Han et al. investigated the electrochemical activity of ternary metal sulfides of manganese cobalt sulfide (MCS) with RGO has grown on nickel foam for the application of supercapacitors [215]. The prepared electrode exhibits an outstanding specific capacity of 1356 C/g at 1 A g^{-1} with long cycle stability of 92.9% after 3000 cycles. Li et al. successfully synthesized $NiCo_2S_4$ nanosheets on porous graphitic carbon nitride (g-C_3N_4) NSs and employed as electrode material for supercapacitor [430]. The $NiCo_2S_4$/P-g-C_3N_4 electrode showed a high specific capacitance of 506 C/g at 1 A g^{-1} with 99% of cycling stability after 5000 continuous cycles. Du et al. studied the superior electrochemical performance of the $CoNi_2S_4$/graphene nanocomposite electrode prepared by a facile physical approach [431]. At a current density of 1 A g^{-1}, the constructed $CoNi_2S_4$/graphene composite achieved a specific capacitance of 2009.1 F g^{-1} and maintained 755.4 F g^{-1} at 4 A g^{-1} even after 2000 continuous charge–discharge cycles. Lv et al. constructed a high-performance asymmetric solid-state supercapacitor based on hierarchical zinc cobalt sulfide@nickel sulfide ($Zn_{0.76}Co_{0.24}S$@Ni_3S_2) nanosheet cores through a simple hydrothermal method followed by sulfurization technique. The designed ASC achieved a high specific capacitance of 1209 C/g at 2 A g^{-1} with 94.9% of capacitance retention after 5000 cycles. Also, it exhibits an energy density of 53.8 Wh kg^{-1} at a power density of 853 W kg^{-1} with excellent rate performance. Li et al. created 3D manganese molybdenum sulfide with rGO/NF using a two-step hydrothermal process and employed it as an electrode material for supercapacitor applications [432]. The result obtained showed that MMS/rGO/NF composite achieved a specific capacitance of 1637.1 C/g at 1 A g^{-1} with long-term cycling stability of 96.5% after 8000 cycles. Sahoo et al. synthesized a novel Cu_2MoS_4 NPs embedded rGO sheets through a simple one-pot hydrothermal method [433]. It exhibits a specific capacitance of 231.51 F g^{-1} at 5 mV s^{-1} than the pristine Cu_2MoS_4 (135.78 F g^{-1}) electrode. Sazonov et al. demonstrated the electrochemical performance of $CoMoS_4/Co_3V_2O_8$ nanocomposite prepared by a chemical precipitation method. It exhibits a specific capacitance of 584 F g^{-1} at 0.5 A g^{-1} with superior cycling stability after 3000 cycles [434].

Also, morphology and structures are very significant to enhance the electrochemical properties of electroactive materials and thereby facilitate excellent contact with electrolyte. On this concern, Zhu et al. reported a novel architecture of sea urchin–like cobalt manganese sulfide NWs arrays through a two-step hydrothermal method followed

by anion-exchange sulfuration process [435]. It displayed a specific capacitance of 502 C/g at current density of 1 A g^{-1} with excellent capacitance maintenance at 107% after 2000 cycles. An et al. synthesized a coral-like $Ni_{0.9}Co_{1.92}Se_4$ nanostructural electrode through a two-step solvothermal method that exhibits a specific capacitance of 1021.1 F g^{-1} at 2 mA. cm^{-2} with excellent rate capability of 77% over 2–5 mA. cm^{-2} and cycling stability of 88.39% after 5000 cycles [436]. Yang et al. synthesized a highly exposed active surface of $(Ni_xCo_{1-x})_9Se_8$ series through a one-step growth solid solution reaction for high-performance solid-state supercapacitor [437]. The prepared $(Ni_{0.1}Co_{0.9})_9Se_8$ nanodendrites delivered a specific capacitance of 3762 F g^{-1} at 5 A g^{-1} and retain 94.8% of its initial capacitance after 5000 cycles. For the first time, Zhang et al. investigated the formation and electrochemical performance of double-shelled zinc cobalt sulfide dodecahedral cages through a sequential chemical etching and sulfurization method [438]. The optimized zinc cobalt sulfide showed enhanced electrochemical performance with an outstanding specific capacitance of 1266 F g^{-1} at 1 A g^{-1} and retains 91% of the capacitance over 10,000 cycles. Yu and Lin studied the morphological variation and electrochemical performance of nickel ions delivered by Ni foam and nickel salt in the hydrothermal route for preparing nickel cobalt sulfide [439]. The as-prepared NCS electrode at a current density of 4 A g^{-1} exhibits a specific capacitance of 2206 F g^{-1} with a good rate capacity of 1655.8 F g^{-1} and retains about 94.6% of capacitance after 2000 cycles. Nan et al. studied the intrinsic energy storage mechanism of low crystallinity $NiCo_2S_4$ for supercapacitor application, which delivered a high specific capacitance of 666.27 F g^{-1} at 5 A g^{-1} and retains about 65.29% of its initial capacitance after 10,000 cycles [440]. Talha et al. used a one-step facile method for preparing copper-cobalt sulfide for the application of supercapacitors [441]. The copper-cobalt sulfide electrode achieved a high specific capacitance of ~ 516 F g^{-1} even at higher current density of 10 A g^{-1} with a rate performance of ~ 72% and retains ~ 66% of capacitance after 10,000 cycles. The assembled supercapacitor exhibits high energy and power densities of ~ 35.2 Wh kg^{-1} and ~ 6.6 kW kg^{-1}, respectively. Chen et al. synthesized hierarchical core–shell $NiMoO_4$@NiCoS nanorods grown on Ni foam by two-step method [442]. The well-designed nanorods exhibit a specific capacitance of 1892 F g^{-1} at 5 mA.cm^{-2} with a retention of 91.7% capacitance after 6000 cycles. He et al. studied the improved supercapacitors performance by introducing the hierarchical Ni-Co-S@Ni-W–O core–shell NSAs on nickel foam by a facile three-step hydrothermal method [443]. These hybrid nanosheet arrays provide a high specific capacitance of 1988 F g^{-1} at 2 A g^{-1} current density, and the constructed supercapacitor using this hybrid NSAs offers a high energy and power densities of 55.1 Wh kg^{-1} and 799.8 W kg^{-1}, respectively. Tang et al. prepared a highly electronic conductive cobalt–nickel sulfide dendrite/quasi-spherical nanocomposite through a facile hydrothermal method. The constructed $Co_{1.5}Ni_{1.5S}S_4$ electrode-based supercapacitor at a power density of 103.4 W kg^{-1} achieved an energy density of 32.4 Wh kg^{-1} and served with better cyclic stability.

Hussain et al. prepared rod-like zinc cobalt sulfide through a single-step hydrothermal method and used as an electrode material for supercapacitor [444]. At a current density of 1 A g^{-1}, the ZCS-based electrode exhibits an outstanding specific capacitance of 2418 F g^{-1} and 83% of long cycling stability over 10,000 cycles. Ai et al. studied the application of a supercapacitor by using a novel 3D flower-like $CoNi_2S_4$/carbon nanotube composite through a simple and facile precursor transformation approach [445]. The electrochemical activity of $CoNi_2S_4$/carbon nanotubes showed a specific capacitance of 2094 F g^{-1} at 1 A g^{-1} with a 72% rate capacity even at 10 A g^{-1}. Wang et al. first prepared a novel rhombic dodecahedron ZIF-67-derived amorphous $CoNi_2S_4$ nanocage structure through a sulfurization technique and employed as electrode material for supercapacitor [446]. The electrochemical performance of $CoNi_2S_4$ nanocage reached an ultrahigh specific capacitance of 1890 F g at 4 A g^{-1} with superior capacitance retention of 89.9% over 1000 charge–discharge cycles. Moreover, the constructed supercapacitor attained outstanding energy and power density of 35 Wh kg^{-1} and 640 W kg^{-1}, respectively. Wang et al. designed a kelp-like structured $NiCo_2S_4$-C-MoS_2 composite electrode-based supercapacitor, which achieved a specific capacitance of 1601 F g^{-1} at a current density of 0.5 A g^{-1} [447]. The ASC based on this composite exhibits superior energy and power densities of 27.7 Wh kg^{-1} and 400 W kg^{-1}, respectively, with cycling stability of 60% after 1000 cycles.

Due to their relatively high cycle stability and specific capacitance, transition metal oxysulfides (TMOS) have been considered promising electrode materials for energy storage devices. Liu prepared cobalt–nickel oxysulfide through a hydrothermal method, which delivered a specific capacitance of 592 F g^{-1} at 5 A g^{-1} current density with retention of 81.5% of its initial capacitance after 2000 cycles [448]. In another work, Liu synthesized manganese cobalt oxysulfide grown on Ni foam via a two-step hydrothermal route that parades a specific capacitance of 490 C/g at 2 A g^{-1} with excellent cycling stability of 86.5% after 3000 cycles. Also, Liu studied the electrochemical performance of zinc cobalt oxysulfide for energy storage applications and revealed a specific capacity of 645.5 C/g at 1 A g^{-1} with capacitance retention of 76% after 1000 cycles. Yao et al. used the electrochemical deposition technique for the synthesis of manganese oxysulfide, which exhibits an enhanced specific capacitance of 214 F g^{-1} at 1 mA. cm^{-2} with 75.4% of cycling stability after 1000 cycles. Based on this works, Asen et al.

employed an electrochemical deposition method for the preparation of iron vanadium oxysulfide nanostructures with different ratios [449]. The iron vanadium oxysulfide at 2:1 ratio showed an improved specific capacitance of 217 F g^{-1} at 3 A g^{-1} with 92% of capacitance retention after 4000 cycles. The summary of bimetal chalcogenide-based electrode materials and their supercapacitor performances are shown in Table 7.

6 Trimetallic chalcogenides and its composites

Compared to monometallic (NiS, CoS, FeS, etc.) and bimetallic sulfides (nickel cobalt, nickel manganese, etc.), the electrochemical influences of cobalt, nickel, manganese, and ions in the trimetallic sulfides delivered rich redox reactions resulting in outstanding specific capacitance. Generally, Co, Ni, and Mn-based supercapacitors displayed a high specific capacitance, energy density, and power density at low current density. Also, it is reported that electrodes of mixed transition metals offer superior electrochemical performance than single TMSs. Thus, the coupling of three metal species could render the mixed TMO/TMSs and will surely increase the redox reaction with high electrical conductivity, which is favorable for the application of energy storage devices. Wei et al. prepared a yolk-shell hollow sphere of nickel cobalt manganese sulfide via a self-templating strategy, which possesses a high specific capacitance of 1360 F g^{-1} at a current density of 1 A g^{-1} [524]. The fabricated nickel cobalt manganese sulfide supercapacitor device showed an energy and power densities of 49.8 Wh kg^{-1} and 1700 W kg^{-1}, respectively, with only a 1.8% loss of its initial capacitance even after 6000 cycles. Sahoo et al. used a cathodic electrodeposition method for preparing nickel cobalt manganese sulfide (NCMS) nanosheets on Ni foam for the fabrication of high-performance supercapacitors [525]. The optimized NCMS, at 1 A g^{-1}, offers a larger specific capacitance of 2717 F g^{-1} with great cycle life and energy density (94.7 Wh kg^{-1}). Gao et al. synthesized a single-phase $CuCo_{2-x}Ni_xS_4$ electrode through a facile two-step hydrothermal method to improve the electrochemical activity of supercapacitor [526]. The electrochemical performance of the $CuCo_{2-x}Ni_xS_4$ electrode reached up to 647 F g^{-1} of specific capacitance at 1 A g^{-1} of current density with ~ 98% of capacitance retention after 10,000 cycles. Verma et al. investigated the pseudocapacitive behavior of cobalt manganese nickel sulfide (CoMnNiS) nanosheet grown on Ni-foam through a simple electrodeposition method [527]. The designed CoMnNiS electrode achieved a specific capacitance of 257.4 mAh/g at 2.5 A g^{-1}. They fabricated an asymmetric supercapacitor based on both CoMnNiS/NiCuO and CoMnNiS/CNT electrodes with a superior energy density of 8.4 and 6.3 Wh kg^{-1} at a power density of 985 and 211 W kg^{-1}, respectively. Isacfranklin et al. developed a newer form of chalcogenides using copper, iron, and tin to form Cu2FeSnS4/PVP/rGO-decorated nanocomposite that are prepared by simple hydrothermal method and followed by nucleation process in later studies in quaternary chalcogenides for use as electrode material [528]. The developed electrode material exhibits an excellent specific capacitance value of 328 F g^{-1} (45.55 mA h/g) at 0.5 A g^{-1}, and the symmetric cell made using this electrode exhibits energy and power densities of 73 Wh kg^{-1} and 749 W kg^{-1} at 1 A g^{-1}. With 20,000 cycles, it has a coulombic efficiency of 99.99% and a 63% capacity retention. They also developed marigold flower-like structured Cu_2NiSnS_4 by employing simple solvothermal process, and the electrode revealed high 1029 F g^{-1} specific capacitance at 0.5 A g^{-1} current density. To prove its application towards practical technology development, a full-cell asymmetric solid-state device is fabricated which delivers 41.25 Wh kg^{-1} and 750 W kg energy and power density at 0.5 A g^{-1} [529]. Song et al. developed $Ni_xCo_yMn_zS/Ni(SeO_3)$ (NCMS/NSeO) heterostructure that is prepared on Ni-plated carbon cloth and employed them as electrode for supercapacitor; the optimized electrodes exhibit a high capacity of 536 mAh g^{-1} at 1 A g^{-1}, the assembled asymmetric supercapacitor achieves an ultrahigh energy density of 141 Wh kg^{-1}, and the main highlight of this work is an impressive high-rate capability and cyclability combination with 124% capacitance retention after 10,000 cycles at a large current density of 50 A g^{-1} [530].

7 Outlook and future prospects

For high energy storage, long cycle, and reliability, supercapacitors are the most predominant technology that can complement the strength of batteries. Firstly, we pointed out the advantages and disadvantages of carbonaceous materials like graphene, MWCNT, metal oxides, and polymers that fail to provide high specific capacitance and cycling stability in supercapacitors. In this study, we collected many transition metal chalcogenides and their composites with different morphologies-based electrode materials that offer high ratings in supercapacitors. From the above discussion, the TMCs and their composite-based electrode material possess better specific capacitance with high-rate capability and long-term stability than carbon-based materials. Despite being promising candidates, it has some demerits of having low energy and power density compared to batteries. Hence, many morphological changes and doping of metals have been done to rectify these limitations. Recently, researchers

Table 7 Summary of bimetal chalcogenide–based electrode materials with various synthesis methods and their supercapacitor performances

Electrode material for supercapacitor	Method of synthesis	Specific capacitance	Capacitance retention	Ref
3D NCS/CNS composite	Hydrothermal method	15.6 F cm^{-2} @ 10 mA. cm^{-2}	93% after 5000 cycles	[415]
$NiCo_2S_4$/RGO hybrids	One-pot refluxing method	1526 F g^{-1} @ 1 A g^{-1}	83% after 2000 cycles	[450]
Ni_2CoS_4@$NiCoO_4$/N-doped carbon xerogels	Hydrothermal method	1501 F g^{-1} @ 1 mA. cm^{-2}	87.6% after 10,000 cycles	[451]
$NiCo_2S_4$	One-step potentiostatic deposition method	1080 F g^{-1} @ 1 A g^{-1}	93.4% after 1500 cycles	[452]
$NiCo_2S_4$ composite	Co-deposition method	1418 F g^{-1} @ 5 A g^{-1}	90.6% after 50,000 cycles	[453]
$NiCo_2S_4$ NT @ $NiCo_2S_4$ NSs on Ni foam	Hydrothermal method	4.38 F. cm^{-2} @ 5 mA. cm^{-2}	81% after 5000 cycles	[454]
$NiCo_2S_4$ on Ni foam	Chemical liquid method	1777 F g^{-1} @ 1 A g^{-1}	83% after 3000 cycles	[455]
Tremelliform $NiCo_2S_4$	One-step hydrothermal method	150.9 F g^{-1} @ 1 A g^{-1}	88.3% after 5000 cycles	[456]
$NiCo_2S_4$@$NiCO_2O_4$ NCAs	Facile method	2258.9 F g^{-1} @ 0.5 A g^{-1}	92.5% after 6000 cycles	[457]
$CuCo_2S_4$ NRAs	Two-step hydrothermal method	1536.9 F g^{-1} @ 1 A g^{-1}	88% after 5000 cycles	[457]
Hierarchical $NiCo_2S_4$@$NiCo_xS_y$ core/shell NAs	Two-step hydrothermal route	3.9 F cm^{-2} @ 1 mA. cm^{-2}	77% after 1500 cycles	[458]
$NiCo_2S_4$ nanotubes	Hydrothermal and ion-exchange reaction	1005 F g^{-1} @ 1 A g^{-1}	79.34% after 5000 cycles	[459]
$CuCo_2S_4$ nanowire arrays	Two-step hydrothermal method	2446 F g^{-1} @ 1 A g^{-1}	78% after 10,000 cycles	[460]
$CuCo_2S_4$ on graphene	Solvothermal method	668 F g^{-1} @ 1 A g^{-1}	72% after 8000 cycles	[461]
$MnCo_2S_4$ NPs	Hydrothermal method	1150 F g^{-1} @ 1 A g^{-1}	88.2% after 5000 cycles	[462]
HM-NCS ellipsoids	Hydrothermal method	~495 F g^{-1} @ 10 A g^{-1}	~99% after 5000 cycles	[463]
$Ni_{3x}Co_{3-3x}S_4$@ carbon	Hydrothermal method	696 F g^{-1} @ 1 A g^{-1}	73% after 2000 cycles	[464]
$NiCOS_4$	Solvothermal method	2215 F g^{-1} @ 0.5 A g^{-1}	90.16% after 10,000 cycles	[465]
Porous $NiCo_2S_4$ nanotubes	Sacrificial template method	1093 F g^{-1} @ 0.2 A g^{-1}	63% after 1000 cycles	[466]
NiCoS/PAN	Electrospinning method	1513 F g^{-1} @ 5A g^{-1}	82.2% after 5000 cycles	[467]
$NiCo_2S_4$ nanosheet	Chemical bath deposition method	1155 F g^{-1} @ 10 mV s^{-1}	95% after 2000 cycles	[468]
Core–shell $NiCo_2S_4$ nanostructure on nickel foam	Two-step hydrothermal method	1948 mF. cm^{-2} @ 1 mA. cm^{-2}	94% after 5000 cycles	[469]
CS@Ni-Co-S core–shell microstructure	Hydrothermal method	724.4 F g^{-1} @ 2 A g^{-1}	97.9% after 2000 cycles	[470]
Fe-Co-S/NF	Solvothermal sulfurization	2695 F g^{-1} @ 1 A g^{-1}	84% after 1000 cycles	[471]
Ni-Co sulfide nanowires on nickel foam	Two-step hydrothermal method	2415 F g^{-1} @ 2.5 mA. cm^{-2}	78.5% after 3000 cycles	[472]
Ni-Co-sulfide NSs	Micelle-confined growth and sulfurization	1304 F g^{-1} @ 2 A g^{-1}	93.5% after 6000 cycles	[473]
Zn-Co-S nanowires	Two-step method	366.7 mAh/g @ 3 mA. cm^{-2}	93.2% after 10,000 cycles	[474]
$Zn_xCo_{1-x}S$ nanoartichokes	Facile oil phase approach	486.2 F g^{-1} @ 2 A g^{-1}	86.4% after 2000 cycles	[475]
$NiCo_2S_4$/GA composite	Solvothermal method	704.34 F g^{-1} @ 1 A g^{-1}	80.3% after 1500 cycles	[476]
$NiCo_2S_4$@MnO_2	Hydrothermal route	1337.8 F g^{-1} @ 2 A g^{-1}	82% after 2000 cycles	[477]
ZCS microspheres	Solvothermal method	1516 F g^{-1} @ 1 A g^{-1}	94% after 2000 cycles	[478]
ZCS NPs	Hydrothermal method	1269.1 F g^{-1} @ 0.5 A g^{-1}	91.6% after 5000 cycles	[479]
CS-NCS composite	One-step hydrothermal method	1093 F g^{-1} @ 0.5 A g^{-1}	91% after 8000 cycles	[480]
$MnCo_2S_4$	Hydrothermal method	2067 F g^{-1} @ 1 A g^{-1}	89% after 5000 cycles	[481]
$NiCo_2S_4$ NTs/carbon cloth	Two-step hydrothermal method	578 C/g @ 0.5 A g^{-1}	71.13% after 6000 cycles	[482]
$FeCo_2S_4$ nanowire	Two-step hydrothermal method	337 mAh/g @ 2 A g^{-1}	90% after 2000 cycles	[483]
Hierarchical NCS	Two-step hydrothermal method	574 C/g @ 1 A g^{-1}	88% after 1500 cycles	[484]
$Zn_{0.76}Co_{0.24}S$@Ni_3S_2 on Ni foam	Hydrothermal and sulfurization method	1209 C/g @ 2 A g^{-1}	94.9% after 5000 cycles	[485]
$Zn_{0.76}Co_{0.24}S$	Two-step synthesis	2484 F g^{-1} @ 2 A g^{-1}	~99% after 10,000 cycles	[486]
$NiCo_2S_4$/RGO-C	Solvothermal method	1467 F g^{-1} @ 0.5 A g^{-1}	83% after 10,000 cycles	[487]
Mixed NCSs	Solvothermal method	2599.6 F g^{-1} @ 10 mV s^{-1}	95% after 3000 cycles	[488]
$NiCo_2S_4$ NTs on nickel foam	Two-step method	738 F g^{-1} @ 4 A g^{-1}	93.4% after 4000 cycles	[489]

Table 7 (continued)

Electrode material for supercapacitor	Method of synthesis	Specific capacitance	Capacitance retention	Ref
$NiCo_2S_4$@NCNT composite	Hydrothermal method	783.5 C/g @ 1 A g^{-1}	88.9% after 3000 cycles	[490]
$CuCo_2S_4$-glycerol	Solvothermal method	5030 F g^{-1} @ 20 A g^{-1}	79.5% after 2000 cycles	[491]
$Ni_{1.77}Co_{1.23}S_4$	Hydrothermal method	224.5 mAh/g @ 0.25 A g^{-1}	64.82% after 1000 cycles	[492]
$CoFe_2Se/CoNiSe_2$ composite	Facile method	183.4 mAh/g @ 1 A g^{-1}	99.2% after 3000 cycles	[493]
N-GNTs@$NiCoSe_2/Ni_3Se_4$	One-step electrodeposition method	1308 F g^{-1} at 1 A g^{-1}	94.4% after 10,000 cycles	[494]
$CoNi_2S_4$@NiSe NAs	Three-step solution based method	312.95 mF. cm^{-2} @ 5 mV s^{-1}	97.59% after 1000 cycles	[495]
3D flower-like $CoNi_2S_4$/G-NF	Chemical vapor deposition method	6.528 F cm^{-2} @ 6 mA. cm^{-2}	85% after 3500 cycles	[496]
$CoNi_2S_4$ NPs/ 3D-CNT	Electrodeposition method	1530 F g^{-1} @ 1 A g^{-1}	85% after 10,000 cycles	[497]
rGO/$CoNiS_x$/N–C nanocomposite	One-step carbonization/sulfurization method	1028.2 F g^{-1} @ 1 A g^{-1}	93.6% after 2000 cycles	[498]
$CoNi_2S_4$ nanosheet arrays/NF	One-step potentiostatic deposition method	1932 F g^{-1} @ 2 A g^{-1}	89.2% after 1000 cycles	[499]
rGO-$CoNi_2S_4$/ NF	Two-step hydrothermal method	1680 F g^{-1} @ 1 A g^{-1}	62% after 5000 cycles	[500]
$CoNi_2S_4$ nanosheet arrays on Ni foam	Two-step hydrothermal method	2906 F g^{-1} @ 5 mA. cm^{-2}	98% after 3000 cycles	[501]
Reduced $CoNi_2S_4$ NSs	Facile moderate-reduction process	1117 C/g @ 2 A g^{-1}	80% after 10,000 cycles	[502]
Ultrathin $CoNi_2S_4$ nanosheet	Microwave-assisted method	247 mAh/g @ 8 A g^{-1}	82% after 10,000 cycles	[503]
$CoNi_2S_4$/RGO composite	One-pot hydrothermal method	1709 F g^{-1} @ 0.5 A g^{-1}	92% after 2000 cycles	[504]
$NiCo_2S_4$/NiS hollow nanospheres	Two-step hydrothermal method	1947.5 F g^{-1} @ 3 mA. cm^{-2}	90.3% after 1000 cycles	[505]
$Ni_xCo_{9-x}S_8$@C	Two-step solvothermal method	1404 F g^{-1} @ 2 A g^{-1}	95.8% after 2000 cycles	[506]
$CoNi_2S_4/Co_9S_8$ composite	Chemical bath deposition method	1183.3 F g^{-1} @ 2 A g^{-1}	97.3% after 1000 cycles	[507]
$CoNi_2S_4$-G-$MoSe_2$ composite	Ultrasonication and hydrothermal method	1141 F g^{-1} @ 20 A g^{-1}	108% after 2000 cycles	[508]
$CoMoS_4$	Chemical co-precipitation method	415 F g^{-1} @ 0.5 A g^{-1}	100% after 10,000 cycles	[509]
$CoMo_2S_4$/3DSG composite	Hydrothermal method	1288.33 F g^{-1} @ 1 A g^{-1}	90% after 2000 cycles	[510]
Nickel-molybdenum-sulfide/NF	SILAR method	2224 C/g @ 4 mA. cm^{-2}	95% after 5000 cycles	[511]
GN-$CoMoS_4$ hybrid	Hydrothermal method	774 F g^{-1} @ 1 A g^{-1}	94.49% after 6000 cycles	[512]
T-$Mn_xMo_{1-x}S_{2-y}Se_y$	Hydrothermal method	0.76 mAh/cm^2 @ 1 mA. cm^{-2}	81% after 10,000 cycles	[513]
$MoFe_2S_{4-z}Se_z$	Hydrothermal method	0.534 mAh/cm^2 @ 1 mA. cm^{-2}	86.2% after 10,000 cycles	[513]
Co–W–S	Wet chemical method	1929 F g^{-1} @ 5 mV s^{-1}	66% after 10,000 cycles	[514]
Ag-decorated Ni–Fe-Te	Wet chemical method	1.1 mAh/cm^2 @ 3 mA. cm^{-2}	80.4% after 3000 cycles	[515]
CF@$NiCoO_4Se_3/Ni_2Co$-LDH		3270 F g^{-1} @ 1 A g^{-1}	95.6% after 10,000 cycles	[516]
Cu_3SbS_4	Solution-based method	397 F g^{-1} @ 5 mV s^{-1}	-	[517]
Flowery $EuZrSe_3$	Wet chemical method	1543 F g^{-1} @ 3 A g^{-1}	93.58% after 10,000 cycles	[518]
$NiCo_2Se_4$/RGO microsphere	Hydrothermal method	1776.1 F g^{-1} @ 2 A g^{-1}	93.5% after 5000 cycles	[519]
$Cu_{0.5}Co_{0.5}Se_2$ nanosheets	Hydrothermal method	1695 F g^{-1} @ 1 A g^{-1}	91.1% after 10,000 cycles	[520]
FeO@$CuCo_2S_4$ microfilms	Hydrothermal and magnetron sputtering	3213 F g^{-1} @ 1 A g^{-1}	116% after 10,000 cycles	[521]
$NbMo_6S_8$/NC	Hydrothermal method	167.89 mAh/g @ 0.25 A g^{-1}	87.60% after 15,000 cycles	[522]
Ni-Co–C-N-OS	Electrochemical deposition	555.35 µAh/cm^2 @ 1 mA cm^{-2}	100% after 45,000 cycles	[523]

have developed supercapacitors with a novel ternary meta for energy storage systems due to their large surface area, high conductivity, and feasibility towards electrochemical performance. In addition, the morphology-controlled ternary metals are attractive at high-temperature operations. Also, a few recent reports show that the trimetallic-based electrode is a promising candidate in supercapacitor with extraordinary specific capacitance and power density. Hence, we conclude that among various electrodes, bi- and trimetallic-based electrodes offer high efficiency in comparison with lithium-based batteries. Lastly, we conclude that the efficient electrode materials used in testing supercapacitors must be practically developed and used in the commercial market.

Author contribution E. S. Sowbakkiyavathi: methodology, writing, and reviewing the original draft; Arunachala Kumar S. P.: methodology, writing, and reviewing the original draft; Dheeraj K. Maurya, B. Balakrishnan, and John Zhanhu Guo: review and editing; A. Subramania: methodology, conceptualization, supervision, funding acquisition, review, and editing.

Funding Prof. A.S thank the University Grants Commission (UGC), New Delhi, for their financial support under BSR Mid-Career Award Scheme (No. F.19–214/2018).

Data availability The data that support the findings of this review article are available in the cited references and sources. Additional data related to this study are available upon request from the corresponding author.

Declarations

Competing interests The authors declare no competing interests.

References

1. Miller JR (1979) Simon P (2008) Materials science: electrochemical capacitors for energy management. Science 321:651–652. https://doi.org/10.1126/science.1158736
2. Hong H, Lin Gao, Yawen Zheng, Xueli Xing, Fan Sun, Taixiu Liu, Murugadoss V, Zhanhu Guo, Ming Yang, Zhang H (2021) A path of multi-energy hybrids of concentrating solar energy and carbon fuels for low CO2 emission. ES Energy Environ 13:1–7. https://doi.org/10.30919/esee8c520
3. Qin C, Gong H, Sun C, Wu X (2022) Optical properties of a core/shell/shell shape metal-insulator-metal composite nanoparticle for solar energy absorption. Eng Sci 17:224–230. https://doi.org/10.30919/es8e509
4. Kanekar PP, Kulkarni SO, Dhakephalkar PK, Saxena N, Pathan HM (2021) Bacteriorhodopsin producing halophilic archaea isolated from solar salt pan saline environment for conversion of light energy into electrical energy. ES Energy Environ 13:57–64. https://doi.org/10.30919/esee8c444
5. Frackowiak E (2007) Carbon materials for supercapacitor application. Phys Chem Chem Phys 9:1774–1785. https://doi.org/10.1039/b618139m
6. Poonam SK, Arora A, Tripathi SK (2019) Review of supercapacitors: materials and devices. J Energy Storage 21:801–825. https://doi.org/10.1016/j.est.2019.01.010
7. Pandolfo AG, Hollenkamp AF (2006) Carbon properties and their role in supercapacitors. J Power Sources 157:11–27. https://doi.org/10.1016/j.jpowsour.2006.02.065
8. Navathe GJ, Prasad SR, Mane AM, Barge SH, Dongale TD, Shaikh V, Karanjkar MM, Teli SB, Patil PS, Prasad NR (2022) A critical review on design and development of new generation energy storage devices. ES Energy Environ 17:11–32. https://doi.org/10.30919/esee8c739
9. Thota SP, Bag PP, Vadlani PV, Belliraj SK (2022) Plant biomass derived multidimensional nanostructured materials: a green alternative for energy storage . Engineered Science 18:31–58. https://doi.org/10.30919/es8d664
10. Wang G, Zhang L, Zhang J (2012) A review of electrode materials for electrochemical supercapacitors. Chem Soc Rev 41:797–828. https://doi.org/10.1039/c1cs15060j
11. Pan H, Li J, Feng YP (2010) Carbon nanotubes for supercapacitor. Nanoscale Res Lett 5:654–668. https://doi.org/10.1007/s11671-009-9508-2
12. Largeot C, Portet C, Chmiola J, Taberna P, Gogotsi Y, Simon P (2008) [255] Size and pore size for an electric double-layer.pdf. 2730–2731. https://doi.org/10.1016/j.carbon.2007.10.023.(15)
13. Conway BE (1999) Electrochemical supercapacitors. Springer, US, Boston, MA
14. Frackowiak E, Beguin F (2001) Carbon materials for the electrochemical storage of energy in capacitors. Carbon N Y 39:937–950. https://doi.org/10.1016/S0008-6223(00)00183-4
15. Raymundo-Piñero E, Kierzek K, Machnikowski J, Béguin F (2006) Relationship between the nanoporous texture of activated carbons and their capacitance properties in different electrolytes. Carbon N Y 44:2498–2507. https://doi.org/10.1016/j.carbon.2006.05.022
16. Sun H, Xu Z, Gao C (2013) Multifunctional, ultra-flyweight, synergistically assembled carbon aerogels. Adv Mater 25:2554–2560. https://doi.org/10.1002/adma.201204576
17. Chien HC, Cheng WY, Wang YH, Lu SY (2012) Ultrahigh specific capacitances for supercapacitors achieved by nickel cobaltite/carbon aerogel composites. Adv Funct Mater 22:5038–5043. https://doi.org/10.1002/adfm.201201176
18. Chen JH, Li WZ, Wang DZ, Yang SX, Wen JG, Ren ZF (2002) Electrochemical characterization of carbon nanotubes as electrode in electrochemical double-layer capacitors. Carbon N Y 40:1193–1197. https://doi.org/10.1016/S0008-6223(01)00266-4
19. Emmenegger C, Mauron P, Züttel A, Nützenadel C, Schneuwly A, Gallay R, Schlapbach L (2000) Carbon nanotube synthesized on metallic substrates. Appl Surf Sci 162:452–456. https://doi.org/10.1016/S0169-4332(00)00232-4
20. Xia J, Chen F, Li J, Tao N (2009) Measurement of the quantum capacitance of graphene. Nat Nanotechnol 4:505–509. https://doi.org/10.1038/nnano.2009.177
21. Stoller MD, Park S, Zhu Y, An J, Ruoff RS (2008) Graphene-based ultracapacitors. Nano Lett 8:3498–3502. https://doi.org/10.1021/nl802558y
22. Kim I-H, Kim K-B (2006) Electrochemical characterization of hydrous ruthenium oxide thin-film electrodes for electrochemical capacitor applications. J Electrochem Soc 153:A383. https://doi.org/10.1149/1.2147406
23. Jow TR, Zheng JP (1995) Amorphous thin film ruthenium oxide as an electrode material for electrochemical capacitors. Mater Res Soc Symp - Proc 393:433–438. https://doi.org/10.1557/proc-393-433
24. Long JW, Swider KE, Merzbacher CI, Rolison DR (1999) Voltammetric Characterization of ruthenium oxide-based aerogels and other RuO2 solids: the nature of capacitance in nanostructured materials. Langmuir 15:780–784. https://doi.org/10.1021/la980785a
25. Pang SC, Anderson MA (2000) Novel electrode materials for electrochemical capacitors: part II. Material characterization of sol-gel-derived and electrodeposited manganese dioxide thin films. J Mater Res 15:2096–2106. https://doi.org/10.1557/JMR.2000.0302
26. Nagarajan N, Humadi H, Zhitomirsky I (2006) Cathodic electrodeposition of MnOx films for electrochemical supercapacitors. Electrochim Acta 51:3039–3045. https://doi.org/10.1016/j.electacta.2005.08.042
27. Kayani ZN, Arshad S, Riaz S, Naseem S (2019) Investigation of structural, optical and magnetic characteristics of Co 3 O 4 thin films. Appl Phys A Mater Sci Process 125:. https://doi.org/10.1007/s00339-019-2501-4
28. Deori K, Ujjain SK, Sharma RK, Deka S (2013) Morphology controlled synthesis of nanoporous Co3O4 nanostructures and their charge storage characteristics in supercapacitors. ACS Appl

Mater Interfaces 5:10665–10672. https://doi.org/10.1021/am4027482
29. Cheng J, Cao GP, Yang YS (2006) Characterization of sol-gel-derived NiOx xerogels as supercapacitors. J Power Sources 159:734–741. https://doi.org/10.1016/j.jpowsour.2005.07.095
30. Lee HY, Goodenough JB (1999) Ideal supercapacitor behavior of amorphous V2O5·nH2O in potassium chloride (KCl) aqueous solution. J Solid State Chem 148:81–84. https://doi.org/10.1006/jssc.1999.8367
31. Halper MS, Ellenbogen JC (2006) Supercapacitors: a brief overview. The MITRE Corporation, McLean, Virginia, USA
32. Arbizzani C, Mastragostino M, Soavi F (2001) New trends in electrochemical supercapacitors. J Power Sources 100:164–170. https://doi.org/10.1016/S0378-7753(01)00892-8
33. Li H, Wang J, Chu Q, Wang Z, Zhang F, Wang S (2009) Theoretical and experimental specific capacitance of polyaniline in sulfuric acid. J Power Sources 190:578–586. https://doi.org/10.1016/j.jpowsour.2009.01.052
34. Kim JH, Lee YS, Sharma AK, Liu CG (2006) Polypyrrole/carbon composite electrode for high-power electrochemical capacitors. Electrochim Acta 52:1727–1732. https://doi.org/10.1016/j.electacta.2006.02.059
35. Zhou C, Zhang Y, Li Y, Liu J (2013) Construction of high-capacitance 3D CoO@Polypyrrole nanowire array electrode for aqueous asymmetric supercapacitor. Nano Lett 13:2078–2085. https://doi.org/10.1021/nl400378j
36. Najib S, Erdem E (2019) Current progress achieved in novel materials for supercapacitor electrodes: Mini review. Nanoscale Adv 1:2817–2827. https://doi.org/10.1039/c9na00345b
37. Chen C, Xie X, Yang M, Zhang H, Seok I, Guo Z, Jiang Q, Wangila G, Liu Q (2021) Recent advances in solar energy full spectrum conversion and utilization. ES Energy & Environment 11:3–18. https://doi.org/10.30919/esee8c416
38. Hu X, Wu H, Liu S, Gong S, Du Y, Li X, Lu X, Qu J (2022) Fabrication of organic shape-stabilized phase change material and its energy storage applications. Engineered Science 17:1–27. https://doi.org/10.30919/es8d474
39. Theerthagiri J, Karuppasamy K, Durai G, Rana A ul HS, Arunachalam P, Sangeetha K, Kuppusami P, Kim HS (2018) Recent advances in metal chalcogenides (MX; X = S, Se) nanostructures for electrochemical supercapacitor applications: a brief review. Nanomaterials 8:. https://doi.org/10.3390/nano8040256
40. Ganesan P, Sivanantham A, Shanmugam S (2016) Inexpensive electrochemical synthesis of nickel iron sulphides on nickel foam: super active and ultra-durable electrocatalysts for alkaline electrolyte membrane water electrolysis. J Mater Chem A Mater 4:16394–16402. https://doi.org/10.1039/c6ta04499a
41. Gautam AK, Faraz M, Khare N (2020) Enhanced thermoelectric properties of MoS2 with the incorporation of reduced graphene oxide (RGO). J Alloys Compd 838:. https://doi.org/10.1016/j.jallcom.2020.155673
42. Hong S, Choi DW, Kim HN, Park CG, Lee W, Park HH (2020) Protein-based nanoparticles as drug delivery systems. Pharmaceutics 12:1–28
43. Bokov D, Turki Jalil A, Chupradit S, Suksatan W, Javed Ansari M, Shewael IH, Valiev GH, Kianfar E (2021) Nanomaterial by sol-gel method: synthesis and application. Adv Mater Sci Eng 2021:5102014. https://doi.org/10.1155/2021/5102014
44. Oloore LE, Gondal MA, Popoola IK, Popoola A (2019) CdS quantum dots-organometallic halide perovskites bilayer electrodes structures for supercapacitor applications. ChemElectroChem 7:486–492. https://doi.org/10.1002/celc.201901969
45. Chen L, Zuo Y, Zhang Y, Gao Y (2018) Cadmium sulfide anchored in three-dimensional graphite cage for high performance supercapacitors. Appl Phys Lett 112:223901-1–223904. https://doi.org/10.1063/1.5025128
46. Patil DS, Pawar SA, Shin JC (2018) Alteration of Ag nanowires to Ag/Ag2S nanowires@CdS core-shell architectures for electrochemical supercapacitors. J Alloys Compd 768:1076–1082. https://doi.org/10.1016/j.jallcom.2018.07.244
47. Patil DS, Pawar SA, Shin JC (2018) Core-shell structure of Co 3 O 4 @ CdS for high performance electrochemical supercapacitor. Chem Eng J 335:693–702. https://doi.org/10.1016/j.cej.2017.11.007
48. He Z, Zhu Y, Xing Z, Wang Z (2015) Reduced graphene – cadmium sulfide hybrid nanopowders : solvothermal synthesis and enhanced electrochemical performance. J Mater Sci: Mater Electron 26:5697–5702. https://doi.org/10.1007/s10854-015-3124-y
49. Wang X, Shi Bo, Fang Y, Huang F, Ronghui Que MS (2017) High capacitance and rate capability of Ni3S2@CdS core-shell nanostructures supercapacitor. J Mater Chem A Mater 5:7165–7172. https://doi.org/10.1039/C7TA00593H
50. Safdar B, Rajesh JA, Kang S, Kim H, Ahn K (2020) Enhanced capacitive performances and excellent stability of cadmium-sulfide-concealed nickel sulfide (Ni3S2/CdS) for electrochemical capacitors. J Alloys Compd 826:154211. https://doi.org/10.1016/j.jallcom.2020.154211
51. Krishnamoorthy K, Pazhamalai P, Jae S (2017) Ruthenium sulfide nanoparticles as a new pseudocapacitive material for supercapacitor. Electrochim Acta 227:85–94. https://doi.org/10.1016/j.electacta.2016.12.171
52. Bae J, Paik U, Kee D (2016) Novel semiconducting CdSe quantum dot based electrochemical capacitors. Mater Lett 162:230–234. https://doi.org/10.1016/j.matlet.2015.10.004
53. Pawar SA, Patil DS, Shin JC (2017) Cadmium selenide microspheres as an electrochemical supercapacitor. Mater Today Chem 4:164–171. https://doi.org/10.1016/j.mtchem.2017.04.002
54. Nisha MMP, Dhanuskodi FS, Muralidharan NMG (2018) High performance supercapacitor behavior of hydrothermally synthesized CdTe nanorods. J Mater Sci: Mater Electron 29:17397–17404. https://doi.org/10.1007/s10854-018-9837-y
55. Pande SA, Pandit B, Sankapal BR (2017) Electrochemical approach of chemically synthesized HgS nanoparticles as supercapacitor electrode. Mater Lett 209:97–101. https://doi.org/10.1016/j.matlet.2017.07.084
56. Pande SA, Pandit B, Sankapal BR (2017) Facile chemical route for multiwalled carbon nanotube/mercury sulfide nanocomposite: high performance supercapacitive electrode. J Colloid Interface Sci 514:740–749. https://doi.org/10.1016/j.jcis.2017.12.068
57. Yun X, Wu S, Li J, Li L, Zhou J, Lu P, Tang H, Zhu Y (2019) Facile synthesis of crystalline RuSe 2 nanoparticles as a novel pseudocapacitive electrode material for supercapacitors †. ChemComm 55:12320–12323. https://doi.org/10.1039/c9cc06023e
58. Mo Z, Liu P, Guo R, Deng Z, Zhao Y, Sun Y (2012) Graphene sheets / Ag 2 S nanocomposites : synthesis and their application in supercapacitor materials. Mater Lett 68:416–418. https://doi.org/10.1016/j.matlet.2011.11.006
59. Nair N, Sankapal BR (2016) Cationic-exchange approach for conversion of two dimensional CdS to two dimensional Ag 2 S nanowires with an intermediate core – shell. New J Chem 40:10144–10152. https://doi.org/10.1039/C6NJ02411D
60. Pawar SA, Patil DS, Shin JC (2018) Electrochemical battery-type supercapacitor based on chemosynthesized Cu 2 S e Ag 2 S composite electrode. Electrochim Acta 259:664–675. https://doi.org/10.1016/j.electacta.2017.11.006
61. Wang Min, Zhang Li, Zhong Yujia, Huang Meirong, Zhen Zhen, Zhu Hongwei (2018) In-situ electrodeposition of polypyrrole onto TaSe2 nanobelts quasi-arrays for high-capacitance supercapacitor. Nanoscale 10:17341–17346. https://doi.org/10.1039/C8NR05261A
62. Chakravarty D, Kumar P, Ugale VS, Late DJ (2015) Microwave-assisted synthesis of few-layered TaTe 2 and its application as

supercapacitor. Eur J Inorg Chem 1598–1603. https://doi.org/10.1002/ejic.201403220
63. Parvaz M, Ahmed S, Khan MB, Ahmad S, Khan ZH (2018) Synthesis of TiS 2 nanodiscs for supercapacitor application. AIP Conf Proc 1953:030121-1–30125. https://doi.org/10.1063/1.5032456
64. Ramachandran R, Saranya M, Kollu P, Raghupathy BPC, Soon Kwan Jeong ANG (2015) Solvothermal synthesis of zinc sulfide decorated graphene (ZnS / G) nanocomposites for novel supercapacitor electrodes. Electrochim Acta 178:647–657. https://doi.org/10.1016/j.electacta.2015.08.010
65. Hou X, Peng T, Cheng J, Yu Q, Luo R, Lu Y, Liu X (2016) Ultrathin ZnS nanosheet / carbon nanotube hybrid electrode for high-performance flexible all-solid-state supercapacitor. Nano Res 10:2570–2583. https://doi.org/10.1007/s12274-017-1459-9
66. Iqbal MF, Razaq A, Ashiq MN, Kaneti YV, Azhar AA, Yasmeen F, Saleem Joya K, Abbass S (2018) Excellent effect of graphene oxide thin films on growth and electrochemical performance of hierarchical zinc sulfide nanoweb for supercapacitor applications. ChemElectroChem 5:2636–2644. https://doi.org/10.1002/celc.201800633
67. Javed MS, Chen J, Chen L, Xi Yi, Zhang C, Buyong Wan CH (2015) Flexible full-solid state supercapacitor based on zinc sulfide spheres growing on carbon textile with superior charge storage. J Mater Chem A Mater 4:667–674. https://doi.org/10.1039/C5TA08752J
68. Arul NS, Cavalcante LS, In Han J (2017) Facile synthesis of ZnS/MnS nanocomposites for supercapacitor applications. J Solid State Electrochem 22:303–313. https://doi.org/10.1007/s10008-017-3782-1
69. Li X, Sun J, Feng L, Zhao L, Ye L, Zhang W (2018) Cactus-like ZnS / Ni 3 S 2 hybrid with high electrochemical performance for supercapacitors. J Alloys Compd 753:508–516. https://doi.org/10.1016/j.jallcom.2018.04.236
70. Li X, Cao J, Yang L, Wei M, Liu X, Liu Q, Hong Y, Yue Zhou JY (2019) One-pot synthesis of ZnS nanowires/Cu7S4 nanoparticles/reduced graphene oxide nanocomposites for supercapacitors and photocatalytic applications. Dalton Trans 48:2442–2454. https://doi.org/10.1039/C8DT04097D
71. Wei B, Liang H, Wang R, Zhang D, Qi Z, Wang Z (2018) One-step synthesis of graphitic-C 3 N 4 / ZnS composites for enhanced supercapacitor performance. J Energy Chem 27:472–477. https://doi.org/10.1016/j.jechem.2017.11.015
72. Cao H, Wang X, Chen X (2017) Hollow cubic double layer structured Cu7S4/NiS nanocomposites for high-performance supercapacitors. J Mater Chem A: Mater Energ Sustain 5:20729–20736. https://doi.org/10.1039/C7TA05784A
73. Hussain I, Shaheen I, Ahmad R, Ali I, Hussain K, Hussain SS, Alsaiari NS, Katubi KM, Eldin SM, Ansari MZ (2023) Binder-free cupric-ion containing zinc sulfide nanoplates-like structure for flexible energy storage devices. Chemosphere 314:137660. https://doi.org/10.1016/j.chemosphere.2022.137660
74. Pandit B, Bommineedi LK, Sankapal BR (2018) Electrochemical engineering approach of high performance solid-state flexible supercapacitor device based on chemically synthesized VS2 nanoregime structure. J Energy Chem 31:79–88. https://doi.org/10.1016/j.jechem.2018.05.011
75. Guo Z, Yang L, Wang W, Cao L, Dong B (2018) Ultrathin VS2 nanoplate with in-plane and out-of-plane defects for electrochemical supercapacitor with ultrahigh specific capacitance. J Mater Chem A Mater 6:14681–14688. https://doi.org/10.1039/C8TA03812K
76. Masikhwa TM, Barzegar F, Dangbegnon JK, Bello A, Madito MJ, Momodu D, Manyala N (2016) Asymmetric supercapacitor based on VS2 nanosheets and activated carbon materials. RSC Adv 6:38990–39000. https://doi.org/10.1039/C5RA27155J
77. Pandit B, Karade SS, Sankapal BR (2017) Hexagonal VS2 anchored MWCNTs : first approach to design flexible solid-state symmetric supercapacitor device. Appl Mater Interfaces 9:44880–44891. https://doi.org/10.1021/acsami.7b13908
78. Meyer E, Bede A, Mutukwa D, Taziwa R, Zingwe N (2020) Optimization, and analysis of carbon supported VS 2 nanocomposites as potential electrodes in supercapacitors. J Energy Storage 27:101074. https://doi.org/10.1016/j.est.2019.101074
79. Fang L, Zhang Z, Li X, Zhou H, Ma K, Ge L, Huang K (2016) Fabrication of hybrid cauliflower-like nanoarchitectures by in situ grown ZnO nanoparticals on VS 2 ultrathin nanosheets for high performance supercapacitors. Colloids Surf A Physicochem Eng Asp 501:42–48. https://doi.org/10.1016/j.colsurfa.2016.04.047
80. Kalam NA, Sengottaiyan C, Jayavel R, Ariga K, Shrestha RG, Subramani T, Sambasivam Sankar LKS (2018) Vanadium sulfide / reduced graphene oxide composite with enhance d supercapacitance performance. J Taiwan Inst Chem Eng 92:72–79. https://doi.org/10.1016/j.jtice.2018.01.040
81. Sun R, Wei Q, Li Q, Luo W, An Q, Sheng J, Di Wang WC, Mai L (2015) Vanadium sulfide on reduced graphene oxide layer as promising anode for sodium ion battery. Appl Mater Interfaces 7:20902–20908. https://doi.org/10.1021/acsami.5b06385
82. Wang X, Zhang Y, Zheng J, Liu X, Meng C (2019) Hydrothermal synthesis of VS 4 / CNTs composite with petal-shape structures performing a high specific capacity in a large potential range for high-performance symmetric supercapacitors. J Colloid Interface Sci 554:191–201. https://doi.org/10.1016/j.jcis.2019.06.105
83. Wang X, Zhang Y, Zheng J, Jiang H, Dong X, Liu X, Meng C (2020) Fabrication of vanadium sulfide (VS4) wrapped with carbonaceous materials as an enhanced electrode for symmetric supercapacitors. J Colloid Interface Sci 574:312–323. https://doi.org/10.1016/j.jcis.2020.04.072
84. Nguyen TT, Balamurugan J, Aravindan V, Kim NH, Lee JH (2019) Boosting the energy density of flexible solid-state supercapacitors via both ternary NiV2Se 4 and NiFe2Se 4 nanosheet Arrays. Chem Mater 31:4490–4504. https://doi.org/10.1021/acs.chemmater.9b01101
85. Marri SR, Ratha S, Rout CS, Behera JN (2017) 3D cuboidal vanadium diselenide embedded reduced graphene oxide hybrid structures with enhanced supercapacitor properties. Communications 53:228–231. https://doi.org/10.1039/C6CC08035A
86. Xu J, Zhang S, Wei Z, Yan W, Wei X, Huang K (2021) Orientated VSe2 nanoparticles anchored on N-doped hollow carbon sphere for high-stable aqueous energy application. J Colloid Interface Sci 585:12–19. https://doi.org/10.1016/j.jcis.2020.11.065
87. Ramu M, Chellan JR, Goli N, Joaquim P, Cristobal V, Kim BC (2020) A self-branched lamination of hierarchical patronite nanoarchitectures on carbon fiber cloth as novel electrode for ionic liquid electrolyte-based high energy density supercapacitors. Adv Funct Mater 30:1906586. https://doi.org/10.1002/adfm.201906586
88. Hussain S, Vikraman D, Sarfraz M, Faizan M, Patil SA, Batoo KM, Nam K-W, Kim H-S, Jung J (2023) Small 19:2205881. https://doi.org/10.1002/smll.202205881
89. Ratha S, Rout CS (2013) Supercapacitor electrodes based on layered tungsten disul fi de- reduced graphene oxide hybrids synthesized by a facile hydrothermal method. Appl Mater Interfaces 5:11427–11433
90. Tu C, Lin L, Xiao B, Chen Y (2016) Highly efficient supercapacitor electrode with two-dimensional tungsten disul fi de and reduced graphene oxide hybrid nanosheets. J Power Sources 320:78–85. https://doi.org/10.1016/j.jpowsour.2016.04.083
91. Shang X, Chi J, Lu S, Gou J, Dong B, Li X, Liu Y, Yan K, Chai Y, Liu C (2017) Carbon fiber cloth supported interwoven WS2

nanosplates with highly enhanced performances for supercapacitors. Appl Surf Sci 392:708–714. https://doi.org/10.1016/j.apsusc.2016.09.058
92. Qui X, Luning Wang L-ZF (2018) Immobilization of tungsten disulfide nanosheets on active carbon fiber as electrode materials for high performance quasi-solid state asymmetric supercapacitors. J Mater Chem A Mater 6:7835–7841. https://doi.org/10.1039/C8TA01047A
93. Ansari MZ, Ansari SA, Parveen N, Moo Hwan Cho TS (2018) lithium ion storage ability, supercapacitor electrode performance, and photocatalytic performance of tungsten disulfide nanosheets. New J Chem 42:5859–5867. https://doi.org/10.1039/C8NJ00018B
94. Gopi CVVM, Reddy AE, Bak J, Cho I, Kim H (2018) One-pot hydrothermal synthesis of tungsten diselenide / reduced graphene oxide composite as advanced electrode materials for supercapacitors. Mater Lett 223:57–60. https://doi.org/10.1016/j.matlet.2018.04.023
95. Yu P, Fu W, Zeng Q, Lin J, Yan C, Lai Z, Tang B (2017) Controllable synthesis of atomically thin Type-II Weyl semimetal WTe 2 nanosheets : an advanced electrode material for all-solid-state flexible supercapacitors. Communications 29:1–9. https://doi.org/10.1002/adma.201701909
96. Karade SS, Dwivedi P, Majumder S, Bidhan Pandit BRS (2017) First report on FeS based 2 V operating flexible solid-state symmetric supercapacitor dvice. Sustain Energy Fuels 1:1366–1375. https://doi.org/10.1039/C7SE00165G
97. Zhao C, Shao X, Zhu Z, Zhao C, Qian X (2017) One-pot hydrothermal synthesis of RGO / FeS composite on Fe foil for high performance supercapacitors. Electrochim Acta 246:497–506. https://doi.org/10.1016/j.electacta.2017.06.090
98. Sridhar V, Park H (2018) Carbon nanofiber linked FeS2 mesoporous nano-alloys as high capacity anodes for lithium-ion batteries and supercapacitors. J Alloys Compd 732:799–805. https://doi.org/10.1016/j.jallcom.2017.10.252
99. Zhong Y, Liu J, Lu Z, Xia H (2016) Hierarchical FeS2 nanosheet@Fe2O3 nanosphere heterostructure as promising electrode material for supercapacitors. Mater Lett 166:223–226. https://doi.org/10.1016/j.matlet.2015.12.092
100. Sun Z, Lin H, Zhang F, Yang X, Jiang H, Wang Q, Qu F (2018) Rapid microwave-assisted synthesis of high-rate FeS2 nanoparticles anchored on graphene for hybrid supercapacitors with ultrahigh energy density. J Mater Chem A Mater 6:14956–14966. https://doi.org/10.1039/C8TA05818K
101. Manikandan R, Justin Raj C, Nagaraju G, Velayutham R, Moulton SE, Puigdollers J, Chul Kim B (2021) Selenium enriched hybrid metal chalcogenides with enhanced redox kinetics for high-energy density supercapacitors. Chem Eng J 414:128924. https://doi.org/10.1016/j.cej.2021.128924
102. Shit M, Das P, Paul S, Samnta A, Aziz SkM, Ray PP, Sinha C (2022) In quest of new energy material: 3D Mn (II)-coordination polymer, the Schottky device and theoretical interpretation. ES Mater Manuf 19:. https://doi.org/10.30919/esmm5f804
103. Tang Y, Chen T, Yu S (2015) Morphology controlled synthesis of monodispersed manganese sulfide nanocrystals and their primary application in supercapacitors with high performances. Chem Commun 51:9018–9021. https://doi.org/10.1039/C5CC01700A
104. Li M, Liang J, Chai Y, Li D, Lu J, Li L (2017) One-step synthesis of alpha-MnS nanosheets for supercapacitor electrode materials. Micro Nano Lett 12:735–737. https://doi.org/10.1049/mnl.2017.0157
105. Pujari RB, Lokhande AC, Yadav AA, Kim JH, Lokhande CD (2016) Synthesis of MnS microfibers for high performance flexible supercapacitors. Mater Des 108:510–517. https://doi.org/10.1016/j.matdes.2016.07.038
106. Mohamed SG, Attia SY, Barakat YF, Hassan HH (2018) Hydrothermal synthesis of a -MnS nanoflakes @ nitrogen and sulfur co-doped rGO for high-performance hybrid supercapacitor. ChemPubSoc 3:6061–6072. https://doi.org/10.1002/slct.201801042
107. Tang Y, Chen T, Shengxue Yu, Qiao Y, Shichun Mu, Jie Hu FG (2015) Synthesis of graphene oxide anchored porous manganese sulfide nanocrystal via the nanoscale Kirkendall effect for supercapacitor. J Mater Chem A Mater 3:12913–12919. https://doi.org/10.1039/C5TA02480C
108. Naveenkumar P, Kalaignan GP (2018) Electrodeposited MnS on graphene wrapped Ni-foam for enhanced supercapacitor applications. Electrochim Acta 289:437–447. https://doi.org/10.1016/j.electacta.2018.09.100
109. Ragupathi V, Panigrahi P, Subramaniam NG (2019) g-C3N4 doped MnS as high performance electrode material for supercapacitor application. Mater Lett 246:88–91. https://doi.org/10.1016/j.matlet.2019.03.054
110. Pujari RB, Lokhande VC, Patil UM, Lee DW, Lokhande CD (2019) Controlled sulfurization of MnCO 3 microcubes architectured MnS 2 nanoparticles with 1.7 fold capacitance increment for high energy density supercapacitor. Electrochim Acta 301:366–376. https://doi.org/10.1016/j.electacta.2019.01.185
111. Chen T, Tang Y, Qiao Y, Liu Z, Guo W, Song J, Mu S, Yu S, Zhao Y, Gao F (2016) All-solid-state high performance asymmetric supercapacitors based on novel MnS nanocrystal and activated carbon materials. Sci Rep 6:. https://doi.org/10.1038/srep23289
112. Huang X, Zhang Z, Li H, Zhao Y, Wang H, Ma T (2017) Novel fabrication of Ni3S2/MnS composite as high performance supercapacitor electrode. J Alloys Compd 722:662–668. https://doi.org/10.1016/j.jallcom.2017.06.166
113. Kumbhar VS, Lee YR, Ra CS, Tuma D, Min B, Shim J (2017) Modified chemical synthesis of MnS nanoclusters on nickel foam for high performance all-solid-state asymmetric supercapacitors †. RSC Adv 7:16348–16359. https://doi.org/10.1039/C7RA00772H
114. Arul NS, In J, Mangalaraj HD (2017) Fabrication of highly flexible conducting electrode based on MnS nanoparticles / graphite / scotch tape for supercapacitor applications. J Mater Sci: Mater Electron 29:1636–1642. https://doi.org/10.1007/s10854-017-8075-z
115. Zhang G, Kong M, Yao Y, Long L, Yan M (2017) One-pot synthesis of γ -MnS / reduced graphene oxide with enhanced performance for aqueous asymmetric supercapacitors. Nanotechnology 28:1–12
116. Quan H, Cheng B, Chen D, Su X, Xiao Y, Lei S (2016) One-pot synthesis of α-MnS/nitrogen-doped reduced graphene oxide hybrid for high-performance asymmetric supercapacitors. Electrochim Acta 210:557–566. https://doi.org/10.1016/j.electacta.2016.05.031
117. Javed MS, Shoaib S, Shah A, Hussain S (2019) Tuning the phase of hierarchical mesoporous manganese-selenide microflowers towards significantly enhanced electrochemical performance as a flexible symmetric 1 . 8 V supercapacitor. Chem Eng J 122814. https://doi.org/10.1016/j.cej.2019.122814
118. Tang H, Yuan Y, Meng L, Wang W, Lu J, Zeng Y (2018) Low-resistance porous nanocellular MnSe electrodes for hybrid devices. Advanced Material Technology 3:1–8. https://doi.org/10.1002/admt.201800074
119. Sahoo S, Pazhamalai P, Krishnamoorthy K, Kim S (2018) Hydrothermally prepared a -MnSe nanoparticles as a new pseudocapacitive electrode material for supercapacitor. Electrochim Acta 268:403–410. https://doi.org/10.1016/j.electacta.2018.02.116
120. Ranganatha S, Munichandraiah N (2018) γ-MnS nanoparticles anchored reduced graphene oxide: electrode materials for high

performance supercapacitors. J Sci Adv Mater Dev 3:359–365. https://doi.org/10.1016/j.jsamd.2018.07.001
121. Balamuralitharan B, Karthick SN, Balasingam SK, Hemalatha KV, Selvam S, Raj JA, Prabakar K, Jun Y, Kim HJ (2017) Hybrid reduced graphene oxide/MnSe2 cubes: a new electrode material for supercapacitors. Energ Technol 5:1953–1962. https://doi.org/10.1002/ente.201700097
122. Yasoda KY, Baji DS, Kumar MS, Santhanagopalan D, Batabyal SK (2023) Sustainable development of manganese sulfoselenide nanoparticles anchored graphene oxide nanocomposite for high-performance supercapacitor and lithium-ion battery applications. J Alloys Compd 930:167282. https://doi.org/10.1016/j.jallcom.2022.167282
123. Huang K, Zhang J, Fan Y (2015) One-step solvothermal synthesis of different morphologies CuS nanosheets compared as supercapacitor electrode materials. J Alloys Compd 625:158–163. https://doi.org/10.1016/j.jallcom.2014.11.137
124. Heydari H, Moosavifard SE, Elyasi S, Shahraki M (2016) Nanoporous CuS nano-hollow spheres as advanced material for high-performance supercapacitors. Appl Surf Sci 394:425–430. https://doi.org/10.1016/j.apsusc.2016.10.138
125. Hsu Y, Chen Y, Lin Y (2014) Synthesis of copper sulfide nanowire arrays for high-performance supercapacitors. Electrochim Acta 139:401–407. https://doi.org/10.1016/j.electacta.2014.06.138
126. Zhang J, Feng H, Yang J, Qin Q, Fan H, Calying Wei WZ (2015) Solvothermal Synthesis of 3D Hierarchical CuS microspheres from a Cu-based ionic liquid precursor for high-performance asymmetric supercapacitors. Appl Mater Interfaces 7:21735–21744
127. Jin K, Zhou M, Zhao H, Zhai S, Ge F, Zhao Y, Cai Z (2018) Electrodeposited CuS nanosheets on carbonized cotton fabric as flexible supercapacitor electrode for high energy storage. Electrochimica Acta 295:668–676. https://doi.org/10.1016/j.electacta.2018.10.182
128. Patil AM, Lokhande VC, Ji T, Lokhande CD (2019) New design of all-solid state asymmetric flexible supercapacitor with high energy storage and long term cycling stability using m-CuO/FSS and h-CuS/FSS electrodes. Electrochim Acta 307:30–42. https://doi.org/10.1016/j.electacta.2019.03.108
129. De B, Kuila T, Kim NH, Lee JH (2017) Carbon dot stabilized copper sulphide nanoparticles decorated graphene oxide hydrogel for high performance asymmetric supercapacitor. Carbon N Y 122:247–257. https://doi.org/10.1016/j.carbon.2017.06.076
130. Naveed M, Younas W, Zhu Y, Rafai S, Zhao Q, Tahir M, Mushtaq N, Cao C (2019) Template free and facile microwave-assisted synthesis method to prepare mesoporous copper sul fi de nanosheets for high-performance hybrid supercapacitor. Electrochim Acta 319:49–60. https://doi.org/10.1016/j.electacta.2019.06.169
131. Kumar DR, Kesavan S, Baynosa ML, Shim J (2018) Flower-like Cu1.8S nanostructures for high-performance flexible solid-state supercapacitors. Appl Surf Sci 448:547–558. https://doi.org/10.1016/j.apsusc.2018.03.247
132. Durga IK, Rao SS, Reddy AE, Gopi CVVM, Kim H (2018) Achieving copper sulfide leaf like nanostructure electrode for high performance supercapacitor and quantum-dot sensitized solar cells. Appl Surf Sci 435:666–675. https://doi.org/10.1016/j.apsusc.2017.11.171
133. Bulakhe RN, Sahoo S, Chandrakant TTN, Lokhande D, Roh C, Yong Rok Lee J-JS (2016) Chemical synthesis of 3D copper sulfide with different morphologies for high performance supercapacitors application. RSC Adv 6:14844–14851. https://doi.org/10.1039/C5RA25568F
134. Zeraati M, Tahmasebi K (2019) Supercapacitor behavior of SiC coated copper hydroxide and copper sulfide nanowires. J Alloys Compd 786:798–807. https://doi.org/10.1016/j.jallcom.2019.01.373
135. Cui Y, Zhang J, Li G, Sun Y, Zhang G, Zheng W (2017) Ionic liquid-assisted synthesis of rGO wrapped three-dimensional CuS ordered nanoerythrocytes with enhanced performance for asymmetric supercapacitors. Chem Eng J 325:424–432. https://doi.org/10.1016/j.cej.2017.05.069
136. Ba Y, Zhou S, Jiao S, Pan W (2018) Fabrication of polyaniline / copper sulfide / poly (ethylene terephthalate) thread electrode for flexible fiber-shaped supercapacitors. J Appl Polym Sci 135:1–8. https://doi.org/10.1002/app.46769
137. Hou X, Liu X, Lu Y, Cheng J, Luo R (2017) Copper sulfide nanoneedles on CNT backbone composite electrodes for high-performance supercapacitors and Li-S batteries. J Solid State Electrochem 21:349–359. https://doi.org/10.1007/s10008-016-3322-4
138. Alshammari W, Patil DS, Pawar SA, Shin JC (2017) Silver nanowires-copper sulfide core/shell nanostructure for electrochemical supercapacitors. Mater Today Chem 5:72–80. https://doi.org/10.1016/j.mtchem.2017.07.004
139. Hong J, Kim B, Yang S, Jang A, Lee Y, Pak S, Lee S, Cho Y, Kang D, Shin HS, Hong JP, Morris SM, Cha S, Sohn JI, Kim JM (2019) Chalcogenide solution-mediated activation protocol for scalable and ultrafast synthesis of single-crystalline 1-D copper sulfide for supercapacitor. J Mater Chem A Mater 7:2529–2535. https://doi.org/10.1039/c8ta10743b
140. You X, Zhao X, Liu X, Ye M, Trans D, Cdta DOI (2018) Hierarchical Cu2S nanorods with different crystal phases for asymmetrical supercapacitors and visible-light photocatalysis. Dalton Trans 47:15189–15196. https://doi.org/10.1039/C8DT03794A
141. Zhao T, Yang W, Zhao X, Peng X, Hu J, Tang C, Li T (2018) Facile preparation of reduced graphene oxide/copper sulfide composite as electrode materials for supercapacitors with high energy density. Compos B Eng 150:60–67. https://doi.org/10.1016/j.compositesb.2018.05.058
142. Javed MS, Dai S, Wang M, Xi Yi, Lang Q, Donglin Guo CH (2015) Faradic redox active material of Cu7S4 nanowires with high conductance for flexible solid state supercapacitor. Nanoscale 7:13610–13618. https://doi.org/10.1039/C5NR03363B
143. Liu Y, Qi X, Li L, Zhang S, Bi T (2019) MOF-derived PPy / carbon-coated copper sulfide ceramic nanocomposite as high-performance electrode for supercapacitor. Ceram Int 45:17216–17223. https://doi.org/10.1016/j.ceramint.2019.05.277
144. Zhou K, Liang J, Liu J, Sun P, Bu J, Zhang W, Chen G (2016) Synthesis of porous Cu7.2S4 sub-microspheres by an ion exchange method for high-performance supercapacitors. RSC Adv 6:16832–16837. https://doi.org/10.1039/C5RA26976H
145. Xu P, Miao C, Cheng K, Ye K, Yin J, Cao D (2016) High electrochemical energy storage performance of controllable synthesis of nanorod Cu 1. 92 S accompanying nanoribbon CuS directly grown on copper foam. Electrochim Acta 214:276–285. https://doi.org/10.1016/j.electacta.2016.08.049
146. Wang Y, Liu F, Ji Y, Yang M, Liu W, Wang W, Sun Q, Zhang Z, Zhao X, Liu X (2015) Controllable synthesis of various kinds of copper sulfides (CuS, Cu7S4, Cu9S5) for high-performance supercapacitors. Dalton Trans 44:1043–10437. https://doi.org/10.1039/C5DT00402K
147. Pazhamalai P, Krishnamoorthy K, Kim SJ (2016) Hierarchical copper selenide nanoneedles grown on copper foil as a binder free electrode for supercapacitors. Int J Hydrogen Energy 41:14830–14835. https://doi.org/10.1016/j.ijhydene.2016.05.157
148. Shinde SK, Ghodake GS, Dubal DP, Patel RV, Saratale RG, Kim D (2017) Electrochemical synthesis : monoclinic Cu 2 Se nanodendrites with high performance for supercapacitors. J Taiwan

Inst Chem Eng 75:271–279. https://doi.org/10.1016/j.jtice.2017.01.028
149. Jin R, Meng M, Zhang S, Lixia Yang GL (2018) CNTs@Cu2-xSe hybrid materials: an advanced electrode for high performance lithium batteries and supercapacitors. Energ Technol 6:2179–2187. https://doi.org/10.1002/ente.201800236
150. Huang K, Zhang J, Xing K (2014) One-step synthesis of layered CuS / multi-walled carbon nanotube nanocomposites for supercapacitor electrode material with ultrahigh specific capacitance. Electrochim Acta 149:28–33. https://doi.org/10.1016/j.electacta.2014.10.079
151. Sulphide NGC, Chen C, Zhang Q, Ma T, Fan W (2017) Synthesis and electrochemical properties of nitrogen-doped graphene/copper sulphide nanocomposite for supercapacitor. J Nanosci Nanotechnol 17:2811–2816. https://doi.org/10.1166/jnn.2017.12668
152. Brown JW, Ramesh PS, Geetha D (2018) Fabrication of mesoporous iron (Fe) doped copper sulfide (CuS) nanocomposite in the presence of a cationic surfactant via mild hydrothermal method for supercapacitors. Mater Res Express 5:1–8
153. Huang K, Zhang J, Jia Y, Xing K, Liu Y (2015) Acetylene black incorporated layered copper sulfide nanosheets for high-performance supercapacitor. J Alloys Compd 641:119–126. https://doi.org/10.1016/j.jallcom.2015.04.075
154. Hu H, Qi J, Sui Y, Zhou Y, Wei F, He Y (2017) Facile synthesis of copper sulfides with different shapes for high- performance supercapacitors. J Mater Sci: Mater Electron 28:10720–10729. https://doi.org/10.1007/s10854-017-6848-z
155. Huang K, Zhang J, Liu Y, Liu Y (2015) Synthesis of reduced graphene oxide wrapped- copper sulfide hollow spheres as electrode material for supercapacitor. Int J Hydrogen Energy 40:10158–10167. https://doi.org/10.1016/j.ijhydene.2015.05.152
156. Properties E, Krishnamoorthy K, Veerasubramani GK (2015) Preparation of copper sulfide nanoparticles by sonochemical method and study on their. J Nanosci Nanotechnol 15:4409–4413. https://doi.org/10.1166/jnn.2015.9594
157. Liu Y, Zhou Z, Zhang S, Luo W, Zhang G (2018) Controllable Synthesis of CuS hollow microflowers hierarchical structures for asymmetric supercapacitors. Appl Surf Sci 442:711–719. https://doi.org/10.1016/j.apsusc.2018.02.220
158. Kanaka Durga I, Srinivasa Rao S, Ahn JW, Park TY, Jin-Soo B, Ho CI, Prabakar K, Kim HJ (2018) Dice-like nanostructures of a CuS@PbS composite for high-performance supercapacitor electrode applications. Energies (Basel) 11:1624–1635. https://doi.org/10.3390/en11071624
159. Xiao W, Zhou W, Feng T, Zhang Y, Liu H (2016) One-pot solvothermal synthesis of flower-like copper sulfide / reduced graphene oxide composite superstructures as high- performance supercapacitor electrode materials. J Mater Sci: Mater Electron 28:5931–5940. https://doi.org/10.1007/s10854-016-6267-6
160. Wang G, Mingyuan Zhang LuLu, Hongfeng Xu, Zuoyi Xiao SG (2018) One-pot synthesis of CuS nanoflower-decorated active carbon layer for high-performance asymmetric supercapaciotrs. ChemNanoMat 4:946–971. https://doi.org/10.1002/cnma.201800179
161. Xu W, Liang Y, Su Y, Zhu S, Cui Z, Yang X, Inoue A, Wei Q, Liang C (2016) Synthesis and properties of morphology controllable copper sulphide nanosheets for supercapacitor application. Electrochim Acta 211:891–899. https://doi.org/10.1016/j.electacta.2016.06.118
162. Podili S, Geetha D, Ramesh PS Preparation and characterization of porous hollow sphere of Ni doped CuS nanostructures for electrochemical supercapacitor electrode material. Recent Trends Mater Sci Appl 277–288. https://doi.org/10.1007/978-3-319-44890-9
163. Peng S, Fan L, Wei C, Liu X, Zhang H, Xu W, Xu J (2017) Flexible polypyrrole / copper sulfide / bacterial cellulose nanofibrous composite membranes as supercapacitor electrodes. Carbohydr Polym 157:344–352. https://doi.org/10.1016/j.carbpol.2016.10.004
164. Peng H, Ma G, Sun K, Mu J, Lei Z (2014) High-performance supercapacitor based on multi-structural CuS@polypyrrole composites prepared by in situ oxidative polymerization. J Mater Chem A Mater 2:3303–3307. https://doi.org/10.1039/c3ta13859c
165. Peng H, Ma G, Mu J, Sun K, Lei Z (2014) Controllable synthesis of CuS with hierarchical structures via a surfactant-free method for high-performance supercapacitors. Mater Lett 122:25–28. https://doi.org/10.1016/j.matlet.2014.01.173
166. Naveenkumar P, Paruthimal G, Subramanian K, Sambandam A (2018) Solvothermal synthesis of CuS / Cu (OH) 2 nanocomposite electrode materials for supercapacitor applications. J Mater Sci: Mater Electron 29:16853–16863. https://doi.org/10.1007/s10854-018-9780-y
167. Kumar YA, Rao SS, Punnoose D, Tulasivarma CV, Gopi CVVM, Prabakar K, Kim H, Kim H (2017) Influence of solvents in the preparation of cobalt sulfide for supercapacitors. R Soc Open Sci 49:1–10
168. Zhang D, Liu H, Zhang J, Wang X, Zhang R, Zhou J (2016) Synthesis of novel CoS 2 nanodendrites with high performance supercapacitors. 11:6791–6798. https://doi.org/10.20964/2016.08.44
169. Amaresh S, Karthikeyan K, Jang IC, Lee YS (2014) Single-step microwave mediated synthesis of the CoS2 anode material for high rate hybrid supercapacitor. J Mater Chem A Mater 2:11099–11106. https://doi.org/10.1039/c4ta01633e
170. Liu L, Rong H, Li J, Tong X, Wang Z (2017) Synthesis of hierarchical cobalt sulfide/cobalt basic salt nanocomposite via a vapor-phase hydrothermal method for supercapacitors. New J Chem 41:12147–12152. https://doi.org/10.1039/C7NJ02350B
171. Chen Q, Li H, Cai C, Yang S, Huang K, Wei X, Zhong J (2013) In-situ shape and phase transformation synthesis of Co3S4 nanosheet arrays for high-performance electrochemical supercapacitor. RSC Adv 3:22922–22926. https://doi.org/10.1039/b000000x
172. Aloqayli S, Ranaweera CK, Wang Z, Siam K, Kahol PK, Tripathi P, Srivastava ON (2017) Nanostructured cobalt oxide and cobalt sul fi de for fl exible, high performance and durable supercapacitors. Energy Storage Mater 8:68–76. https://doi.org/10.1016/j.ensm.2017.05.006
173. Das CK (2015) Hydrothermal growth of hierarchical Ni3S2 and Co3S4 on reduced graphene oxide hydrogel @ Ni foam : high energy density aqueous asymmetric supercapacitor. Appl Mater Interfaces 7:1122–1131
174. Liu S, Mao C, Niu Y, Yi F, Hou J, Lu S, Jiang J, Xu M, Li C (2015) Facile synthesis of novel networked ultralong cobalt sul fi de nanotubes and its application in supercapacitors. Appl Mater Interfaces 7:25568–25573. https://doi.org/10.1021/acsami.5b08716
175. Cao F, Zhao M, Yu Y, Chen B, Huang Y, Yang J, Cao X (2016) Synthesis of two-dimensional CoS 1.097 /nitrogen-doped carbon nanocomposites using metal – organic framework nanosheets as precursors for supercapacitor application. J Am Chem Soc 138:6924–6927. https://doi.org/10.1021/jacs.6b02540
176. Chang Y, Sui Y, Qi J, Jiang L, He Y, Wei F, Meng Q, Jin Y (2017) Facile synthesis of Ni 3 S 2 and Co 9 S 8 double-size nanoparticles decorated on rGO for high-performance supercapacitor electrode materials. Electrochim Acta 226:69–78. https://doi.org/10.1016/j.electacta.2016.12.184
177. Zhu F, Yan M, Liu Y, Shen H, Lei Y, Shi W (2017) Hexagonal prism-like hierarchical Co9S8@Ni(OH)2 core-shell nanotubes

on carbon fibers for high-performance asymmetric supercapacitors. J Mater Chem A Mater 5:22782–22789. https://doi.org/10.1039/C7TA07160D
178. Han X, Tao K, Wang D, Han L (2018) Design of a porous cobalt sulfide nanosheet array on Ni foam from zeolitic imidazolate frameworks as an advanced electrode for supercapacitors. Nanoscale 10:2735–2741. https://doi.org/10.1039/c7nr07931a
179. Chen T, Li S, Gui P, Wen J, Xuemei Fu GF (2018) Bifunctional bamboo-like CoSe2 arrays for high performance asymmetric supercapacitor and electrocatalytic oxygen evolution. Nanotechnology 29:1–21
180. Bose R, Patil B, Jothi VR, Kim T, Arunkumar P, Ahn H, Yi SC (2018) Co3Se4 nanosheets embedded on N-CNT as an efficient electroactive material for hydrogen evolution and supercapacitor applications. J Ind Eng Chem 65:62–71. https://doi.org/10.1016/j.jiec.2018.04.013
181. Peng H, Ma G, Sun K, Zhang Z, Li J, Zhou X (2015) A novel aqueous asymmetric supercapacitor based on petal-like cobalt selenide nanosheets and nitrogen-doped porous carbon networks electrodes. J Power Sources 297:351–358. https://doi.org/10.1016/j.jpowsour.2015.08.025
182. Kirubasankar B, Murugadoss V, Angaiah S (2017) Hydrothermal assisted in situ growth of CoSe onto graphene nanosheets as a nanohybrid positive electrode for asymmetric supercapacitors †. RSC Adv 7:5853–5862. https://doi.org/10.1039/C6RA25078E
183. Zhang X, Gong J, Zhang K, Zhu W, Li J (2019) All-solid-state asymmetric supercapacitor based on porous cobalt selenide thin fi lms. J Alloys Compd 772:25–32. https://doi.org/10.1016/j.jallcom.2018.09.023
184. Zhao X, Li X, Zhao Y, Su Z, Wang R (2017) Facile synthesis of tremelliform Co 0. 85 Se nanosheets for supercapacitor. J Alloys Compd 697:124–131. https://doi.org/10.1016/j.jallcom.2016.12.124
185. Zhang Y, Pan A, Wang Y, Cao X, Zhou Z, Zhu T (2017) Self-templated synthesis of N-doped CoSe 2 / C double-shelled dodecahedra for high-performance supercapacitors. Energy Storage Mater 8:28–34. https://doi.org/10.1016/j.ensm.2017.03.005
186. Manikandan M, Subramani K (2020) Hydrothermal synthesis of cobalt telluride nanorods for a high performance hybrid asymmetric supercapacitor. RSC Adv 10:13632–13641. https://doi.org/10.1039/c9ra08692g
187. Xiao Mi, Yupeng Su, Du Meilian Zhao B (2019) Synthesis of CoTe nanowires: a new electrode material for supercapacitor with high-stability and high-performance. Nanotechnology 31:1–14
188. Mao H, Yu J, Li J, Zheng T, Cen J, Ye Y (2019) A high-performance supercapacitor electrode based on nano flower-shaped CoTe2. Ceram Int 46:6991–6994. https://doi.org/10.1016/j.ceramint.2019.11.141
189. Ye B, Gong C, Huang M, Fan L, Lin J, Wu J (2018) Improved performance of a CoTe // AC asymmetric supercapacitor using a redox additive aqueous electrolyte. RSC Adv 8:7997–8006. https://doi.org/10.1039/C7RA12919J
190. Gong C, Huang M, Zhou P, Sun Z, Fan L (2016) Mesoporous Co0.85Se nanosheets supported on Ni foam as a positive electrode material for asymmetric supercapacitor. Appl Surf Sci 362:469–476. https://doi.org/10.1016/j.apsusc.2015.11.194
191. Younas W, Naveed M, Cao C, Khalid S, Rafai S, Wang Z, Wu Y, Yang L (2020) Rapid and simplistic microwave assisted method to synthesise cobalt selenide nanosheets; a prospective material for high performance hybrid supercapacitor. Appl Surf Sci 505:144618. https://doi.org/10.1016/j.apsusc.2019.144618
192. Chen T, Li S, Wen J, Gui P, Guo Y, Guan C, Liu J (2018) Rational construction of hollow core-branch CoSe 2 nanoarrays for high-performance asymmetric supercapacitor and efficient oxygen evolution. Small 14:1–8. https://doi.org/10.1002/smll.201700979
193. Sun P, Liang J, Chen G, Zhou K, Li Y, Liu J, Zhang W, Niu F, Zhang W (2017) Direct growth of bundle-like cobalt selenide nanotube arrays on Ni foam as binder-free electrode for high-performance supercapacitor. Res Chem Intermed 43:1969–1978. https://doi.org/10.1007/s11164-016-2742-1
194. Yang J, Yuan Y, Wang W, Tang H, Ye Z, Lu J (2017) Interconnected Co 0. 85 Se nanosheets as cathode materials for asymmetric supercapacitors. J Power Sources 340:6–13. https://doi.org/10.1016/j.jpowsour.2016.11.061
195. Zhu Y, Huang Z, Hu Z, Xi L, Ji X, Liu Y (2018) 3D interconnected ultrathin cobalt selenide nanosheets as cathode materials for hybrid supercapacitors. Electrochim Acta 269:30–37. https://doi.org/10.1016/j.electacta.2018.02.146
196. Bao S, Li CM, Guo C, Qiao Y (2008) Biomolecule-assisted synthesis of cobalt sulfide nanowires for application in supercapacitors. J Power Sources 180:676–681. https://doi.org/10.1016/j.jpowsour.2008.01.085
197. Chen C, Shih Z, Yang Z, Chang H (2012) Carbon nanotubes / cobalt sul fi de composites as potential high-rate and high-ef fi ciency supercapacitors. J Power Sources 215:43–47. https://doi.org/10.1016/j.jpowsour.2012.04.075
198. Cheng JP, Chen WQ, Gao SQ, Guo SH, Liu F (2018) Low crystalline 2D CoS x derived from cobalt carbonate hydroxide by sul fi dation at room temperature for supercapacitor. Electrochim Acta 286:14–21. https://doi.org/10.1016/j.electacta.2018.08.035
199. Chiu JM, Lin LY, Yeh PH, Lai CY, Teng K, Tu CC, Yang SS, Yu JF (2015) Synthesizing highly conductive cobalt sulfide hydrangea macrophylla using long carbon-chain sulfur source for supercapacitor. RSC Adv 5:83383–83390. https://doi.org/10.1039/C5RA16920H
200. Dai K, Lu L, Liang C, Geng L, Zhu G (2016) Large-scale synthesis of cobalt sul fi de / carbon nanotube hybrid and its excellent electrochemical capacitance performance. Mater Lett 176:42–45. https://doi.org/10.1016/j.matlet.2016.04.063
201. Dubal DP, Gund GS, Lokhande CD, Holze R (2014) Controlled growth of CoS x nanostrip arrays (CoS x -NSA) on nickel foam for asymmetric supercapacitors. Energ Technol 2:401–408. https://doi.org/10.1002/ente.201300193
202. El-gendy DM, Afifi IM, Allam NK (2019) Eco-friendly, one-step synthesis of cobalt sulfide-decorated functionalized graphene for high-performance supercapacitors. J Energy Storage 24:100760. https://doi.org/10.1016/j.est.2019.100760
203. Grace AN, Ramachandran R, Vinoba M, Choi Y (2014) Facile synthesis and electrochemical properties of Co 3 S 4 - nitrogen-doped graphene nanocomposites for supercapacitor applications. Electroanalysis 26:199–208. https://doi.org/10.1002/elan.201300262
204. Hu H, Guan BY, Wen X, Lou D, Hu H, Guan BY, Wen X, Lou D (2016) Construction of complex CoS hollow structures with enhanced electrochemical properties for hybrid supercapacitors construction of complex CoS hollow structures with enhanced electrochemical properties for hybrid supercapacitors. Chem 1:102–113. https://doi.org/10.1016/j.chempr.2016.06.001
205. Huang K, Zhang J, Shi G, Liu Y (2014) One-step hydrothermal synthesis of two-dimensional cobalt sul fi de for high-performance supercapacitors. Mater Lett 131:45–48. https://doi.org/10.1016/j.matlet.2014.05.148
206. Ji Y, Liu X, Liu W, Wang Y, Zhang H, Yang M, Wang X (2014) A facile template-free approach for the solid-phase synthesis of CoS 2 nanocrystals and their enhanced storage energy in supercapacitors †. RSC Adv 4:50220–50225. https://doi.org/10.1039/C4RA08614G
207. Jiang Z, Lu W, Li Z, Ho H, Li X (2014) Synthesis of amorphous cobalt sulfide polyhedral nanocages for high performance supercapacitors †. J Mater Chem A Mater 2:8603–8606. https://doi.org/10.1039/c3ta14430e

208. Jiang D, Xu Q, Meng S, Xia C, Chen M (2017) Construction of cobalt sulfide/graphitic carbon nitride hybrid nanosheet composites for high performance supercapacitor electrodes. J Alloys Compd 706:41–47. https://doi.org/10.1016/j.jallcom.2017.02.204
209. Kale SB, Lokhande AC, Pujari RB, Lokhande CD (2018) Cobalt sulfide thin films for electrocatalytic oxygen evolution reaction and supercapacitor applications. J Colloid Interface Sci 532:491–499. https://doi.org/10.1016/j.jcis.2018.08.012
210. Krishnamoorthy K, Kumar G, Jae S (2015) Hydrothermal synthesis, characterization and electrochemical properties of cobalt sulfide nanoparticles. Mater Sci Semicond Process 40:781–786. https://doi.org/10.1016/j.mssp.2015.06.070
211. Li H, Gao Y, Shao Y, Su Y, Wang X (2015) Vapor-phase atomic layer deposition of Co 9 S 8 and its application for supercapacitors. Nano Lett 15:6689–6695. https://doi.org/10.1021/acs.nanolett.5b02508
212. Li B, Hu Y, Li J, Liu M, Kong L, Hu Y, Kang L (2016) Mechanical alloying synthesis of Co 9 S 8 particles as materials for supercapacitors. Metals (Basel) 6:6–11. https://doi.org/10.3390/met6060142
213. Li Ye, Liu S, Chen W, Li S, Luolin Shi YZ (2017) Facile synthesis of flower-like cobalt sulfide hierarchitectures with superior electrode performance for supercapacitors. J Alloys Compd 712:139–146. https://doi.org/10.1016/j.jallcom.2017.04.064
214. Li L, Ding Y, Huang H, Yu D, Zhang S, Chen H, Ramakrishna S, Peng S (2019) Controlled synthesis of unique Co 9 S 8 nanostructures with carbon coating as advanced electrode for solid-state asymmetric supercapacitors. J Colloid Interface Sci 540:389–397. https://doi.org/10.1016/j.jcis.2019.01.002
215. Li H, Xuan H, Gao J, Liang T, Han X, Guan Y, Yang J, Han P, Du Y (2019) Construction of core-shell cobalt sul fi de / manganese molybdate nanostructure on reduced graphene oxide / Ni foam as an advanced electrode for high-performance asymmetric supercapacitor. Electrochim Acta 312:213–223. https://doi.org/10.1016/j.electacta.2019.05.008
216. Lin JY, Chou SW (2013) Cathodic deposition of interlaced nanosheet-like cobalt sulfide films for high-performance supercapacitors. RSC Adv 3:2043–2048. https://doi.org/10.1039/c2ra22373b
217. Lin T-W, Dai C-S, Tsai T-T, Chou S-W, Jeng-Yu Lin H-HS (2015) High-performance asymmetric supercapacitor based on Co 9 S 8 / 3D graphene composite and graphene hydrogel. Chem Eng J 279:241–249. https://doi.org/10.1016/j.cej.2015.05.011
218. Liang Xu YL (2015) One-step synthesis of cobalt sulfide/reduced graphene oxide xcomposite used as electrode material for supercapacitor. RSC Adv 5:67518–67523. https://doi.org/10.1039/C5RA11711A
219. Luo F, Li J, Yuan H, Xiao D (2014) Rapid synthesis of three-dimensional flower-like cobalt sulfide hierarchitectures by microwave assisted heating method for high-performance supercapacitors. Electrochim Acta 123:183–189. https://doi.org/10.1016/j.electacta.2014.01.009
220. Mao M, Mei L, Wu L, Li Q, Zhang M (2014) Facile synthesis of cobalt sulfide/carbon nanotube shell / core composites for high performance. RSC Adv 4:12050–12056. https://doi.org/10.1039/c4ra00485j
221. Meng X, Sun H, Zhu J, Bi H, Han Q, Xiaoheng Liu XW (2016) Graphene-based cobalt sulfides composite hydrogel with enhanced electrochemical properties for supercapacitors. New J Chem 40:2843–2849. https://doi.org/10.1039/C5NJ03423J
222. Mohammadi A, Arsalani N, Tabrizi AG, Moosavifard SE, Naqshbandi Z, Ghadimi LS (2017) Engineering rGO-CNT wrapped Co 3 S 4 nanocomposites for high-performance. Chem Eng J 334:66–80. https://doi.org/10.1016/j.cej.2017.10.029
223. Patil SJ, Kim JH, Lee DW (2017) Graphene-nanosheet wrapped cobalt sulphide as a binder free hybrid electrode for asymmetric solid-state supercapacitor. J Power Sources 342:652–665. https://doi.org/10.1016/j.jpowsour.2016.12.096
224. Pu J, Wang Z, Wu K, Yu N, Sheng E (2014) Co9S8 nanotube arrays supported on nickel foam for high-performance supercapacitors †. Phys Chem Chem Phys 16:785–791. https://doi.org/10.1039/c3cp54192d
225. Rakhi RB, Alhebshi NA, Anjum DH, Alshareef HN (2014) Nanostructured cobalt sulfide-on-fiber with tunable morphology as electrodes for asymmetric hybrid supercapacitors. J Mater Chem A: Mater Energ Sustain 2:16190–16198. https://doi.org/10.1039/C4TA03341H
226. Ray RS, Sarma B, Jurovitzki AL, Misra M (2014) Fabrication and characterization of titania nanotube/cobalt sulfide supercapacitor electrode in various electrolytes. Chem Eng J 260:671–683. https://doi.org/10.1016/j.cej.2014.07.031
227. Ren R, Faber MS, Dziedzic R, Wen Z, Jin S (2015) Metallic CoS 2 nanowire electrodes for high cycling performance supercapacitors. Nanotechnology 26:494001. https://doi.org/10.1088/0957-4484/26/49/494001
228. Shi J, Li X, He G, Zhang L, Li M (2015) Electrodeposition of high-capacitance 3D CoS/graphene nanosheets on nickel foam for high-performance aqueous asymmetric supercapacitors. J Mater Chem A Mater 3:20619–20626. https://doi.org/10.1039/C5TA04464B
229. Su C, Xiang J, Wen F, Song L, Mu C, Xu D, Hao C, Liu Z (2016) Microwave synthesized three-dimensional hierarchical nanostructure CoS 2 / MoS 2 growth on carbon fiber cloth : a bifunctional electrode for hydrogen evolution reaction and supercapacitor. Electrochim Acta 212:941–949. https://doi.org/10.1016/j.electacta.2016.07.012
230. Subramani K, Sudhan N, Divya R, Sathish M (2017) All solid-state asymmetric supercapacitors based on cobalt hexacyanoferrate-derived CoS and activated carbon. RSC Adv 7:6648–6659. https://doi.org/10.1039/C6RA27331A
231. Yang Z, Ma Q, Han L, Tao K (2019) Design of Mo-doped cobalt sulfide hollow nanocages from zeolitic imidazolate framework as advanced electrodes for supercapacitors. Inorg Chem Front 6:2178–2184. https://doi.org/10.1039/C9QI00663J
232. Yin L, Wang L, Liu X, Gai Y, Su L, Qu B, Gong L (2015) Ultrafast microwave synthesis of 3D flower-like Co 9 S 8 hierarchical architectures for high-performance supercapacitor applications. Eur J Inorg Chem 2015:24572462. https://doi.org/10.1002/ejic.201500120
233. Zhang Z, Wang Q, Zhao C, Min S, Qian X (2015) One-step hydrothermal synthesis of 3D petal-like Co9S8 / RGO / Ni3S2 composite on nickel foam for high-performance supercapacitors one-step hydrothermal synthesis of 3D petal-like Co 9 S 8 / RGO / Ni 3 S 2 composite on nickel foam for high-performance Sup. Appl Mater Interfaces 7:4861–4868. https://doi.org/10.1021/am5088192
234. Xu N, Lei H, Hou T, Wang X, Hu Y, Peng H, Ma G (2023) Constructing an asymmetric supercapacitor based on Prussian blue analogues-derived cobalt selenide nanoframeworks and iron oxide nanoparticles. Electrochim Acta 439:141686. https://doi.org/10.1016/j.electacta.2022.141686
235. Du N, Zheng W, Li X, He G, Wang L, Shi J (2017) Nanosheet-assembled NiS hollow structures with double shells and controlled shapes for high-performance supercapacitors. Chem Eng J 323:415–424. https://doi.org/10.1016/j.cej.2017.04.127
236. Gaikar P, Pawar SP, Mane RS, Nuashad M, Shinde DV (2016) Synthesis of nickel sulfide as a promising electrode material for pseudocapacitor application. RSC Adv 6:112589–112593. https://doi.org/10.1039/c0xx00000x

237. Fu W, Zhao Y, Mei J, Wang F, Han W, Xie E (2018) Honeycomb-like Ni3S2 nanosheet arrays for high-performance hybrid supercapacitors Wenbin. Electrochim Acta 283:737–743. https://doi.org/10.1016/j.electacta.2018.07.014
238. Akbarzadeh R, Dehghani H (2018) From nickel oxalate dihydrate microcubes to NiS 2 nanocubes for high performance supercapacitors. J Solid State Electrochem 22:3375–3382
239. Gou J, Xie S, Liu C (2017) Hollow sphere NiS 2 as high-performance hybrid supercapacitor electrode materials. AIP Conf Proc 179:1–5. https://doi.org/10.1063/1.4971922
240. Li Z, Han J, Fan L, Guo R (2015) Template-free synthesis of Ni7S6 hollow spheres with mesoporous shells for high performance supercapacitors. CrystEngComm 17:1952–1958. https://doi.org/10.1039/C4CE02548B
241. Nandhini S, Christina AJ, Muralidharan G (2018) Facile microwave-hydrothermal synthesis of NiS nanostructures for supercapacitor applications. Appl Surf Sci 449:485–491. https://doi.org/10.1016/j.apsusc.2018.01.024
242. Cheng Y, Zhai M, Guo M, Yu Y, Hu J (2018) A novel electrode for supercapacitors : spicules-like Ni 3 S 2 shell grown on molybdenum nanoparticles doped nickel foam. Appl Surf Sci 467–468:1113–1121. https://doi.org/10.1016/j.apsusc.2018.10.230
243. Gao AR, Zhang Q, Soyekwo F (2017) Novel amorphous nickel sulfide @ CoS double-shelled polyhedral nanocages for supercapacitor electrode materials with superior electrochemical properties. Electrochim Acta 237:94–101. https://doi.org/10.1016/j.electacta.2017.03.214
244. Chen T, Liu Z, Liu Z, Tao X, Fan H, Guo L (2019) Fabrication of interconnected 2D / 3D NiS / Ni 3 S 4 composites for high performance supercapacitor. Mater Lett 248:1–4. https://doi.org/10.1016/j.matlet.2019.03.125
245. Li S, Chen T, Wen J, Gui P, Fang G (2017) In-situ grown Ni9S8 nanorod/O-MoS2 nanosheet nanocomposite on carbon cloth as a free binder supercapacitor electrode and hydrogen evolution catalyst. Nanotechnology 28:1–26
246. Gu Y, Du W, Darrat Y, Saleh M, Huang Y, Zhang Z, Wei S (2019) In situ growth of novel nickel diselenide nanoarrays with high specific capacity as the electrode material of flexible hybrid supercapacitors. Appl Nanosci 10:1591–1601. https://doi.org/10.1007/s13204-019-01234-8
247. H Li, J Gong, J Li, X Zhang, C Tang, H Yao, Q Ding, 2020 Synthesis of nickel selenide thin films for high performance all-solid-state asymmetric supercapacitors. Chinese Chemical Letters In press: https://doi.org/10.1016/j.cclet.2020.03.010
248. Yu AD, Li Z, Zhao G, Zhang H (2019) Network of porous ultrathin NiSe nanosheets on nickel foam for high-performance hybrid supercapacitor. ChemS 13:1–9. https://doi.org/10.1002/cssc.201901766
249. Du L, Du W, Ren H, Wang N, Yao Z, Shi X, Zhang B, Zai J, Qian X (2017) Honeycomb-like metallic nickel selenide nanosheet arrays as binder-free electrodes for high-performance hybrid asymmetric supercapacitors†. J Mater Chem A Mater 5:22527–22535. https://doi.org/10.1039/c7ta06921a
250. Wu L, Xue Y, Chen H, Zhang K, Qin A, Chen S (2020) Synthesis of Ni 3 Se 2 on nickel foam with different morphologies for high - performance supercapacitor electrode. J Mater Sci: Mater Electron 31:6140–6149. https://doi.org/10.1007/s10854-020-03167-3
251. Gu Y, Id LF, Huang J, Geng C, Lin J (2018) Hydrothermal synthesis of Co-Doped NiSe 2 nanowire for high-performance asymmetric supercapacitors. Materials 11:1–15. https://doi.org/10.3390/ma11081468
252. Arul NS, Han JI (2018) Enhanced pseudocapacitance of NiSe2/Ni(OH)2 nanocomposites for supercapacitor electrode. Mater Lett 234:87–91. https://doi.org/10.1016/j.matlet.2018.09.064
253. Gu Y, Fan L, Huang J, Geng C, Lin J (2019) N-doped reduced graphene oxide decorated NiSe 2 nanoparticles for high- performance asymmetric supercapacitors. J Power Sources 425:60–68. https://doi.org/10.1016/j.jpowsour.2019.03.123
254. Jiang S, Wu J, Ye B, Fan Y, Ge J, Guo Q, Huang M (2017) Growth of Ni 3 Se 2 nanosheets on Ni foam for asymmetric supercapacitors. J Mater Sci: Mater Electron 29:4649–4657. https://doi.org/10.1007/s10854-017-8416-y
255. Kirubasankar B, Murugadoss V, Lin J, Ding T, Dong M, Liu H, Zhang J, Li T, Wang N, Guo Z, Angaiah S (2018) In situ grown nickel selenide on graphene nanohybrid electrodes for high energy density asymmetric supercapacitors. Nanoscale 10:20414–20425. https://doi.org/10.1039/c8nr06345a
256. Peng H, Zhou J, Sun K, Zhang Z, Feng E, Lei Z (2017) High-performance asymmetric supercapacitor designed with a novel NiSe @ MoSe nanosheet arrays and nitrogen-doped carbon nanosheet high-performance asymmetric supercapacitor designed with a novel NiSe @ MoSe 2 nanosheet arrays and nitrogen-doped carbon nan. Sustain Chem Eng 5:5951–5963
257. Manikandan M, Subramani K, Sathish M, Dhanuskodi S (2018) NiTe nanorods as electrode material for high performance supercapacitor applications. Chem Select 3:9034–9040. https://doi.org/10.1002/slct.201801421
258. Zhou P, Fan L, Wu J, Gong C, Zhang J, Tu Y (2016) Facile hydrothermal synthesis of NiTe and its application as positive electrode material for asymmetric supercapacitor. J Alloys Compd 685:384–390. https://doi.org/10.1016/j.jallcom.2016.05.287
259. Deshagani S, Ghosal P, Deepa M (2020) Altered crystal structure of nickel telluride by selenide doping and a poly (N-methylpyrrole) coating amplify supercapacitor performance. Electrochim Acta 345:136200. https://doi.org/10.1016/j.electacta.2020.136200
260. Ye B, Huang M, Jiang S, Fan L, Lin J, Wu J (2018) In-situ growth of Se-doped NiTe on nickel foam as positive electrode material for high-performance asymmetric supercapacitor. Mater Chem Phys 211:389–398. https://doi.org/10.1016/j.matchemphys.2018.03.011
261. Ye B, Huang M, Bao Q, Jiang Si, Ge J, Zhao H, Leqing Fan JL, Jihuai W (2017) Construction of NiTe/NiSe composites on Ni foam for high-performance asymmetric supercapacitor. ChemElectroChem 5:1–27. https://doi.org/10.1002/celc.201701033
262. Guo K, Yang F, Cui S, Chen W, Mi L (2016) Controlled synthesis of 3D hierarchical NiSe microspheres for high-performance supercapacitor. RSC Adv 6:46523–46530. https://doi.org/10.1039/c6ra06909f
263. Kuai Y, Wang T, Liu M, Ma H, Zhang C (2019) Flower-like Ni 0 $ 85 Se nanosheets with enhanced performance toward hybrid supercapacitor. Electrochim Acta 321:134701. https://doi.org/10.1016/j.electacta.2019.134701
264. Ma S, Zhou S, Wang S, Liu M (2017) Controlled synthesis of Ni0.85Se microstructures with different morphologies and their morphology-dependent electrochemical supercapacitor properties. J Alloys Compd 728:592–599. https://doi.org/10.1016/j.jallcom.2017.08.257
265. Shi X, Key J, Ji S, Linkov V, Liu F, Wang H, Gai H, Wang R (2018) Ni (OH) 2 nanoflakes supported on 3D Ni 3 Se 2 nanowire array as highly efficient electrodes for asymmetric supercapacitor and Ni / MH battery. Small 15:1–10. https://doi.org/10.1002/smll.201802861
266. Tang C, Pu Z, Liu Q, Asiri AM, Sun X, Luo Y (2015) In situ growth of NiSe nanowire film on nickel foam as an electrode for high-performance supercapacitors. ChemElectroChem 2:1903–1907. https://doi.org/10.1002/celc.201500285
267. Wang S, Li W, Xin L, Wu M, Long Y, Huang H, Lou X (2017) Facile synthesis of truncated cube-like NiSe 2 single crystals

for high- performance asymmetric supercapacitors. Chem Eng J 330:1334–1341. https://doi.org/10.1016/j.cej.2017.08.078
268. Shaolan Wang SM (2019) Facile fabrication of Ni0.85Se nanowires by composite alkali salt method as a novel cathode material for asymmetric supercapacitors. Dalton Trans 48:3906–3913. https://doi.org/10.1039/C9DT00041K
269. Wu S, Hu Q, Wu L, Li J, Peng H, Yang Q (2019) One-step solvothermal synthesis of nickel selenide nanoparticles as the electrode for high-performance supercapacitors. J Alloys Compd 784:347–353. https://doi.org/10.1016/j.jallcom.2019.01.026
270. Yang Q, Chen X, Zhan H, Wu S, Hu Q, Zhou R (2019) Mixing solvothermal synthesis of surfactant free nano fl ower-sphere-like nickel selenide for supercapacitor application. Synth Met 257:116167. https://doi.org/10.1016/j.synthmet.2019.116167
271. Yuan Y, Chen R, Zhang H, Liu Q, Liu J, Yu J (2018) Hierarchical NiSe@Co2(CO3)(OH)2 heterogeneous nanowire arrays on nickel foam as electrode with high areal capacitance for hybrid supercapacitors. Electrochim Acta 2:325–336. https://doi.org/10.1016/j.electacta.2018.10.058
272. Zhang Y, Wang T, Wang Y, Wang Y, Wu L, Sun Y, Zhou X, Hou W, Du Y, Zhong W (2019) Metal organic frameworks derived hierarchical hollow Ni 0. 85 Se j P composites for high-performance hybrid supercapacitor and ef fi cient hydrogen evolution. Electrochim Acta 303:94–104. https://doi.org/10.1016/j.electacta.2019.02.069
273. Chen H, Li J, Long C, Wei T, Ning G, Yan J, Fan Z (2014) Nickel sulfide / graphene / carbon nanotube composites as electrode material for the supercapacitor application in the sea flashing signal system. J Marine Sci Appl 1:462–466. https://doi.org/10.1007/s11804-014-1279-1
274. Dhaiveegan P, Hsu Y, Tsai Y, Hsieh C, Lin J (2018) Pulse-reversal deposition of Ni 3 S 2 thin fi lms on carbon fi ber cloths for supercapacitors. Surf Coat Technol 350:1003–1009. https://doi.org/10.1016/j.surfcoat.2018.02.079
275. Dai S, Zhao B, Qu C, Dang D, Song B, Ben M, Hu C, Wong C, Liu M, Dai S, Zhao B, Qu C, Chen D (2017) Controlled synthesis of three-phase NixSy/rGO nanoflake electrodes for hybrid supercapacitors with high-energy and power density. Nano Energy 33:522–531. https://doi.org/10.1016/j.nanoen.2017.01.056
276. Dai Z, Zang X, Yang J, Sun C, Si W, Huang W, Dong X (2015) Template synthesis of shape-tailorable NiS2 hollow prisms as high-performance supercapacitor materials template synthesis of shape-tailorable NiS 2 hollow prisms as high-performance supercapacitor materials. Appl Mater Interfaces 7:25396–25401
277. Dai C, Chien P, Lin J, Chou S, Wu W, Li P, Wu K, Lin T (2013) Hierarchically structured Ni 3 S 2 / carbon nanotube composites as high performance cathode materials for asymmetric supercapacitors. Appl Mater Interfaces 5:12168–12174
278. Cheng L, Hu Y, Ling L, Qiao D, Cui S, Jiao Z (2018) One-step controlled synthesis of hierarchical hollow Ni 3 S 2 / NiS @ Ni 3 S 4 core / shell submicrospheres for high-performance supercapacitors. Electrochim Acta 283:664–675. https://doi.org/10.1016/j.electacta.2018.07.013
279. Chen F, Wang H, Ji S, Linkov V, Wang R (2019) High-performance all-solid-state asymmetric supercapacitors based on sponge-like NiS / Ni 3 S 2 hybrid nanosheets. Mater Today Energy 11:211–217. https://doi.org/10.1016/j.mtener.2018.12.002
280. Chen L (2019) Morphology control of Ni 3 S 2 multiple structures and their effect on supercapacitor performances. J Mater Sci 54:12737–12746. https://doi.org/10.1007/s10853-019-03808-x
281. Chen S, Li Y, Wu B, Wu Z, Li F, Wu J, Liu P (2018) 3D meso / macroporous Ni 3 S 2 @ Ni composite electrode for high-performance supercapacitor. Electrochim Acta 275:40–49. https://doi.org/10.1016/j.electacta.2018.04.152
282. Chen F, Wang H, Ji S, Linkov V, Wang R (2018) Core-shell structured Ni 3 S 2 @ Co (OH) 2 nano-wires grown on Ni foam as binder-free electrode for asymmetric supercapacitors. Chem Eng J 345:48–57. https://doi.org/10.1016/j.cej.2018.03.152
283. Rao SS, Punnoose D, Bae J, Durga IK, Thulasi-varma CV, Naresh B, Subramanian A, Raman V, Kim H (2017) Preparation and electrochemical performances of NiS with PEDOT : PSS chrysanthemum petal like nanostructure for high performance supercapacitors. Electrochim Acta 254:269–279. https://doi.org/10.1016/j.electacta.2017.09.134
284. Luo Y, Yang C, Tian Y, Tang Y, Yin X, Que W (2020) A long cycle life asymmetric supercapacitor based on advanced nickel-sulfide / titanium carbide (MXene) nanohybrid and MXene electrodes. J Power Sources 450:227694. https://doi.org/10.1016/j.jpowsour.2019.227694
285. Harish S, Naveen AN, Abinaya R, Archana J, Ramesh R, Navaneethan M, Shimomura M, Hayakawa Y (2018) Enhanced performance on capacity retention of hierarchical NiS hexagonal nanoplate for highly stable asymmetric supercapacitor. Electrochim Acta 283:1053–1062. https://doi.org/10.1016/j.electacta.2018.06.161
286. He J, Guo C, Zhou S, Zhao Y, Wang Q, Yang S, Yang J, Wang Q (2019) Dual carbon-modified nickel sulfide composites toward high-performance electrodes for supercapacitors. Inorg Chem Front 6:226–232. https://doi.org/10.1039/c8qi01024b
287. Guo D, Song X, Tan L, Ma H, Pang H, Wang X, Zhang L (2018) Hierarchical structured Ni3S2@rGO@NiAl-LDHs nanoarrays: a competitive electrode material for advanced asymmetrical supercapacitors. ACS Sustain Chem Eng 7:2803–2810. https://doi.org/10.1021/acssuschemeng.8b06053
288. He Y, Zhang P, Huang H, Li X, Zhai X, Chen B, Guo Z (2020) Rationally design nickel sul fi de @ PEDOT arrays as binder-free cathode for durable asymmetric supercapacitor and aqueous Ni e Zn battery. Electrochim Acta 343:136140. https://doi.org/10.1016/j.electacta.2020.136140
289. Han T, Jiang L, Jiu H, Chang J (2017) Hydrothermal synthesis of the clustered network-like Ni 3 S 2 -Co 9 S 8 with enhanced electrochemical behavior for supercapacitor electrode. J Phys Chem Solids 110:1–8. https://doi.org/10.1016/j.jpcs.2017.05.024
290. Gou J, Xie S, Yang Z, Liu Y, Chen Y, Liu Y, Liu C (2017) A high-performance supercapacitor electrode material based on NiS / Ni 3 S 4 composite. Electrochim Acta 229:299–305. https://doi.org/10.1016/j.electacta.2017.01.111
291. Li GC, Liu M, Wu MK, Liu PF, Zhou Z, Zhu SR, Liu R, Han L (2016) MOF-derived self-sacrificing route to hollow NiS2/ZnS nanospheres for high performance supercapacitors. RSC Adv 6:103517–103522. https://doi.org/10.1039/C6RA23071G
292. Li T, Zuo Y, Lei X, Li N, Liu J, Han H (2016) Regulating the oxidation degree of nickel foam: a smart strategy to controllably synthesize active Ni3S2 nanorod/nanowire arrays for high-performance supercapacitors. J Mater Chem A Mater 4:8029–8040. https://doi.org/10.1039/C6TA01547F
293. Li W, Wang S, Xin L, Wu M, Lou X (2016) Single-crystal β-NiS nanorods arrays with hollow-structured Ni3S2 framework for supercapacitor applications. J Mater Chem A Mater 4:7700–7709. https://doi.org/10.1039/C6TA01133K
294. Kang J, Ryu I, Choe G, Kim G, Yim S (2017) Simple fabrication of nickel sulfide nanostructured electrode using alternate dip-coating method and its supercapacitive properties. Int J Electrochem Sci 12:9588–9600. https://doi.org/10.20964/2017.10.27
295. Jothi PR, Salunkhe RR, Pramanik M, Shanthi Kannan YY (2016) Surfactant-assisted synthesis of nanoporous nickel sulfide flakes and their hybridization with reduced graphene oxides for supercapacitor applications Palani. RSC Adv 6:21246–21253. https://doi.org/10.1039/C5RA26946F

296. Krishnamoorthy K, Kumar G, Radhakrishnan S, Jae S (2014) One pot hydrothermal growth of hierarchical nanostructured Ni 3 S 2 on Ni foam for supercapacitor application. Chem Eng J 251:116–122. https://doi.org/10.1016/j.cej.2014.04.006
297. Ji F, Jiang D, Chen X, Pan X, Kuang L, Zhang Y, Alameh K, Ding B (2016) Simple in-situ growth of layered Ni 3 S 2 thin film electrode for the development of high-performance supercapacitors. Appl Surf Sci 399:432–439. https://doi.org/10.1016/j.apsusc.2016.12.106
298. Huang F, Sui Y, Wei F, Qi J, Meng Q, He Y (2017) Ni 3 S 4 supported on carbon cloth for high-performance flexible all- solid-state asymmetric supercapacitors. J Mater Sci: Mater Electron 29:2525–2536. https://doi.org/10.1007/s10854-017-8175-9
299. Huang L, Hou H, Liu B, Zeinu K, Yuan X, Zhu X, He X, Wu L, Hu J, Yang J (2016) Phase-controlled solvothermal synthesis and morphology evolution of nickel sulfide and its pesudocapacitance performance. Elsevier
300. Hu Q, Zou X, Huang Y, Wei Y, Chen F, Xiang B (2020) Graphene oxide-drove transformation of NiS / Ni 3 S 4 microbars towards Ni 3 S 4 polyhedrons for supercapacitor. J Colloid Interface Sci 559:115–123. https://doi.org/10.1016/j.jcis.2019.10.010
301. Huang F, Yan A, Sui Y, Wei F, Qi J, Meng Q (2017) One-step hydrothermal synthesis of Ni3S4@MoS2 nanosheet on carbon fiber paper as a binder-free anode for supercapacitor. J Mater Sci: Mater Electron 28:12747–12754. https://doi.org/10.1007/s10854-017-7100-6
302. Huo H, Zhao Y, Xu C (2014) 3D Ni3S2 nanosheet arrays supported on Ni foam for high-performance supercapacitor and non- enzymatic glucose detection. J Mater Chem A: Mater Ener Sustain 2:15111–15117. https://doi.org/10.1039/C4TA02857K
303. Liu Y, Liu G, Nie X, Pan A, Liang S, Zhu T (2019) In-situ formation of Ni3S2-Cu1.8S nanosheets to promote hybrid supercapacitor performance. J Mater Chem A Mater 7:11044–11052. https://doi.org/10.1039/C9TA01880H
304. Liu T, Jiang C, Cheng B, You W, Yu J (2017) Novel hierarchical NiS/N-doped carbon composite hollow spheres as an enhanced-performance electrode for hybrid supercapacitors. J Mater Chem A Mater 5:21257–21265. https://doi.org/10.1039/C7TA06149H
305. Lin H, Liu F, Wang X, Ai Y, Yao Z, Chu L, Han S, Zhuang X (2016) Graphene-coupled flower-like Ni 3 S 2 for a free-standing 3D aerogel with an ultra-high electrochemical capacity. Electrochim Acta 191:705–715. https://doi.org/10.1016/j.electacta.2016.01.064
306. Li Z, Li B, Liao C, Liu Z, Li D, Wang H, Li Q (2017) One-pot construction of 3-D graphene nanosheets / Ni 3 S 2 nanoparticles composite for high-performance supercapacitors. Electrochim Acta 253:344–356. https://doi.org/10.1016/j.electacta.2017.09.070
307. Li J, Wang S, Xiao T, Tan X, Xiang P, Jiang L, Deng C, Li W, Li M (2017) Controllable preparation of nanoporous Ni3S2 films by sulfuration of nickel foam as promising asymmetric supercapacitor electrodes. Appl Surf Sci 420:919–926. https://doi.org/10.1016/j.apsusc.2017.05.206
308. Li L, Yang H, Yang J, Zhang L, Miao J, Zhang Y, Sun C, Huang W, DongLiu XB (2016) Hierarchical carbon@Ni3S2@MoS2 double core-shell nanorods for high-performance supercapacitors. J Mater Chem A Mater 4:1319–1325. https://doi.org/10.1039/C5TA08714G
309. Li Z, Gu A, Sun J, Zhou Q (2015) Facile hydrothermal synthesis of NiS hollow microspheres with mesoporous shells for high-performance supercapacitors. New J Chem 40:1663–1670. https://doi.org/10.1039/C5NJ02425K
310. Li Z, Yu X, Gu A, Tang H, Wang L, Lou Z (2017) Anion exchange strategy to synthesis of porous NiS hexagonal nanoplates for supercapacitors. Nanotechnology 28:1–12
311. Peng L, Ji X, Wan H, Ruan Y, Xu K, Chen C, Miao L, Jiang J (2015) Nickel sul fi de nanoparticles synthesized by microwave-assisted method as promising supercapacitor electrodes : an experimental and computational study. Electrochim Acta 182:361–367. https://doi.org/10.1016/j.electacta.2015.09.024
312. Parveen N, Ansari SA, Ansari SG, Fouad H, Abd NM, El-Salam MHCP (2018) Solid-state symmetrical supercapacitor based on hierarchical flower-like nickel sulfide with shape-controlled morphological evolution. Electrochim Acta 268:82–93. https://doi.org/10.1016/j.electacta.2018.01.100
313. Lokhande A, Chodankar NR, Ji T, Kim JH, Lokhande CD (2016) Ultrathin nickel sulfide nano-flames as an electrode for high performance supercapacitor Comparison of symmetric FSS-SCs and electrochemical SCs device. RSC Adv 6:68388–68401. https://doi.org/10.1039/C6RA12018K
314. Naresh B, Punnoose D, Rao SS, Subramanian A, Ramesh BR, Kim HJ (2018) Hydrothermal synthesis and pseudocapacitive properties of morphology tuned nickel sulfide (NiS) nanostructures. New J Chem 42:2733–2742. https://doi.org/10.1039/C7NJ05054B
315. Pang H, Wei C, Li X, Li G, Li S, Chen J, Zhang J, Nis U (2014) Microwave-assisted synthesis of NiS 2 nanostructures for supercapacitors and cocatalytic enhancing photocatalytic H 2 production. Sci Rep 4:1–8. https://doi.org/10.1038/srep03577
316. Namdarian A, Goljanian A, Maseleno A (2018) One step synthesis of rGO-Ni 3 S 2 nano-cubes composite for high-performance supercapacitor electrodes. Int J Hydrogen Energy 43:17780–17787. https://doi.org/10.1016/j.ijhydene.2018.07.178
317. Long L, Yao Y, Yan M, Wang H, Zhang G, Kong M (2017) Ni 3 S 2 @ polypyrrole composite supported on nickel foam with improved rate capability and cycling durability for asymmetric supercapacitor device applications. J Mater Sci 52:3642–3656. https://doi.org/10.1007/s10853-016-0529-9
318. Ma X, Zhang L, Xu G, Zhang C, Song H, He Y, Zhang C, Jia D (2017) Facile synthesis of NiS hierarchical hollow cubes via Ni formate frameworks for high performance supercapacitors. Chem Eng J 320:22–28. https://doi.org/10.1016/j.cej.2017.03.033
319. Ma X, Kang Z (2018) A facile electrodeposition technique for synthesis of nickel sulfides / carbon nanotubes nanocomposites as high performance electrodes for supercapacitor. Mater Lett 236:468–471. https://doi.org/10.1016/j.matlet.2018.10.157
320. Mun C, Muralee CVV, Vinodh R, Sambasivam S, Obaidat IM, Kim H (2019) Micro fl ower-like nickel sul fi de-lead sul fi de hierarchical composites as binder-free electrodes for high-performance supercapacitors. J Energy Storage 26:1–7. https://doi.org/10.1016/j.est.2019.100925
321. Qu C, Zhang L, Meng W, Liang Z, Zhu B, Dang D, Dai S, Zhao B, Tabassum H, Gao S, Zhang H, Guo W, Zhao R, Huang X, Liu M, Zou R (2018) MOF-derived α-NiS nanorods on graphene as an electrode for high-energy-density supercapacitors. J Mater Chem A: Mater Energ Sustain 6:4003–4012. https://doi.org/10.1039/C7TA11100B
322. Raju GSR, Pavitra E, Nagaraju G, Sekhar SC, Ghoreishian SM, Kwak CH, Yu JS, Huh YS, Han Y (2018) Rational design of forest-like nickel sulfide hierarchical architectures with ultra-high areal capacity as a binder-free cathode material for hybrid supercapacitors†. J Mate 6:13178–13190. https://doi.org/10.1039/c8ta02597e
323. Reddy BJ, Vickraman P, Justin AS (2019) Electrochemical performance of nitrogen-doped graphene anchored nickel sul fi de nano fl akes for supercapacitors. Appl Surf Sci 483:1142–1148. https://doi.org/10.1016/j.apsusc.2019.03.292
324. Ruan Y, Jiang J, Wan H, Ji X, Miao L, Peng L, Zhang B, Lv L (2016) Rapid self-assembly of porous square rod-like nickel persul fi de via a facile solution method for high-performance

supercapacitors. J Power Sources 301:122–130. https://doi.org/10.1016/j.jpowsour.2015.09.116
325. Sahoo S, Satpati AK, Sahoo PK, Naik PD (2018) Incorporation of carbon quantum dots for improvement of supercapacitor performance of nickel sul fi de. ACS Omega 3:17936–17946. https://doi.org/10.1021/acsomega.8b01238
326. Shi Z, Yue L, Wang X, Lei X, Sun T, Li Q, Guo H, Yang W (2019) 3D mesoporous hemp-activated carbon / Ni 3 S 2 in preparation of a binder-free Ni foam for a high performance all-solid-state asymmetric supercapacitor. J All 791:665–673. https://doi.org/10.1016/j.jallcom.2019.03.259
327. Justin AS, Vickraman P, Reddy BJ (2019) Carbon sphere@ nickel sulfide core-shell nanocomposite for high performance supercapacitor application. Curr Appl Phys 19:295–302. https://doi.org/10.1016/j.cap.2018.12.010
328. Sun C, Yang J, Zhang Y, Chen P, Huang W, Dong X (2014) Phase-controlled synthesis of a -NiS nanoparticles confined in carbon nanorods for high performance supercapacitors. Sci Rep 4:1–6. https://doi.org/10.1038/srep07054
329. Tan Y, Xue W, Zhang Y, He D, Wang W, Zhao R (2019) Solvothermal synthesis of hierarchical a -NiS particles as battery-type electrode materials for hybrid supercapacitors. J Alloys Compd 806:1068–1076. https://doi.org/10.1016/j.jallcom.2019.07.222
330. Wang A, Wang H, Zhang S, Mao C, Song J, Niu H, Jin B, Tian Y (2013) Controlled synthesis of nickel sulfide / graphene oxide nanocomposite for high-performance supercapacitor. Appl Surf Sci 282:704–708. https://doi.org/10.1016/j.apsusc.2013.06.038
331. Wang H, Liang M, Duan D, Shi W, Song Y, Sun Z (2018) Rose-like Ni3S4 as battery-type electrode for hybrid supercapacitor with excellent charge storage performance. Chem Eng J 350:523–533. https://doi.org/10.1016/j.cej.2018.05.004
332. Wang F, Zhu Y, Tian W, Lv X, Zhang H, Hu Z, Zhang Y, Ji J, Jiang W (2018) Co-doped Ni3S2@CNTs array anchored on graphite foam with hierarchical conductive network for high-performance supercapacitor and hydrogen evolution electrode. J Mater Chem A Mater 6:10490–10496. https://doi.org/10.1039/C8TA03131B
333. Hayat M, Zhou Y, Shah MZ, Hanif MB, Hou H, Arif U, Khan S, Hassan AM, Tighezza AM, Sajjad M, Vadla R (2023) Exploring the electrochemical properties of CuSe-decorated NiSe2 nanocubes for battery-supercapacitor hybrid devices. Chemosphere 340:139720. https://doi.org/10.1016/j.chemosphere.2023.139720
334. Online VA, Choudhary N, Patel M, Ho Y, Dahotre NB, Lee W, Hwang JY, Choi W (2015) Directly deposited MoS 2 thin fi lm electrodes for high performance supercapacitors. J Mater Chem A Mater 3:24049–24054. https://doi.org/10.1039/C5TA08095A
335. Huang K, Zhang J, Shi G, Liu Y (2014) Hydrothermal synthesis of molybdenum disulfide nanosheets as supercapacitors electrode material. Electrochim Acta 132:397–403. https://doi.org/10.1016/j.electacta.2014.04.007
336. Karade SS, Dubal DP, Sankapal BR (2016) MoS2 ultrathin nanoflakes for high performance supercapacitors: room temperature chemical bath deposition (CBD). RSC Adv 6:39159–39165. https://doi.org/10.1039/C6RA04441G
337. Li D, Zhou W, Zhou Q, Ye G, Tongzhou Wang JW, Yanan Chang JX (2017) Transparent 1T-MoS2 nanofilm robustly anchored on substrate by layer-by-layer self- assembly and its ultra-high cycling stability as supercapacitors. Nanotechnology 28:1–23
338. Gupta H, Mothkuri S, Mcglynn R, Carolan D, Maguire P, Mariotti D, Rao TN, Padmanabham G, Chakrabarti S, Materials N, Balapur PO (2020) Activated functionalized carbon nanotube and 2D nanostructured MoS2 hybrid electrode material for high performnce supercapacitor application. IPSS Appl Mater Sci 217:1900855. https://doi.org/10.1002/pssa.201900855
339. Li H, Jiang N, Deng Q, Wang X (2019) Vertically MoS 2 on reduced graphene oxide with superior durability for quasi-solid-state supercapacitor. Chemistry Select 4:12815–12823. https://doi.org/10.1002/slct.201903517
340. Ali S, Fouad H, Ansari SG, Sk P, Hwan M (2017) Mechanically exfoliated MoS 2 sheet coupled with conductive polyaniline as a superior supercapacitor electrode material. J Colloid Interface Sci 504:276–282. https://doi.org/10.1016/j.jcis.2017.05.064
341. Bai L, Wang Y, Cheng S, Li F, Zhang Z, Liu Y (2018) Synthesis and electrochemical performance of molybdenum disulfide-reduced graphene oxide-polyaniline ternary composites for supercapacitors. Front Chem 6:1–7. https://doi.org/10.3389/fchem.2018.00218
342. Chanda K, Thakur S, Maiti S, Acharya A, Paul T, Besra N, Sarkar S, Sardar K, Chattopadhyay KK (2018) Hierarchical heterostructure of MoS 2 flake anchored on TiO 2 sphere for supercapacitor application. AIP Conf Proc 030138:1–5. https://doi.org/10.1063/1.5032473
343. Chang C, Yang X, Xiang S, Que H (2017) Layered MoS 2 / PPy nanotube composites with enhanced performance for supercapacitors. J Mater Sci: Mater Electron 28:1777–1784. https://doi.org/10.1007/s10854-016-5725-5
344. Chao J, Yang L, Liu J, Hu R, Zhu M (2018) Oxygen incorporated and polyaniline intercalated 1T / 2H hybrid MoS2 nanosheets arrayed on reduced graphene oxide for high performance supercapacitors. J Phys Chem C 122:8128–8136. https://doi.org/10.1021/acs.jpcc.8b01473
345. Fan L, Liu G, Zhang C, Wu J, Wei Y (2015) Facile one-step hydrothermal preparation of molybdenum disulfide / carbon composite for use in supercapacitor. Int J Hydrogen Energy 40:10150–10157. https://doi.org/10.1016/j.ijhydene.2015.06.061
346. Niu SF, Zheng JH (2018) Mo2S3@Ni3S2 nanowries on nickel foam as a highly-stable supercapacitor material. J Alloys Compd 737:809–814. https://doi.org/10.1016/j.jallcom.2017.12.051
347. Taylor P, Jiang L, Zhang S, Kulinich SA, Song X, Zhu J, Wang X (2015) Optimizing hybridization of 1T and 2H phases in MoS 2 monolayers to improve capacitances of supercapacitors. Mater Res Lett 3:37–41. https://doi.org/10.1080/21663831.2015.1057654
348. Gao Y, Huang K, Shuai H, Liu L (2017) Synthesis of sphere-feature molybdenum selenide with enhanced electrochemical performance for supercapacitor. Mater Lett 209:319–322. https://doi.org/10.1016/j.matlet.2017.08.044
349. Aziz RA, Muzakir SK, Misnon II, Ismail J, Jose R (2016) Hierarchical Mo9Se11 nanoneedles on nanosheet with enhanced electrochemical properties as a battery-type electrode for asymmetric supercapacitors. J Alloys Compd 673:390–398. https://doi.org/10.1016/j.jallcom.2016.02.221
350. Jia J, Wu J, Dong J, Tu Y, Lan Z, Fan L, Wei Y (2016) High-performance molybdenum diselenide electrodes used in dye-sensitized solar cells and supercapacitors. IEEE J Photovolt 6:1196–1202. https://doi.org/10.1109/JPHOTOV.2016.2585021
351. Balasingam SK, Lee JS, Jun Y (2016) Molybdenum diselenide/reduced graphene oxide based hybrid nanosheets for supercapacitor applications. Dalton Trans 45:9646–9653. https://doi.org/10.1039/C6DT00449K
352. Karade SS, Sankapal BR (2017) Two dimensional cryptomelane like growth of MoSe2 over MWCNTs: symmetric all-solid-state supercapacitor. J Electroanal Chem 802:131–138. https://doi.org/10.1016/j.jelechem.2017.08.017
353. Huang K, Zhang J, Cai J (2015) Preparation of porous layered molybdenum selenide-graphene composites on Ni foam for high-performance supercapacitor and electrochemical sensing. Electrochim Acta 180:770–777. https://doi.org/10.1016/j.electacta.2015.09.016

354. Liu X, Zhang J, Huang K, Hao P (2016) Net-like molybdenum selenide – acetylene black supported on Ni foam for high-performance supercapacitor electrodes and hydrogen evolution reaction. Chem Eng J 302:437–445. https://doi.org/10.1016/j.cej.2016.05.074
355. He B (2017) Molybdenum diselenide nanosheets wraping carbon aerogel nanospheres as an advanced material for supercapacitor and electrochemical sensing. Electrochim Acta 257:301–310. https://doi.org/10.1016/j.electacta.2017.10.105
356. Kirubasankar B, Vijayan S, Angaiah S (2018) Sonochemical synthesis of a 2D–2D MoSe2/ graphene nanohybrid electrode material for asymmetric supercapacitors†. Sustain Energy Fuels 3:467–477. https://doi.org/10.1039/c8se00446c
357. Kirubasankar B, Palanisamy P, Arunachalam S, Murugadoss V, Angaiah S (2018) 2D MoSe2-Ni(OH)2 nanohybrid as an efficient electrode material with high rate capability for asymmetric supercapacitor applications. Chem Eng J 355:881–890. https://doi.org/10.1016/j.cej.2018.08.185
358. Mariappan VK, Krishnamoorthy K, Pazhamalai P, Kim SJ (2018) Electrodeposited molybdenum selenide sheets on nickel foam as a binder-free electrode for supercapacitor application. Electrochim Acta 265:514–522. https://doi.org/10.1016/j.electacta.2018.01.075
359. Ojha M, Deepa M (2019) Molybdenum selenide nanotubes decorated carbon net for a high performance supercapacitor. Chem Eng J 368:772–783. https://doi.org/10.1016/j.cej.2019.03.002
360. Qiu Y, Li X, Bai M, Wang H, Xue D (2017) Flexible full-solid-state supercapacitors based on self-assembly of mesoporous MoSe2 nanomaterials. Inorg Chem Front 4:675–682. https://doi.org/10.1039/c6qi00569a
361. Pazhamalai P, Krishnamoorthy K, Sahoo S, Kim S (2018) Two-dimensional molybdenum diselenide nanosheets as a novel electrode material for symmetric supercapacitors using organic electrolyte. Electrochim Acta 295:591–598. https://doi.org/10.1016/j.electacta.2018.10.191
362. Wang Z, Yan H, Ze Y, Yu M, Yao F, Gao X, Hao E, Hong G, Zhang J, Qiu W (2019) One-pot hydrothermal synthesis of MoSe 2 nanosheets spheres- reduced graphene oxide composites and application for high- performance supercapacitor. J Mater Sci: Mater Electron 30:8537–8545. https://doi.org/10.1007/s10854-019-01174-7
363. Zhao S, Xu W, Yang Z, Zhang X, Zhang Q (2019) One-pot hydrothermal synthesis of nitrogen and phosphorus Co-doped graphene decorated with flower-like molybdenum sulfide for enhanced supercapacitor performance. Electrochim Acta 331:135265. https://doi.org/10.1016/j.electacta.2019.135265
364. Singha SS, Rudra S, Mondal S, Pradhan M, Nayak AK, Satpati B, Pal P, Das K, Singha A (2020) Mn incorporated MoS 2 nanoflowers : a high performance electrode material for symmetric supercapacitor. Electrochim Acta 338:135815. https://doi.org/10.1016/j.electacta.2020.135815
365. Fu H, Zhang X, Fu J, Shen G, Ding Y, Chen Z, Du H (2020) Single layers of MoS2/Graphene nanosheets embedded in activated carbon nanofibers for high-performance supercapacitor. J Alloys Compd 829:154557. https://doi.org/10.1016/j.jallcom.2020.154557
366. Niu C, Han G, Song H, Yuan S, Hou W (2019) Intercalation pseudo-capacitance behavior of few-layered molybdenum sulfide in various electrolytes. J Colloid Interface Sci 561:117–126. https://doi.org/10.1016/j.jcis.2019.11.107
367. Chang Z, Zhu X, Ju X, Li X, Zheng X, Zhang W, Ren Z (2018) Synthesis of hierarichical hollow urchin-like HGRs/MoS2/MnO2 composite and its excellent supercapacitor performance. J Alloys Compd 775:241–247. https://doi.org/10.1016/j.jallcom.2018.10.166
368. Chao J, Yang L, Liu J, Hu R, Zhu M (2018) Sandwiched MoS 2 / polyaniline nanosheets array vertically aligned on reduced graphene oxide for high performance supercapacitors. Electrochim Acta 270:387–394. https://doi.org/10.1016/j.electacta.2018.03.072
369. Chen M, Dai Y, Wang J, Wang Q, Wang Y, Cheng X, Yan X (2017) Smart combination of three-dimensional- fl ower-like MoS 2 nanospheres / interconnected carbon nanotubes for application in supercapacitor with enhanced electrochemical performance. J Alloys Compd 696:900–906. https://doi.org/10.1016/j.jallcom.2016.12.077
370. Cheng B, Cheng R, Tan F, Liu X, Huo J, Yue G (2019) Highly efficient quasi-solid-state asymmetric supercapacitors based on MoS 2 / MWCNT and PANI / MWCNT composite electrodes. Nanoscal Res Lett 14:1–12
371. Cui X, Chen X, Chen S, Jia F, Yang S, Lin Z, Shi Z, Deng H (2016) Dopamine adsorption precursor enables N-doped carbon sheathing of MoS2 nanoflowers for all-around enhancement of supercapacitor performance. J Alloys Compd 693:955–963. https://doi.org/10.1016/j.jallcom.2016.09.173
372. Geraldo E, Rabelo AC, Dalmaschio CJ, Pinheiro AN, Pereira EC, Schreiner WH, Leite ER (2014) Supercapacitor electrodes obtained by directly bonding 2D MoS 2 on reduced graphene oxide. Adv Energy Mater 4:1–8. https://doi.org/10.1002/aenm.201301380
373. Li X, Li X, Cheng J, Wang B, Wang Z, Li C (2016) Coaxial yarn electrode based on hierarchical MoS2 nanosheets/carbon fiber tows for flexible solid-state supercapacitors. RSC Adv 6:57190–57198. https://doi.org/10.1039/x0xx00000x
374. Han X, Jiang X, Yin S (2013) Application of MoS 2 nanoflakes in supercapacitor. Adv Mat Res 773:524–529. https://doi.org/10.4028/www.scientific.net/AMR.773.524
375. Han AC, Tian Z, Dou H (2018) Vertical crosslinking MoS2/three-dimensional graphene composite towards high performance supercapacito. Chin Chem Lett 29:606–611. https://doi.org/10.1016/j.cclet.2018.01.017
376. Huang K, Wang L, Zhang J, Wang L, Mo Y (2014) One-step preparation of layered molybdenum disul fi de / multi-walled carbon nanotube composites for enhanced performance supercapacitor. Energy 67:234–240. https://doi.org/10.1016/j.energy.2013.12.051
377. Ji H, Liu C, Wang T, Chen J, Mao Z, Zhao J (2015) Porous hybrid composites of few-layer MoS 2 nanosheets embedded in a carbon matrix with an excellent supercapacitor electrode performance. Small 11:6480–6490. https://doi.org/10.1002/smll.201502355
378. Krishnamoorthy K, Veerasubramani G, Pazhamalai P, Kim SJ (2015) Designing two dimensional nanoarchitectured MoS2 sheets grown on Mo foil as a binder free electrode for supercapacitors. Electrochim Acta 190:305–312. https://doi.org/10.1016/j.electacta.2015.12.148
379. Lei X, Yu K, Qi R, Zhu Z (2018) Fabrication and theoretical investigation of MoS 2 -Co 3 S 4 hybrid hollow structure as electrode material for lithium-ion batteries and supercapacitors. Chem Eng J 347:607–617. https://doi.org/10.1016/j.cej.2018.04.154
380. Li X, Zhang C, Xin S, Yang Z, Li Y, Zhang D, Yao P (2016) Facile synthesis of MoS 2 / reduced graphene oxide @ polyaniline for high performance supercapacitor. Appl Mater Interfaces 8:21373–21380. https://doi.org/10.1021/acsami.6b06762
381. Li H, Zhao Y, Wang CA (2018) MoS 2 / CoS 2 composites composed of CoS 2 octahedrons and MoS 2 nano- fl owers for supercapacitor electrode materials. Frontier of material science 12:354–360
382. Li Q, Lu W, Li Z, Ning J, Zhong Y, Hu Y (2020) Hierarchical MoS 2 / NiCo 2 S 4 @ C urchin-like hollow microspheres for

asymmetric supercapacitors. Chem Eng J 380:122544. https://doi.org/10.1016/j.cej.2019.122544
383. Lin AT, Hsiao M, Wang A (2017) Hollow hierarchical carbon spheres decorated with ultrathin molybdenum sulfide nanosheets as high-capacity electrode materials for asymmetric supercapacitors. ChemElectroChem 4:1–27. https://doi.org/10.1002/celc.201600764
384. Lin AT, Sadhasivam T, Wang A (2018) Ternary composite nanosheets with MoS2/WS2/graphene heterostructures as high performance cathode materials for supercapacitors. ChemElectroChem 5:1–22. https://doi.org/10.1002/celc.201800043
385. Liu Y, Zhao D, Liu H, Umar A, Wu X (2018) High performance hybrid supercapacitor based on hierarchical MoS2/Ni3S2 metal chalcogenide. Chin Chem Lett 30:1105–1110. https://doi.org/10.1016/j.cclet.2018.12.024
386. Luo W, Zhang G, Cui Y, Liu Y, Jin C, Jing Hao JZ (2018) One-pot synthesize high stable carbon-MoS2 nano-sphere electrodes by co-growth mechanism for supercapacitors. New J Chem 42:10111–10117. https://doi.org/10.1039/C8NJ01387J
387. Sari FN, Ting JM (2018) MoS2/MoOx nanostructure decorated activated carbon cloth for enhanced supercapacitor performances. Chemsuschem 11:897–906. https://doi.org/10.1002/cssc.201702295
388. Sun T, Li Z, Liu X, Ma L, Wang J (2017) Oxygen-incorporated MoS 2 microspheres with tunable interiors as novel electrode materials for supercapacitors. J Power Sources 352:135–142. https://doi.org/10.1016/j.jpowsour.2017.03.123
389. Tian J, Zhang H, Li Z (2018) Synthesis of double-layer nitrogen-doped microporous hollow carbon @ MoS2 / MoO2 nanospheres for supercapacitors nanospheres for supercapacitors Jingyang Tian, Haiyan Zhang *, Zhenghui Li. Appl Mater Interfaces 10:29511–29520. https://doi.org/10.1021/acsami.8b08534
390. Wang M, Fei H, Zhang P, Yin L (2016) Hierarchically layered MoS 2 / Mn 3 O 4 hybrid architectures for electrochemical supercapacitors with enhanced performance. Electrochim Acta 209:389–398. https://doi.org/10.1016/j.electacta.2016.05.078
391. Zhang S, Hu R, Dai P, Yu X, Ding Z, Wu M, Li G, Ma Y, Tu C (2016) Synthesis of rambutan-like MoS2/mesoporous carbon spheres nanocomposites with excellent performance for supercapacitors. Appl Surf Sci 396:994–999. https://doi.org/10.1016/j.apsusc.2016.11.074
392. Li Y, Wang X, Meng J, Song M, Jiao M, Qin Q, Mi L (2023) Flower-like manganese and phosphorus co-doped MoS2 with high 1T phase content as a supercapacitor electrode material. New J Chem 47:15143–15150. https://doi.org/10.1039/D3NJ02797J
393. Jhankal D, Khan MS, Jhankal KK, Sachdev K (2023) Charge storage kinetics of MoS2 flower decorated reduced graphene oxide for quasi solid-state symmetric supercapacitor. J Phys Chem Solids 173:111117. https://doi.org/10.1016/j.jpcs.2022.111117
394. Vikraman D, Hussain S, Rabani I, Feroze A, Ali M, Seo Y-S, Chun S-H, Jung J, Kim H-S (2021) Engineering MoTe2 and Janus SeMoTe nanosheet structures: first-principles roadmap and practical uses in hydrogen evolution reactions and symmetric supercapacitors. Nano Energy 87:106161. https://doi.org/10.1016/j.nanoen.2021.106161
395. Ghosh K, Pumera M (2021) MXene and MoS3−x coated 3D-printed hybrid electrode for solid-state asymmetric supercapacitor. Small Methods 5:2100451. https://doi.org/10.1002/smtd.202100451
396. Singha SS, Rudra S, Mondal S, Pradhan M, Nayak AK, Satpati B, Pal P, Das K, Singha A (2020) Mn incorporated MoS2 nanoflowers: a high performance electrode material for symmetric supercapacitor. Electrochim Acta 338:135815. https://doi.org/10.1016/j.electacta.2020.135815
397. Cai H, Li X, Li G, Xia H, Wang P, Sun P, Huang J, Wang L (2019) Synthesis of honeycomb-like nickel-manganese sulfide composite nanosheets as advanced battery-type electrodes for hybrid supercapacitor. Mater Lett 255:126505. https://doi.org/10.1016/j.matlet.2019.126505
398. Cao J, Yuan S, Yin H, Zhu Y, Li C, Fan M, Chen H (2018) One-pot synthesis of porous nickel – manganese sulfides with tuneable compositions for high-performance energy storage. J Solgel Sci Technol 85:629–637. https://doi.org/10.1007/s10971-018-4580-7
399. Chen S, Chen H, Li C, Fan M, Lv C, Tian G, Shu K (2017) Tuning the electrochemical behavior of CoxMn3-x sulfides by varying different Co/Mn ratios in supercapacitor. J Mater Sci 52:6687–6696. https://doi.org/10.1007/s10853-017-0903-2
400. Peng H, Wei G, Sun K, Ma G, Feng E, Yang X, Lei Z (2018) Integrated and heterostructured cobalt manganese sulfide nanoneedle arrays as advanced electrodes for high-performance supercapacitors. New J Chem 42:18328–18334. https://doi.org/10.1039/c8nj04364g
401. Bolagam R, Um S (2020) Hydrothermal synthesis of cobalt ruthenium sulfides as promising pseudocapacitor electrode materials. Coatings 10:1–15. https://doi.org/10.3390/coatings10030200
402. Pazhamalai P, Krishnamoorthy K, Sahoo S, Vimal Kumar Mariappan SJK (2019) Copper tungsten sulfide anchored on Ni-foam as a high-performance binder free negative electrode for asymmetric supercapacitor. Chem Eng J 359:409–418. https://doi.org/10.1016/j.cej.2018.11.153
403. Du D, Lan R, Humphreys J, Amari H, Tao S (2018) Preparation of nanoporous nickel-copper sulfide on carbon cloth for high-performance hybrid supercapacitors. Electrochim Acta 273:170–180. https://doi.org/10.1016/j.electacta.2018.04.041
404. Deka BK, Hazarika A, Kim J, Kim N, Eui H, Park Y, Wook H (2019) Bimetallic copper cobalt selenide nanowire-anchored woven carbon fi ber- based structural supercapacitors. Chem Eng J 355:551–559. https://doi.org/10.1016/j.cej.2018.08.172
405. Guo K, Cui S, Hou H, Chen W, Mi L (2016) Hierarchical ternary Ni – Co – Se nanowires for high-performance supercapacitor device design. Dalton Trans 48:19458–19465. https://doi.org/10.1039/c6dt03863h
406. Hu Y, Huang C, Jiang S, Qin Y, Chen HC (2020) Hierarchical nickel-cobalt selenide nanoparticles / nanosheets as advanced electroactive battery materials for hybrid supercapacitors. J Colloid Interface Sci 558:291–300. https://doi.org/10.1016/j.jcis.2019.09.115
407. Quan L, Liu T, Yi M, Chen Q, Cai D, Zhan H (2018) Construction of hierarchical nickel cobalt selenide complex hollow spheres for pseudocapacitors with enhanced performance. Electrochim Acta 281:109–116. https://doi.org/10.1016/j.electacta.2018.05.100
408. Wang Y, Liu R, Sun S, Wu X (2019) Facile synthesis of nickel-cobalt selenide nanoparticles as battery-type electrode for all-solid-state asymmetric supercapacitors. J Colloid Interface Sci 549:16–21. https://doi.org/10.1016/j.jcis.2019.04.049
409. Xie S, Gou J, Liu B, Liu C (2019) Nickel-cobalt selenide as high-performance and long-life electrode material for supercapacitor. J Colloid Interface Sci 540:306–314. https://doi.org/10.1016/j.jcis.2019.01.030
410. Cheng C, Zhang X, Wei C, Liu Y, Cui C, Zhang Q, Zhang D (2018) Mesoporous hollow ZnCo2S4 core-shell nanospheres for high performance supercapacitors. Ceram Int 44:17464–17472. https://doi.org/10.1016/j.ceramint.2018.06.215
411. Elshahawy AM, Guan C, Wang J (2017) Controllable MnCo2S4 nanostructures for high performance hybrid supercapacitors †. J Mater Chem A: Mater Energ Sustain 5:7494–7506. https://doi.org/10.1039/C7TA00943G

412. Guo S, Chen W, Li M, Wang J, Liu F, Cheng JP, Chen W, Li M, Wang J, Liu F, Cheng JP (2018) Effect of reaction temperature on the amorphous-crystalline transition of copper cobalt sulfide for supercapacitor. Electrochim Acta 271:498–506. https://doi.org/10.1016/j.electacta.2018.03.189
413. Huang Y, Zhao Y, Bao J, Lian J, Cheng M, Li H (2018) Tip-welded ferric-cobalt sulfide hollow nanoneedles on highly conductive carbon fibers for advanced asymmetric supercapacitors. Electrochim Acta 292:157–167. https://doi.org/10.1016/j.electacta.2018.08.110
414. Ai Z, Hu Z, Liu Y, Yao M (2016) Capacitance performance of nanostructured CoNi 2 S 4 with different morphology grown on carbon cloth for supercapacitors. ChemPlusChem 81:322–328. https://doi.org/10.1002/cplu.201500413
415. Beka LG, Li X, Liu W (2017) Nickel cobalt sulfide core / shell structure on 3D graphene for supercapacitor application. Sci Rep 7:1–11. https://doi.org/10.1038/s41598-017-02309-8
416. Liang J, Li M, Chai Y, Luo M, Li L (2017) TEOA-mediated formation of hollow core-shell structured CoNi 2 S 4 nanospheres as a high-performance electrode material for supercapacitors. J Power Sources 362:123–130. https://doi.org/10.1016/j.jpowsour.2017.07.023
417. Anthuvan J, Park J, Hong V, Quy V, Myeong J, Chae J, Kang S, Kim H, Ahn K (2018) Rambutan-like cobalt nickel sul fi de (CoNi 2 S 4) hierarchitecture for high-performance symmetric aqueous supercapacitors. J Ind Eng Chem 63:73–83. https://doi.org/10.1016/j.jiec.2018.02.001
418. Zhang S, Yang D, Zhang M, Liu Y, Xu T, Yang J, Yu Z (2020) Synthesis of novel bimetallic nickel cobalt telluride nanotubes on nickel foam for high-performance hybrid supercapacitors †. Inorg Chem Front 7:477–486. https://doi.org/10.1039/c9qi01395d
419. Chandrasekaran NI, Muthukumar H, Sekar AD, Pugazhendhi A, Matheswaran M (2018) High-performance asymmetric supercapacitor from nanostructured tin nickel sulfide (SnNi2S4) synthesized via microwave-assisted technique. J Mol Liq 266:649–657. https://doi.org/10.1016/j.molliq.2018.06.084
420. Balamurugan J, Li C, Thanh TD, Park O, Kim NH, Lee JH (2017) Hierarchical design of Cu1−xNixS nanosheets for high-performance asymmetric solid-state supercapacitors. J Mater Chem A Mater 5:19760–19772. https://doi.org/10.1039/c7ta04071g
421. Ke T-C, Vedhanarayanan B, Li-Dong Shao T-WL (2019) Porous and hierarchically structured ammonium nickel molybdate/nickel sulphide/reduced graphene oxide ternary composite as high performance electrode for supercapacitors. ChemElectroChem 6:1–25. https://doi.org/10.1002/celc.201900885
422. Elkholy AE, Dhmees AS, Heakal FE, Deyab MA (2019) Mesoporous ZnMoS4 as a supercapacitor electrode material with battery-like behavior. New J Chem 43:1987–1992. https://doi.org/10.1039/c8nj05640d
423. Zhang K, Chen H, Wang X, Guo D, Hu C, Wang S, Sun J, Leng Q (2014) Synthesis and structure determination of potassium copper selenide nanowires and solid-state supercapacitor application. J Power Sources 268:522–532. https://doi.org/10.1016/j.jpowsour.2014.06.079
424. Haj YA, Balamurugan J, Nam Hoon Kim JHL (2019) Nitrogen-doped graphene encapsulated cobalt iron sulfide as an advanced electrode for high-performance asymmetric supercapacitors. J Mater Chem A Mater 7:3941–3952. https://doi.org/10.1039/C8TA12396A
425. Xu J, Dong L, Li C, Tang H (2015) Facile synthesis of Mo0.91W0.09S2 ultrathin nanosheets/amorphous carbon composites for high-performance supercapacitor. Mater Lett 162:126–130. https://doi.org/10.1016/j.matlet.2015.09.130
426. Diggikar RS, Ambekar JD, Kulkarni MV, Kale BB (2013) Nanocrystalline silver vanadium sulfide (SVS) anchored polyaniline (PANI): new nanocomposite system for supercapacitor †. New J Chem 37:3236–3243. https://doi.org/10.1039/c3nj00500c
427. Guo M, Balamurugan J, Tran TD, Nam Hoon Kim JHL (2016) Facile fabrication of Co2CuS4 nanoparticles anchored N-doped graphene for high performance asymmetric supercapacitors. J Mater Chem A Mater 4:17560–17571. https://doi.org/10.1039/C6TA07400F
428. Annamalai KP, Liu L, Tao Y (2017) Highly exposed nickel cobalt sulfide-rGO nanoporous structures:an advanced energy storage electrode material. J Mater Chem A Mater 5:9991–9997. https://doi.org/10.1039/C7TA01735A
429. Bahaa A, Balamurugan J, Nam Hoon Kim JHL (2019) Metal organic framework derived hierarchical copper cobalt sulfide nanosheet arrays for high-performance solid-state asymmetric supercapacitors. J Mater Chem A Mater 7:8620–8632. https://doi.org/10.1039/C9TA00265K
430. Li Z, Wu L, Wang L, Gu A, Zhou Q (2017) Nickel cobalt sul fi de nanosheets uniformly anchored on porous graphitic carbon nitride for supercapacitors with high cycling performance. Electrochim Acta 231:617–625. https://doi.org/10.1016/j.electacta.2017.02.087
431. Du W, Wang Z, Zhu Z, Hu S, Zhu X, Shi Y, Pang H, Qian X (2014) Facile synthesis and superior electrochemical performances of CoNi2S4/graphene nanocomposite suitable for supercapacitor electrodes. J Mater Chem A Mater 2:9613–9619. https://doi.org/10.1039/c4ta00414k
432. Li H, Xuan H, Guan Y, Zhang G, Wang R, Liang X, Xie Z, Han P, Wu Y (2020) Preparation and characterization of three-dimensional Mn–Mo–S composites on rGO/Ni foam for battery-supercapacitor electrode with high-performance. Electrochim Acta 345:136260. https://doi.org/10.1016/j.electacta.2020.136260
433. Sahoo S, Krishnamoorthy K, Pazhamalai P, Mariappan VK, Kim S (2019) Copper molybdenum sulfide nanoparticles embedded on graphene sheets as advanced electrodes for wide temperature-tolerant. Inorg Chem Front 6:1775–1784. https://doi.org/10.1039/c9qi00451c
434. Sazonov N, Kong L (2019) Fabrication and characterization of CoMoS 4 / Co 3 V 2 O 8 nanocomposite as electrode material for supercapacitor. Ionics (Kiel) 25:5411–5418
435. Zhu Y, Chen H, Li C (2018) Sea urchin-like architectures and nanowire arrays of cobalt – manganese sulfides for superior electrochemical energy storage performance. Energy Materials 53:6157–6169. https://doi.org/10.1007/s10853-017-1976-7
436. An W, Liu L, Gao Y, Liu Y, Liu J (2016) Ni0.9Co1.92Se4 nanostructures: binder-free electrode of coral-like bimetallic selenide for supercapacitor. RSC Adv 6:75251–75257. https://doi.org/10.1039/c6ra17825a
437. Yang P, Wu Z, Jiang Y, Pan Z, Tian W, Jiang L Fractal (Ni x Co 1 − x) 9 Se 8 Nanodendrite Arrays with Highly exposed (011) surface for wearable, all solid-state supercapacitor. Communications 8:1870116^{-1}–10. https://doi.org/10.1002/aenm.201801392
438. Zhang P, Guan BY, Yu L, Wen X, Lou D (2017) Formation of double-shelled zinc – cobalt sulfide dodecahedral cages from bimetallic zeolitic imidazolate frameworks for hybrid supercapacitors. Angewandte Chemie - International Edition 56:7141–7145. https://doi.org/10.1002/anie.201702649
439. Yu J, Lin L (2016) Structure variation of nickel cobalt sul fi des using Ni foam and nickel salt as the nickel source and the application on the supercapacitor electrode. J Energy Storage 7:295–304. https://doi.org/10.1016/j.est.2016.08.004
440. Nan H, Liu M, Zhang Q, Wang M, Liu S, Qiao L, Hu X, Tian H (2020) Intrinsic energy-storage mechanism of low crystallinity nickel-cobalt sulfide as anode material for supercapacitors. J Power Sources 451:227822-1–227828. https://doi.org/10.1016/j.jpowsour.2020.227822

441. Talha A, Ahmed A, Chavan HS, Jo Y, Cho S, Pawar SM, Gunjakar JL, Inamdar AI, Kim H (2017) One-step facile route to copper cobalt sulfide electrodes for supercapacitor with high-rate long-cycle life performance. J Alloys Compd 744–751. https://doi.org/10.1016/j.jallcom.2017.07.076
442. Chen C, Yan D, Luo X, Gao W, Huang G, Han Z, Zeng Y, Zhu Z (2018) Construction of core-shell $NiMoO_4$@Ni-Co-S nanorods as advanced electrodes for high-performance asymmetric supercapacitors. ACS Appl Mater Interfaces 10:4662–4671. https://doi.org/10.1021/acsami.7b16271
443. He W, Liang Z, Ji K, Sun Q, Zhai T, Xu X (2018) Hierarchical Ni-Co-S @ Ni-W-O core – shell nanosheet arrays on nickel foam for high-performance asymmetric supercapacitors. Nano Res 11:1415–1425
444. Hussain I, Lamiel C, Mohamed SG, Vijayakumar S, Ali A, Shim J (2019) Controlled synthesis and growth mechanism of zinc cobalt sulfide rods on Ni-foam for high-performance supercapacitors. J Ind Eng Chem 71:250–259. https://doi.org/10.1016/j.jiec.2018.11.033
445. Ai Z, Zhonghua Hu, Liu Y, Mengxuan Fan PL (2016) Novel 3D flower-like CoNi2S4/carbon nanotubes composite as high-performance electrode materials for supercapacitor. New J Chem 40:340–347. https://doi.org/10.1039/C5NJ02279G
446. Wang Q, Gao F, Xu B, Cai F, Zhan F, Gao F, Wang Q (2017) ZIF-67 derived amorphous CoNi 2 S 4 nanocages with nanosheet arrays on the shell for a high-performance asymmetric supercapacitor. Chem Eng J 327:387–396. https://doi.org/10.1016/j.cej.2017.06.124
447. Wang D, Zhu W, Yuan Y, Du G, Zhu J, Zhu X, Pezzotti G (2017) Kelp-like structured NiCo2S4-C-MoS2 composite electrodes for high performance supercapacitor. J Alloys Compd 735:1505–1513. https://doi.org/10.1016/j.jallcom.2017.11.249
448. Liua L (2013) Nano-aggregates of cobalt nickel oxysulfide as a high-performance electrode material for supercapacitors. Nanoscale 5:11615–11619. https://doi.org/10.1039/b000000x
449. Asen P, Shahrokhian S, Zad AI (2018) Iron-vanadium oxysulfide nanostructures as novel electrode materials for supercapacitor applications. J Electroanal Chem 818:157–167. https://doi.org/10.1016/j.jelechem.2018.04.035
450. Cai X, Shen X, Ma L, Ji Z (2015) Facile synthesis of nickel-cobalt sulfide/reduced graphene oxide hybrid with enhanced capacitive performance. RSC Adv 5:58777–58783. https://doi.org/10.1039/C5RA09447J
451. Cao L, Tang G, Mei J, Liu H (2017) Construct hierarchical electrode with Ni x Co 3–x S 4 nanosheet coated on NiCo 2 O 4 nanowire arrays grown on carbon fi ber paper for high-performance asymmetric supercapacitors. J Power Sources 359:262–269. https://doi.org/10.1016/j.jpowsour.2017.05.051
452. Chai Z, Wang Z, Wang J, Li X, Guo H (2018) Potentiostatic deposition of nickel cobalt sul fi de nanosheet arrays as binder-free electrode for high-performance pseudocapacitor. Ceram Int 44:15778–15784. https://doi.org/10.1016/j.ceramint.2018.05.254
453. Chen W, Xia C, Alshareef HN, Al CET (2014) One-step electrodeposited nickel cobalt sul fi de nanosheet arrays for high-performance asymmetric supercapacitors. ACS Nano 8:9531–9541
454. Chen H, Chen S, Shao H, Li C, Fan M, Chen D, Tian G (2016) Hierarchical NiCo 2 S 4 nanotube @ NiCo 2 S 4 nanosheet arrays on Ni foam for high-performance supercapacitors. Chem Asian J 11:248–255. https://doi.org/10.1002/asia.201500972
455. Chen X, Chen D, Guo X, Wang R, Zhang H, Accepted J (2017) Facile growth of caterpillar-like NiCo 2 S 4 nanocrystal arrays on nickle foam for high-performance supercapacitors. Appl Mater Interfaces 9:18774–18781
456. Chen X, Ding J, Chen X, Liu X, Zhuang G, Zhang Z (2018) Porous tremella-like NiCo 2 S 4 networks electrodes for high-performance dye- sensitized solar cells and supercapacitors. Sol Energy 176:762–770. https://doi.org/10.1016/j.solener.2018.10.087
457. Cheng S, Shi T, Huang Y, Tao X, Li J, Cheng C, Liao G, Tang Z (2016) Rational design of nickel cobalt sulfide / oxide core- shell nanocolumn arrays for high-performance flexible all-solid-state asymmetric supercapacitors. Ceram Int 43:2155–2164. https://doi.org/10.1016/j.ceramint.2016.10.197
458. Ding R, Zhang M, Yao Y, Gao H (2015) Crystalline NiCo 2 S 4 nanotube array coated with amorphous NiCo x S y for supercapacitor electrodes. J Colloid Interface Sci 467:140–147. https://doi.org/10.1016/j.jcis.2015.12.057
459. Dong M, Wang Z, Li X, Guo H, Wang J (2018) A smart architecture of nickel-cobalt sul fi de nanotubes assembled nanoclusters for high-performance pseudocapacitor. J Alloys Compd 765:505–511. https://doi.org/10.1016/j.jallcom.2018.06.179
460. Du J, Yan Q, Li Y, Cheng K, Ye K, Zhu K, Yan J, Cao D (2019) Hierarchical copper cobalt sul fi des nanowire arrays for high-performance asymmetric supercapacitors. Appl Surf Sci 487:198–205. https://doi.org/10.1016/j.apsusc.2019.04.275
461. Tian Z, Wang X, Li B, Li H, Wu Y (2019) High rate capacbility electrode constructed by anchoring CuCo2S4 on graphene aerogel skeleton toward quasi-solid-state supercapacitor. Electrochim Acta 298:321–329. https://doi.org/10.1016/j.electacta.2018.12.103
462. Zhang F, Cho M, Eom T, Kang C, Lee H (2019) Facile synthesis of manganese cobalt sul fi de nanoparticles as high- performance supercapacitor electrode. Ceram Int 45:20972–20976. https://doi.org/10.1016/j.ceramint.2019.06.240
463. Hou L, Bao R, Chen Z, Rehan M, Tong L, Pang G, Yuan C (2016) Comparative investigation of hollow mesoporous NiCo2S4 ellipsoids with enhanced pseudo-capacitances towards high-performance asymmetric supercapacitors. Electrochim Acta 214:76–84. https://doi.org/10.1016/j.electacta.2016.08.038
464. Huang T, Song XZ, Chen X, Chen XL, Sun FF, Su QF, Li LD, Tan Z (2018) Carbon coated nickel-cobalt bimetallic sulfides hollow dodecahedrons for supercapacitors with enhanced electrochemical performance. New J Chem 42:5128–5134. https://doi.org/10.1039/C7NJ04806H
465. Jiang J, Sun Y, Chen Y, Hu X, Zhu L, Chen H (2019) One-step synthesis of nickel cobalt sulfide nanostructure for high-performance supercapacitor. J Mater Sci 54:11936–11950. https://doi.org/10.1007/s10853-019-03746-8
466. Wan H, Jiang J, Yu J, Xu K, Miao L, Zhang L (2013) NiCo 2 S 4 porous nanotubes synthesis via sacrificial templates: high-performance electrode materials of supercapacitors 3. CrystEngComm 15:7649–7651. https://doi.org/10.1039/c3ce41243a
467. Sami SK, Siddiqui S, Feroze MT, Chung CH (2017) Electrodeposited nickel-cobalt sulfide nanosheet on polyacrylonitrile nanofibers: a binder-free electrode for flexible supercapacitors. Mater Res Express 4:1–31
468. Kim D, Ghodake GS, Maile NC, Kadam AA, Lee DS, Fulari VJ (2017) Chemical synthesis of hierarchical NiCo 2 S 4 nanosheets like nanostructure on flexible foil for a high performance supercapacitor. Sci Rep 7:1–10. https://doi.org/10.1038/s41598-017-10218-z
469. Wei Kong, Chenchen Lu, Wu Zhang, Jun Pu and ZW (2015) Homogeneous core-shell NiCo2S4 nanostructure supported on nickel foam for supercapacitor. https://doi.org/10.1039/C5TA02432C
470. Lamiel C, Nguyen VH, Baynosa M, Huynh DC, Shim J (2016) Hierarchical mesoporous carbon sphere@nickel cobalt sulfide core-shell structures and their electrochemical performance. J Electroanal Chem 771:106–113. https://doi.org/10.1016/j.jelechem.2016.03.047
471. Le K, Gao M, Liu W, Liu J, Wang Z, Wang F (2019) MOF-derived hierarchical core-shell hollow iron-cobalt sul fi des

nanoarrays on Ni foam with enhanced electrochemical properties for high energy density asymmetric supercapacitors. Electrochim Acta 323:134826. https://doi.org/10.1016/j.electacta.2019.134826
472. Li Y, Cao L, Qiao L, Zhou M, Yang Y, Xiao P, Zhang Y (2014) Ni-Co Sulfide nanowires on nickel foam with ultrahigh capacitance for asymmetric supercapacitors. J Mater Chem A Mater 2:6540–6548. https://doi.org/10.1039/c3ta15373h
473. Li X, Li Q, Wu Y, Rui M, Zeng H (2015) Two-dimensional, porous nickel-cobalt sulfide for high-performance asymmetric supercapacitors nickel-cobalt sulfide nanosheets with ultrathin thickness and abundant pores for high-performance asymmetric supercapacitors. Appl Mater Interfaces 7:19316–19323
474. Li C, Balamurugan J, Kim NH, Lee JH (2018) Hierarchical Zn – Co – S nanowires as advanced electrodes for all solid state asymmetric supercapacitors. Adv Energy Mater 8:1–12. https://doi.org/10.1002/aenm.201702014
475. Jun Yang Yu, Zhang CS, Guo G, Sun W, Huang W, Qingyu Yan XD (2015) Controlled synthesis of zinc cobalt sulfide nanostructures in oil phase and their potential applications in electrochemical energy storage. J Mater Chem A Mater 3:11462–11470. https://doi.org/10.1039/C5TA01739D
476. Li B, Tian Z, Li H, Yang Z, Wang Y, Wang X (2019) Self-supporting graphene aerogel electrode intensified by NiCo2S4 nanoparticles for asymmetric supercapacitor. Electrochim Acta 314:32–39. https://doi.org/10.1016/j.electacta.2019.05.040
477. Yang J, Ma M, Sun C, Zhang Y, Huang W (2014) Hybrid NiCo2S4@MnO2 heterostructures for high-performance supercapacitor electrodes. J Mater Chem A: Mater Energ Sustain 3:1258–1264. https://doi.org/10.1039/C4TA05747C
478. Gao X, Chang Q, Hong J, Long D, Jin G, Xiao X (2018) Zinc cobalt sulfide microspheres as a high-performance electrode material for supercapacitors. ChemPubSoc 3:13751–13758. https://doi.org/10.1002/slct.201803095
479. Li H, Li Z, Sun M, Wu Z, Shen W, Qing Y (2019) Zinc cobalt sulfide nanoparticles as high performance electrode material for asymmetric supercapacitor. Electrochim Acta 319:716–726. https://doi.org/10.1016/j.electacta.2019.07.033
480. Liang X, Nie K, Ding X, Dang L, Sun J, Shi F (2018) Highly compressible carbon sponge supercapacitor electrode with enhanced performance by growing nickel-cobalt sulfide nanosheets. ACS Appl Mater Interfaces 10:10087–10095. https://doi.org/10.1021/acsami.7b19043
481. Liu S, Jun SC (2017) Hierarchical manganese cobalt sul fi de core e shell nanostructures for high-performance asymmetric supercapacitors. J Power Sources 342:629–637. https://doi.org/10.1016/j.jpowsour.2016.12.057
482. Liu C, Wu X (2018) NiCo2S4 nanotube arrays grown on flexible carbon fibers as battery-type electrodes for asymmetric supercapacitors. Mater Res Bull 103:55–62. https://doi.org/10.1016/j.materresbull.2018.03.014
483. Liu S, Xu G, Li J, Wang B, Huang Z, Chen Q (2018) Iron-cobalt bi-metallic sulfide nanowires on ni foam for applications in high-performance supercapacitors. ChemPubSoc 5:2250–2255. https://doi.org/10.1002/celc.201800486
484. Lv Z, Zhong Q, Zhao Z, Bu Y (2017) Facile synthesis of hierarchical nickel – cobalt sulfide quadrangular microtubes and its application in hybrid supercapacitors. J Mater Sci: Mater Electron 28:18064–18074. https://doi.org/10.1007/s10854-017-7750-4
485. Lv Y, Liu A, Shi Z, Che H, Mu J, Guo Z, Zhang X (2018) Construction of hierarchical zinc cobalt sul fi de @ nickel sul fi de core-shell nanosheet arrays for high-performance asymmetric solid-state supercapacitors. Chem Eng J 349:397–407. https://doi.org/10.1016/j.cej.2018.05.101
486. Tong H, Bai W, Yue S, Gao Z, Liang Lu, Shen L, Dong S, Zhu J, Jianping He XZ (2016) Zinc cobalt sulfide nanosheets grown on nitrogen-doped graphene/carbon nanotube film as high-performance electrode for supercapacitors. J Mater Chem A Mater 4:11256–11263. https://doi.org/10.1039/C6TA02249A
487. Ma J, Wang L, Yu P, Yan H, Li J, Fu H (2017) Ni – Co bimetallic sulfide coated with reduced graphene oxide and carbon for high-capacitance supercapacitor. J Nanosci Nanotechnol 17:4091–4098. https://doi.org/10.1166/jnn.2017.13428
488. Van NT, Trung L, Manh P, The L, Tien D, Thi N, Van NN, Viet T (2020) One-step solvothermal synthesis of mixed nickel e cobalt sul fi des as high-performance supercapacitor electrode materials. J Alloys Compd 831:154921. https://doi.org/10.1016/j.jallcom.2020.154921
489. Pu J, Wang T, Wang H, Tong Y, Lu C, Kong W (2014) Direct growth of NiCo 2 S 4 nanotube arrays on nickel foam as high-performance binder-free electrodes for supercapacitors. ChemPubSoc 79:577–583. https://doi.org/10.1002/cplu.201300431
490. Luan Y, Zhang H, Yang F, Yan J, Zhu K, Ye K, Wang G, Cheng K, Cao D, Zhang H, Yang F, Yan J, Zhu K, Ye K, Wang G, Cheng K, Cao D (2018) Rational design of NiCo2S4 nanoparticles @ N-doped CNT for hybrid supercapacitor. Appl Surf Sci 447:165–172. https://doi.org/10.1016/j.apsusc.2018.03.236
491. Tang J, Ge Y, Shen J, Ye M (2016) Facile synthesis of CuCo 2 S 4 as a novel electrode material for ultrahigh supercapacitor. Chem Commun 52:1509–1512. https://doi.org/10.1039/C5CC09402J
492. Tang Y, Chen S, Mu S, Chen T, Qiao Y, Yu S, Gao F (2016) Synthesis of capsule-like porous hollow nano-nickel cobalt sulfides via cation exchange based on the Kirkendall effect for high-performance supercapacitors synthesis of capsule-like porous hollow nano-nickel cobalt sulfides via cation exchange based on th. Appl Mater Interfaces 8:9721–9732. https://doi.org/10.1021/acsami.6b01268
493. Gopi CV, Reddy AE, Kim HJ (2018) Wearable superhigh energy density supercapacitors using a hierarchical ternary metal decorated with CoFe 2 Se 4 nanorods †. J Mater Chem A Mater 6:7439–7448. https://doi.org/10.1039/c8ta01141a
494. Meng A, Shen T, Huang T, Song G, Li Z, Tan S (2019) NiCoSe 2 / Ni 3 Se 2 lamella arrays grown on N-doped graphene nanotubes with ultrahigh-rate capability and long-term cycling for asymmetric supercapacitor. Sci China Mater 63:229–239
495. Tang Z, Jia C, Wan Z, Zhou Q, Ye X, Zhu Y (2016) Facile preparation of CoNi2S4@NiSe nano arrays on compressed nickel foam for high performance fl exible supercapacitors †. RSC Adv 6:112307–112316. https://doi.org/10.1039/c6ra20871a
496. Girma L, Li X, Xia X, Liu W (2016) 3D fl ower-like CoNi 2 S 4 grown on graphene decorated nickel foam as high performance supercapacitor. Diam Relat Mater 73:169–176. https://doi.org/10.1016/j.diamond.2016.09.008
497. Cao X, He J, Li H, Kang L, He X, Sun J, Jiang R, Xu H (2018) CoNi 2 S 4 nanoparticle / carbon nanotube sponge cathode with ultrahigh capacitance for highly compressible asymmetric supercapacitor. Small 14:1–10. https://doi.org/10.1002/smll.201800998
498. Chen Q, Miao J, Quan L, Cai D, Zhan H (2018) Bimetallic CoNiSx nanocrystallites embedded in nitrogen-doped carbon anchored on reduced graphene oxide for high-performance supercapacitors. Nanoscale 10:4051–4060. https://doi.org/10.1039/c7nr08284c
499. Gao F, Xu B, Wang Q, Cai F, He S, Zhang M (2016) Potentiostatic deposition of CoNi 2 S 4 nanosheet arrays on nickel foam : effect of depostion time on the morphology and pseudocapacitive performance. J Mater Sci 51:10641–10651. https://doi.org/10.1007/s10853-016-0286-9

500. Gao Z, Chen C, Chang J, Chen L, Wang P, Wu D, Xu F, Guo Y, Jiang K (2018) Enhanced cycleability of faradic CoNi 2 S 4 electrode by reduced graphene oxide coating for ef fi cient asymmetric supercapacitor. Electrochim Acta 281:394–404. https://doi.org/10.1016/j.electacta.2018.05.194
501. Hu W, Chen R, Xie W, Zou L, Qin N, Bao D (2014) CoNi2S4 nanosheet arrays supported on Ni foams with ultrahigh capacitance for aqueous asymmetric supercapacitor applications CoNi 2 S 4 nanosheet arrays supported on Ni foams with ultrahigh capacitance for aqueous asymmetric supercapacitor applications. Appl Mater Interfaces 6:19318–19326. https://doi.org/10.1021/am5053784
502. Li Z, Zhao D, Xu C, Ning J, Zhong Y, Zhang Z, Wang Y, Hu Y (2018) Reduced CoNi 2 S 4 nanosheets with enhanced conductivity for high-performance supercapacitors. Electrochim Acta 278:33–41. https://doi.org/10.1016/j.electacta.2018.05.030
503. Rafai S, Qiao C, Naveed M, Wang Z, Younas W, Khalid S, Cao C (2019) Microwave-anion-exchange route to ultrathin cobalt-nickel-sul fi de nanosheets for hybrid supercapacitors. Chem Eng J 362:576–587. https://doi.org/10.1016/j.cej.2019.01.059
504. Tang J, Shen J, Li N, Ye M, Shen J, Li N, Ye M (2015) One-pot tertbutanol assisted solvothermal synthesis of CoNi2S4/reduced graphene oxide nanocomposite for High-performance supercapacitors. Ceram Int 41:6203–6211. https://doi.org/10.1016/j.ceramint.2015.01.023
505. Xu AR, Lin J, Wu J, Huang M (2017) A two-step hydrothermal synthesis approach to synthesize NiCo 2 S 4 / NiS hollow nanospheres for high-performance asymmetric supercapacitors. Appl Surf Sci 422:597–606. https://doi.org/10.1016/j.apsusc.2017.06.003
506. Zhang Y, Sun C, Haiquan Su, Wei Huang XD (2015) N-doped carbon coated hollow NixCo9-xS8 urchins for high-performance supercapacitor. Nanoscale 7:3155–3163. https://doi.org/10.1039/C4NR06286H
507. Zhao F, Huang W, Zhang H, Zhou D (2017) Facile synthesis of CoNi 2 S 4 / Co 9 S 8 composites as advanced electrode materials for supercapacitors. Appl Surf Sci 426:1206–1212. https://doi.org/10.1016/j.apsusc.2017.07.066
508. Shen J, Wu J, Pei L, Rodrigues MF, Zhang Z (2016) CoNi2S4-graphene^{-2}D-MoSe2 as an advanced electrode material for supercapacitors. Ionics (Kiel) 25:897–901. https://doi.org/10.1002/aenm.201600341
509. Kong L, Shi M, Zhang T, Luo Y, Kang L (2016) Simple synthesis of CoMoS4 based nanostructure and its application for high-performance supercapacitors. RSC Adv 6:7633–7642. https://doi.org/10.1039/C5RA26157K
510. Ma T, Zhang M, Liu H, Wang Y (2019) Electrochimica Acta Three-dimensional sulfur-doped graphene supported cobalt-molybdenum bimetallic sul fi des nanocrystal with highly interfacial storage capability for supercapacitor electrodes. Electrochim Acta 322:134762. https://doi.org/10.1016/j.electacta.2019.134762
511. Manikandan R, Raj CJ, Nagaraju G, Pyo M (2019) Selective design of binder-free hierarchical nickel molybdenum sulfide as a novel battery-type material for hybrid supercapacitors. J Mater Chem A Mater 7:25467–25480. https://doi.org/10.1039/c9ta08527k
512. Wei M, Wang C, Yao Y, Yu S, Liao W, Ren J, Sun R, Wong C (2018) Toward high-performance all-solid-state supercapacitors using facilely fabricated graphite nanosheet-supported CoMoS 4 as electrode material. Chem Eng J 355:891–900. https://doi.org/10.1016/j.cej.2018.08.223
513. Pan UN, Sharma V, Kshetri T, Singh TI, Paudel DR, Kim NH, Lee JH (2020) Freestanding 1T-MnxMo1–xS2–ySey and MoFe2S4–zSez ultrathin nanosheet-structured electrodes for highly efficient flexible solid-state asymmetric supercapacitors. Small 16:2001691. https://doi.org/10.1002/smll.202001691
514. Mohamed AM, Abo El Naga AO, Zaki T, Hassan HB, Allam NK (2020) Bimetallic Co–W–S chalcogenides confined in N, S-codoped porous carbon matrix derived from metal–organic frameworks for highly stable electrochemical supercapacitors. ACS Appl Energy Mater 3:8064–8074. https://doi.org/10.1021/acsaem.0c01513
515. Jayababu N, Jo S, Kim Y, Kim D (2021) Novel conductive Ag-decorated NiFe mixed metal telluride hierarchical nanorods for high-performance hybrid supercapacitors. ACS Appl Mater Interfaces 13:19938–19949. https://doi.org/10.1021/acsami.1c00506
516. Luo R, Yang Q, Liu Y, Sun L, Wang C, Chen M, Shi W (2023) Novel core–shell nanoclusters composed of multiple nickel–cobalt-oxyselenide nanowires wrapped with NiCo-LDH nanosheets for high energy density supercapacitors. Inorg Chem Front 10:192–200. https://doi.org/10.1039/D2QI01739C
517. Sumedha HN, Hausmann JN, Kalra S, Viswanatha R, Menezes PW, Santosh MS (2023) Symmetric supercapacitors based on copper–antimony chalcogenides: a trade-off between S and Se. Ceram Int 49:1756–1763. https://doi.org/10.1016/j.ceramint.2022.09.139
518. Abid AG, Gouadria S, Manzoor S, Katubi KMS, Jabbour K, Abdullah M, Un Nisa M, Aman S, Al-Buriahi MS, Ashiq MN (2023) Uniformly dispersed flowery EuZrSe3 derived from the europium-based metal–organic framework for energy storage devices. Fuel 336:127066. https://doi.org/10.1016/j.fuel.2022.127066
519. Ghosh S, Samanta P, Murmu NC, Kuila T (2020) Investigation of electrochemical charge storage in nickel-cobalt-selenide/reduced graphene oxide composite electrode and its hybrid supercapacitor device. J Alloys Compd 835:155432. https://doi.org/10.1016/j.jallcom.2020.155432
520. Abu Dakka Y, Balamurugan J, Balaji R, Kim NH, Lee JH (2020) Advanced Cu0.5Co0.5Se2 nanosheets and MXene electrodes for high-performance asymmetric supercapacitors. Chem Eng J 385:123455. https://doi.org/10.1016/j.cej.2019.123455
521. Ahmed ATA, Pawar SM, Inamdar AI, Im H, Kim H (2020) Fabrication of FeO@CuCo2S4 multifunctional electrode for ultrahigh-capacity supercapacitors and efficient oxygen evolution reaction. Int J Energy Res 44:1798–1811. https://doi.org/10.1002/er.5027
522. Patil SJ, Chodankar NR, Hwang S-K, Shinde PA, Rama Raju GS, Ranjith KS, Karekar SV, Huh Y-S, Han Y-K (2023) Two-dimensional nanosheets of bimetallic chalcogenide-tagged nitrogen-doped carbon as a cathode for high-performance and durable zinc-ion capacitors. J Mater Chem A Mater 11:5112–5126. https://doi.org/10.1039/D2TA07524E
523. Bhattarai RM, Chhetri K, Le N, Acharya D, Saud S, Nguyen MCHPL, Kim SJ, Mok YS (2023) Oxygen functionalization-assisted anionic exchange toward unique construction of flower-like transition metal chalcogenide embedded carbon fabric for ultra-long life flexible energy storage and conversion. Carbon Energy n/a:e392. https://doi.org/10.1002/cey2.392
524. Wei C, Chen Q, Cheng C, Liu R, Zhang Q, Zhang L (2019) Mesoporous nickel cobalt manganese sulfide yolk-shell hollow spheres for high performance electrochemical energy storage. Inorg Chem Front 6:1851–1860. https://doi.org/10.1039/c9qi00173e
525. Sahoo S, Mondal R, Late DJ, Rout CS (2017) Electrodeposited nickel cobalt manganese based mixed sulfide nanosheets for high performance supercapacitor application. Microporous Mesoporous Mater 244:101–108. https://doi.org/10.1016/j.micromeso.2017.02.043
526. Gao SQ, Zhang PP, Guo SH, Chen WQ, Li M, Liu F, Cheng JP (2019) Synthesis of single-phase CuCo 2-x Ni x S 4 for

high-performance supercapacitors. J Colloid Interface Sci 555:284–293. https://doi.org/10.1016/j.jcis.2019.07.091
527. Verma M, Yadav R, Sinha L, Hong CK, Shirage PM (2018) Pseudocapacitive-battery-like behavior of cobalt manganese nickel sulfide (CoMnNiS) nanosheets grown on Ni-foam by electrodeposition for realizing high capacity. RSC Adv 8:40198–40209. https://doi.org/10.1039/c8ra07471b
528. Isacfranklin M, Yuvakkumar R, Ravi G, Saravanakumar B, Pannipara M, Al-Sehemi AG, Velauthapillai D (2021) Quaternary Cu2FeSnS4/PVP/rGO composite for supercapacitor applications. ACS Omega 6:9471–9481. https://doi.org/10.1021/acsomega.0c06167
529. Isacfranklin M, Yuvakkumar R, Ravi G, Hong SI, Shini F, Thambidurai M, Dang C, Velauthapillai D (2020) Marigold flower like structured Cu2NiSnS4 electrode for high energy asymmetric solid state supercapacitors. Sci Rep 10:19198. https://doi.org/10.1038/s41598-020-75879-9
530. Song J, Fan H, Bai L, Wang Y, Jin Y, Liu S, Xie X, Zheng W, Liu W (2023) Achieving ultrahigh energy-density aqueous supercapacitors via a novel acidic radical adsorption capacity-activation mechanism in Ni(SeO3)/metal sulfide heterostructure. Small Methods 7:2201353. https://doi.org/10.1002/smtd.202201353